Università degli Studi di Camerino

Facoltà di Scienze e Tecnologie
Dipartimento di Fisica

# QUANTUM PHENOMENA UNDER EIT CONDITIONS

Tesi di Dottorato

di

**Carlo Ottaviani**

Dottorato di Ricerca in Fisica (XVIII Ciclo)

Relatori:

Prof. David Vitali

Prof. Paolo Tombesi

Controrelatore:

Prof. Ennio Arimondo

*A mio padre, mia madre*
*e a mio nonno Giovanni (1903-1993)*

# Acknoledgments

I would like to thank my supervisors, prof. Paolo Tombesi and prof. David Vitali for these years of study in the group of Quantum Optics and Quantum Information, and Dr.Stojan Rebic with which I am strongly indebted for his precious help during each day of work for this thesis.
I would like to thank also Dr. Gianni Di Giuseppe, as well as Dr. Stefano Pirandola (*Cobbra*), and Dr. Marco Lucamarini (*Mangusta*) for the useful discussion.

Although it is not possible, obviously, to enumerate all the people that has even unconsciously contributed to this work, I would like to thank my family, my sister Lucia, and all the people apparently not related with my, let's say, *Physical World*, in particular the *ADP Blues band* and the *Hum-pop band* components, Cristiano Porcina, Dr. Leonardo Marchegiani, Roberto Orpianesi, Samuele Elisei.

# List of abbreviations

| | |
|---|---|
| AMS | Asymmetric M-Scheme |
| CPT | Coherent Population Trapping |
| CPS | Conditional Phase Shift |
| CK | Cross Kerr |
| CQED | Cavity Quantum Electro-Dynamics |
| DS | Dark State |
| BS | Bright State |
| EIT | Electromagnetically Induced Transparency |
| EM | Electro-Magnetical |
| IP | Interaction Picture |
| ME | Master Equation |
| RWA | Rotating Wave Approximation |
| QC | Quantum Computation |
| QEC | Quantum Error Correction |
| QECC | Quantum Error Correction Code |
| QPG | Quantum Phase Gate |
| QI | Quantum Information |
| QKD | Quantum Key Distribution |
| QND | Quantum Non-Demolation |
| QT | Quantum Trjactories |
| SK | Self Kerr |
| SMS | Symmetric M-Scheme |
| STIRAP | Atimulated Raman Adiabatic Passage |
| SPM | Self Phase Modulation |
| XPM | Cross Phase Modulation |

# Contents

# List of Figures

# Abstract

This thesis is on the study of the mechanisms for the production of nonlinear photon-photon interaction under the condition of Electromagnetically Induced Transparency (EIT), and on the implementation of a Quantum Error Correction (QEC) scheme adopting a Cavity Quantum Electrodynamics (CQED) set-up. The latter part of the thesis will be treated in the last chapter.

Large non linear effects are usually accompanied, by a large increase of the absorption. This fact makes classical nonlinear devices not useful for the purposes of the rapid developing fields of Quantum Computation and Information. Strong absorption process results in a complete loss of the information represented by the state of the photons. EIT is a well known process of atomic coherence, largely studied starting from the seventies together with the discovery of Coherent Population Trapping (CPT), Lasing Without Inversion (LWI), slow light propagation.
After the recent experimental realization of slowed down light, EIT has experienced a revival in recent years mainly due to the possible application to Quantum Computation and Quantum Information (QC&QI). EIT is a process that makes transparent a previously opaque medium thanks to the interaction with an electromagnetic field. It is a manifestation of the quantum nature of atoms, that exploits a quantum interference process. In this thesis we will show how an EIT medium permits to obtain giant non-linear Kerr interaction (up to eight order of magnitude increase) even at low light level, by the study of several light-atoms scheme. The production and control of giant cross phase modulation (XPM) is analysed and all sources of noise and loss will be included in the treatment.

The main goal of this thesis is to study the photon-photon interaction at the level of single photons in several multilevel schemes. In the full quantum limit we shall concentrate to a specific light-atoms interaction scheme, the symmetric M scheme (SMS) under the condition of EIT. We shall study how to implement a Quantum Phase Gate (QPG). Such a gate has been already experimentally realized for a cavity, but here we want to find the optimal condition to implement the QPG between flying qubits. To this end we adopt EIT in order increase the photon-photon interaction: in a cavity such an increase is provided by the small volume of the cavity, while in EIT it is based on the strong dispersion $dn/d\omega$ at the center of the transparency window.
Photons represent the best candidates for the implementation of transmission lines for carrying quantum information, and this is why strong nonlinear photon-photon interaction is particularly interesting from the point of view of quantum information.
In this scenario the principal goal of this thesis is to analyze the potentiality of a EIT based device in full quantum regime, for the implementation of the QPG. The quantities that define the performance of the gate are calculated in detail including decoherence mechanisms and finding a possible set-up for the experimental realization.

The thesis is organized as follows. In first chapter we review some notions of atom-light interaction in multilevel atoms, and we introduce the most interesting features of the EIT pro-

cess. In the second and in the third chapter, we study three different multilevel atomic schemes in the semiclassical regime. The aim of this chapter is to show how multilevel schemes can be tailored for the generation of Cross Phase Modulation (XPM). In chapter four we concentrate on the SMS for the full quantum analisys of the cross Kerr interaction. Conditions for the implementation of a cross Kerr interaction that gives a conditional phase shift of order $\pi$ are individuated and for the first time a rigorous evaluation of the fidelity of the gate is performed.

In chapter five we approached the problem of the implementation of a QEC protocol based on an experimental set-up composed of Rydberg atoms and cavities. We will describe the various step of the protocol, and we will evaluate the fidelity in the presence of the main decoherence mechanisms.

# Chapter 1

# Interaction of Atoms with Electromagnetic Fields

*In this chapter we introduce the atom-field interaction in the semiclassical approach. After a review of the interaction of a two level atom with an electromagnetic field, we describe the main properties of Electromagnetically Induced Transparency (EIT) in a multilevel atomic system, taking into account in a particular the three level $\Lambda$ configuration. We will describe the linear, nonlinear, as well as the slow light propagation properties of this three level system. We then introduce the Cross Kerr interaction in four level system and review the main schemes for the production of Cross Phase Modulation (XPM). We then give a short introduction to the potential applications of EIT in this field.*

## 1.1 Interaction of an electromagnetic field with two level Atoms

The study of the interaction of atoms with electromagnetic fields plays a crucial role in the analysis of many topics in modern physics. In general the atomic structure is a complicated multilevel one, but for many applications this multilevel structure can be well modelled by a much simpler system, as for example the two level approximation. In this paragraph we study the two level system because, despite its simplicity, it gives a deep insight both for the mathematical technics adopted as well as for the physical behaviour of multilevel systems.

The two level approximation can be adopted when the applied fields are weak and nearly in resonance with the atomic transition. A sketch of an atom approximated by a two level system is represented in Fig.1.1(a). In this situation, only the ground state and the near-resonant excited levels will enter the dynamics of the system, i.e., only these two levels will be populated under the action of the electromagnetic field.

Let us consider the two atomic levels $|1\rangle$ and $|2\rangle$ showed in Fig.1.1 and driven by a classical electromagnetic field. Considering the applied field

$$\mathbf{E} = \mathcal{E}e^{-\imath\omega t} + \mathcal{E}^{\star}e^{-\imath\omega t}, \tag{1.1}$$

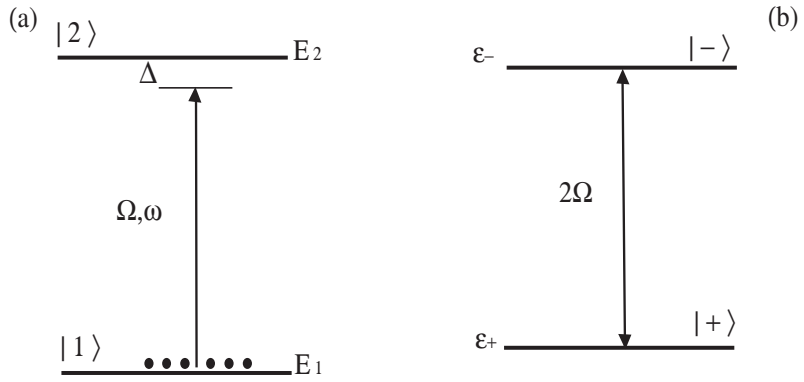


Figure 1.1: Two level scheme in the bare (a) and dressed basis (b).

where $\mathcal{E}$ is the field's amplitude and $\omega$ the angular frequency. In the dipole approximation, the strength of the atom-field interaction is proportional to the atomic dipole operato. Within the two level approximation we truncate the infinite dimensional basis over which we evaluate the dipole moment reducing the Hilbert space to the pair of levels included in the basis $\mathcal{B} = \{|1\rangle, |2\rangle\}$. The dipole moment of the single two level atom is

$$\hat{d} = \sum_n |1\rangle_n \langle 2| \mu_{1,2}^{(n)}, \tag{1.2}$$

where $\mu_{1,2} = \langle 1|e\hat{r}|2\rangle$. The total Hamiltonian is the sum of the two terms

$$H = H_{atom} + H_{int}, \tag{1.3}$$

where $H_{atom}$ represents the free Hamiltonian

$$H_{atom} = \hbar\omega_1 |1\rangle\langle 1| + \hbar\omega_2 |2\rangle\langle 2|, \tag{1.4}$$

and $H_{int}$ is the interaction Hamiltonian, i.e., the energy exchanged by the atoms with the field

$$H_{int} = \hbar\big(|1\rangle\langle 2|\Omega e^{-\imath\omega t} + |2\rangle\langle 1|\Omega^\star e^{\imath\omega t}\big) \tag{1.5}$$

where $\Omega = -\mu_{12}\mathcal{E}/\hbar$ represents the Rabi frequency of the applied field, which will give the time scale at which the atomic population of each atom will oscillate between level $|1\rangle$ and $|2\rangle$. A standard way to proceed to simplify the mathematical description of multilevel system is to pass to the Interaction Picture (IP) and Rotating Wave Approximation (RWA). Representing the physical system in a suitable rotating frame permits to obtain the net effect of the interaction. This is performed defining

$$H_0 = \hbar\omega_1 |1\rangle\langle 1| + \hbar(\omega_2 - \Delta)|2\rangle\langle 2|, \tag{1.6}$$

where $\Delta = \omega_2 + \omega_1 - \omega$ is the detuning, and

$$\mathcal{U}(t) = \exp(-\imath H_0 t/\hbar), \tag{1.7}$$

the associated unitary operator.
Applying $\mathcal{U}(t)$ to the Hamiltonian (1.3), we get the effective Hamiltonian in the IP

$$H_{eff} = \mathcal{U}(t)H\mathcal{U}^\dagger(t) - \imath\hbar\mathcal{U}^\dagger(t)\dot{\mathcal{U}}(t), \tag{1.8}$$

which is exactely given by

$$H_{eff} = \hbar\Delta\sigma_{22} + \hbar\Big(\Omega\sigma_- + \Omega^\star\sigma_+\Big), \tag{1.9}$$

where $\sigma_- = |1\rangle\langle 2|$, and $\sigma_+ = |2\rangle\langle 1|$, are the rising and lowering atomic operators.

### 1.1.1 Schrödinger Equation Treatment

In the two level approximation, we can write the most general state of the system as:

$$|\psi(t)\rangle = C_1(t)|1\rangle + C_2(t)|2\rangle, \tag{1.10}$$

The two coefficients $C_{1,2}$ give the probability amplitude to find the state in level $|1\rangle$ or $|2\rangle$ respectively, and the time evolution will be obtained solving the Schrödinger equation

$$\imath\hbar\frac{d}{dt}|\psi(t)\rangle = H_{eff}|\psi(t)\rangle, \tag{1.11}$$

Which explicitly gives:

$$\begin{aligned}\frac{dC_1}{dt} &= -\imath\frac{\Omega}{2}C_2(t)\\ \frac{dC_2}{dt} &= -\imath\Delta C_2(t) - \imath\frac{\Omega^\star}{2}C_1(t).\end{aligned} \tag{1.12}$$

These equations can be solved exactly but let us consider two special cases that will give an idea of the general behaviour of the two level system.
When $\Delta = 0$ the field is in resonance with the atomic transition. In this case the solutions corresponding to $|\psi(0)\rangle = |1\rangle$ are

$$C_1(t) = \cos\frac{|\Omega|t}{2} \tag{1.13}$$

$$C_2(t) = -\imath\frac{\Omega^\star}{|\Omega|}\imath\sin\frac{|\Omega|t}{2}. \tag{1.14}$$

These equations show that the atomic population oscillates between level $|1\rangle$ and $|2\rangle$, with a period length determined by the Rabi frequency,

$$|\psi(t)\rangle = \cos\frac{\Omega t}{2}|1\rangle - \imath e^{-\imath\arg\Omega}\sin\frac{\Omega t}{2}|2\rangle. \tag{1.15}$$

The opposite situation is when the field is far-detuned from the atomic transition $\Delta \gg \Omega$. In this case, although the field hardly excites the atomic system to the excited level, it will have some effects on the energy of the ground state. If the detuning is much larger then the characteristic Rabi frequency, we can adopt the adiabatic elimination $\dot{C}_2 \simeq 0$ in the second of Eqs.(1.13) so to get

$$C_2(t) = -\frac{\Omega^\star}{\Delta} C_1(t). \tag{1.16}$$

Putting this condition into the first of eq.(1.12) we have the expression for the evolution of the population in level $|1\rangle$,

$$C_1(t) \sim C_1(0) e^{-i|\Omega|^2 t/\Delta}. \tag{1.17}$$

As a consequence, the final population won't be to far from the initial condition. If for example the system starts in the ground state $|1\rangle$ it will remain there, with a phase accumulation depending on the ratio $\Omega/\Delta$. The process that induces the phase accumulation can be seen as a modification of the ground state energy of the atomic system. The energy is shifted by the amount $|\Omega|^2/\Delta$, a process known as the ac-Stark shift that will be of great importance in the next chapters.

An elegant way to describe multilevel systems is based on the *dressed* atomic states. This kind of picture of multilevel systems is particularly useful in the cases where the atomic structure coupled to the fields is particularly complicated. Diagonalizing the time independent Hamiltonian (1.9) we can easily find a basis $\mathcal{B}_{dressed}$ whose elements are the eigenvectors $|\pm\rangle$. Expressed in terms of the bare atomic states $|1\rangle$ and $|2\rangle$ the eigenvectors are

$$|\pm\rangle = \frac{\Omega}{\sqrt{|\Omega|^2 + \epsilon_\pm^2}}|1\rangle + \frac{\epsilon_\pm}{\sqrt{|\Omega|^2 + \epsilon_\pm^2}}|2\rangle, \tag{1.18}$$

where $\epsilon_\pm = \frac{\Delta}{2} \pm \sqrt{\frac{\Delta^2}{4} + |\Omega|^2}$. When $\Delta = 0$ the system is in resonance with the atomic transition, the two dressed states will be $|\pm\rangle = (|1\rangle \pm |2\rangle)/\sqrt{2}$ and the separation in energy of these two states will be twice the applied Rabi frequency $2\Omega$ as showed by Fig.1.1.b.

### 1.1.2 Master Equation for a two level system

A powerful approach for the description of the time evolution of a quantum system is the Master Equation (ME). The ME describes open quantum systems, including in the treatment the effect of the interaction of the system with the environment. The steps to obtain the ME are given in Appendix A.1.Here we give the general expression of the ME for a two level system.
Taking into account the Hamiltonian in IP given by eq.(1.9), the ME for a two level atomic system interacting with an electromagnetic field is given by the following expression

$$\frac{d\rho}{dt} = -\imath\frac{1}{2}\Delta\big[\sigma_{22},\sigma\big] - \imath\frac{\Omega}{2}\big[\sigma_+ + \sigma_-,\sigma\big] + \frac{\gamma}{2}\big(2\sigma_-\sigma\sigma_+ - \sigma_+\sigma_-\sigma - \sigma\sigma_+\sigma_-\big) + \frac{\gamma_{deph}}{2}(2\sigma_z\sigma\sigma_z - \sigma), \tag{1.19}$$

where with $\sigma_{ij} = |i\rangle\langle j|$ we have indicated the projection operators.
The first two terms describe the deterministic evolution given by $H_{eff}$, the other terms describe the various effects of decays and losses due to the interaction with the environment. The first one is determined by the spontaneous decay from level $|2\rangle \rightarrow |1\rangle$, the last last term describe the phase destroying process, that do not affect in general the population of the atomic level but modify the phase of the quantum states describing the atomic levels. This terms are not important in the dynamics of the two level system as they affect only the coherence whose time scale is dominated by the spontaneous emission rate, since $\gamma_{deph} \ll \gamma$. Anyway we include the dephasing rate $\gamma_{deph}$ from now on, as it will be useful in the following.
From the Master Equation (see AppendixA.1), it is possible to obtain the evolution of the elements of the density matrix. This can be done starting from the ME and evaluating the matrix element of $\rho$ on the basis $\mathcal{B} = \{|i\rangle, |j\rangle\}$,

$$\dot{\rho}_{ij} = \langle i|\frac{d\rho}{dt}|j\rangle.$$

We obtain a set of equations that describes the time evolution of populations and atomic coherences. These equations take the name of Optical Bloch Equations (OBE), and for the two level system are

$$\dot{\rho}_{11} = -\imath\frac{\Omega}{2}\big(\rho_{12} - \rho_{21}\big) + \Gamma\rho_{22} \tag{1.20}$$

$$\dot{\rho}_{22} = \imath\frac{\Omega}{2}\big(\rho_{12} - \rho_{21}\big) - \Gamma\rho_{22} \tag{1.21}$$

$$\dot{\rho}_{12} = -\imath\Delta\rho_{12} + \imath\frac{\Omega}{2}\big(\rho_{22} - \rho_{11}\big) + \frac{\Gamma + \gamma_{deph}}{2}\rho_{12}. \tag{1.22}$$

The first two describe the evolution in time of the atomic populations, while the third gives the evolution of the atomic coherence. Atomic coherence is a peculiar feature of the quantum nature of the atoms. With atomic coherence we mean the property of an atomic state to exist in a *coherent superposition* of two or more atomic configuration.

## 1.2 Absorption and Dispersion Properties.

Absorption and dispersion properties of the medium, that interact with the field, are determined by the off-diagonal elements of the density matrix $\rho_{12}$. In fact these terms describe the induced

dipole moment on the atom by the field. The dipole moment of the atom will oscillates with a frequency proportional to the Rabi frequency of the applied field, and the rapidity in the change of the orientation of the atomic dipole will determines the dispersion and absorption properties of the atom. When the dipole is parallel to the electromagnetic field there is no absorption, on the other hand when the dipole is orthogonal to the electromagnetic field the atom absorb energy from it to orient with the field.

The quantity that describes the absorption and dispersion properties is the polarization $\mathcal{P}$ of the medium which is equal to the atomic dipole moment per unit volume and therefore it is given by,

$$\mathcal{P} = \frac{\mathcal{N}_a}{V}\langle p(t)\rangle, \tag{1.23}$$

where $\langle p(t)\rangle = \mathrm{Tr}\{\rho\hat{p}\}$ is the mean dipole moment over the atomic state, $\mathcal{N}_a$ is the number of atoms in the medium, and $V$ is its volume. The Fourier component of the polarization at the frequency $\omega$ is given by the following expression

$$P(\mathbf{r},\omega) = \epsilon_0\chi(\mathbf{r},\omega)E(\mathbf{r},\omega) + \epsilon_0\chi(\mathbf{r},\omega)^{(2)}|E(\mathbf{r},\omega)|^2 + \epsilon_0\chi(\mathbf{r},\omega)^{(3)}|E(\mathbf{r},\omega)|^3 + \ldots, \tag{1.24}$$

here $\mathcal{P}(\omega) = \int dt e^{\imath\omega t}\mathcal{P}(t)$. The term proportional to the square of the applied field describes the second order nonlinear effects, while that proportional to $|E(\mathbf{r},\omega)|^3$ is associated with third order nonlinear Kerr effect[1].

Expressing the dipole moment as a function of the density matrix we have that it is proportional to the off diagonal term $\rho_{12}$, then the susceptibility $\chi^{(1)}$ can be expressed in terms of the off this diagonal

$$\mathcal{P} = \frac{\mathcal{N}_a}{V}\mu_{12}\rho_{12} = \varepsilon_0\chi E_1, \tag{1.25}$$

then from eq(1.20,1.25) we have the single atom polarization

$$\chi = \frac{\mathcal{N}_a}{V}\frac{\mu_{12}\rho_{12}}{E_1\varepsilon_0}, \tag{1.26}$$

The susceptibility is in general a complex number,

$$\chi = \chi' + \imath\chi'', \tag{1.27}$$

where $\chi'$ is the real part of the susceptibility, and $\chi''$ describe the imaginary part of the susceptibility. The real part of the susceptibility gives information on the dispersion properties of the atom while the imaginary part will describe the absorption properties of the medium. Solving eqns.(1.20) at the steady state, we can obtain a simple analytical expression that describe the absorption dispersion profile,

$$\chi = -\frac{\mathcal{N}_a}{V}\frac{\Omega}{2(\Delta - \imath\gamma)}. \tag{1.28}$$

[1] In what follow, we shall consider a homogeneous medium and the dependence of the fields and susceptibility upon the position $\vec{r}$ will not be explicitly written.

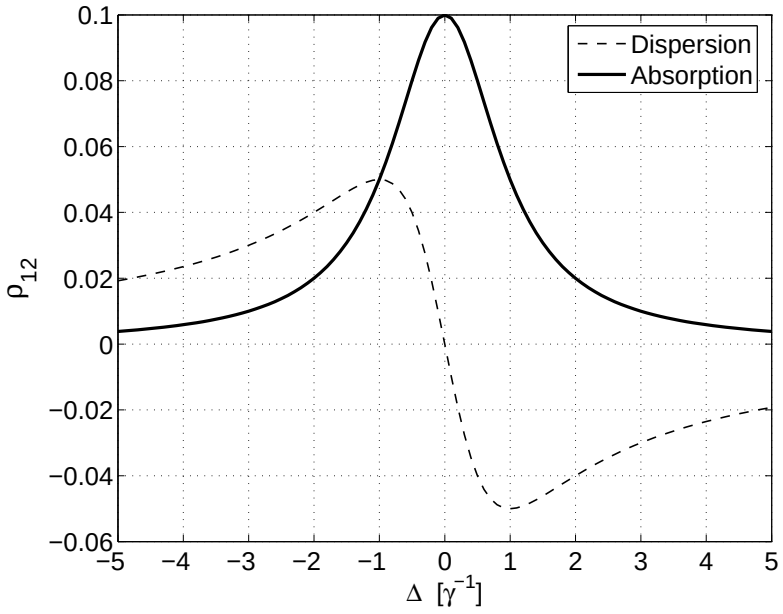


Figure 1.2: This plot shows the profiles of the absorption (continuous line) from the imaginary part of eq.(1.26), and dispersion (dashed) determined by the real part, for a two level system interacting with an electromagnetic field. At resonance ($\Delta = 0$) the field experiences a rapid increase of the absorption.

In Fig.1.2 we see the behavior of the two level medium as described of eq.(1.28). When the electromagnetic field is in resonance with the atomic transition the absorption increases, and at the perfect resonance it reaches its maximum value.

From this picture we see how an interacting light field can modulate the optical properties of the atomic medium. The profile of the imaginary part of the linear susceptibility depicted in Fig.1.2 by the continuous line, suggests that when the field is in resonance with the atomic transition ($\Delta = 0$), its energy is absorbed to promote the atomic system to the excited level $|2\rangle$. At resonance the atom evolves in an anomalous dispersion regime, where the optical properties are radically changed, and group velocity of the light pulses can be radically modified.

In recent years the advent of Quantum Information has induced much more attention to the mechanisms of atom-light interaction. Because of their nature, photons have been individuated as a promising vector of quantum information. The weakness of the decoherence process even for reasonably long distances, the relatively simple transmission and generation have made photons ideal particle to store and process quantum information. Unfortunately this weak decoherence is accompanied by a weak photon-photon interaction, meanly due to the fact that photons are fast, and the interaction time in an *typical* photon-photon interaction device, is too short to have an efficient processing of photon properties. Moreover, in the quantum limit, light pulses are extremely weak, and even a moderate absorption is an obstacle in their use as carriers of quantum information. Therefore one has to look for particular configurations able to give significant photon-photon interaction not accompanied by a large absorption.

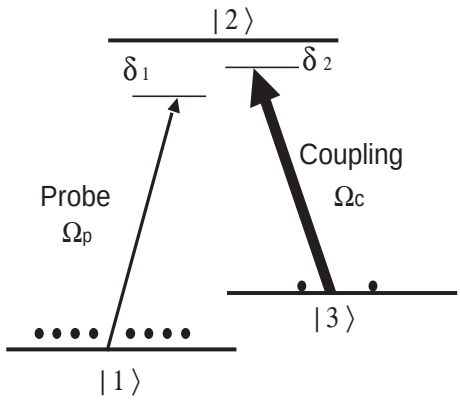


Figure 1.3: Typical atomic configuration for EIT generation.

## 1.3 The EIT interaction

EIT is a phenomenon based on the generation of atomic coherence to modify the optical properties of an atomic medium, in particular EIT-based systems permit the storage and absorption-free propagation of light pulses, even at very low light level, i.e., in the limit of single or quasi-single photon pulses.

To produce EIT we need electromagnetic fields and a multilevel atomic system, i.e., an atomic system that interacts with the light with more than two levels. The prototype of atomic configuration to produce EIT is given by Fig1.3. Two electromagnetic fields, whose Rabi frequency are $\Omega_p$ and $\Omega_c$ are coupled with the atomic transitions $|1\rangle \rightarrow |2\rangle$ and $|3\rangle \rightarrow |2\rangle$, respectively. We will show how this interaction scheme will leads to the propagation of light without absorption. Let us consider a system of Fig.1.3 with an initial population in the two ground states $|1\rangle$ and $|3\rangle$. We want to induce a loss-free propagation of the probe field. For this reason the first field to turn on is the *coupling* field with frequency $\omega_c$, and Rabi frequency $\Omega_c$. This process will pump the largest part of population in level $|1\rangle$, and only a small amount of population will remain in level $|3\rangle$. At this stage the atomic system evolves into a coherent superposition of the two ground state $|1\rangle$ and $|3\rangle$.

If we now turn on also the second field, the *probe* with frequency $\omega_p$, the atomic system will have two possible paths to be promoted to the common excited level $|2\rangle$: directly from $|1\rangle \rightarrow |2\rangle$ or from the indirect way $|3\rangle \rightarrow |2\rangle \rightarrow |1\rangle \rightarrow |2\rangle$. Both of these paths have an of probability that is proportional to the coupling field's Rabi frequency $\Omega_c$, but with opposite sign. The result is a mutual cancellation of the total amplitude probability of find an atom in the level $|2\rangle$. This is a quantum interference process. The results is that the atomic system is *trapped* in a pure state that is a coherent superposition of the two level $|1\rangle$ and $|3\rangle$.

Let us obtain a more detailed description of the process: we have a three level atomic system in the $\Lambda$ configuration. The two applied electromagnetic fields, are applied to the transition $|1\rangle \rightarrow |2\rangle$ and $|3\rangle \rightarrow |2\rangle$ respectively. We consider the most general case, both fields are slightly detuned from resonance. The probe detuning is $\delta_1 = \omega_{21} - \omega_p$ where $\omega_{21}$ is the frequency difference between the level $|2\rangle$ and $|1\rangle$, while the coupling field's detuning is $\delta_2 = \omega_{23} - \omega_c$.

Since we are working in the semiclassical approximation, the Hamiltonian will be of the form,

$$\begin{aligned} H_{tot} &= H_{atom} + H_{int} \\ &= \sum_{i=0}^{3} E_i |i\rangle\langle i| + \frac{\hbar}{2}\big[\Omega_p e^{-\imath\omega_p t}|2\rangle\langle 1| + \Omega_p^\star e^{\imath\omega_p t}|1\rangle\langle 2|\big] + \frac{\hbar}{2}\big[\Omega_c e^{-\imath\omega_c t}|2\rangle\langle 3| + \Omega_c^\star e^{\imath\omega_c t}|3\rangle\langle 2|\big] \end{aligned} \tag{1.29}$$

where $E_i$ for $i = 1, 2, 3$ are the energies of the atomic levels. Now we fix the zero of the energy in correspondence of the ground state $|1\rangle$, and we define the detunings so that

$$\begin{aligned} E_1 &= 0 \\ E_2 &= \hbar\delta_1 + \hbar\omega_p \\ E_3 &= E_2 - \hbar\delta_2 - \hbar\omega_c. \end{aligned} \tag{1.30}$$

Adopting the IP with respect to the following free Hamiltonian

$$H_0 = \hbar\omega_p|2\rangle\langle 2| + \hbar(\omega_p - \omega_c)|3\rangle\langle 3|,$$

we can write the effective Hamiltonian $H_{eff}$ in the IP, in the following form without any explicit time dependence,

$$H_{eff} = \hbar\delta_1|2\rangle\langle 2| + \hbar(\delta_1 - \delta_2)|3\rangle\langle 3| + \frac{\hbar}{2}\big[\Omega_p|2\rangle\langle 1| + \Omega_p^\star|1\rangle\langle 2|\big] + \frac{\hbar}{2}\big[\Omega_c|2\rangle\langle 3| + \Omega_c^\star|3\rangle\langle 2|\big]. \tag{1.31}$$

To fulfill the two photon Raman condition, we have to impose that the two detunings have to be equal ($\delta_1 = \delta_2$), or equivalently we have to set the frequency of the field so that the difference of the two detuning is equal to the frequency difference between the two ground levels $|1\rangle$ and $|2\rangle$. When Raman conditions are satisfied we obtain the best transparency.
On the basis of the three bare atomic states $\mathcal{B} = \big\{|1\rangle, |2\rangle, |3\rangle\big\}$, the matrix form of $H_{eff}$ is

$$H_{eff} = \frac{\hbar}{2}\begin{pmatrix} 0 & \Omega_p^\star & 0 \\ \Omega_p & \delta_1 & \Omega_c^\star \\ 0 & \Omega_c & \delta_1 - \delta_2 \end{pmatrix}. \tag{1.32}$$

Let us describe the dynamics of the system within the dressed state picture, i.e., let us evaluate the eigenvalues and eigenvectors of this Hamiltonian. Under the Raman condition $\delta_1 = \delta_2$ we can easily do this and in the limit of small probe detuning, as showed by [4,6,12], we obtain the following energies

$$\lambda_+ = \frac{\Omega}{2}, \tag{1.33}$$

$$\lambda_0 = 0, \tag{1.34}$$

$$\lambda_- = -\frac{\Omega}{2}, \tag{1.35}$$

corresponding to the three eigenvectors

$$|BS\rangle_+ = \frac{1}{\sqrt{2}}\big[\frac{\Omega_p}{\Omega}|1\rangle + |2\rangle + \frac{\Omega_c}{\Omega}|3\rangle\big], \tag{1.36}$$

$$|DS\rangle = \frac{1}{\Omega}\big[\Omega_c|1\rangle - \Omega_p|3\rangle\big], \tag{1.37}$$

$$|BS\rangle_- = \frac{1}{\sqrt{2}}\big[\frac{\Omega_p}{\Omega}|1\rangle - |2\rangle + \frac{\Omega_c}{\Omega}|3\rangle\big], \tag{1.38}$$

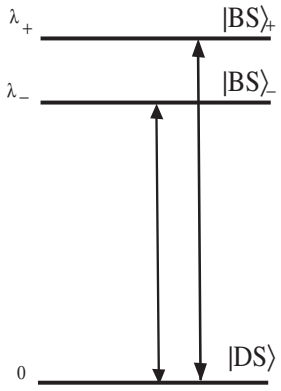


Figure 1.4: Dressed State picture of a three level Λ scheme.

where $\Omega = \sqrt{|\Omega_p|^2 + |\Omega_c|^2}$. The dressed state picture for the Λ scheme is in Fig.1.3. The three eigenvectors are named *bright-state* $|BS\rangle_\pm$, and *Dark-state* $|DS\rangle$. The reason of the name relies on their structure: $|BS\rangle_\pm$ have a component from the excited level $|2\rangle$, while $|DS\rangle$ has no contribution from $|2\rangle$. This implies that spontaneous emission affects only $|BS_\pm\rangle$ and not $|DS\rangle$. For this reason if the atom is initially prepared in $|DS\rangle$ (for example with the procedure described at the beginning of this section), or if we wait for a sufficient long time, the system relaxes to the dark state after an initial passage through the bright-states. We can notice, in fact, that $|DS\rangle$ is in fact an eigenstate of the the effective Hamiltonian $H_{eff}$ with eigenvalue $\lambda_0 = 0$, i.e., it does not evolves in time, it is decoupled from the effective Hamiltonian (1.32) . As much as we approach the zero detuning condition the atomic system becomes more and transparent to the propagation of the probe field. This is clear from the fact that the state to which the system evolves has no $|2\rangle$ components. The general expression for the dark state when the two photon resonance is not fulfilled $\delta_{12} = \delta_1 - \delta_2 \neq 0$ is given by

$$|DS\rangle = \frac{\left[\Omega_c|1\rangle + \delta_{12}|2\rangle - \Omega_p|3\rangle\right]}{\sqrt{\Omega^2 + \delta_{12}^2}}, \tag{1.39}$$

and is evident as the dark state decouples from the Hamiltonian function at the Raman condition.

The early days of EIT start with the first experimental and analytical analysis of the Λ scheme that was performed in the 1976 [4]. In this experiment the Coherent Population Trapping (CPT) [4] was realized. In a spectroscopic analysis of the Na atoms they recorded the absence of fluorescence spectrum in correspondence of some precise frequencies as the consequence of the application of two coherent field to the atomic transition of a Λ scheme. The theoretical description In subsequent theoretical works [3,5], developed the description in terms of the dark state configuration of the evolution of a three level atomic system. The pumping of the atoms into the uncoupled $|DS\rangle$ determine the absence of absorption, and of the consequent emission.

## 1.4 Optical Response Under EIT Conditions

The EIT process can be implemented in a number of schemes with more than two effective levels. During the years, the analysis of other three level configurations alternative to the $\Lambda$ scheme, have shown that although EIT is possible also in other atomic schemes, e.g. see Fig.1.7, the efficiency of the process of absorption suppression and resonant nonlinear enhancement that we will discuss in the next sections are smaller in the scheme designed in Fig.1.7. This is mainly due to the fact that only the $\Lambda$ configuration evolves to a dark state that has zero contribution from the excited level.

## 1.5 Linear Susceptibility and Group Velocity Slow Down

When two photon resonance conditions are fulfilled, both real and imaginary parts of the susceptibility are radically modified by the two *two possible paths absorption*. In a two level system, see Fig.1.2, the profile of the imaginary part $\chi''$, is a Lorentzian with a width depending on the spontaneous decay $\gamma_{21}$. In the three level $\Lambda$ scheme, this profile is radically modified as represented in Fig.1.5. Here the linear part of the probe susceptibility is plotted for resonant coupling field, and as a function of the probe detuning $\delta_1$. In correspondence of the two photon resonance ($\delta_1 = \delta_2 = 0$), the eigenstate of the Hamiltonian (1.31) is the $|DS\rangle$ state,i.e., the system is pumped to the dark state. No contribution from the excited level $|2\rangle$ are involved in the steady state, and no absorption take place.

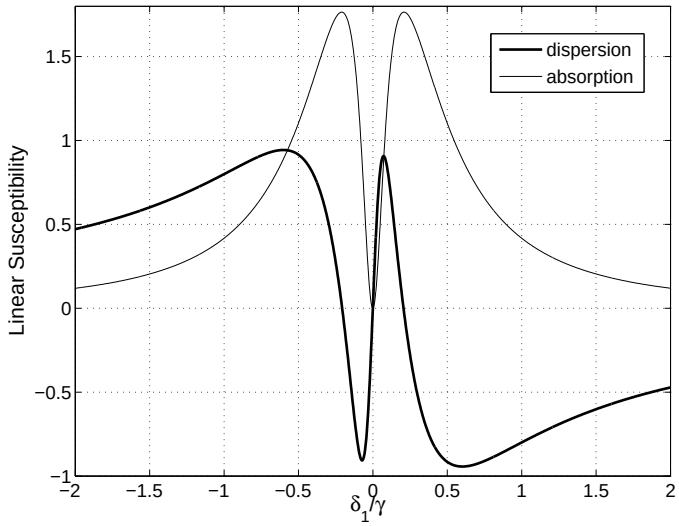


Figure 1.5: Linear susceptibility profiles of the real part of and of the imaginary part in the $\Lambda$ scheme for the probe field $\Omega_1$. At the two photon resonance conditions $\delta_1 = \delta_2$ the EIT is established and a steep variation of the dispersion properties are accompanied by the dramatic reduction in the probe field absorption.

The range of frequency for which perfect transmission is possible is named *transparency window* $\Delta\omega \propto |\Omega|^2/\Gamma_{21}$, and corresponds to the range of frequencies for which the two-photon absorption condition is fulfilled.

The fact that region of frequency exists for which we can obtain a perfect transmission of a probe pulse, is not particularly new. For example a two level system is perfectly transparent to light propagation, provided that the light pulse is sufficiently far from the resonant condition. What is new in EIT are two aspects. First of all the fact that the condition of perfect transparency is accompanied by a steep variation of the refractive index that determines the slow down of light pulse,i.e., the true novelty of the EIT process is the bandwidth at which the transparency take place.

The reduction of group velocity in EIT media can be evaluated analytically by solving the Bloch equation and obtaining analytical expression of the linear susceptibility. Let us consider a collection of $\mathcal{N}_a$ identical atoms in the $\Lambda$ configuration. We can start from the effective Hamiltonian (1.31) to evaluate the OBE following the scheme we have adopted for the two level procedure given in the previous sections,

$$\begin{aligned}
\dot{\rho}_{11} &= i\Omega_1\rho_{21} - i\Omega_1^\star\rho_{12} + \Gamma_{21}\rho_{22}, \\
\dot{\rho}_{22} &= -i\Omega_p\rho_{21} + i\Omega_p^\star\rho_{12} - i\Omega_c\rho_{23} + i\Omega_c^\star\rho_{32} - \Gamma_2\rho_{22}, \\
\dot{\rho}_{33} &= i\Omega_c\rho_{23} - i\Omega_c^\star\rho_{32} + \Gamma_{23}\rho_{22}, \\
\dot{\rho}_{12} &= -i\delta_1\rho_{12} + i\Omega_p(\rho_{22} - \rho_{11}) - i\Omega_c\rho_{13} - \frac{\Gamma_2 + \gamma_{12}}{2}\rho_{12}, \\
\dot{\rho}_{13} &= -i\delta_{12}\rho_{13} + i\Omega_p\rho_{23} - i\Omega_c^\star\rho_{12} - \frac{\gamma_{13}}{2}\rho_{13}, \\
\dot{\rho}_{23} &= i\delta_2\rho_{23} + i\Omega_p^\star\rho_{13} + i\Omega_c^\star(\rho_{33} - \rho_{22}) - \frac{\Gamma_2 + \gamma_{23}}{2}\rho_{23},
\end{aligned} \tag{1.40}$$

where the terms $\Gamma_2 = \Gamma_{21} + \Gamma_{23}$ are global decay terms from the excited level, and $\gamma_{ij}$ with $i, j = 1, 2, 3$ we mean the decay of coherence induced by random dephasing process, caused for exemple by the collision of atoms inside an atomic cloud.
We assume the the atom is initially prepared in the ground date $|1\rangle$, so that applying a strong coupling field ($\Omega_c$) the dark state will coincide with the ground state $|DS\rangle \simeq |1\rangle$. Solving this set of equation at the steady state and perturbatively developping the obtained expression at first order in the probe field Rabi frequency $\Omega_p$ we obtain the following expression for the probe susceptibility

$$\chi_P^{(1)} = \frac{|\mu_{12}|^2}{\hbar\varepsilon_0} \frac{\delta_{12} - i\gamma_{13}/2}{(\delta_1 - i\Gamma_2/2)(\delta_{12} - i\gamma_{13}/2) - |\Omega_c|^2}. \tag{1.41}$$

We see that in this expression both the real and imaginary part go to zero for two photon absorption $\delta_{12} = \delta_1 - \delta_2 = 0$ and for no spontaneous decay $\Gamma_2 = 0$. In fact without the spontaneous emission we cannot produce the interference between absorption paths explained at the beginning of the section 1.3. Eq.(1.41) is almost general, in fact it can straightforwardly generalized in the case of an EIT interaction produced in an atomic cloud with an atomic density $\mathcal{N}_a/V$ instead of a single atom, simply by multiplying the previous expression for the atomic density.

Together with the transparency, the steep variation of the real part of the linear susceptibility produces the group velocity slow down. The group velocity represent the velocity at which propagate the in-phase front of an optical pulse [7], in term of polarization, i.e., susceptibility it is defined as

$$v_g = \frac{c}{1 + n_g}, \tag{1.42}$$

where $n_g$ is the group index and is defined as

$$n_g = Re\left[\chi^{(1)}\right] + \frac{\omega_p}{2}\frac{\partial Re\left[\chi^{(1)}\right]}{\partial \omega_p}. \tag{1.43}$$

For the three level system the *group index* $n_g$ is

$$n_g = \frac{\mathcal{N}_a|\Omega_p|^2}{V|\Omega_c|^2}, \tag{1.44}$$

This expression shows how the reduction of the group velocity takes place. The group index depends upon the density of the medium and on the coupling field. Increasing the density, i.e., increasing the number of atoms or reducing the coupling field, the denominator of eq.(1.42) can be increased to be much larger than unity, giving the reduction of $v_g$.

## 1.6 Kerr Nonlinearity based on EIT.

The second typical feature of EIT is that the dramatic reduction of the group velocity is accompanied by an increase of the optical nonlinearities. In fact a profile analogous to that of the linear susceptibility can be obtained for the nonlinear one. This means that in an EIT medium together with the slow down of a light pulse, we are able to produce strong nonlinear interaction, i.e., we can *produce* efficient third order nonlinear optical (Kerr) effects. The Kerr effect is proportional to the intensity of the light beam, and for this reason the effect that is possible to appreciate after a photon has passed through a Kerr medium, is a phase accumulation proportional to the intensity of the field.
Solving the set of OBE, for $\Omega_p \ll \Omega_c$, we can see in Fig.1.6 the nonlinear susceptibility. It is evident that as soon as the system goes out of resonance from the two photon transition, the real part grows up much more rapidly then the imaginary one. This reflects in a large increase of the self-phase modulation with very small absorption. This situation is largely different from the two level system where all resonant effects are affected by the linear absorption that determines a complete lost of the pulse.

## 1.7 Amplitude Variables Method: Inclusion of loss mechanisms in the Schrödinger formalisms

In a realistic model of the atom-field interaction, together with the unitary evolution given by the Hamiltonian, we are faced with various loss mechanisms. These loss mechanisms can be seen as the results of the interaction of the quantum system with a system or *environment* that possesses many more degrees of freedom.
In our case the system is the three level atom of Fig.1.7(a), in the so-called cascade system. The ground level $|1\rangle$ is a stable or meta-stable state, so there is no radiative decay from $|1\rangle$ to other states. A probe field, with frequency $\omega_p$, is applied to the atomic transition $|1\rangle \rightarrow |2\rangle$ with a detuning $\delta_1$ from the resonance, while a coupling field, whose frequency is $\omega_c$, is applied to the $|1\rangle \rightarrow |2\rangle$ transition with the detuning $\delta_2$. The Rabi frequencies are $\Omega_1$ for the probe field and

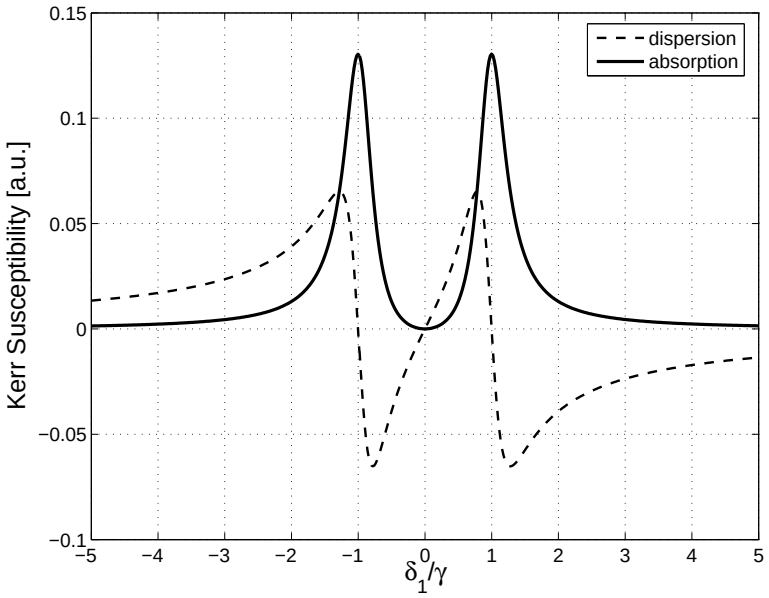


Figure 1.6: Nonlinear susceptibility in a three level $\lambda$. A small perturbation from the two photon absorption condition produces large nonlinear effects, and a large nonlinear phase accumulation

$\Omega_2$ for the coupling field. The Hamiltonian of the system

$$H_{cascade} = \sum_{i=1}^{3} \hbar\omega_i + \hbar\Big(\Omega_1 e^{\imath\omega_p t}|2\rangle\langle 1| + \Omega_1^\star e^{\imath\omega_p t}|1\rangle\langle 2|\Big) + \hbar\Big(\Omega_3 e^{\imath\omega_t t}|3\rangle\langle 2| + \Omega_3^\star e^{\imath\omega_t t}|2\rangle\langle 3|\Big). \quad (1.45)$$

With respect to the following $H_0$ we can pass to the IP

$$H_0 = \hbar\omega_p|2\rangle\langle 2| + \hbar(\omega_p + \omega_t)|3\rangle\langle 3|, \quad (1.46)$$

we arrive at the effective Hamiltonian in the time independent form

$$H_{eff}^{cascade} = \hbar\delta_1|2\rangle\langle 2| + \hbar(\delta_1 + \delta_2)|3\rangle\langle 3| + \hbar\Big(\Omega_1|2\rangle\langle 1| + \Omega_1^\star|1\rangle\langle 2|\Big) + \hbar\Big(\Omega_3|3\rangle\langle 2| + \Omega_3^\star|2\rangle\langle 3|\Big), \quad (1.47)$$

where the detunings and the energy level have been defined

$$\hbar\delta_1 = E_2 - \hbar\omega_p \quad (1.48)$$

$$\hbar\delta_3 = E_3 - E_2 - \hbar\omega_t. \quad (1.49)$$

The loss terms can be included in the Schrödinger description by a phenomenological theory. From the Schrödinger equation, and from the effective Hamiltonian of eq.(1.47), defining the quantum state of the atomic system as

$$|\psi(t)\rangle = c_1(t)|1\rangle + c_2(t)|2\rangle + c_3(t)|3\rangle$$

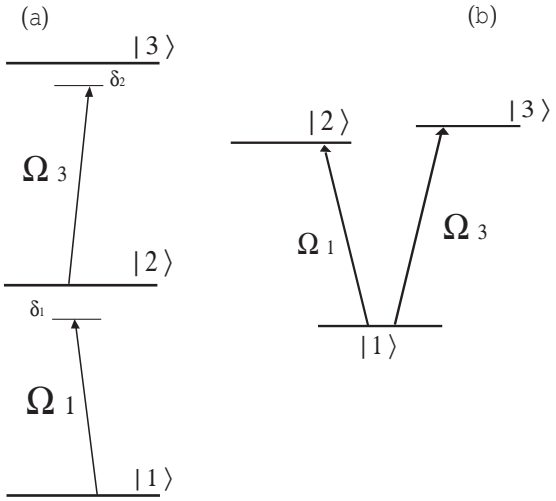


Figure 1.7: Three level schemes in two different configurations, the cascade (A), and the V (B). Both of these configuration permit to have EIT but with limited efficiency compared to the $\Lambda$ scheme.

we obtain the the time evolution of the amplitudes $c_i$ for $i = 1, 2, 3$

$$\dot{c}_1(t) = -\imath\Omega_1^\star c_2(t) \tag{1.50}$$
$$\dot{c}_2(t) = -\imath\delta_1 c_2(t) - \imath\Omega_1 c_1(t) - \imath\Omega_3^\star c_3(t) \tag{1.51}$$
$$\dot{c}_3(t) = -\imath(\delta_1 - \delta_3)c_3(t) - \imath\Omega_3 c_2(t) \tag{1.52}$$

The noise terms can be added phenomenologically by adding terms that give an exponential decay of each amplitude, so to get

$$\dot{c}_1(t) = \imath\Omega_1^\star c_2(t) - \frac{\Gamma_1}{2}c_1(t) \tag{1.53}$$
$$\dot{c}_2(t) = \imath\delta_1 c_2(t) - \frac{\Gamma_2}{2}c_2(t) + \imath\Omega_1 c_1(t) + \imath\Omega_3^\star c_3(t) \tag{1.54}$$
$$\dot{c}_3(t) = \imath(\delta_1 + \delta_3)c_3(t) - \frac{\Gamma_3}{2}c_3(t) + \imath\Omega_3 c_2(t), \tag{1.55}$$

where $\Gamma_1$ has the to be seen as a dephasing process A.1, while the two terms $\Gamma_{2,3}$ are spontaneous decay rates from level $|2\rangle$ and from level $|3\rangle$ respectively.

This equation can be easily solved, at the steady state. However, in order to acquire a real physical meaning, the equation of the AV approach has to be solved not finding the exact solution of the system at the steady state (which would be $C_j = 0 \quad \forall j$), but adjusting "by hand" the normalization condition. Usually we assume that at the steady state the population will be concentrated in one of the level involved in the dynamics. By imposing that almost the totality of the atomic population is in one of the states $|i\rangle$ for $i = 1, 2, 3$, we can obtain an approximated solution for the amplitude coefficients $c_{1,2,3}$ at the steady state, while the relation

$$\rho_{ij} = c_i^\star c_j, \tag{1.56}$$

gives the steady state values of the density matrix elements.

## 1.8 Cross-Phase Modulation

The generation of a phase accumulation on the quantum state of a field, proportional to the intensity of a second field is named Cross Phase Modulation (XPM) and is realized by the nonlinear Kerr interaction.
Let us assume that a couple of weak light pulses, i.e., ideally two single photon pulses, *probe* and *trigger*, interact simultaneously with an atomic medium, composed by $\mathcal{N}_a$ identical atoms in a suitable configuration that for the moment we do not specify for the moment. If the interaction between the two pulses is of Kerr type, the dynamics of the two pulses can be described by the following Hamiltonian

$$H_{kerr} = \hbar\chi\hat{a}_p^\dagger\hat{a}_p\hat{a}_t^\dagger\hat{a}_t, \tag{1.57}$$

where $\hat{a}_p$ and $\hat{a}_t$ are the annihilation operators of the probe and trigger field respectively.
The evolution of the field's operators $\hat{a}_{p,t}$ and $\hat{a}_{p,t}^\dagger$ is then given by

$$\hat{a}_{p,(t)}(t) = \hat{a}_{p,(t)}(0)e^{-\imath\chi\hat{a}_{t,(p)}^\dagger\hat{a}_{t,(p)}t_{int}}, \tag{1.58}$$

where $t_{int}$ represent the interaction time, $\chi$ the parameter containing the Kerr interaction. It is evident that a modulation in the amplitude of the field produces phase variation at the output. In the case of the XPM this phase accumulation is induced on the probe (trigger) by the intensity of the trigger (probe) with the consequent production of a *conditional dynamics*.

### 1.8.1 Cross Phase Modulation with cascade system

Let us now consider the XPM for a more specific atomic configuration. We have an ensemble of $N_a$ atoms in the cascade configuration interacting with two EM fields. The cascade scheme permits to induce XPM. In the cascade scheme we obtain the modification of the nonlinear interaction on the probe field ($\Omega_1$) by the presence of the trigger field ($\Omega_3$) on the transition $|2\rangle \rightarrow |3\rangle$, and vice versa.
The atomic system starts in the ground level $|1\rangle$. Solving the system (1.53) at the steady state, and developing in series of power of $\Omega_3$, which is assumed to be smaller than the detuning ad the decay rates, we obtain the following expression for the $\rho_{21} = c_2c_1^\star$ coherence

$$\chi^{(1)} = -\frac{\Omega_1}{d_{12}} - \frac{\Omega_1|\Omega_3|^2}{d_{12}^2 d_{13}}, \tag{1.59}$$

where the "complex detunings" have been introduced $d_{12} = \delta_1 - \imath\Gamma_2/2$, and $d_{13} = \delta_1 + \delta_3 - \imath\Gamma_4/2$. From eq.(1.59) we obtain the following expression for the real part of the cross-Kerr nonlinear effect

$$Re\{\chi^{(3)}\} = -\frac{N_a}{V}\frac{|\mu_{12}|^2|\mu_{23}|^2}{\hbar^3\varepsilon_0}\frac{1}{\delta_1^2\delta_{13}}, \tag{1.60}$$

If we want to increase the XPM we have to reduce the single photon detuning $\delta_1$, putting the

probe field close to resonance. But when the XPM increases, the linear absorption increases even faster, because

$$Im\{\chi^{(1)}\} = -\frac{N_a}{V}\frac{|\mu_{12}|^2}{\hbar\varepsilon_0}\frac{\Gamma_2/2}{\delta_1^2}. \tag{1.61}$$

This relation shows the intrinsic limitation of the cascade scheme for the generation of a large XPM. If we want to increase the XPM effect we have to decrease the detuning, increasing at the same time the absorption.

## 1.9 Cross Nonlinear Interaction in EIT Medium

Recently Schmidt and Imamoğlu [13] have showed how to use an EIT medium to modulate the phase of a weak field proportional to the intensity of another weak field. Schmidt and Imamoğlu based their analysis on a four-level atomic system in the N configuration (see Fig.1.9).

In this scheme we put at resonance a standard three level atomic system in the $\Lambda$ configuration,

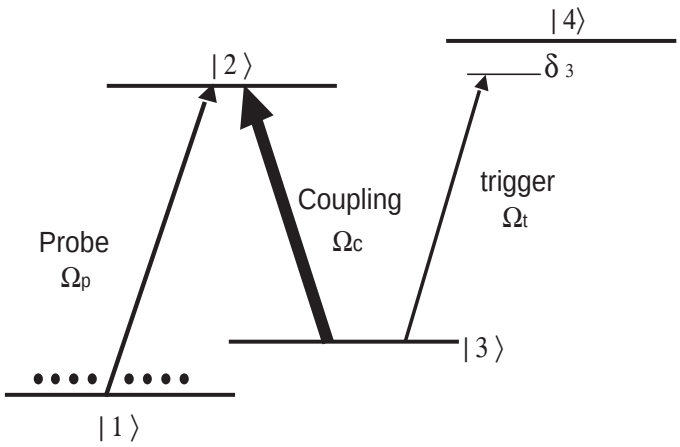


Figure 1.8: N multilevel scheme for giant cross Kerr effect between weak pulse proposed by Schmidt and Imamoğlu [13]. The atomic system is prepared on level $|1\rangle$.The presence of the trigger field $\Omega_3$ coupled to the level $|4\rangle$ induce an AC-Stark shift of level $|3\rangle$. This put out of resonance the first lambda composed by level $|1\rangle, |2\rangle, |3\rangle$ shifting the resonance condition of an amount proportional to the intensity of the trigger field.

and complete the scheme by adding a third weak field $\Omega_3$ coupled to a fourth atomic level $|4\rangle$. This field, that we shall call *trigger*, is put out of resonance with the $|3\rangle \rightarrow |4\rangle$ transition by an amount $\delta_3$, . The trigger field induces an ac-Stark shift on level $|3\rangle$ proportional to $|\Omega_3|^2/\delta_3$, perturbing in this way the EIT resonance and generating a non-linear interaction proportional to the intensity of the trigger field. If compared to previous XPM obtained from the cascade three level scheme of Fig.1.7, this EIT based set-up has a cross Kerr interaction which can be as much as 6-7 order of magnitude larger for the same field and density. This is because due to EIT, the phase accumulation is in practice loss-free, so that we can approach resonance without inducing absorption.

This result has given a great impulse in the search for the optimal conditions for an efficient XPM even at very low-light level and ideally at the single photon level.

On the other hand, we have to stress that limitations occur for the N scheme.
In fact, the weak probe field is subject to EIT, and the $\Lambda$ structure and the atomic population on level $|1\rangle$ permits to have a strong reduction of its group velocity. This does not take place for the trigger pulse, which can be considered to be involved in a V atomic configuration and it is largely detuned. Hence the trigger field does not experience a significant slowing down as the probe does, resulting in an short effective interaction time during which the weak pulse can accumulate the phase. It is evident that in order to obtain a joint and large XPM between the probe and trigger field, their group velocity has to be comparable, i.e. of the same order. If this condition is not fulfilled, instead of a XPM that increase linearly with the interaction length, we will have a saturation of the accumulated phase.

The problem of group velocity matching was first solved by Lukin and Imamoglu [77]. They propose to use a medium composed of an atomic cloud of $\mathcal{N}_a$ atoms appropriately distributed between two different isotopes of Rb, $Rb^{87}$ and $Rb^{85}$. The first kind of atoms will induce the XPM due to the four level $N$ scheme of Schmidt - Imamoğlu, while the $Rb^{85}$ atoms, that experience a standard three-level $\Lambda$ interaction between trigger and $\Omega_t$ and coupling $\Omega_c$ fields, have the role of reducing the trigger group velocity. In this way the interaction time is increased. With such a scheme, ideally it should be possible to obtain very large XPM between few photon with a simultaneous and comparable reduction of the group velocity for both the probe and the trigger fields. In fact the density of the two isotopes could be carefully balanced do to have perfect group velocity matchig.
Recently Kurizki et al. [73] have proposed a scheme based on only one atomic species involving six atomic levels, while others authors [74, 75] have studied the possibility of resonant enhancement of high order nonlinearity in chains of lambda schemes.

## 1.10 Quantum Information with EIT: Quantum Gates and Quantum Memory

EIT has attracted much attention for its potential application to high sensitivity magnetometers [19], or for four wave mixing and sum frequency generation [20–23], as well as for the design of single photon detectors and single photon devices as single photons guns [36] and quantum memories [26–30]. The XPM properties of EIT have been used to verify experimentally protocols for Quantum Non Demolition Measurement (QND) [16], and finally, all optical Quantum Phase Gate (QPG) for single photon flying qubits. In this thesis we will concentrate on the potential application of EIT in the implementation of devices for the Quantum Information where information is encoded in the quantum states of photons.

Several works [41–45], have shown how, on hypothetical Quantum computers, i.e., a computing device able to take advantage of some properties of quantum system, have the ability to solve problem exponentially faster than a classical computer. Moreover it has been shown that Quantum Mechanical properties could be usefully adopted to perform Quantum Communications that permits novel and much more secure way s of transferring information [46].
Quantum Information developed rapidly during last years. The growing in the interest in both theoretical and experimental aspects of this field, rely on the need of finding novel physical architecture for the implementation of automatized calculations [24]. Moreover the need for secure

communication against eavesdroppers attacks has attracted much interest as the increase of the request for secure communications.

In Quantum Information science the minimal amount of information that can be sent or processed is the qubit (quantum bit),i.e., the state living in a Hilbert space of dimension two, which can be written as,

$$|\psi\rangle = \alpha|1\rangle + \beta|0\rangle, \tag{1.62}$$

where $|\alpha|^2 + |\beta|^2 = 1$, and where with the logical basis $|1\rangle, |0\rangle$ we have indicated two orthogonal states of a quantum system, like for example the polarization states of a photon, or the state of an electron around the nucleus, or any other observable property of a quantum system.
The main properties that make quantum systems so attractive for quantum information, is that the qubits can occupy generic linear superpositions and not only the two states $|0\rangle$ and $|1\rangle$ as its classical counterpart. The fact that a quantum state can be in an arbitrary superposition of two or more possible states, is at the basis of the massive quantum parallelism [41, 42, 44] achievable by quantum computation. Moreover it has been shown how a number of novel possibilities in quantum communication are possible taking advantage of the entaglement properties of interacting quantum particles. Entanglement based technologies are ,e.g., Quantum Teleportation, secure Quantum Key Distribution (QKD), Quantum Cloning.

In this domain EIT has attracted much attention for its ability to permit the propagation of weak light pulses through dense media, accompanied by strong slow down group velocity and giant enhancement of Kerr nonlinearties. The group velocity reduction have been studied for the possibility of store single photon to build quantum memories, while the giant nonlinearities achievable in EIT media are interesting for the tailoring of devices able to perform conditional photon-photon operations on single flying qubit states.

A medium able to realize a significant cross-phase modulation is the key ingredient for the implementation of a quantum gate between two optical qubits. In fact such a gate implies the existence of conditional quantum dynamics, which is, in fact, realized in the cross-Kerr effect where an optical field acquires a phase shift conditioned to the state of another optical field. Using cross phase modulation one can implement a QPG, which is a device able to process, in a deterministic, and ideally reversible way, the quantum state of a qubit.

**The Conditional phase shift** Several authors [79, 80] have showed that *almost any quantum logic gate, involving two qubits, is universal*, and how these quantum gates could be implemented. The statement of the universality of a quantum gate is important because this conclusion permits to wire together copies of the same gate to compose more complex operation. It has pointed out that the conditional dynamics between qubit, could be realized whenever a nonlinear interaction between qubit, is implemented. Nonlinear XPM can then be adopted for such a scope, in particular for the implementation of the Quantum Phase Gate (QPG) universal gate.
Let us consider a two-qubit state at the input of a black box that performs a certain operation on the two input qubits. The operation that a QPG (see Fig.1.9) has to performs is a two-qubit unitary operation that induces a phase shift on the state of a qubit conditioned to the state of another qubit. In general each input state on the basis $\mathcal{B}_L = \{|00\rangle, |10\rangle, |01\rangle, |11\rangle\}$ can acquire a phase depending on its state according to

$$|i\rangle_1|j\rangle_2 \rightarrow \exp\{i\phi_{ij}\}|i\rangle_1|j\rangle_2 \quad i, j = 0, 1.$$

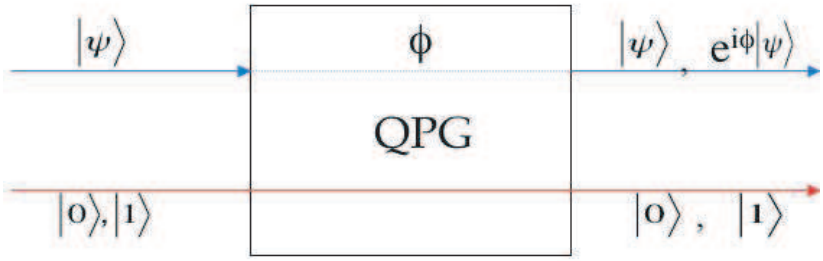


Figure 1.9: Quantum phase gate for a two qubit system. At the input we have two qubits the *target* qubit ($|\psi\rangle$), and the *control* qubit ($\alpha|0\rangle + \beta|1\rangle$). At the output, the state of the target qubit is modified depending on the state of the controller. In a QPG, the phase of $|\psi\rangle$ is changed by an amount $\phi$ *conditioned* to the quantum state of the control qubit ($|0\rangle$, or $|1\rangle$).

For example, if we adopt a pair of photons to encode information, the orthogonal quantum states could correspond to two orthogonal polarizations. In this case one can implement a universal QPG by means of a nontrivial cross-phase modulation effect between probe and trigger fields that arises for only one of the four possible input configurations of their polarization.
In matrix representation in the logical basis $\mathcal{B}_L$, the QPG is defined as

$$\mathcal{U}_{QPG} = \begin{pmatrix} e^{i\phi_{00}} & 0 & 0 & 0 \\ 0 & e^{i\phi_{10}} & 0 & 0 \\ 0 & 0 & e^{i\phi_{01}} & 0 \\ 0 & 0 & 0 & e^{i\phi_{11}} \end{pmatrix}. \tag{1.63}$$

The *Conditional Phase Shift* $\phi$ is defined as

$$\phi = \phi_{11} + \phi_{00} - \phi_{10} - \phi_{01}, \tag{1.64}$$

It represents the net effect of a nonlinear interaction that takes place between two qubits. When this quantity is non zero, $\phi \neq 0$, the quantum phase gate is an *entangling* gate, i.e. an input state of two qubits, initially in a factorized state, will evolve to an entangled one after the action of the QPG. Moreover the QPG is equivalent, up to single qubit unitary operations, to a CNOT

gate when $\phi = \pi$ [24, 79, 97]

$$\mathcal{U}_{CNOT} = \begin{pmatrix} 1 & 0 & 0 & 0 \\ 0 & 1 & 0 & 0 \\ 0 & 0 & 0 & 1 \\ 0 & 0 & 1 & 0 \end{pmatrix}. \tag{1.65}$$

Travelling optical pulses are the natural candidates for the realization of quantum communication schemes and many experimental demonstrations of quantum key distribution [47, 48] and quantum teleportation schemes [49–53] have been already performed. Optical systems have been also proposed for the implementation of quantum computing, even though the absence of significant photon-photon interactions is an obstacle for the realization of efficient two-qubit quantum gates, which are needed for implementing universal quantum computation [24].Various schemes have been proposed to circumvent this problem. Knill and co-workers have proposed to adopt linear optics for quantum computation. Recently liner optics quantum computation has demonstrated in the work of [55, 56]. Other schemes, like ours, explicitly exploit optical nonlinearities for quantum gate implementations.

The strong nonlinear properties of the EIT media have all the characteristic to permits the implementation of strong nonlinear photon-photon interaction. In fact they increase the interaction time, they induce Giant Kerr interaction, and permits perfect transparency.
The key point is to find an atom-field interaction scheme that produce large nonlinear interaction in a conditional way at single photon level and for a sufficiently long interaction time.

The first experimental realization of a conditional dynamics between photons, and the first analysis of the truth table of a QPG, has been realized by the Kimble's group [97]. The Caltech's group found a conditional phase shift $\phi \simeq 16^\circ$ between two frequency-distinct high-Q cavity modes, due to the effective cross modulation mediated by a beam of Cs atoms. However, the complete truth table of the gate has not been determined in this experiment. A conditional phase shift $\phi \simeq 8^\circ$ has been instead obtained between weak coherent pulses, using a second-order nonlinear crystal [58]. However, this experiment did not demonstrate a standard two-qubit gate. In such a gate in fact, $\phi$ depends on the input states, and the gate can be defined only for a restricted class of inputs (weak coherent states). In practice this is not a *bona fide* QPG. A $\pi$ conditional phase shift has been realized in the domain of CQED [67], where a quantum phase gate has been realized adopting a mixed atom-cavity field two-qubit system. Here we will try to do something different being our purpose to study a quantum phase gate for flying optical qubits.

In the next chapters we will show how to design several schemes able to produce strong nonlinear interaction between photons for long interaction time, by taking advantage of EIT properties.

# Chapter 2

# The *Tripod* Scheme for Giant-Kerr Interaction

*In this chapter we will analyze the nonlinear optical response of a specific four-level atomic system driven into a Tripod configuration for XPM. We will discuss the atomic structure and the population distribution to fulfill the need of large cross-Kerr nonlinearities and group velocity reduction. The Cross-Kerr interaction is calculated in the semiclassical and in quantum regime adopting the Lukin and Imamoğlu few photon approach [77]. The experimental feasibility of such a gate is here examined in detail.*

## 2.1 Non linear interaction in a Tripod System

In this chapter we propose an alternative scheme for phase gating that can greatly reduce, when compared with other schemes, the experimental effort for its realizability. The mechanism relies on an enhanced cross-phase modulation effect which occurs in a relatively simple and robust four atomic level *tripod* configuration. Our scheme only requires good control over frequencies and intensities of the laser beams. We consider a QPG for qubits in which binary information is encoded in the polarization of an optical field. The four level tripod configuration that we adopt here has been extensively studied in the past few years. For example, Unanyan *et al.* [60] used a tripod configuration to achieve stimulated Raman adiabatic passage (STIRAP) for creating an arbitrary coherent superposition of two atomic states in a controlled way. Paspalakis and et al. [61–63], in particular, developed the interesting possibility of using a tripod scheme for efficient nonlinear frequency generation. Moreover, it was shown that the group velocity of a probe pulse may be significantly reduced, as in conventional $\Lambda$ system [61]. The work of Malakyan [64] was the first to hint that the tripod scheme may be used to entangle a pair of very weak optical fields in an atomic sample. This work has been recently extended to the case of quantum probe and trigger fields in [65], where an adiabatic treatment similar to that of [77] is adopted.

The purpose of this chapter is thus twofold. *First*, we adopt a standard density matrix approach, including spontaneous emission and dephasings, to analyse the nonlinear optical response of a four-level tripod configuration. In particular, we examine the conditions under which large cross-Kerr nonlinearities may occur in a cold atomic sample. *Second*, we study the possibility of employing such an enhanced cross-phase modulation to devise a polarization phase-gating mechanism which turns out to be rather robust and apt to actual experimental investigations.

The chapter is organized as follows. In Sec. 2.2, dressed states of the atomic tripod are analyzed and their significance emphasized. In Sec. 2.3, we solve the set of Bloch equations and derive expressions for linear and nonlinear susceptibilities. In Sec. 2.4 group velocity matching is discussed in detail, while Sec. 2.5 discusses the operation of a polarization phase gate.

## 2.2 Dressed States of the Tripod System

The energy level scheme of a tripod system is given in Fig. 2.1. Transitions $|1\rangle \rightarrow |0\rangle$ and $|3\rangle \rightarrow |0\rangle$ are driven by a probe and trigger fields of respective Rabi frequencies $\Omega_P$ and $\Omega_T$, while the transition $|2\rangle \rightarrow |0\rangle$ is driven by a control (or pump) field of Rabi frequency $\Omega$. The system Hamiltonian is

$$\begin{aligned}\mathcal{H} &= \hbar\sum_{i=0}^{3}\omega_i|i\rangle\langle i| + \hbar\left(\Omega_P^{\star}e^{\imath\omega_p t}|1\rangle\langle 0| + \Omega_P e^{-\imath\omega_p t}|0\rangle\langle 1|\right) + \hbar\left(\Omega^* e^{\imath\omega t}|2\rangle\langle 0| + \Omega e^{\imath\omega t}|0\rangle\langle 2|\right) \\ &\quad +\hbar\left(\Omega_T^* e^{\imath\omega_t t}|3\rangle\langle 0| + \Omega_T e^{-\imath\omega_t t}|0\rangle\langle 3|\right). \end{aligned} \tag{2.1}$$

Defining $\delta_j = \omega_0 - \omega_j - \omega_j^{(L)}$ the laser (frequency $\omega_j^{(L)}$) detunings from the respective transitions $|j\rangle \leftrightarrow |0\rangle$, and adopting the IP with respect to the Hamiltonian

$$H_0 = \hbar\omega_0|0\rangle\langle 0| + \hbar\omega_2|2\rangle\langle 2| + \hbar\omega_3|3\rangle\langle 3|, \tag{2.2}$$

and in the dipole and rotating wave approximations, we have the following time-independent Hamiltonian

$$\begin{aligned}\mathcal{H}_{int} &= \hbar\delta_1|0\rangle\langle 0| + \hbar(\delta_1-\delta_2)|2\rangle\langle 2| + \hbar(\delta_1-\delta_3)|3\rangle\langle 3| + \hbar\left(\Omega_P^*|1\rangle\langle 0| + \Omega_P|0\rangle\langle 1|\right) + \\ &\quad +\hbar\left(\Omega^*|2\rangle\langle 0| + \Omega|0\rangle\langle 2|\right) + \hbar\left(\Omega_T^*|3\rangle\langle 0| + \Omega_T|0\rangle\langle 3|\right), \end{aligned} \tag{2.3}$$

Spontaneous emission and dephasing are included below [see Eqs. 2.6] as done in the previous chapter, by means of the Master Equation and the optical Bloch equations.

There are four eigenstates of Hamiltonian (2.3) [60]. When the three detunings are equal, $\delta_i = \delta$, $i = 1, 2, 3$, two of them are degenerate with energy equal to $\delta$ and assume the following form:

$$|e_1\rangle = \frac{\Omega_T|1\rangle - \Omega_P|3\rangle}{\sqrt{\Omega_P^2+\Omega_T^2}}, \tag{2.4a}$$

$$|e_2\rangle = \frac{\Omega_T\Omega_P|1\rangle + \Omega\Omega_P|3\rangle - \left(\Omega_P^2+\Omega_T^2\right)|2\rangle}{\sqrt{\left(\Omega_P^2+\Omega_T^2\right)\left(\Omega_P^2+\Omega^2+\Omega_T^2\right)}}. \tag{2.4b}$$

Since these states do not contain any contribution of the excited states $|0\rangle$, they belong to the class of dark states. The other two eigenstates have energies $\delta \pm \sqrt{\Omega_P^2+\Omega^2+\Omega_T^2}$ and are

$$|e_\pm\rangle = \frac{\Omega_P|1\rangle \pm |0\rangle + \Omega_T|3\rangle + \Omega|2\rangle}{\sqrt{\Omega_P^2+\Omega^2+\Omega_T^2}}. \tag{2.5}$$

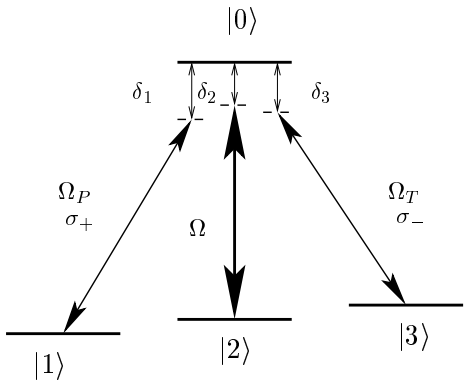


Figure 2.1: Energy level scheme for a tripod. Probe and trigger fields have Rabi frequencies $\Omega_P$ and $\Omega_T$ and polarizations $\sigma_+$ and $\sigma_-$. The pump Rabi frequency is $\Omega$ while $\delta_j = \omega_0 - \omega_j - \omega_j^{(L)}$ denote the laser (frequency $\omega_j^{(L)}$) detunings from the respective transitions $|j\rangle \leftrightarrow |0\rangle$.

In the case of different detunings, the expression of the eigenstates becomes more complicated, and the degeneracy of the two dark states is removed because their energies shift from $\delta$ to $\delta_2$ and $\delta_3$ respectively.

To achieve a giant Cross-Kerr interaction with the interaction scheme of Fig. 2.1 by EIT, we have to verify some conditions:

1. probe and trigger must be tuned to dark states,
2. the transparency frequency window for each of these dark states has to be narrow and with a steep dispersion to enable significant group velocity reduction,
3. there must be a degree of symmetry between the two transparency windows so that trigger and probe group velocities can be made to be equal [59, 66, 77].

These conditions can be satisfied by taking all three detunings nearly equal, in this way the two dark states are degenerate, and they will have an identical transparency window for both fields. However, as we seen in previous chapter, the three detunings cannot be exactly equal. In fact in such conditions the Tripod scheme is linear, i.e., the dispersive part of the nonlinear susceptibility vanishes [see Eqs. (2.11)]. Hence, the exact resonance condition will have to be violated. We will show that if the frequency mismatch is small (within the transparency window width), then strong, cross-Kerr modulation with group velocity matching can still be achieved and phase gate operation realized.

## 2.3 Bloch Equations and Susceptibilities

We will write down the OBE for the tripod system. From the eqns.(2.3,A.21) and eq.(A.22), we can calculate the Bloch equations for the density matrix elements (including atomic spontaneous

emission and dephasing) and obtain

$$\begin{aligned}
i\dot{\sigma}_{00} &= -i(\gamma_{11}+\gamma_{22}+\gamma_{33})\sigma_{00}+\Omega_P^*\sigma_{10}-\Omega_P\sigma_{01} \\
&\quad +\Omega^*\sigma_{20}-\Omega\sigma_{02}+\Omega_T^*\sigma_{30}-\Omega_T\sigma_{03}, && \text{(2.6a)}\\
i\dot{\sigma}_{11} &= i\gamma_{11}\sigma_{00}+i\gamma_{12}\sigma_{22}+i\gamma_{13}\sigma_{33}+\Omega_P\sigma_{01}-\Omega_P^*\sigma_{10}, && \text{(2.6b)}\\
i\dot{\sigma}_{22} &= i\gamma_{22}\sigma_{00}-i\gamma_{12}\sigma_{22}+i\gamma_{23}\sigma_{33}+\Omega\sigma_{02}-\Omega^*\sigma_{20}, && \text{(2.6c)}\\
i\dot{\sigma}_{33} &= i\gamma_{33}\sigma_{00}-i(\gamma_{13}+\gamma_{23})\sigma_{33}+\Omega_T\sigma_{03}-\Omega_T^*\sigma_{30}, && \text{(2.6d)}\\
i\dot{\sigma}_{10} &= -d_{10}\sigma_{10}+\Omega_P\sigma_{00}-\Omega_P\sigma_{11}-\Omega\sigma_{12}-\Omega_T\sigma_{13}, && \text{(2.6e)}\\
i\dot{\sigma}_{20} &= -d_{20}\sigma_{20}+\Omega\sigma_{00}-\Omega\sigma_{22}-\Omega_P\sigma_{21}-\Omega_T\sigma_{23}, && \text{(2.6f)}\\
i\dot{\sigma}_{30} &= -d_{30}\sigma_{30}+\Omega_T\sigma_{00}-\Omega_P\sigma_{33}-\Omega_P\sigma_{31}-\Omega\sigma_{32}, && \text{(2.6g)}\\
i\dot{\sigma}_{12} &= -d_{12}\sigma_{12}+\Omega_P\sigma_{02}-\Omega^*\sigma_{10}, && \text{(2.6h)}\\
i\dot{\sigma}_{13} &= -d_{13}\sigma_{13}+\Omega_P\sigma_{03}-\Omega_T^*\sigma_{10}, && \text{(2.6i)}\\
i\dot{\sigma}_{23} &= -d_{23}\sigma_{23}+\Omega\sigma_{03}-\Omega_T^*\sigma_{20}, && \text{(2.6j)}
\end{aligned}$$

where decay rates $\gamma_{ij}$ describe decay of populations and coherences, and we have defined complex "effective" global detunings as $d_{j0}=\delta_j+i\gamma_{j0}$ and $d_{ij}=\delta_j-\delta_i-i\gamma_{ij}$, with $i,j=1,2,3$.

We consider the steady state solutions of the Bloch equations. As we did in the previous chapter for the simpler two and three level system, we put to zero the time derivatives, and assume that the final population distribution will be symmetric with respect to the $1\leftrightarrow 3$ exchange, i.e., $\sigma_{11}\approx\sigma_{33}\approx 1/2$, with the population of the other two levels vanishing. This condition is fulfilled provided the intensity of the pump field is stronger than the intensity of both probe and trigger $|\Omega|^2\gg|\Omega_{P,T}|^2$, and the detunings and decay rates are of the same order of magnitude. This allows to decouple the equations for the populations from those of the coherences. This simplifies the problem, and permits to obtain the steady state solution for the latter, yielding the probe and trigger susceptibilities according to

$$\begin{aligned}
\chi_P &= -\lim_{t\to\infty}\frac{\mathcal{N}_a|\mu_{\mathbf{P}}|^{\mathbf{2}}}{\hbar\epsilon_0}\times\frac{\sigma_{10}(t)}{\Omega_P}, && \text{(2.7a)}\\
\chi_T &= -\lim_{t\to\infty}\frac{\mathcal{N}_a|\mu_{\mathbf{T}}|^{\mathbf{2}}}{\hbar\epsilon_0}\times\frac{\sigma_{30}(t)}{\Omega_T}, && \text{(2.7b)}
\end{aligned}$$

where $\mathcal{N}_a$ is the atomic density and $\mu_{\mathbf{P},\mathbf{T}}$ the electric dipole matrix elements for probe and trigger transitions respectively. Rabi frequencies are defined in terms of electric field amplitudes $E_{P,T}$ as $\Omega_{P,T}=-\left(\mu_{\mathbf{P},\mathbf{T}}\cdot\varepsilon_{\mathbf{P},\mathbf{T}}\right)E_{P,T}/\hbar$, with $\varepsilon_{\mathbf{P},\mathbf{T}}$ being the polarization unit vector of probe and trigger beams. The resulting general expression for the steady-state ($ss$) probe and trigger susceptibilities are

$$\begin{aligned}
\frac{(\sigma_{10})_{ss}}{\Omega_P} &= \left(1+\frac{1}{4}\frac{\left(d_{12}d_{23}/d_{13}^2\right)|\Omega_P|^2|\Omega_T|^2}{\left(d_{10}d_{12}-|\Omega|^2\right)\left(d_{30}^*d_{23}-|\Omega|^2\right)}\right)^{-1}\left\{-\frac{1}{2}\frac{d_{12}d_{13}}{d_{10}d_{12}d_{13}-d_{13}|\Omega|^2-d_{12}|\Omega_T|^2}\right. \\
&\quad \left.-\frac{1}{2}\frac{d_{12}d_{13}d_{23}|\Omega_T|^2}{d_{30}^*d_{13}d_{23}-d_{13}|\Omega|^2-d_{23}|\Omega_P|^2}\right\}, && \text{(2.8a)}\\
\frac{(\sigma_{30})_{ss}}{\Omega_T} &= \left(1+\frac{1}{4}\frac{\left(d_{23}^*d_{12}^*/d_{13}^{*2}\right)|\Omega_P|^2|\Omega_T|^2}{\left(d_{30}d_{23}^*-|\Omega|^2\right)\left(d_{10}^*d_{12}^*-|\Omega|^2\right)}\right)^{-1}\left\{-\frac{1}{2}\frac{d_{23}^*d_{13}^*}{d_{30}d_{23}^*d_{13}^*-d_{13}^*|\Omega|^2-d_{23}^*|\Omega_P|^2}\right. \\
&\quad \left.-\frac{1}{2}\frac{d_{23}^*d_{13}^*d_{12}^*|\Omega_P|^2}{d_{10}^*d_{13}^*d_{12}^*-d_{13}^*|\Omega|^2-d_{12}^*|\Omega_T|^2}\right\}. && \text{(2.8b)}
\end{aligned}$$

We are interested in the XPM between probe and trigger fields. Therefore, we keep the two lowest order contributions: linear and third-order nonlinear susceptibilities, neglecting the higher orders in the expansion. This yields

$$\chi_P = \chi_P^{(1)} + \chi_P^{(3)}|E_T|^2, \tag{2.9a}$$

$$\chi_T = \chi_T^{(1)} + \chi_T^{(3)}|E_P|^2 \tag{2.9b}$$

that is, each susceptibility has a linear and a cross–Kerr nonlinear term, while self-phase modulation terms are of higher order. Both susceptibilities have a linear contribution because of the nonzero stationary population in levels 1 and 3. Linear susceptibilities are given by

$$\chi_P^{(1)} = \frac{\mathcal{N}_a|\mu_{\mathbf{P}}|^2}{\hbar\epsilon_0} \times \frac{1}{2}\frac{d_{12}}{d_{10}d_{12} - |\Omega|^2}, \tag{2.10a}$$

$$\chi_T^{(1)} = \frac{\mathcal{N}_a|\mu_{\mathbf{T}}|^2}{\hbar\epsilon_0} \times \frac{1}{2}\frac{d_{23}^*}{d_{30}d_{23}^* - |\Omega|^2}, \tag{2.10b}$$

where the factor 1/2 in each equation comes from the symmetric steady state population distribution. The cross-Kerr susceptibilities are instead given by

$$\chi_P^{(3)} = \mathcal{N}_a \frac{|\mu_{\mathbf{P}}|^2|\mu_{\mathbf{T}}|^2}{\hbar^3\epsilon_0} \times \frac{1}{2}\frac{d_{12}/d_{13}}{d_{10}d_{12} - |\Omega|^2}\left(\frac{d_{12}}{d_{10}d_{12} - |\Omega|^2} + \frac{d_{23}}{d_{30}^*d_{23} - |\Omega|^2}\right), \tag{2.11a}$$

$$\chi_T^{(3)} = \mathcal{N}_a \frac{|\mu_{\mathbf{T}}|^2|\mu_{\mathbf{P}}|^2}{\hbar^3\epsilon_0} \times \frac{1}{2}\frac{d_{23}^*/d_{13}^*}{d_{30}d_{23}^* - |\Omega|^2}\left(\frac{d_{12}^*}{d_{10}^*d_{12}^* - |\Omega|^2} + \frac{d_{23}^*}{d_{30}d_{23}^* - |\Omega|^2}\right). \tag{2.11b}$$

Note that Eqs. (2.10) and (2.11) are completely symmetric with respect to the $1 \leftrightarrow 3$ exchange. This exchange symmetry is ensured by the complex conjugate terms in (2.10b) and it is expected because of the symmetry of the system and of the population distribution. Note also that in the absence of dephasing, the nonlinear susceptibility has a singularity at $\delta_1 = \delta_3$. The necessary regularization is provided by the nonzero dephasing term $i\gamma_{13}$.

Paspalakis and Knight [61] have recently analyzed the properties of the tripod system in a somewhat different setup. It is nevertheless instructive to compare the results of this Section with theirs. In the scheme of [61], population is assumed to be initially in the ground state $|1\rangle$. Provided that $|\Omega_P|^2 \ll |\Omega|^2$, $|\Omega_T|^2$ population remains in $|1\rangle$ in the steady state. Paspalakis and Knight calculate the expression for probe susceptibility to the first order in $\Omega_P$. It is easy to see that their expression is consistent (up to a factor 1/2 determined by the different population distribution) to our result in Eq. (2.8a): considering only terms to the first order in $\Omega_P$ leaves only the first term in the curly brackets of (2.8a). Additional terms in Eqs. (2.8) arise because we are looking for a cross-Kerr nonlinearity in both probe and trigger, so that all the terms of third order have to be included.

## 2.4 Group Velocity Matching

The linear and nonlinear susceptibilities of Eqs. (2.10) and (2.11) have all the properties required for a large cross-phase modulation. In fact, our tripod system can be seen as formed by two adjacent $\Lambda$ systems, one involving the probe field and one involving the trigger field, sharing the same control field. Therefore both fields exhibit EIT, which here manifests itself through the presence of two generally distinct transparency windows, corresponding to the two dark states of Eq. (2.4). Perfect simultaneous EIT for both fields takes place when the two transparency windows coincide, i.e., when the two dark states are degenerate, which is achieved when the three detunings $\delta_i$ are all equal. In this case all physical effects related to standard EIT are present and in particular the steep dispersion responsible for the reduction of the group velocity which is at the basis of the giant cross-Kerr nonlinearity (see Fig. 2.2). The condition of equal detunings (exact double EIT-resonance condition) is important also for another reason. In fact, together with the symmetry of Eqs. (2.10) and (2.11) with respect to the $1 \leftrightarrow 3$ exchange, it also guarantees identical dispersive properties for probe and trigger and therefore the same group velocity. As first underlined by Lukin and Imamoğlu [77], group velocity matching is another fundamental condition for achieving a large nonlinear mutual phase shift because only in this way the two optical pulses interact in a transparent nonlinear medium for a sufficiently long time.

The group velocity of a light pulse is given in general by eq.(1.42), where $c$ is the speed of light in vacuum and $n_g$, is given by equation (1.43)

$$n_g = \frac{1}{2}\mathrm{Re}[\chi] + \frac{\omega_0}{2}\left(\frac{\partial \mathrm{Re}[\chi]}{\partial \omega}\right)_{\omega_0}$$

is the group index, $\omega_0$ being the laser frequency. In the tripod configuration the group index of previous equation and of eq. (1.43) is essentially determined by the linear susceptibility $\chi^{(1)}$, because contributions from the nonlinear terms are orders of magnitude smaller and can be neglected. Using Eqs. (2.10), it is possible to get a simple expression for the two group velocities in the case of equal detunings. This condition corresponds to the center of the transparency window for each field, where $\mathrm{Re}[\chi^{(1)}]$ vanishes, and the group velocity is reduced due to a large dispersion gradient. One has

$$(v_g)_P \approx \frac{4\hbar c\epsilon_0}{\omega_P \mathcal{N}_a |\mu_{\mathbf{P}}|^{\mathbf{2}}} \left(|\Omega|^2 + |\Omega_T|^2\right), \tag{2.12a}$$

$$(v_g)_T \approx \frac{4\hbar c\epsilon_0}{\omega_T \mathcal{N}_a |\mu_{\mathbf{T}}|^{\mathbf{2}}} \left(|\Omega_P|^2 + |\Omega|^2\right), \tag{2.12b}$$

so that, as expected from the $1 \leftrightarrow 3$ symmetry, group velocity matching is achieved for $|\Omega_P| = |\Omega_T|$.

In the previous expression for the group velocity the nonlinear contribution are different from zero. The presence of the cross-Kerr for both the weak fields, gives a group velocity that depends upon the non-linear interaction. This fact can give bad propagation dynamics of the light pulse. The presence of nonlinear dynamics determines the splitting of the original pulse in several components, each with a different amplitude and propagating with its own group velocity. The consequent destruction of the group velocity matching condition is straightforward. Our tripod-scheme set-up is not affected by such a problem, because choosing probe and trigger field much weaker than the coupling field ($\Omega_{P,T} \ll \Omega$). The group index is dominated by the coupling field and there is no appreciable nonlinear effect on the propagation dynamics.

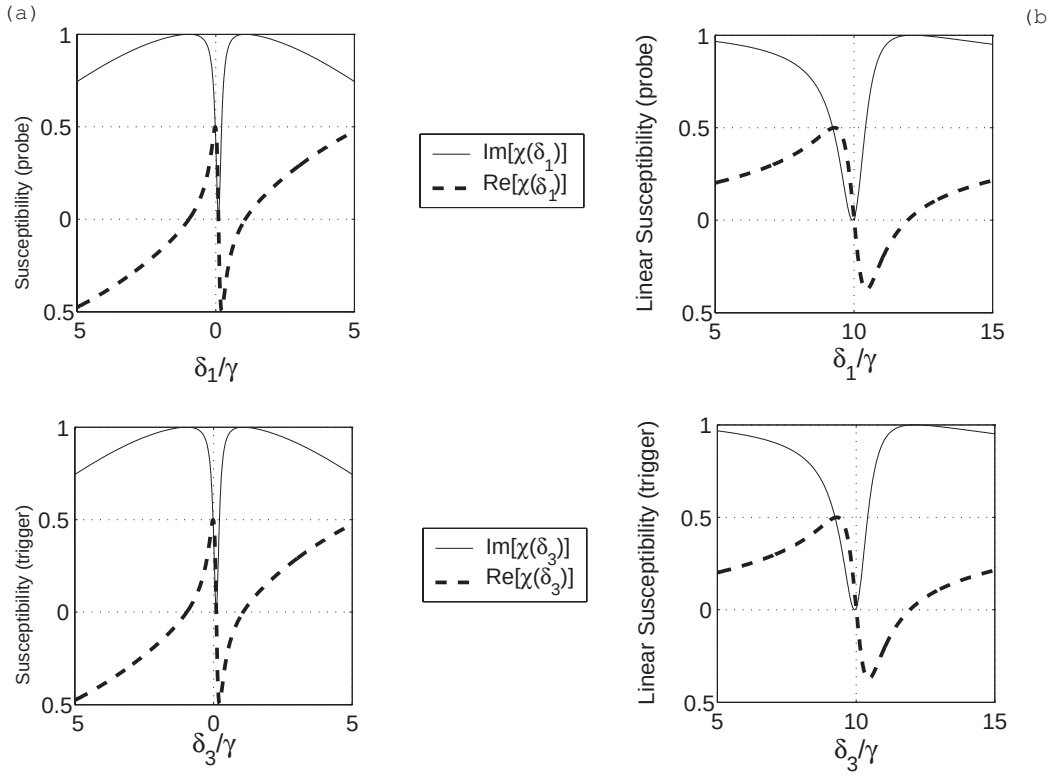


Figure 2.2: Plots (a) represent absorption and dispersion for probe and trigger, plotted versus their respective frequencies (in arbitrary units). Parameters are: $\Omega_P = \Omega_T = 0.1\gamma$, $\Omega = \gamma$, $\delta_2 = 0.1\gamma$. For probe plot $\delta_3 = 0.1\gamma$, and for trigger plot $\delta_1 = 0.1\gamma$. Plots (b) shows absorption and dispersion for probe and trigger, plotted versus their respective frequencies (in arbitrary units), for the set of parameters that permits to have the symmetric group velocity slow down and the symmetric cross kerr interaction on the two weak fields (see eq.(A.14)). Parameters are: $\Omega_P = \Omega_T = \gamma$, $\Omega = 4.5\gamma$, $\delta_2 = 10\gamma$. For probe plot $\delta_3 = 10.02\gamma$, and for trigger plot $\delta_1 = 10.01\gamma$.

Unfortunately, it is possible to check from Eqs. (2.11) that when $\delta_i = \delta$, $\forall i$ exactly, the system becomes linear, i.e., the real part of the nonlinear susceptibilities vanish and there is no cross-phase modulation. This means that we have to "disturb" the exact EIT resonance conditions, by taking slightly different detunings. This is a general conclusion, valid for any atomic level scheme resembling multiple $\Lambda$ systems [59, 74, 75]. If the double EIT-resonance condition is disturbed by a small amount, one remains within the common transparency window and the absorption is still negligible. Moreover, the two group velocities can be matched also in the non-resonant case. In fact, from the symmetry of Eqs. (2.10), one has that the gradients - and hence the group velocities - can be kept symmetric and all the conclusions for the exact resonance remain valid in the vicinity of resonance as well.

## 2.5 Phase Gate Operation in the Tripod System

Experimentally during last years there have been a lot of work on the EIT realization on Rb atoms. The typically adopted transition lines are the $D_1$ and $D_2$. In the case of the tripod a possible experimental configuration employing the giant Kerr nonlinear phase shift achievable in the tripod scheme discussed above is provided by a $^{87}$Rb cell in a magnetic field, in which states are in the $D_1$ line, and more precisely $|1\rangle$, $|2\rangle$ and $|3\rangle$ correspond to the ground state Zeeman sublevels $|5S_{1/2}, F = 1, m = \{-1, 0, 1\}\rangle$, and state $|0\rangle$ corresponds to the excited state $|5P_{3/2}, F = 0\rangle$. One realizes the tripod scheme of Fig. 1 (and therefore a significant nonlinear phase shift) only when the probe has $\sigma_+$ polarization and the trigger has $\sigma_-$ polarization. When either the probe or the trigger polarizations (or both) are changed, the phase shifts acquired by the two pulses do not involve the nonlinear susceptibilities and are different, so that the resulting conditional phase shift is nonzero. In fact, when they have the "wrong" polarization (probe $\sigma^-$ polarized or trigger $\sigma^+$ polarized) there is no sufficiently close level which the atoms can be driven to and the fields acquire the trivial vacuum phase shift $\phi_0^j = k_j l$, $j = P, T$, where $l$ in the length of the gas cell. Instead, when only one of them has the right polarization, it acquires a linear phase shift $\phi_{lin}^j$, $j = P, T$, where

$$\phi_{lin}^j = k_j l \left(1 + 2\pi\chi_j^{(1)}\right). \tag{2.13}$$

Denoting with $\phi_{nlin}^{P,T}$ the corresponding probe and trigger nonlinear phase shift when the tripod configuration is realized, we can write the following truth table for the polarization QPG

$$|\sigma^-\rangle_P|\sigma^-\rangle_T \rightarrow e^{-i(\phi_0^P+\phi_{lin}^T)}|\sigma^-\rangle_P|\sigma^-\rangle_T, \tag{2.14a}$$
$$|\sigma^-\rangle_P|\sigma^+\rangle_T \rightarrow e^{-i(\phi_0^P+\phi_0^T)}|\sigma^-\rangle_P|\sigma^+\rangle_T, \tag{2.14b}$$
$$|\sigma^+\rangle_P|\sigma^+\rangle_T \rightarrow e^{-i(\phi_{lin}^P+\phi_0^T)}|\sigma^+\rangle_P|\sigma^+\rangle_T, \tag{2.14c}$$
$$|\sigma^+\rangle_P|\sigma^-\rangle_T \rightarrow e^{-i(\phi_+^P+\phi_-^T)}|\sigma^+\rangle_P|\sigma^-\rangle_T, \tag{2.14d}$$

with the conditional phase shift being

$$\phi = \phi_+^P + \phi_-^T - \phi_{lin}^P - \phi_{lin}^T, \tag{2.15}$$

with $\phi_+^P = \phi_{lin}^P + \phi_{nlin}^P$ and $\phi_-^T = \phi_{lin}^T + \phi_{nlin}^T$.

For a Gaussian trigger pulse of time duration $\tau_T$, whose peak Rabi frequency is $\Omega_T$, moving with group velocity $v_g^T$ through the atomic sample, the nonlinear probe phase shift can be written as

$$\phi_{nlin}^P = k_P l \frac{\pi^{3/2}\hbar^2|\Omega_T|^2}{4|\mu_{\mathbf{T}}|^{\mathbf{2}}} \frac{\mathrm{erf}[\zeta_\mathrm{P}]}{\zeta_P} \mathrm{Re}[\chi_P^{(3)}], \tag{2.16a}$$

where $\zeta_P = (1 - v_g^P/v_g^T)\sqrt{2}l/v_g^P\tau_T$. The trigger phase shift is simply obtained by changing $P \leftrightarrow T$ in the equation above

$$\phi_{nlin}^T = k_T l \frac{\pi^{3/2}\hbar^2|\Omega_P|^2}{4|\mu_{\mathbf{P}}|^{\mathbf{2}}} \frac{\mathrm{erf}[\zeta_\mathrm{T}]}{\zeta_T} \mathrm{Re}[\chi_T^{(3)}], \tag{2.16b}$$

with the same appropriate changes in the definition of $\zeta_T$.

In the $^{87}$Rb level configuration chosen above, the decay rates are equal $\gamma_{j0} = \gamma$, and we choose equal dephasing rates $\gamma_{ij} = \gamma_d$ for simplicity. For $\Omega_P \approx \Omega_T = \gamma$, $\Omega = 4.5\gamma$, and detunings $\delta_1 = 10.01\gamma$, $\delta_2 = 10\gamma$, $\delta_3 = 10.02\gamma$, by assuming a low dephasing rate $\gamma_d = 10^{-2}\gamma$, we obtain a conditional phase shift of $\pi$ radians, in a gas cell of length $l = 0.7$ cm, density $\mathcal{N}_a = 3 \times 10^{12}$ cm$^{-3}$. With these parameters, group velocities are virtually the same, giving $\mathrm{erf}[\zeta_\mathrm{P}]/\zeta_\mathrm{P} = \mathrm{erf}[\zeta_\mathrm{T}]/\zeta_\mathrm{T} \approx 2/\sqrt{\pi}$. Probe and trigger susceptibilities corresponding to these parameter values are shown in Fig. 2.2(b). Note that the absorption vanishes over a wide range of frequencies due to the large size of atomic detunings. The values of the Rabi frequencies correspond to classical probe and trigger fields. The above parameter choice shows that a demonstration of a deterministic polarization QPG can be made using present technologies.

As discussed above, we had to move from the exact double EIT-resonance condition in order to have a nonzero nonlinearity and in such a condition the linear susceptibilities do not vanish. Actually, the linear contribution is predominant. In fact, the ratios of nonlinear to linear phase shifts are given by

$$\frac{\phi_P^{nlin}}{\phi_P^{lin}} = \frac{|\Omega_T|^2}{4}\mathrm{Re}\left[\frac{1}{d_{13}}\left(\frac{d_{12}}{d_{10}d_{12} - |\Omega|^2} + \frac{d_{23}}{d_{30}^* d_{23} - |\Omega|^2}\right)\right], \tag{2.17a}$$

$$\frac{\phi_T^{nlin}}{\phi_T^{lin}} = \frac{|\Omega_P|^2}{4}\mathrm{Re}\left[\frac{1}{d_{13}^*}\left(\frac{d_{12}}{d_{10}^* d_{12}^* - |\Omega|^2} + \frac{d_{23}^*}{d_{30}^* d_{23}^* - |\Omega|^2}\right)\right], \tag{2.17b}$$

and for the above choice of parameters, they are of order $\sim 1/64$. This means that under the optimal conditions corresponding to a $\pi$ conditional phase shift, the total phase shift in each input–output transformation is very large, of the order of $65\pi$. The experimental demonstration of the QPG requires the measurement of the conditional phase shift, i.e., of a phase difference and therefore it is important to keep the errors in the phase measurements small. These errors are mainly due to the fluctuations of the laser intensities and of the detunings. In particular, intensity fluctuations of 1% yield an error of about 4% in the phase measurement. It is more important to minimize the effects of relative detuning fluctuations but this can be achieved by taking all lasers tightly phase locked to each other.

Another important limitation is that due to dephasing of the ground state coherences, whose main effect is to increase absorption. Absorption is a crucial issue in the case of single photon polarization qubits. In fact a non negligible absorption implies a nonzero gate failure probability (one or both qubits missing at the output), making therefore the present QPG, which is deterministic in principle, a probabilistic gate. In our scheme, it can be checked that, if the dephasings do not become very large, i.e., $\gamma_d = 2\pi \times 10$ kHz, or $\gamma_d \sim 10^{-2}\gamma$, this increase of absorption is negligible, as shown in Fig. 2.3.

It should be mentioned that the conclusion above holds for strong control field strengths of order $\Omega \sim \gamma$. If a weaker control is used, the dephasing must also be lower in order to keep absorption negligible.

## 2.6 Quantized probe and trigger fields

We now consider the case when probe and trigger fields are quantized [72]. Pump field is still considered much stronger than the probe and the trigger and therefore its quantum fluctuations are neglected and is thus kept classical. We adopt the formalism developed by Lukin and Imamoğlu [77] and Fleischhauer and Lukin [68] and apply it to the atoms in tripod configuration. A similar approach has been followed in the recent work of Petrosyan and Malakyan [65].

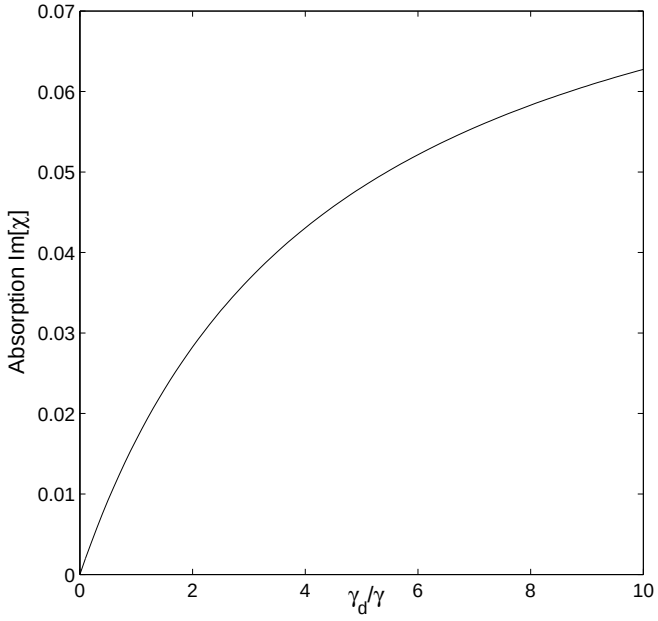


Figure 2.3: Probe absorption (scaled) at the center of probe transparency window, plotted against the dephasing rate, for $\Omega_P = \Omega_T = \gamma$, $\Omega = 4.5\gamma$, $\delta_j = 0$.

The interaction Hamiltonian is

$$\begin{aligned} H_{int} &= -\int \frac{dz}{L} N[\hbar\delta_1\sigma_{00} + \hbar(\delta_1 - \delta_2)\sigma_{22} + \hbar(\delta_1 - \delta_3)\sigma_{33}] \\ &\quad +\hbar g_P(\hat{E}_P\sigma_{01} + \hat{E}_P^\dagger\sigma_{10}) + \hbar g_T\left(\hat{E}_T\sigma_{03} + \hat{E}_T^\dagger\sigma_{30}\right) + \hbar\Omega(\sigma_{02} + \sigma_{20})], \end{aligned} \quad (2.18)$$

where $L$ is the interaction length along the propagation axis $z$, $g_{P,T}$ denotes coupling strengths of probe and trigger fields $\hat{E}_{P,T}$ to the respective atomic transitions, and $\sigma_{ij} = \frac{1}{N}\sum_k \sigma_{ij}^{(k)}$ are the collective operators for the atomic populations and transitions for $N$ atoms in a medium.

The equations for probe and trigger pulses propagating along $z-$axis through the tripod-media are given by

$$\left(\frac{\partial}{\partial t} + c\frac{\partial}{\partial z}\right)\hat{E}_P(z,t) = -ig_P N\sigma_{10}, \quad (2.19a)$$

$$\left(\frac{\partial}{\partial t} + c\frac{\partial}{\partial z}\right)\hat{E}_T(z,t) = -ig_T N\sigma_{30}, \quad (2.19b)$$

while the equations for the atomic coherences operators

$$\dot{\sigma}_{10} = -id_{10}\sigma_{10} - ig_P\hat{E}_P(\sigma_{11}-\sigma_{00}) - ig_T\hat{E}_T\sigma_{13} - i\Omega\sigma_{12}, \tag{2.19c}$$
$$\dot{\sigma}_{20} = -id_{20}\sigma_{20} - ig_P\hat{E}_P\sigma_{21} - ig_T\hat{E}_T\sigma_{23} - i\Omega(\sigma_{22}-\sigma_{00}), \tag{2.19d}$$
$$\dot{\sigma}_{30} = -id_{30}\sigma_{30} - ig_P\hat{E}_P\sigma_{31} - ig_T\hat{E}_T(\sigma_{33}-\sigma_{00}) - i\Omega\sigma_{32}, \tag{2.19e}$$
$$\dot{\sigma}_{12} = -id_{12}\sigma_{12} + ig_P\hat{E}_P\sigma_{02} - i\Omega\sigma_{10}, \tag{2.19f}$$
$$\dot{\sigma}_{13} = -id_{13}\sigma_{13} + ig_P\hat{E}_P\sigma_{03} - i\hat{E}_T^{\dagger}\sigma_{10}, \tag{2.19g}$$
$$\dot{\sigma}_{23} = -id_{23}\sigma_{23} - ig_T\hat{E}_T^{\dagger}\sigma_{20} + i\Omega\sigma_{03}, \tag{2.19h}$$

where the generalized detunings $d_{ij}$ for $i,j = 0,\ldots,3$ have been previously defined.

We proceed by assuming low intensity for probe and trigger fields, $g_j\langle\hat{E}_j\rangle \ll \Omega$ and strong pump $|\Omega|^2/\gamma_{0j}\gamma_{ij} \gg 1$. The latter condition also implies that the EIT resonances for both, probe and trigger fields are strongly saturated. Furthermore, if $g_P \sim g_T$, for a probe and trigger fields of equal mean amplitudes $\langle\hat{E}_j\rangle$, we can assume $\langle\sigma_{00}\rangle \approx \langle\sigma_{22}\rangle \approx 0$ and $\langle\sigma_{11}\rangle \approx \langle\sigma_{33}\rangle \approx \frac{1}{2}$, as in the semiclassical case. Solving the equations (2.19c) for weak probe and trigger field, we can write $\sigma_{10}$ in function of $\sigma_{12}$, and in the same way, the $\sigma_{30}$ in function of $\sigma_{32}$. This gives the following equations for the pulse propagation,

$$\sigma_{10} = -\Big(\frac{\partial}{\partial t} + \imath d_{12}\Big)\frac{\sigma_{12}}{\Omega} \tag{2.20}$$
$$\sigma_{10} = -\Big(\frac{\partial}{\partial t} - \imath d_{23}\Big)\frac{\sigma_{32}}{\Omega}. \tag{2.21}$$

This equations permits to obtain the following relations

$$\left(\frac{\partial}{\partial t} + c\frac{\partial}{\partial z}\right)\hat{E}_P(z,t) \cong \frac{g_P N}{\Omega}\left(\frac{\partial}{\partial t} + id_{12}\right)\sigma_{12}, \tag{2.22a}$$
$$\left(\frac{\partial}{\partial t} + c\frac{\partial}{\partial z}\right)\hat{E}_T(z,t) \cong \frac{g_T N}{\Omega}\left(\frac{\partial}{\partial t} - id_{23}\right)\sigma_{32}. \tag{2.22b}$$

The symmetry of these equations with respect to the exchange of the probe and trigger, with respect to the related density matrix elements, shows full symmetry between the probe and the trigger dynamics. Note also that the symmetry is intimately linked to the atomic population being equally distributed between $|1\rangle$ and $|3\rangle$ atomic states.

If, furthermore, a slow change in the pump - or a constant, coherent - $\Omega$ is assumed, we can perform an adiabatic elimination of the atomic variables. From the equation for $\dot{\sigma}_{12}$ and $\dot{\sigma}_{32}$ we have

$$\sigma_{10} = \frac{\imath}{\Omega}\Big(\frac{\partial}{\partial t} + \imath d_{12}\Big)\sigma_{12} + \frac{g_P}{\Omega}\hat{E}_P\sigma_{02} \tag{2.23}$$
$$\sigma_{30} = \frac{\imath}{\Omega}\Big(\frac{\partial}{\partial t} - \imath d_{23}\Big)\sigma_{32} + \frac{g_T}{\Omega}\hat{E}_T\sigma_{02}. \tag{2.24}$$

From eq.(2.19c) we have

$$\Big(\frac{\partial}{\partial t} + \imath d_{10}\Big)\sigma_{10} + \imath\frac{g_P}{2}\hat{E}_P + \imath g_T\hat{E}_T\sigma_{13} = -\imath\Omega\sigma_{12}, \tag{2.25}$$

and from here we can obtain an expression for the $\sigma_{12}$ as a function of eq.(2.23)

$$\begin{aligned}\sigma_{12} &= \frac{\imath}{\Omega}\Big(\frac{\partial}{\partial t}+\imath d_{10}\Big)\frac{\imath}{\Omega}\Big(\frac{\partial}{\partial t}+\imath d_{12}\Big)\sigma_{12}+\frac{g_P}{\Omega^2}\Big(\frac{\partial}{\partial t}+\imath d_{12}\Big)\hat{E}_P\sigma_{02}\\ &\quad -\frac{g}{2\Omega}\hat{E}_P-\frac{g}{\Omega}\hat{E}_T\sigma_{13}.\end{aligned} \tag{2.26}$$

This equation will give us an approximate expression of the $\sigma_{12}$ coherence, where the small terms proportional to the product between the weak probe field $g_P\hat{E}_P$ terms and the small coherence $\sigma_{02}$ have been dropped out,

$$\sigma_{12}\simeq\frac{1}{2|\Omega|^2}\frac{g_P d_{10}}{d_{10}d_{12}-|\Omega|^2}\frac{\partial}{\partial t}\hat{E}_P+\frac{1}{2}\frac{g_P\Omega}{d_{10}d_{12}-|\Omega|^2}\hat{E}_T\sigma_{13}. \tag{2.27}$$

Now we have to eliminate the dependency on $\sigma_{13}$ in the previous expression. From eqns.(2.19c) at the steady state we have

$$\begin{aligned}\sigma_{13} &= \frac{g_p}{d_{13}}\hat{E}_P\sigma_{03}-\frac{g_T}{d_{13}}\hat{E}_T\sigma_{10},\\ &\quad -\frac{g_P g_T}{2d_{13}}\Big(\frac{d_{23}}{d_{30}d_{23}-|\Omega|^2}+\frac{d_{12}}{d_{10}d_{12}-|\Omega|^2}\Big)\hat{E}_T^\dagger\hat{E}_P=\sigma_{31}^\dagger.\end{aligned} \tag{2.28}$$

Adopting the same steps to the trigger field $g_T\hat{E}_T$ we can evaluate the atomic coherence and perform the adiabatic elimination also for the trigger field. Inserting the previous relations in the eq.(2.22a) we arrive at the following expression:

$$\left(\frac{\partial}{\partial z}+\frac{1}{v_g^{(P)}}\frac{\partial}{\partial t}\right)\hat{E}_P = -\kappa_P\hat{E}_P+\beta_P\frac{\partial^2}{\partial t^2}\hat{E}_P+i\eta_P\hat{E}_T^\dagger\hat{E}_T\hat{E}_P, \tag{2.29a}$$

$$\left(\frac{\partial}{\partial z}+\frac{1}{v_g^{(T)}}\frac{\partial}{\partial t}\right)\hat{E}_T = -\kappa_T\hat{E}_T+\beta_T\frac{\partial^2}{\partial t^2}\hat{E}_T+i\eta_T\hat{E}_T\hat{E}_P^\dagger\hat{E}_P, \tag{2.29b}$$

where group velocities of probe and trigger pulses, $v_g^{(P)}, v_g^{(T)}$ are given by the usual definition (see eq.(1.43)) in terms of the respective group indices $n_g^{(i)}$

$$n_g^{(P)} = \frac{1}{2}\frac{g_P^2 N}{d_{10}d_{12}-|\Omega|^2}, \tag{2.30a}$$

$$n_g^{(T)} = \frac{1}{2}\frac{g_T^2 N}{d_{30}d_{23}^*-|\Omega|^2}, \tag{2.30b}$$

These expressions are consistent with the semiclassical case for the case of equal couplings $g_j$, equal detunings and low intensity probe and trigger. The low intensity condition $g_j\langle\hat{E}_j\rangle\ll\Omega$ has its semiclassical analogue in $|\Omega_{P,T}|\ll|\Omega|$.

The terms $-\kappa_P E_P$ and $-\kappa_T E_T$ describe single-photon loss due to dephasing and the corresponding rates are

$$\kappa_P = i\frac{d_{12}n_g^{(P)}}{c}, \tag{2.30c}$$

$$\kappa_T = i\frac{d_{23}^*n_g^{(T)}}{c}. \tag{2.30d}$$

The last terms in eqs.(2.29) are associated with the cross-Kerr interaction between the two pulses, and their coupling coefficients are given by

$$\eta_P = \frac{lg_P^2 g_T^2 N}{2\pi c^2} \times \frac{1}{2}\frac{d_{12}/d_{13}}{d_{10}d_{12}-|\Omega|^2} \times \left(\frac{d_{12}}{d_{10}d_{12}-|\Omega|^2} + \frac{d_{23}}{d_{30}^* d_{23}-|\Omega|^2}\right), \tag{2.30e}$$

$$\eta_T = \frac{lg_P^2 g_T^2 N}{2\pi c^2} \times \frac{1}{2}\frac{d_{23}^*/d_{13}^*}{d_{30}d_{23}^*-|\Omega|^2} \times \left(\frac{d_{12}^*}{d_{10}^* d_{12}^*-|\Omega|^2} + \frac{d_{23}^*}{d_{30}d_{23}^*-|\Omega|^2}\right). \tag{2.30f}$$

Finally the second order derivative terms describe the dispersion of the pulses, with coefficients

$$\beta_P = \frac{d_{10}^* n_g^{(P)}}{c|\Omega|^2}, \tag{2.30g}$$

$$\beta_T = \frac{d_{30} n_g^{(T)}}{c|\Omega|^2}. \tag{2.30h}$$

The transparency window widths are

$$d\omega_{tr}^{(P,T)} = \sqrt{\frac{c}{\gamma l}\frac{|\Omega|^2}{n_g^{(P,T)}}}, \tag{2.31}$$

where we assumed $\gamma_{j0} = \gamma$. In general case, $\gamma \to \gamma_{10}$ for probe and $\gamma \to \gamma_{30}$ for trigger.

When single photon loss $\kappa_{P,T}$ and wave dispersion $\beta_{P,T}$ are negligible, the solution of these coupled equations can be written as

$$\hat{E}_P(z,t) = \hat{E}_P(t') \exp\left[i\eta_P \hat{E}_T^\dagger(t')\hat{E}_T(t')\right], \tag{2.32a}$$

$$\hat{E}_T(z,t) = \hat{E}_T(t') \exp\left[i\eta_T \hat{E}_P^\dagger(t')\hat{E}_P(t')\right], \tag{2.32b}$$

where we adopted a reference moving at the group velocity $v_g$, i.e. the new time is defined as $t' = t - z/v_g$. Following the approach of Lukin and Imamoğlu [77], we conclude that for an initial multimode coherent states $|\alpha_P, \alpha_T\rangle$ (see Appendix C), the probe and trigger fields after propagation through the medium of length $l$ become

$$\langle \hat{E}_P(z,t)\rangle = \alpha_P(t') \times \exp\left\{\left[-2\sin^2(\Phi_P/2) + i\sin\Phi_P\right]\frac{|\alpha_T(t')|^2}{d\omega}\right\}, \tag{2.33a}$$

$$\langle \hat{E}_T(z,t)\rangle = \alpha_T(t') \times \exp\left\{\left[-2\sin^2(\Phi_T/2) + i\sin\Phi_T\right]\frac{|\alpha_P(t')|^2}{d\omega}\right\}. \tag{2.33b}$$

where $\Phi_{P,T} = \left(\frac{c\eta_{P,T}}{l}\right) l\Delta\omega = c\eta_{P,T}\Delta\omega$ ($\Delta\omega$ being pulse spread) is the quantum phase shift obtained due to the nonlinear interaction between probe and trigger.

It can be shown further that a pair of single photon wave packets, one being probe and the other trigger, acquire respective phase shifts $\Phi_{P,T}$ as a result of the nonlinear interaction. This is a general property of a solutions for field operators given by Eqs. (2.32), and has been proven by Lukin and Imamoğlu [77]. As shown by Petrosyan and Malakyan [65], these large nonlinear phase shifts can be used to create quantum entanglement.

However, we have to stress that the validity of the previous *quantum description* of the tripod system, is limited by the validity of the adiabatic elimination, and within the approximation

that the probe and trigger quantum fields are well described by weak coherent states. Therefore, even though quantum, this treatment is not fully satisfactory.
In chapter four we will develop an analytical and numerical approach to treat the multilevel system dynamics in the full quantum limit, without any adiabatic elimination of the atomic dynamics.

# Chapter 3

# Five level M scheme for Giant Kerr interaction: Semiclassical treatment

*In this section we take into account the five level* M*-scheme configuration. Like n the previous chapter, the aim is to give an analytical description of the system, and to find the optimal conditions to obtain a giant Cross-Kerr interaction between optical pulses. Moreover we perform a detailed study of the group velocity of the involved fields. We find the conditions under which it is possible to match the group velocities, and we give an estimate of the possible use of such a scheme for a QPG implementation. The analysis we have performed is at a semiclassical level, adopting an AV and an OBE description.*

## 3.1 Atom-field interaction

In a standard three-level cascade scheme, shown in Fig. 1.7a, nonlinear effects are obtained alongside absorption, which increase as the fields are tuned closer to the atomic transition [13]. To reduce the absorption to an acceptable level, light fields need to be strongly detuned from the intermediate atomic level $|2\rangle$, simultaneously reducing however the size of the nonlinearity, since both are inversely proportional to the square of the detuning.
The double $\Lambda$ nature of a five level $M$ configuration offers the opportunity to have a strong and stable EIT process that reflects in cross Kerr interaction and a simultaneous group velocity reduction for pulses propagating inside the atomic sample.

In this chapter we perform a semiclassical analysis of the interaction of light with atoms in the $M$ configuration, in which the amplitude of the four fields involved is described in terms of the corresponding Rabi frequency. The aim is to estimate the effects of noise sources, such as

dephasing and spontaneous emission, both on the nonlinear interaction and on group velocity matching. The semiclassical regime offers a clear picture of the physical aspects involved in EIT-based nonlinear optics, and well describes a number of recent experiments [37, 89, 90]. To this end we consider two different configurations of atom-field interactions, which we will call the *asymmetric* (see Fig. 3.1) and the *symmetric* (see Fig. 3.9) $M$ scheme. The chapter is thus composed of two main parts. In Sec. 3.2 we describe the physics of the asymmetric $M$-scheme. We start by defining the system and calculating the susceptibilities using an approximate treatment employing amplitude equations. These analytical calculations are then compared with the results of the numerical solution of the full system of Bloch equations. Finally, the conditions for group velocity matching are analyzed. In Sec. 3.3 the physics of the symmetric $M$-scheme is described by following the same order as in Sec. 3.2. Conclusions are drawn in Sec. 3.4.1.

## 3.2 The Asymmetric M Scheme

The $M$-system under consideration has a double adjacent $\Lambda$ structure as shown in Fig. 3.1, where atoms with five levels (three ground states $|1\rangle$, $|3\rangle$, $|5\rangle$, and two excited states $|2\rangle$, $|4\rangle$) interact with four electromagnetic fields [84]. This configuration can be realized in Zeeman-splitted alkali atoms, such as $^{87}$Rb atoms.
On transitions $|3\rangle \leftrightarrow |2\rangle$ and $|5\rangle \leftrightarrow |4\rangle$ we apply two strong fields, the *coupler* $\Omega_2$ and the *tuner* $\Omega_4$ respectively. On the transition $|1\rangle \leftrightarrow |2\rangle$ a *probe* field is applied (with $\Omega_1$), while on the transition $|3\rangle \leftrightarrow |4\rangle$ a *trigger* field (with $\Omega_3$) is applied. In this chapter, we will analyze the XPM and the group velocity matching between the *probe* and the *trigger* fields. We call the scheme of Fig. 2 the *asymmetric M* scheme due to the asymmetric distribution of the initial atomic population. All the atoms are in fact assumed to be initially in state $|1\rangle$ so that they directly feel the effect of the probe field only, while the effect of the trigger field is only indirect. Due to this inherent asymmetry, the dynamics experienced by probe and trigger fields are always different, even when the corresponding parameters (Rabi frequencies, decay rates, detunings) are equal. The symmetric version of this scheme will be analyzed in Sec. 3.3.

The detunings $\delta_i$ (see Fig. 3.1) are defined as follows

$$E_2 - E_1 = \hbar\omega_1 + \hbar\delta_1 \tag{3.1a}$$
$$E_2 - E_3 = \hbar\omega_2 + \hbar\delta_2 \tag{3.1b}$$
$$E_4 - E_3 = \hbar\omega_3 + \hbar\delta_3 \tag{3.1c}$$
$$E_4 - E_5 = \hbar\omega_4 + \hbar\delta_4, \tag{3.1d}$$

where $E_i$, $(i = 1, \ldots, 5)$ is the energy of level $|i\rangle$, and $\omega_i$ is the frequency of the field with Rabi frequency $\Omega_i$.

The Hamiltonian of the system is

$$\begin{aligned} H_A = & \sum_i^5 E_i|i\rangle\langle i| + \hbar\left(\Omega_1 e^{-i\omega_1 t}|2\rangle\langle 1| + \Omega_2 e^{-i\omega_2 t}|2\rangle\langle 3|\right. \\ & \left. + \Omega_3 e^{-i\omega_3 t}|4\rangle\langle 3| + \Omega_4 e^{-i\omega_4 t}|4\rangle\langle 5| + h.c.\right), \end{aligned} \tag{3.2}$$

where *h.c.* denotes the hermitian conjugate. Moving to the interaction picture with respect to the following free Hamiltonian

$$H_0 = E_1|1\rangle\langle 1| + (E_2 - \hbar\delta_1)|2\rangle\langle 2| + (E_3 - \hbar\delta_{12})|3\rangle\langle 3| + (E_4 - \hbar\delta_{13})|4\rangle\langle 4| + (E_5 - \hbar\delta_{14})|5\rangle\langle 5| \tag{3.3}$$

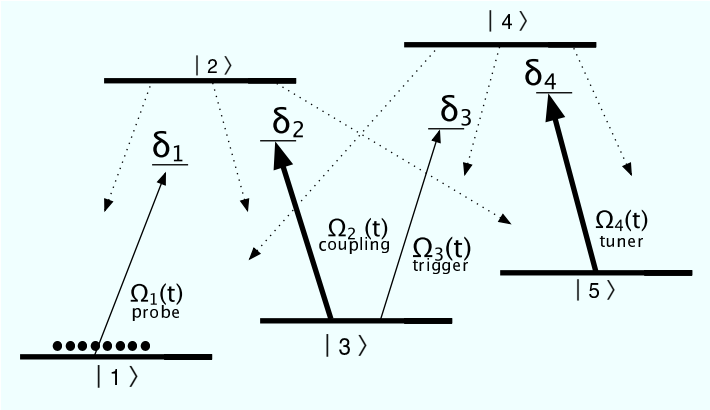


Figure 3.1: Asymmetric $M$ scheme. The probe and the trigger fields, with Rabi frequencies $\Omega_1$ and $\Omega_3$ respectively, together with the stronger pump fields, the coupler and the tuner (with Rabi frequencies $\Omega_2$ and $\Omega_4$, respectively) drive the corresponding transitions. All the atoms are assumed to be in state $|1\rangle$ and the detunings are defined in Eqs. (3.1).

where

$$\delta_{12} = \delta_1 - \delta_2, \tag{3.4a}$$
$$\delta_{13} = \delta_1 - \delta_2 + \delta_3, \tag{3.4b}$$
$$\delta_{14} = \delta_1 - \delta_2 + \delta_3 - \delta_4, \tag{3.4c}$$

we get the following effective time-independent Hamiltonian

$$\begin{aligned} H_{eff}^{AS} = {} & \hbar\delta_1|2\rangle\langle 2| + \hbar\delta_{12}|3\rangle\langle 3| + \hbar\delta_{13}|4\rangle\langle 4| + \hbar\delta_{14}|5\rangle\langle 5| \\ & + \hbar\Omega_1|2\rangle\langle 1| + \hbar\Omega_2|2\rangle\langle 3| + \hbar\Omega_3|4\rangle\langle 3| + \hbar\Omega_4|4\rangle\langle 5| + h.c. \end{aligned} \tag{3.5}$$

### 3.2.1 Amplitude variables approach

We now study the dynamics driven by Eq. (3.5). As we saw in first chapter, we can include the spontaneous emission and dephasing process in the description of the system, first in a phenomenological manner by including decay rates $\Gamma_i^{AV}$ for each atomic level $|i\rangle$ in the equations for the amplitude variables (AV) of the atomic wave-function. From an intuitive point of view, for the excited levels $|2\rangle$ and $|4\rangle$ these rates describe the total spontaneous decay rates, while for the ground states the associated decay rates describe dephasing processes [6]. Therefore, the evolution equations for the amplitudes $b_i(t)$ of the atomic state

$$|\psi(t)\rangle = \sum_{i=1}^{5} b_i(t)|i\rangle \tag{3.6}$$

become

$$\dot{b}_1 = -\frac{\Gamma_1^{AV}}{2} b_1 - i\Omega_1^{\star} b_2, \tag{3.7a}$$

$$\dot{b}_2 = -\left(\frac{\Gamma_2^{AV}}{2} + i\delta_1\right) b_2 - i\Omega_1 b_1 - i\Omega_2 b_3, \tag{3.7b}$$

$$\dot{b}_3 = -\left(\frac{\Gamma_3^{AV}}{2} + i\delta_{12}\right) b_3 - i\Omega_2^{\star} b_2 - i\Omega_3^{\star} b_4, \tag{3.7c}$$

$$\dot{b}_4 = -\left(\frac{\Gamma_4^{AV}}{2} + i\delta_{13}\right) b_4 - i\Omega_3 b_3 - i\Omega_4 b_5, \tag{3.7d}$$

$$\dot{b}_5 = -\left(\frac{\Gamma_5^{AV}}{2} + i\delta_{14}\right) b_5 - i\Omega_4^{\star} b_4. \tag{3.7e}$$

The system's initial state is assumed to be the ground state $|1\rangle$. Since an efficient XPM requires a dispersive interaction, we tailor the dynamics in such a way that this initial condition on the populations remains essentially unaltered, even when the system reaches the steady-state, i.e.,

$$b_1^{ss} \simeq 1. \tag{3.8}$$

To this end we assume that the control field $\Omega_2$ is stronger then the probe field $\Omega_1$, with the system being approximately on Raman resonance for the first and the second $\Lambda$ subsystems ($\delta_1 \sim \delta_2$ and $\delta_3 \sim \delta_4$). Equations (3.7) are then solved in the steady-state. In order to get a consistent expression for the nonlinear susceptibilities one has to consider higher order contributions to Eq. (3.8), which is obtained by imposing the normalization of the atomic wavefunction of Eq. (3.6) at second order in $|\Omega_1/\Omega_2|$. One gets the following expression for the steady state amplitudes

$$b_1^{ss} = 1 - \frac{|\Omega_1|^2 \left[|d_3|^2 + |\Omega_2|^2\right]}{2\left|d_2 d_3 - |\Omega_2|^2\right|^2}, \tag{3.9a}$$

$$b_2^{ss} = \Omega_1 \frac{d_3\left[|\Omega_4|^2 - d_4 d_5\right] + |\Omega_3|^2 d_5}{D_a} b_1^{ss} \tag{3.9b}$$

$$b_3^{ss} = -\Omega_1 \Omega_2^{\star} \frac{|\Omega_4|^2 - d_4 d_5}{D_a} b_1^{ss} \tag{3.9c}$$

$$b_4^{ss} = -\frac{\Omega_1 \Omega_2^{\star} \Omega_3 d_5}{D_a} b_1^{ss} \tag{3.9d}$$

$$b_5^{ss} = \frac{\Omega_1 \Omega_2^{\star} \Omega_3 \Omega_4^{\star}}{D_a} b_1^{ss}, \tag{3.9e}$$

where we have defined

$$d_2 = \delta_1 - \imath\Gamma_2^{AV}/2, \tag{3.10a}$$

$$d_3 = \delta_{12} - \imath\Gamma_3^{AV}/2, \tag{3.10b}$$

$$d_4 = \delta_{13} - \imath\Gamma_4^{AV}/2, \tag{3.10c}$$

$$d_5 = \delta_{14} - \imath\Gamma_5^{AV}/2, \tag{3.10d}$$

$$D_a = \left[d_2 d_3 - |\Omega_2|^2\right]\left[d_4 d_5 - |\Omega_4|^2\right] - d_2 d_5 |\Omega_3|^2. \tag{3.11}$$

These results can be used to determine the probe and trigger susceptibilities, which are defined as

$$\chi_P = \frac{N\mu_{12}}{V\varepsilon_0 \mathcal{E}_1} b_2^{ss} b_1^{ss,\star} = -\frac{N|\mu_{12}|^2}{V\hbar\varepsilon_0 \Omega_1} b_2^{ss} b_1^{ss,\star}, \tag{3.12a}$$

$$\chi_T = \frac{N\mu_{34}}{V\varepsilon_0 \mathcal{E}_3} b_4^{ss} b_3^{ss,\star} = -\frac{N|\mu_{34}|^2}{V\hbar\varepsilon_0 \Omega_3} b_4^{ss} b_3^{ss,\star}, \tag{3.12b}$$

where $N$ is the number of atoms interacting with the electromagnetic field, $V$ is the volume occupied by the gas, and $\varepsilon_0$ is the vacuum dielectric constant. Doppler broadening is neglected here. It is well known that first order Doppler effect can be cancelled by using co-propagating laser fields [4]. In particular we emphasize that this is valid for cold atomic media in a magneto-optical trap as well as for a standard gas cell.

Inserting Eqs. (3.9) into Eqs. (3.12) and expanding in series at the lowest orders in the probe and trigger electric fields, $\mathcal{E}_1$ and $\mathcal{E}_3$ respectively, one gets

$$\chi_P \simeq \chi_P^{(1)} + \chi_P^{(3,sk)} |\mathcal{E}_1|^2 + \chi_P^{(3,ck)} |\mathcal{E}_3|^2 \tag{3.13a}$$

$$\chi_T \simeq \chi_T^{(3,ck)} |\mathcal{E}_1|^2, \tag{3.13b}$$

where we have introduced the linear susceptibility $\chi_P^{(1)}$, the third-order self-Kerr susceptibility $\chi_P^{(3,sk)}$ and the third-order cross-Kerr susceptibilities $\chi_{P,T}^{(3,ck)}$. Eqs. (3.13) clearly show the asymmetry of the scheme between the probe and trigger fields, with the latter possessing a nonzero cross-Kerr susceptibility only. This is a consequence of the asymmetry of the population distribution, which essentially remains in the ground state $|1\rangle$ all the time. This means that the trigger field drives a virtually empty transition, hence the contribution to the susceptibility comes only from higher order (see [71] for discussion on the link between the population distribution and a linear contribution to susceptibility). It will be shown in Sec. 3.3 that the symmetric $M$-scheme brings about both a linear and a self-Kerr contribution to the trigger susceptibility.

By using Eqs. (3.9) and the definitions of Eqs. (3.10) into Eqs. (3.12), and comparing with Eqs. (3.13) at the corresponding order in the electric fields, one gets the explicit dependence of the linear and nonlinear susceptibilities as a function of the system parameters, i.e.,

$$\chi_P^{(1)} = \frac{N|\mu_{12}|^2}{V\hbar\varepsilon_0} \frac{\delta_{12} - i\Gamma_3^{AV}/2}{\left(\delta_1 - i\Gamma_2^{AV}/2\right)\left(\delta_{12} - i\Gamma_3^{AV}/2\right) - |\Omega_2|^2} \tag{3.14}$$

for the probe linear susceptibility, and

$$\chi_P^{(3,sk)} = \frac{N|\mu_{12}|^4}{V\hbar^3\varepsilon_0} \frac{-d_{12}^{as}\left[|d_{12}^{as}|^2 + |\Omega_2|^2\right]}{\left[d_1^{as}d_{12}^{as} - |\Omega_2|^2\right]|d_1^{as}d_{12}^{as} - |\Omega_2|^2|^2}, \tag{3.15}$$

$$\chi_P^{(3,ck)} = \frac{N|\mu_{12}|^2|\mu_{34}|^2}{V\hbar^3\varepsilon_0} \frac{|\Omega_2|^2 d_{14}^{as}}{\left[d_1^{as}d_{12}^{as} - |\Omega_2|^2\right]^2\left[d_{13}^{as}d_{14}^{as} - |\Omega_4|^2\right]}, \tag{3.16}$$

$$\chi_T^{(3,ck)} = \frac{N|\mu_{12}|^2|\mu_{34}|^2}{V\hbar^3\varepsilon_0} \frac{|\Omega_2|^2 d_{14}^{as}}{|d_1^{as}d_{12}^{as} - |\Omega_2|^2|^2\left[d_{13}^{as}d_{14}^{as} - |\Omega_4|^2\right]}, \tag{3.17}$$

for the third-order nonlinear susceptibilities. The complex detunings $d_1^{as}, d_{12}^{as}, d_{13}^{as}, d_{14}^{as}$ have been defines as

$$d_1^{as} = \delta_1 - i\Gamma_2^{AV}/2 \tag{3.18}$$

$$d_{12}^{as} = \delta_{12} - i\Gamma_3^{AV}/2 \tag{3.19}$$

$$d_{13}^{as} = \delta_{13} - i\Gamma_4^{AV}/2 \tag{3.20}$$

$$d_{14}^{as} = \delta_{14} - i\Gamma_5^{AV}/2. \tag{3.21}$$

The two cross-Kerr susceptibilities are identical whenever the quantity

$$\left(\delta_1 - i\Gamma_2^{AV}/2\right)\left(\delta_{12} - i\Gamma_3^{AV}/2\right) - |\Omega_2|^2,$$

is (at least approximately) real. This happens in the typical EIT situation we are considering in which $|\Omega_2|$ is large enough. In fact, when $|\Omega_2|^2 \gg \left|\left(\delta_1 - i\Gamma_2^{AV}/2\right)\left(\delta_{12} - i\Gamma_3^{AV}/2\right)\right|$, one has [59]

$$\chi_P^{(3,ck)} = \chi_T^{(3,ck)} = \frac{N|\mu_{12}|^2|\mu_{34}|^2}{V\hbar^3\varepsilon_0} \frac{\delta_{14} - i\Gamma_5^{AV}/2}{|\Omega_2|^2\left[\left(\delta_{13} - i\Gamma_4^{AV}/2\right)\left(\delta_{14} - i\Gamma_5^{AV}/2\right) - |\Omega_4|^2\right]}. \tag{3.22}$$

We shall see in the next section that these approximate expressions for the nonlinear susceptibilities fit very well with the numerical solution of the exact dynamics of the system.

The asymmetric $M$-scheme can be seen as an extension of the four level $N$-scheme introduced in Ref. [13], with the addition of the coupling to an additional level $|5\rangle$ provided by the tuner field with Rabi frequency $\Omega_4$. In fact, it easy to check that upon setting $\Omega_4 = 0$ in Eq. (3.15b), one recovers the third-order nonlinear susceptibility of the four-level $N$-scheme derived in Refs. [13, 37]). As we will see below, the role of the tuner field is to enable a fine tuning of the group velocities, in order to achieve group velocity matching between probe and trigger [59, 73, 77].

### 3.2.2 Comparison with the Optical Bloch Equations

We now study the dynamics of the asymmetric $M$ scheme of Fig. 3.1 by means of the optical Bloch equations (OBE) (see Appendix A), which allow to describe spontaneous emission and dephasing rigorously and no more phenomenologically as in the AV treatment presented in the preceding section. We consider six spontaneous decay channels, i.e., the decay of the excited state $|2\rangle$ onto the three ground state sublevels $|1\rangle$, $|3\rangle$, and $|5\rangle$ with rates $\Gamma_{21}$, $\Gamma_{23}$ and $\Gamma_{25}$ respectively, and the corresponding decay of the excited state $|4\rangle$ onto the three sublevels $|1\rangle$,

$|3\rangle$, and $|5\rangle$ with rates $\Gamma_{41}$, $\Gamma_{43}$ and $\Gamma_{45}$ respectively. Moreover we consider dephasing of the each level $|i\rangle$ with dephasing rate $\gamma_{ii}$, so that the master equation for the atomic density operator $\sigma$ is given by

$$\begin{aligned}\dot{\sigma} &= -\frac{i}{\hbar}\left[H_{eff}^{AS},\sigma\right] + \sum_{l=2,4}\sum_{k=1,3,5}\frac{\Gamma_{lk}}{2}\left(2\hat{\sigma}_{kl}\sigma\hat{\sigma}_{kl}^{\dagger} - \hat{\sigma}_{kl}^{\dagger}\hat{\sigma}_{kl}\sigma - \sigma\hat{\sigma}_{kl}^{\dagger}\hat{\sigma}_{kl}\right) \\ &\quad + \sum_{k=1}^{5}\frac{\gamma_{kk}}{2}\left(2\hat{\sigma}_{kk}\sigma\hat{\sigma}_{kk} - \hat{\sigma}_{kk}\sigma - \sigma\hat{\sigma}_{kk}\right), \end{aligned} \tag{3.23}$$

where $H_{eff}^{AS}$ is given by Eq. (3.5) and $\hat{\sigma}_{kl} = |k\rangle\langle l|$. The corresponding system of OBE's for the mean values $\sigma_{ij}(t) \equiv \langle\hat{\sigma}_{ij}(t)\rangle \equiv \sigma_{ji}(t)$ is displayed in Appendix A.2.1 as Eqs. (A.23) and (A.24), where we have defined for convenience the total decay rates

$$\Gamma_2 = \Gamma_{21} + \Gamma_{23} + \Gamma_{25}, \tag{3.24}$$

$$\Gamma_4 = \Gamma_{41} + \Gamma_{43} + \Gamma_{45}, \tag{3.25}$$

and the composite dephasing rates

$$\gamma_{ij} = \gamma_{ii} + \gamma_{jj}, \quad i = 1\ldots 5. \tag{3.26}$$

The OBE for the $M$ scheme are quite involved and less suited for an approximate analytical treatment with respect to the AV equations of the preceding section. In fact, if we consider again the condition $|\Omega_1/\Omega_2| \ll 1$ and, consistently with Eq. (3.8), we assume that

$$\sigma_{11} \approx 1, \tag{3.27a}$$

$$\sigma_{jj} \approx 0, \quad j = 2,\ldots,5, \tag{3.27b}$$

at the steady state, it is possible to see that by inserting Eqs. (3.27) into Eqs. (A.24) for the coherences, one gets a satisfactory expression for the probe linear susceptibility only. To be more specific, only the approximate linear susceptibility fits well with the numerical solution of the OBE, while it turns out to be extremely difficult to derive analytical expressions from Eqs. (A.23) and (A.24) for the nonlinear susceptibilities, as simple as those of Eqs. (3.15), and which reproduce in the same way the exact numerical solution in the EIT regime we are studying. Obviously, one can exactly solve analytically the OBE, but the resulting expressions are very cumbersome and not physically transparent such as those of Eqs. (3.15). For this reason we will analytically derive from the OBE the probe linear susceptibility only, and we will then use the OBE only for the numerical determination of the atomic steady state. Additionally, deriving this result will enable us to draw a formal analogy between the AV and OBE treatments (see Eqs. (3.30) below).

The probe susceptibility is defined in terms of the atomic coherence $\sigma_{12}$ as (see also Eq. (3.12a))

$$\chi_P = \frac{N\mu_{12}}{V\varepsilon_0\mathcal{E}_1}\sigma_{12} = -\frac{N|\mu_{12}|^2}{V\hbar\varepsilon_0\Omega_1}\sigma_{12}. \tag{3.28}$$

Using Eqs. (3.27) and performing a series expansion at the lowest order in the probe and trigger fields, we arrive at an approximate solution for $\sigma_{12}$, which, inserted into Eq. (4.27), gives the following expression for the probe linear susceptibility

$$\chi_P^{(1)} = \frac{N|\mu_{12}|^2}{V\hbar\varepsilon_0}\frac{\delta_{12} - i\gamma_{13}/2}{\left[\delta_{12} - i\gamma_{13}/2\right]\left[\delta_1 - i\left(\Gamma_2 + \gamma_{12}\right)/2\right] - |\Omega_2|^2}. \tag{3.29}$$

By comparing Eq. (3.29) with Eq. (3.14), one can immediately see that the AV and OBE predictions for the probe linear susceptibility coincide provided that the phenomenological decay rates $\Gamma_i^{AV}$ are appropriately interpreted, i.e.,

$$\Gamma_2^{AV} \leftrightarrow \Gamma_2 + \gamma_{12}, \tag{3.30a}$$

$$\Gamma_3^{AV} \leftrightarrow \gamma_{13}. \tag{3.30b}$$

This comparison shows therefore that the AV approach provides a treatment of the atomic dynamics simpler than the OBE's approach, but roughly equivalent, and that the intuitive interpretation of its phenomenological decay rates $\Gamma_i^{AV}$ as spontaneous emission total decay rates for the excited states, and as dephasing rates in the case of ground state sublevels, is essentially correct, especially in the typical case in which dephasing rates are much smaller than spontaneous emission decay rates (see Eqs. (3.30)).

We then consider the numerical solution of the OBE and we compare it with the analytical treatment based on the AV approach presented above. The numerical calculations are performed in the range of parameters corresponding to EIT, i.e., $|\Omega_1|, |\Omega_2| \ll |\Omega_3|, |\Omega_4|$ and we stay near two-photon resonance for both the probe and the trigger field. In Figs. 3.2-3.5 we compare the analytical solutions of Eq. (3.14) and Eqs. (3.15) with the numerical solution of the complete set of Bloch equations given in the Appendix A. From these plots it is evident that our analytical treatment works satisfactorily well, except for a small interval of values of the detuning, corresponding to the maximum probe (or trigger) absorption. In such a case, the detunings match the Rabi frequencies of the two pumps, and the probe (or trigger) field is in resonance with a single atomic transition. The atoms are significantly pumped to the excited levels and the population assumption of Eq. (3.8) is not fulfilled. In fact, the discrepancy between the exact numerical solution of the OBE and the AV approach is strictly related to the atomic population out of level $|1\rangle$ which, in the case of Fig. 3.2, is about 14% of the total population.

Figs. 3.2-3.5 refer to a situation with small dephasing rates ($\forall$ i,j, $\gamma_{ij} = \Gamma_3^{AV} = \Gamma_5^{AV} = 10^{-4}\Gamma_4 \sim$ few kHz) which are typical for not too dense gases. For larger values of the dephasing rates (some tens of kHz), we have seen that the analytical prediction of the AV approach of the preceding section starts to depart from the exact solution of the OBE.

### 3.2.3 Group velocity matching

The propagation equation for the slowly varying electric field amplitudes $\varepsilon_i(z,t)$, $i = P, T$, defined as

$$\mathcal{E}_i(z,t) = \varepsilon_i(z,t) \exp\{ik_i z - i\omega_i t\} + c.c. \;\; i = P, T,$$

is given by

$$\left(\frac{\partial}{\partial z} + \frac{1}{v_g^i}\frac{\partial}{\partial t}\right)\varepsilon_i(z,t) = i\frac{k_i}{2}\chi_i(z,t)\varepsilon_i(z,t), \;\; i = P, T, \tag{3.31}$$

where $v_g^i$ is the group velocity, generally defined as $v_g^i = c/(1 + n_g^i)$, with $c$ the speed of light in vacuum and

$$n_g^i = \frac{1}{2}\mathrm{Re}[\chi_i] + \frac{\omega_i}{2}\left(\frac{\partial \mathrm{Re}[\chi_i]}{\partial \omega}\right)_{\omega_i} \tag{3.32}$$

the group index, $\omega_i$ being the central frequency of pulse $i$. The solution of Eq. (3.31) is

$$\varepsilon_i(z,t) = \varepsilon_i(0, t - \frac{z}{v_g^i}) \exp\left\{i\frac{k_i}{2}\int_0^z dz' \chi_i(z',t)\right\}, \tag{3.33}$$

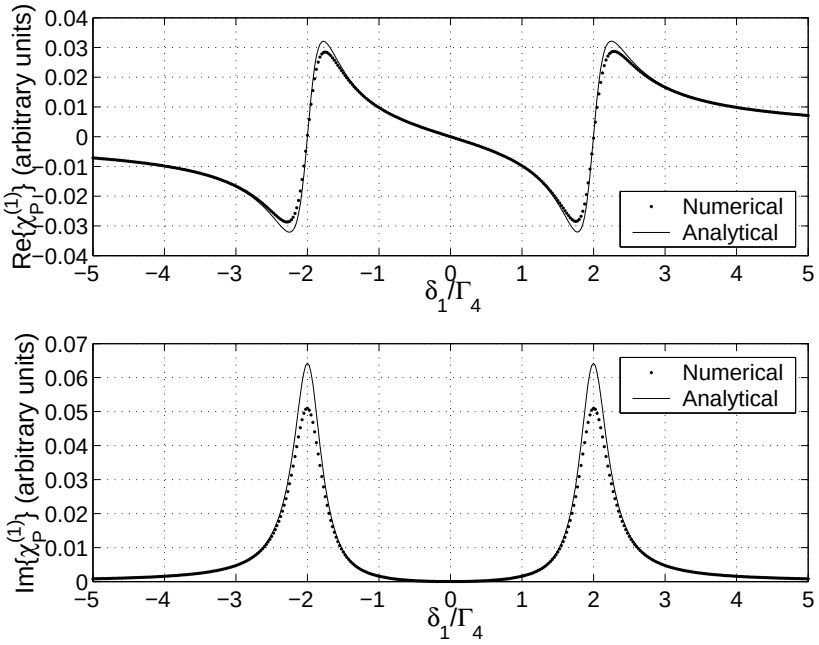


Figure 3.2: Comparison of the numerical solution (dotted line) of the OBE with the analytical prediction of Eq. (3.14) (full line) for the real part (above) and imaginary part (below) of the linear probe susceptibility versus the normalized probe detuning $\delta_1/\Gamma_4$. The parameter used are the following: $\Gamma_2^{AV} = \Gamma_2 = 36$ MHz, $\Gamma_4^{AV} = \Gamma_4 = 38$ MHz, $\delta_2 = \delta_3 = \delta_4 = 0$, $\forall$ i,j $\gamma_{ij} = \Gamma_3^{AV} = \Gamma_5^{AV} = 10^{-4}\Gamma_4$, $\Omega_1 = 0.08\Gamma_4$, $\Omega_2 = 2\Gamma_4$, $\Omega_3 = 0.04\Gamma_4$, $\Omega_4 = \Gamma_4$.

so that, using Eqs. (3.13), the nonlinear cross-phase shift for the two fields of interest is given by

$$\phi_P^{ck} = \frac{\omega_1}{2c}\int_0^l dz \mathrm{Re}[\chi_P^{3,ck}]\,|\varepsilon_T(z,t)|^2\,, \tag{3.34a}$$

$$\phi_T^{ck} = \frac{\omega_3}{2c}\int_0^l dz \mathrm{Re}[\chi_T^{3,ck}]\,|\varepsilon_P(z,t)|^2\,, \tag{3.34b}$$

where $l$ is the length of the atomic medium. These nonlinear cross-phase shifts are of fundamental importance also for quantum information processing applications. In fact, the CPS of Eq. (4.3) is determined only by these cross-Kerr contributions to the total phase shift, because the linear and self-Kerr contributions cancel out, as shown in Refs. [59, 71].

For Gaussian probe and trigger pulses of time durations $\tau_P$ and $\tau_T$, and with peak Rabi frequencies $\Omega_P^{peak}$ and $\Omega_T^{peak}$ respectively, the nonlinear cross-phase shifts can be written as (see also Refs. [59, 71])

$$\phi_P^{ck} = \frac{\omega_1 l}{4c}\frac{\sqrt{\pi}\hbar^2|\Omega_T^{peak}|^2}{|\mu_{34}|^2}\frac{\mathrm{erf}[\zeta_\mathrm{P}]}{\zeta_P}\,\mathrm{Re}[\chi_P^{3,ck}], \tag{3.35a}$$

$$\phi_T^{ck} = \frac{\omega_3 l}{4c}\frac{\sqrt{\pi}\hbar^2|\Omega_P^{peak}|^2}{|\mu_{12}|^2}\frac{\mathrm{erf}[\zeta_\mathrm{T}]}{\zeta_T}\,\mathrm{Re}[\chi_T^{3,ck}], \tag{3.35b}$$

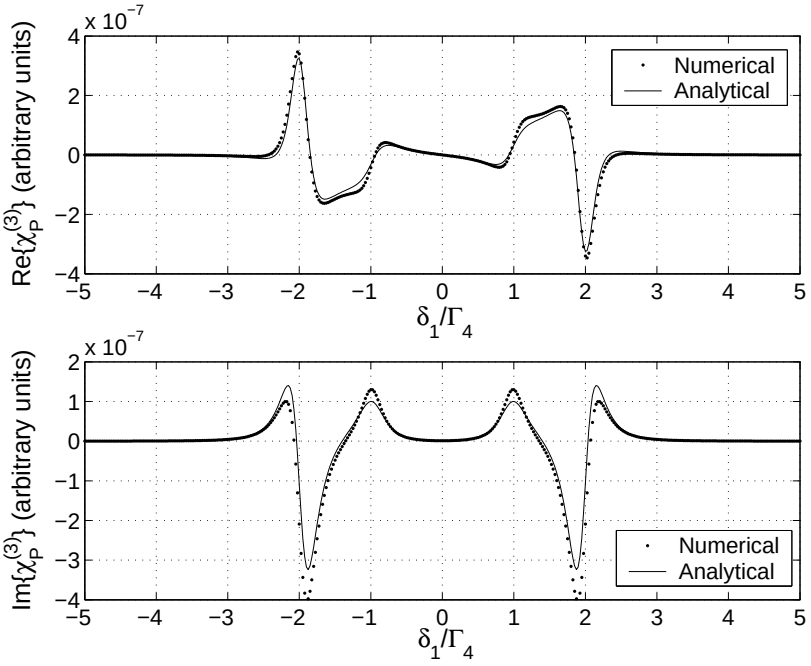


Figure 3.3: Comparison of the numerical solution (dotted line) of the OBE with the analytical prediction of Eq. (3.15b) (full line) for the real part (above) and imaginary part (below) of the probe cross-Kerr susceptibility versus the normalized probe detuning $\delta_1/\Gamma_4$. To reduce as much as possible the influence of the self-Kerr susceptibility we have considered a probe Rabi frequency $\Omega_1$ much smaller than that of the trigger field. Parameters are: $\Gamma_2^{AV} = \Gamma_2 = 36$ MHz, $\Gamma_4^{AV} = \Gamma_4 = 38$ MHz, $\delta_2 = \delta_3 = \delta_4 = 0$, $\forall$ i,j $\gamma_{ij} = \Gamma_3^{AV} = \Gamma_5^{AV} = 10^{-4}\Gamma_4$, $\Omega_1 = 0.004\Gamma_4$, $\Omega_2 = 2\Gamma_4$, $\Omega_3 = 0.04\Gamma_4$, $\Omega_4 = \Gamma_4$.

where $\zeta_P = (1 - v_g^P/v_g^T)\sqrt{2}l/v_g^P\tau_T$ and $\zeta_T$ is obtained from $\zeta_P$ upon interchanging the indices $P \leftrightarrow T$. Large nonlinear cross-phase shifts take place for appreciably large values of the two cross-Kerr susceptibilities real parts, and especially when probe and trigger velocities become *equal*, i.e., when $\zeta_{P,T} \to 0$, in which case the $\mathrm{erf}[\zeta]/\zeta$ reaches the maximum value $2/\sqrt{\pi}$. In this limit the cross-phase phase shifts linearly increase with the length of the atomic medium $l$. This explains why achieving group velocity matching, $v_g^P = v_g^T$, is of fundamental importance. Moreover group velocities become small for large group indices and this condition can be achieved within the EIT transparency window, where $\mathrm{Re}[\chi]$ vanishes, and the group velocity is strongly reduced due to a large dispersion gradient $\partial\mathrm{Re}[\chi]/\partial\omega$.

Let us see how small and equal probe and trigger group velocities can be obtained. We consider the approximate analytical expressions for the susceptibilities of Eqs. (3.13)-(3.15) derived above within the AV approach, and which we have seen to work very well in the EIT regime. Assuming to stay at the center of the transparency window for the probe ($\delta_{12} = 0$) where the dispersion gradient is maximum, and neglecting dephasing rates $\Gamma_3^{AV}$ and $\Gamma_5^{AV}$, which

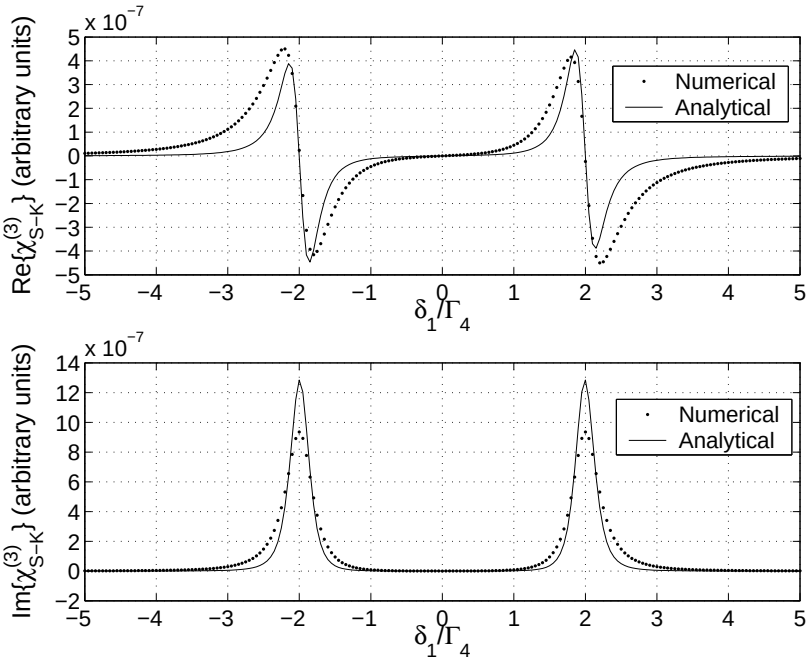


Figure 3.4: Comparison of the numerical solution (dotted line) of the OBE with the analytical prediction of Eq. (3.15a) (full line) for the real part (above) and imaginary part (below) of the probe self-Kerr susceptibility versus the normalized probe detuning $\delta_1/\Gamma_4$. To reduce as much as possible the influence of the cross-Kerr susceptibility we have considered a trigger Rabi frequency $\Omega_3$ much smaller than that of the probe field. Parameters are: $\Gamma_2^{AV} = \Gamma_2 = 36$ MHz, $\Gamma_4^{AV} = \Gamma_4 = 38$ MHz, $\delta_2 = \delta_3 = \delta_4 = 0$, $\forall$ i,j $\gamma_{ij} = \Gamma_3^{AV} = \Gamma_5^{AV} = 10^{-4}\Gamma_4$, $\Omega_1 = 0.5\Gamma_4$, $\Omega_2 = 2\Gamma_4$, $\Omega_3 = 0.005\Gamma_4$, $\Omega_4 = \Gamma_4$.

are typically much smaller than all the other parameters, one gets

$$n_g^P \simeq \frac{N}{V}\frac{|\mu_{12}|^2\omega_1}{2\hbar\epsilon_0|\Omega_2|^2}(1+|\Omega_3|^2\beta), \tag{3.36a}$$

$$n_g^T \simeq \frac{N}{V}\frac{|\mu_{34}|^2\omega_3}{2\hbar\epsilon_0|\Omega_2|^2}|\Omega_1|^2\beta, \tag{3.36b}$$

where [59]

$$\beta = \frac{\left(\delta_{14}^2+|\Omega_4|^2\right)\left[\left(\delta_{13}\delta_{14}-|\Omega_4|^2\right)^2-\delta_{14}^2\left(\Gamma_4^{AV}/2\right)^2\right]}{\left[\left(\delta_{13}\delta_{14}-|\Omega_4|^2\right)^2+\delta_{14}^2\left(\Gamma_4^{AV}/2\right)^2\right]^2}. \tag{3.37}$$

In the EIT situation we are considering it is $n_g^P, n_g^T \gg 1$, so that, using Eqs. (3.36),

$$v_g^P \simeq \frac{c}{n_g^P} \simeq \frac{2\hbar\epsilon_0 c|\Omega_2|^2}{(N/V)|\mu_{12}|^2\omega_1(1+|\Omega_3|^2\beta)}, \tag{3.38a}$$

$$v_g^T \simeq \frac{c}{n_g^T} \simeq \frac{2\hbar\epsilon_0 c|\Omega_2|^2}{(N/V)|\mu_{34}|^2\omega_3|\Omega_1|^2\beta}. \tag{3.38b}$$

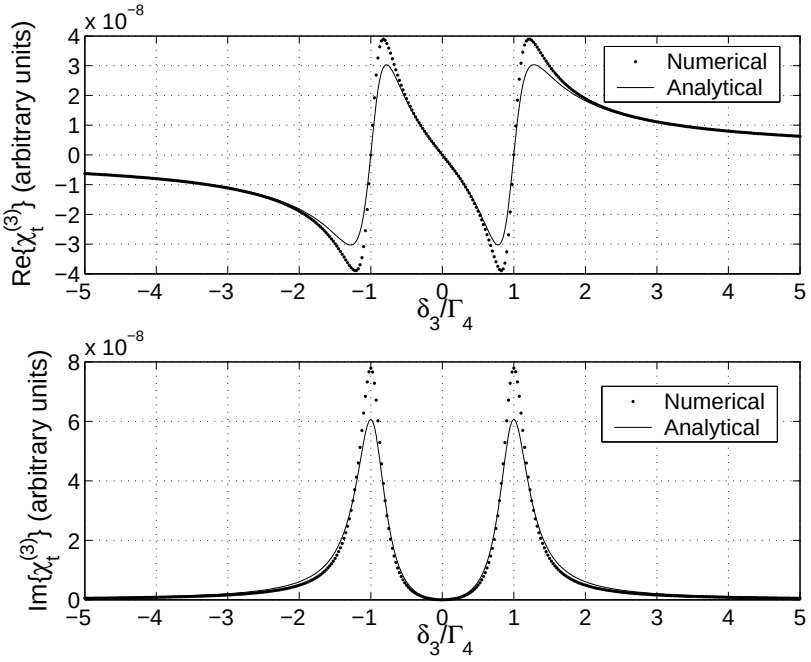


Figure 3.5: Comparison of the numerical solution (dotted line) of the OBE with the analytical prediction of Eq. (3.15c) (full line) for the real part (above) and imaginary part (below) of the trigger cross-Kerr susceptibility as a function of the normalized trigger's detuning $\delta_3/\Gamma_4$. Parameters are similar to those of Fig. 3.2, $\Gamma_2^{AV} = \Gamma_2 = 36$ MHz, $\Gamma_4^{AV} = \Gamma_4 = 38$ MHz, $\delta_1 = \delta_2 = \delta_4 = 0$, $\forall$ i,j $\gamma_{ij} = \Gamma_3^{AV} = \Gamma_5^{AV} = 10^{-4}\Gamma_4$, $\Omega_1 = 0.08\Gamma_4$, $\Omega_2 = 2\Gamma_4$, $\Omega_3 = 0.04\Gamma_4$, $\Omega_4 = \Gamma_4$.

As expected, the asymmetric $M$-scheme does not yield equal slow down of both trigger and probe pulse automatically as, for example, the scheme of Petrosyan and Kurizki [73] does. In fact, the two expressions of the group velocities are generally different. Nonetheless, Eqs. (3.38) show that group velocity matching is always achievable by properly adjusting the parameter $\beta$, which means adjusting the tuner intensity $|\Omega_4|^2$ and the composite detuning $\delta_{14}$. This shows that the present asymmetric $M$-scheme can be seen as a modified version of the $N$-scheme of Ref. [13], in which the tuner pump field is added just in order to "tune" the group velocity of the trigger pulse so to make it equal to that of the probe. The possibility to achieve group velocity matching is shown in Fig. 3.6, where both the numerical result derived form the OBE and the approximate analytical expressions of Eqs. (3.38) are plotted versus the trigger detuning $\delta_3$. Two different values of $\delta_3$ exist for which $v_g^P = v_g^T \simeq 1000$ m/s (see Fig. 3.6). Parameter values here correspond to typical values for a cell of $^{87}$Rb atoms, i.e., $\Gamma_2^{AV} = \Gamma_2 \simeq 36$ MHz, $\Gamma_4^{AV} = \Gamma_4 \simeq 38$ MHz, $N/V \simeq 3 \times 10^{13}$ cm$^{-3}$, $\delta_1 = \delta_2 = 0$, $\delta_4 \simeq \delta_3 \simeq 20\Gamma_4$, $\Omega_1 = 0.08\Gamma_4$, $\Omega_2 = 2\Gamma_4$, $\Omega_3 = 0.04\Gamma_4$, $\Omega_4 = \Gamma_4$, $\forall$ i,j, $\gamma_{ij} = \Gamma_3^{AV} = \Gamma_5^{AV} = 10^{-4}\Gamma_4$. Moreover Fig. 3.6 clearly shows that the simple expressions of Eqs. (3.38) well reproduce the exact numerical solution of the OBE.

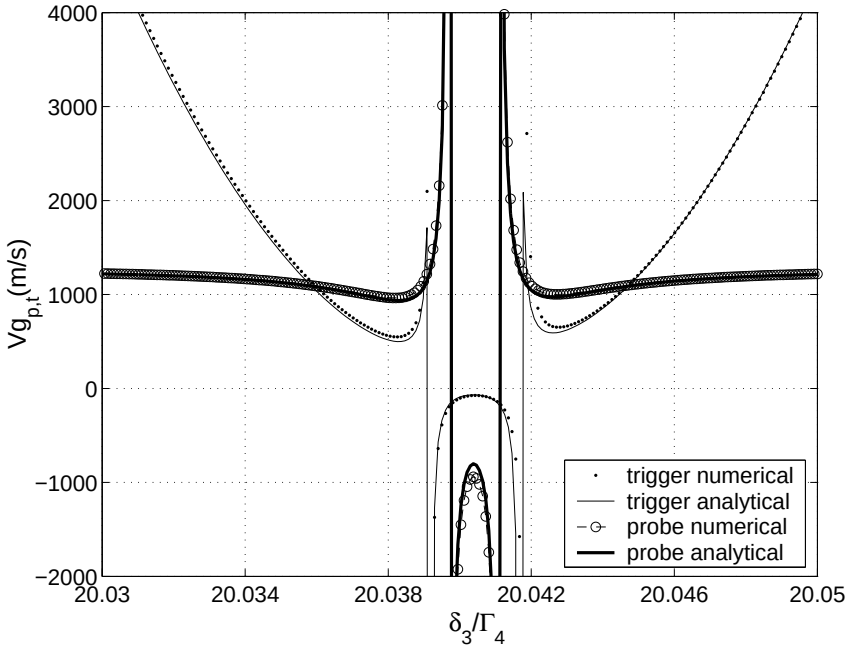


Figure 3.6: Group velocity of the probe and trigger pulses versus the normalized trigger detuning $\delta_3/\Gamma_4$. Full lines denote the analytical predictions of Eqs. (3.38) (the thick line refers to the probe and the thin line to the trigger). Circles and dots refer to the numerical solution of the OBE for the probe and trigger group velocity, respectively. This figure shows how it is possible to obtain group velocity matching in the asymmetric $M$-scheme: two different values of $\delta_3$ exist for which $v_g^P = v_g^T \simeq 1000$ m/s. The parameters are those of the $D_1$ and $D_2$ line in the $^{87}$Rb spectrum: $\Gamma_2^{AV} = \Gamma_2 \simeq 36$ MHz, $\Gamma_4^{AV} = \Gamma_4 \simeq 38$ MHz, $\delta_1 = \delta_2 = 0$, $\delta_4 \simeq \delta_3 \simeq 20\Gamma_4$, $\Omega_1 = 0.08\Gamma_4$, $\Omega_2 = 2\Gamma_4$, $\Omega_3 = 0.04\Gamma_4$, $\Omega_4 = \Gamma_4$, $\forall$ i,j, $\gamma_{ij} = \Gamma_3^{AV} = \Gamma_5^{AV} = 10^{-4}\Gamma_4$, $N/V = 3.0 \cdot 10^{13}$ cm$^{-3}$.

### 3.2.4 Pulse propagation

In previous Section, we have addressed the problem of group velocity matching between probe and trigger fields in the asymmetric M-scheme. It should be emphasized that the analysis and the results presented there are strictly valid for the continuous-wave (cw) fields. We would now address that same problem but with the pulsed probe and trigger fields in mind. At first look, Eqs. (34) appear to suggest that the group velocity matching would not be possible in the pulsed regime. As the group velocity of the trigger pulse is inversely proportional to the square of the probe pulse, trigger suffers anomalous nonlinear dispersion, i.e. in the presence of a pulsed probe, the trigger pulse will get distorted, splitting into several components, each having a different group velocity.

It will be shown in this Section that the above conclusion is an artifact of the usual approximations made to obtain a closed and compact expression for group velocities. In particular, the pulse propagation in this approximation is described by Eqs. (3.31), with group velocities $v_g^i$ given by Eqs. (3.38) and nonlinear susceptibilities $\chi_i$ being those of Eqs. (3.15). This is equivalent to the adiabatic elimination of the atomic degrees of freedom. Such adiabatic elimination, strictly speaking, is not valid in the parameter regime explored in this paper: strong nonlin-

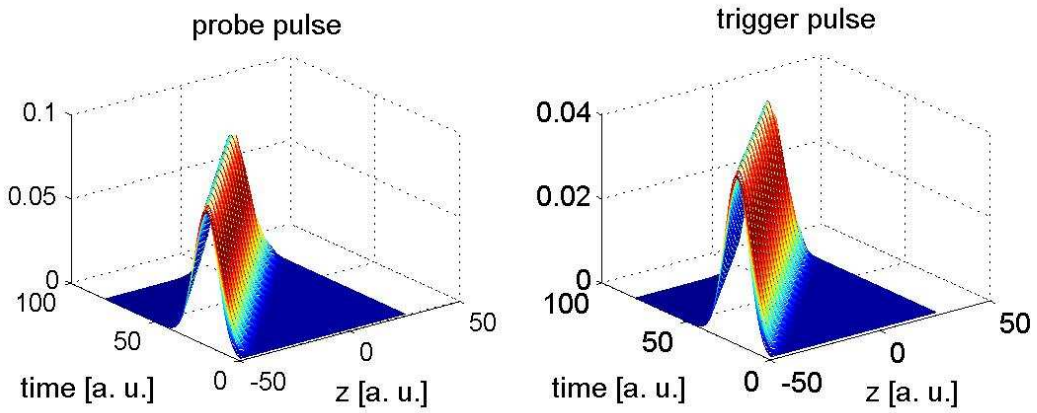


Figure 3.7: Pulse propagation in the AMS, in regime of long pulses in time.

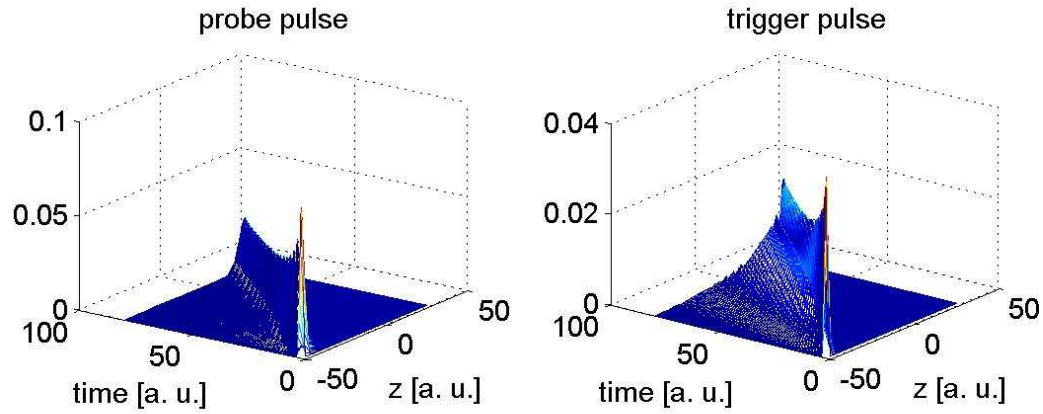


Figure 3.8: Pulse propagation in the AMS in regime of short pulses in time.

ear interaction between probe and trigger pulses suggests that the contribution of the atomic medium is far from being adiabatic. Also, it should be noted that the dephasing processes have been neglected in the derivation of $v_g^i$. For the adiabatic case, the above conclusion is correct: the trigger pulse suffers anomalous dispersion and its group velocity becomes singular towards the edges of a probe pulse. However, pulse propagation through the asymmetric M-system do not follow such a simple approximate evolution. Full propagation problem must then be solved which includes adding the time-dependent equations for the pulses to the OBEs A.23, and numerically solving the resulting system of equations. In the above equation, it is understood that $\sigma_P = \sigma_{12}$ and $\sigma_T = \sigma_{34}$.

$$\Big(\frac{\partial}{\partial z} + \frac{1}{c}\frac{\partial}{\partial t}\Big)\mathcal{E}_i(z,t) = \imath\frac{k_i}{2}\frac{N\mu_i}{V\epsilon_0}\sigma_i(z,t), \qquad i = P,T, \tag{3.39}$$

results are shown in Fig.3.7 and in Fig.3.8, for the same set of parameters that give group velocity matching in previous sections. Vertical axes are scaled with the spontaneous emission

parameters. We can see the emergence of two different regimes, a long-pulse regime, and a short-pulse regime. Here with long and short we mean in time. The inverse of this "length" is compared with the transparency window. Long pulse (narrow frequency bandwidth) fit well in the transparency window, while long pulse (wide frequency band) do not. In the case of long pulses propagate troughs the medium with untouched amplitude, only a small reduction of the amplitude is due to the presence of not perfect EIT condition and then to the non-zero imaginary part of susceptibility. For the short pulses the situation is completely different. It is clear from Fig.3.8, that the pulses are distorted, because they spread outside the transparency window. Trigger, as the probe, shows a reduction of the amplitude, moreover it also split into several components which then continue to propagate with a different group velocity each.

It is also noted that in the long-pulse regime, both of the pulses propagate virtually undistorted, with a group velocity uniform across each of the pulses. Our simulations suggest that the approximate Eqs. (34) are valid, as long as the Rabi frequencies there are considered to be taken at the peak of the pulse, i.e. $\Omega_i \to \Omega_{peak}$.

## 3.3 The Symmetric M–scheme

In this section we analyze the symmetric M–scheme [84], schematically shown in Fig. 3.9. The initial conditions and the configuration of the fields are slightly different from those of the asymmetric case of Sec. 3.2. The same five levels could be used, but all the atoms are now initially prepared in level $|3\rangle$ (see Fig. 3.9). Moreover, the role of the probe and of the coupler fields are exchanged, i.e., now the probe field (still with Rabi frequency $\Omega_1$ and central frequency $\omega_1$) couples levels $|2\rangle$ and $|3\rangle$, while the coupler (still with Rabi frequency $\Omega_2$ and central frequency $\omega_2$) induces transitions between levels $|1\rangle$ and $|2\rangle$. The role of trigger and tuner fields remains unchanged. In such a way, the scheme becomes symmetric for probe and trigger, and the two fields experience *exactly* the same dynamics whenever the corresponding parameters are made equal, i.e., when the Rabi frequencies are correspondingly equal ($\Omega_1 = \Omega_3$, $\Omega_2 = \Omega_4$), as well as the detunings, ($\delta_1 = \delta_3$, $\delta_2 = \delta_4$), which are now defined similarly to those of the asymmetric $M$ scheme (see Eqs. (3.1)) except for probe-coupler exchange, i.e.,

$$E_2 - E_1 = \hbar\omega_2 + \hbar\delta_2, \tag{3.40a}$$
$$E_2 - E_3 = \hbar\omega_1 + \hbar\delta_1, \tag{3.40b}$$
$$E_4 - E_3 = \hbar\omega_3 + \hbar\delta_3, \tag{3.40c}$$
$$E_4 - E_5 = \hbar\omega_4 + \hbar\delta_4. \tag{3.40d}$$

In this way, the scheme can be seen again as formed by two adjacent $\Lambda$, one for the probe and one for the trigger, now however symmetrically placed with respect to state $|3\rangle$. As we have done for the asymmetric $M$ scheme, we assume to stay close to the two-photon resonance conditions, $\delta_1 \simeq \delta_2$ and $\delta_3 \simeq \delta_4$, and moreover that $|\Omega_1| \ll |\Omega_2|$, and $|\Omega_3| \ll |\Omega_4|$, so that both probe and trigger will experience EIT. As we have seen above, a large XPM is obtained when the group velocities are equal [31, 59, 71, 73, 77, 83], and the advantage of the present symmetric M–scheme is that group velocity matching is automatically achieved once that the scheme is exactly symmetric between probe and trigger.

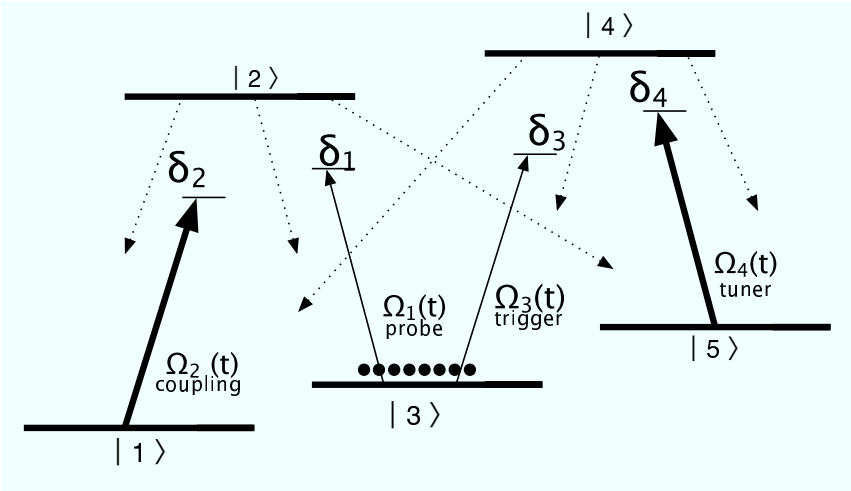


Figure 3.9: Symmetric $M$ scheme. The probe and the trigger fields, with Rabi frequencies $\Omega_1$ and $\Omega_3$ respectively, together with the stronger pump fields, the coupler and the tuner (with Rabi frequencies $\Omega_2$ and $\Omega_4$, respectively) drive the corresponding transitions. All the atoms are assumed to be in state $|3\rangle$ and the detunings are defined in Eqs. (4.2).

The Hamiltonian of the system is

$$\begin{aligned} H_S &= \sum_i^5 E_i|i\rangle\langle i| + \hbar\left(\Omega_1 e^{-i\omega_1 t}|2\rangle\langle 3| + \Omega_2 e^{-i\omega_2 t}|2\rangle\langle 1|\right. \\ &\quad \left. + \Omega_3 e^{-i\omega_3 t}|4\rangle\langle 3| + \Omega_4 e^{-i\omega_4 t}|4\rangle\langle 5| + h.c.\right). \end{aligned} \tag{3.41}$$

Moving to the interaction picture with respect to the following free Hamiltonian

$$\begin{aligned} H_0' &= E_3|3\rangle\langle 3| + (E_2 - \hbar\delta_1)|2\rangle\langle 2| + (E_1 - \hbar\delta_{12})|1\rangle\langle 1| \\ &\quad +(E_4 - \hbar\delta_3)|4\rangle\langle 4| + (E_5 - \hbar\delta_{34})|5\rangle\langle 5|, \end{aligned} \tag{3.42}$$

where

$$\delta_{12} = \delta_1 - \delta_2, \tag{3.43a}$$

$$\delta_{34} = \delta_3 - \delta_4, \tag{3.43b}$$

we get the following effective Hamiltonian

$$\begin{aligned} H_{eff}^S &= \hbar\delta_1|2\rangle\langle 2| + \hbar\delta_{12}|1\rangle\langle 1| + \hbar\delta_3|4\rangle\langle 4| + \hbar\delta_{34}|5\rangle\langle 5| \\ &+\hbar\Omega_1|2\rangle\langle 3| + \hbar\Omega_2|2\rangle\langle 1| + \hbar\Omega_3|4\rangle\langle 3| + \hbar\Omega_4|4\rangle\langle 5| \\ &+\hbar\Omega_1^\star|3\rangle\langle 2| + \hbar\Omega_2^\star|1\rangle\langle 2| + \hbar\Omega_3^\star|3\rangle\langle 4| + \hbar\Omega_4^\star|5\rangle\langle 4|. \end{aligned} \tag{3.44}$$

### 3.3.1 Amplitude Variables Approach

We first study the system dynamics by means of the AV approach, in which the state of the atom is described by the wave-function of Eq. (3.6), whose time evolution is determined by

the Hamiltonian of Eq. (3.44), supplemented with phenomenological decay rates $\Gamma_i^{AV}$ for each atomic level $|i\rangle$. The corresponding evolution equations for the amplitudes $b_i(t)$ are

$$\begin{aligned}
\dot{b}_1(t) &= -\imath d_1 b_1(t) - \imath\Omega_2^\star b_2(t), && (3.45a)\\
\dot{b}_2(t) &= -\imath d_2 b_2(t) - \imath\Omega_2 b_1(t) - \imath\Omega_1 b_3(t), && (3.45b)\\
\dot{b}_3(t) &= -\imath d_3 b_3 - \imath\Omega_1^\star b_2(t) - \imath\Omega_3^\star b_4(t), && (3.45c)\\
\dot{b}_4(t) &= -\imath d_4 b_4(t) - \imath\Omega_3 b_3(t) - \imath\Omega_4 b_5(t), && (3.45d)\\
\dot{b}_5(t) &= -\imath d_5 b_5(t) - \imath\Omega_4^\star b_4(t), && (3.45e)
\end{aligned}$$

where, similarly to what we have done for the asymmetric case, we have defined

$$\begin{aligned}
d_1 &= \delta_{12} - \imath\Gamma_1^{AV}/2, && (3.46a)\\
d_2 &= \delta_1 - \imath\Gamma_2^{AV}/2, && (3.46b)\\
d_3 &= -\imath\Gamma_3^{AV}/2, && (3.46c)\\
d_4 &= \delta_3 - \imath\Gamma_4^{AV}/2, && (3.46d)\\
d_5 &= \delta_{34} - \imath\Gamma_5^{AV}/2. && (3.46e)
\end{aligned}$$

Since we choose again $|\Omega_1/\Omega_2| \ll 1$ and $|\Omega_3/\Omega_4| \ll 1$, it is reasonable to assume that the atomic population remains in the initial state $|3\rangle$ to a good approximation

$$b_3^{ss} \sim 1. \tag{3.47}$$

The set of equations (3.45) is then solved in the steady-state. In order to get a consistent expression for the nonlinear susceptibilities one has to consider higher order contributions to Eq. (3.47), which is obtained by imposing the normalization of the atomic wave-function of Eq. (3.6) at second order in $|\Omega_1/\Omega_2|$ and $|\Omega_3/\Omega_4|$. One gets the following expression for the steady state amplitudes

$$\begin{aligned}
b_3^{ss} &= 1 - \frac{|\Omega_1|^2\left[|d_1|^2 + |\Omega_2|^2\right]}{2\left|d_1 d_2 - |\Omega_2|^2\right|^2} - \frac{|\Omega_3|^2\left[|d_5|^2 + |\Omega_4|^2\right]}{2\left|d_4 d_5 - |\Omega_4|^2\right|^2}, && (3.48a)\\
b_2^{ss} &= -\frac{\Omega_1 d_1}{d_1 d_2 - |\Omega_2|^2} b_3^{ss}, && (3.48b)\\
b_4^{ss} &= -\frac{\Omega_3 d_5}{d_5 d_4 - |\Omega_4|^2} b_3^{ss}, && (3.48c)\\
b_1^{ss} &= \frac{\Omega_1\Omega_2^\star}{d_1 d_2 - |\Omega_2|^2} b_3^{ss}, && (3.48d)\\
b_5^{ss} &= \frac{\Omega_3\Omega_4^\star}{d_5 d_4 - |\Omega_4|^2} b_3^{ss}. && (3.48e)
\end{aligned}$$

These results can be used to determine the probe and trigger susceptibilities, which are now defined as (see Eqs. (3.12))

$$\begin{aligned}
\chi_P &= \frac{N\mu_{32}}{V\varepsilon_0\mathcal{E}_1} b_2^{ss} b_3^{ss,\star} = -\frac{N|\mu_{32}|^2}{V\hbar\varepsilon_0\Omega_1} b_2^{ss} b_3^{ss,\star}, && (3.49a)\\
\chi_T &= \frac{N\mu_{34}}{V\varepsilon_0\mathcal{E}_3} b_4^{ss} b_3^{ss,\star} = -\frac{N|\mu_{34}|^2}{V\hbar\varepsilon_0\Omega_3} b_4^{ss} b_3^{ss,\star}. && (3.49b)
\end{aligned}$$

Inserting Eqs. (3.48) into Eqs. (3.49) and expanding in series at the lowest orders in the probe and trigger electric fields, $\mathcal{E}_1$ and $\mathcal{E}_3$ respectively, one gets

$$\chi_P \simeq \chi_P^{(1)} + \chi_P^{(3,sk)}|\mathcal{E}_1|^2 + \chi_P^{(3,ck)}|\mathcal{E}_3|^2, \tag{3.50a}$$
$$\chi_T \simeq \chi_T^{(1)} + \chi_T^{(3,sk)}|\mathcal{E}_3|^2 + \chi_T^{(3,ck)}|\mathcal{E}_1|^2, \tag{3.50b}$$

where we have again distinguished the third-order self-Kerr susceptibilities $\chi_{P,T}^{(3,sk)}$ from the third-order cross-Kerr susceptibilities $\chi_{P,T}^{(3,ck)}$. Using Eqs. (3.48) and the definitions of Eqs. (3.46), we get the following expressions for the linear susceptibilities,

$$\chi_P^{(1)} = \frac{N|\mu_{32}|^2}{V\hbar\varepsilon_0}\frac{\delta_{12} - i\Gamma_1^{AV}/2}{\left(\delta_1 - i\Gamma_2^{AV}/2\right)\left(\delta_{12} - i\Gamma_1^{AV}/2\right) - |\Omega_2|^2} \tag{3.51a}$$
$$\chi_T^{(1)} = \frac{N|\mu_{34}|^2}{V\hbar\varepsilon_0}\frac{\delta_{34} - i\Gamma_5^{AV}/2}{\left(\delta_3 - i\Gamma_4^{AV}/2\right)\left(\delta_{34} - i\Gamma_5^{AV}/2\right) - |\Omega_4|^2} \tag{3.51b}$$

and the following ones for the nonlinear susceptibilities,

$$\chi_P^{(3,sk)} = \frac{N|\mu_{32}|^4}{V\hbar^3\varepsilon_0}\frac{-d_{12}^{sym}\left[|d_{12}^{sym}|^2 + |\Omega_2|^2\right]}{\left[d_1^{sym}d_{12}^{sym} - |\Omega_2|^2\right]\left|d_1^{sym}d_{12}^{sym} - |\Omega_2|^2\right|^2}, \tag{3.52a}$$
$$\chi_T^{(3,sk)} = \frac{N|\mu_{34}|^4}{V\hbar^3\varepsilon_0}\frac{-d_{34}^{sym}\left[|d_{34}^{sym}|^2 + |\Omega_4|^2\right]}{\left[d_3^{sym}d_{34}^{sym} - |\Omega_4|^2\right]\left|d_3^{sym}d_{34}^{sym} - |\Omega_4|^2\right|^2}, \tag{3.52b}$$
$$\chi_P^{(3,ck)} = \frac{N|\mu_{32}|^2|\mu_{34}|^2}{V\hbar^3\varepsilon_0}\frac{-d_{12}^{sym}\left[|d_{34}^{sym}|^2 + |\Omega_4|^2\right]}{\left[d_1^{sym}d_{12}^{sym} - |\Omega_2|^2\right]\left|d_3^{sym}d_{34}^{sym} - |\Omega_4|^2\right|^2}, \tag{3.52c}$$
$$\chi_T^{(3,ck)} = \frac{N|\mu_{32}|^2|\mu_{34}|^2}{V\hbar^3\varepsilon_0}\frac{-d_{34}^{sym}\left[|d_{12}^{sym}|^2 + |\Omega_2|^2\right]}{\left[d_3^{sym}d_{34}^{sym} - |\Omega_4|^2\right]\left|d_1^{sym}d_{12}^{sym} - |\Omega_2|^2\right|^2}, \tag{3.52d}$$

where the complex detuning $d_1^{sym}, d_3^{sym}$, and $d_{12}^{sym}, d_{34}^{sym}$ have been defined as

$$d_1^{sym} = \delta_1 - i\Gamma_2^{AV}/2 \tag{3.53}$$
$$d_{12}^{sym} = \delta_{12} - i\Gamma_1^{AV}/2 \tag{3.54}$$
$$d_3^{sym} = \delta_3 - i\Gamma_4^{AV}/2 \tag{3.55}$$
$$d_{34}^{sym} = \delta_{34} - i\Gamma_5^{AV}/2. \tag{3.56}$$

From previous equations, first of all, we note that the expressions of the probe and trigger susceptibilities above are completely symmetric. This means that probe and trigger experience the same linear and Kerr susceptibilities, as soon as the corresponding parameters correspond, i.e., $\mu_{32} = \mu_{34}$, $\Omega_1 = \Omega_3$, $\Omega_2 = \Omega_4$, $\delta_1 = \delta_3$, $\delta_2 = \delta_4$, $\Gamma_1^{AV} = \Gamma_5^{AV}$, $\Gamma_2^{AV} = \Gamma_4^{AV}$. Moreover, the probe linear susceptibility of Eq. (3.51a) and the self-Kerr susceptibility of Eq. (3.52a) coincide with the corresponding ones of the asymmetric case, Eq. (3.14) and Eq. (3.15a) respectively, because the phenomenological decay rate $\Gamma_1^{AV}$ here plays just the same role of the phenomenological decay rate $\Gamma_3^{AV}$ of the asymmetric scheme. This is not surprising, since the probe response in the absence of the trigger field is the same in the two $M$ scheme studied

here. Finally the cross-Kerr susceptibilities of the two schemes are generally different, both for the probe and the trigger, even though they possess a similar structure. The main relevant difference between the two cross-Kerr susceptibilities is in the dependence of their real parts upon the detunings. In fact, in the asymmetric case both real parts are proportional to the composite detuning $\delta_{14} = \delta_{12} + \delta_{34}$ (see Eqs. (3.4) and (3.43)), so that one has a nonzero XPM as soon as one of the two $\Lambda$ subsystem is shifted from the two-photon resonance condition. In the symmetric case instead, $\mathrm{Re}\{\chi_P^{(3,ck)}\}$ is proportional to $\delta_{12}$ and $\mathrm{Re}\{\chi_T^{(3,ck)}\}$ is proportional to $\delta_{34}$, and the two-photon resonance condition has to be violated by *both* $\Lambda$ subsystems if each field has to experience a nonzero XPM.

### 3.3.2 Comparison with the Optical Bloch Equations

We now study the dynamics of the symmetric $M$ scheme of Fig. 3.9 by means of the OBE, which allows to describe spontaneous emission and dephasing more rigorously. Due to the similarity of the symmetric and asymmetric $M$ schemes, we consider the same spontaneous emission and dephasing processes described in section 3.2.2. As a consequence, the master equation for the atomic density operator $\sigma$ is again given by Eq. (3.23), with the only difference that the Hamiltonian $H_{eff}^{AS}$ is replaced by the corresponding Hamiltonian $H_{eff}^{S}$ of the symmetric scheme, given by Eq. (3.44). The corresponding system of OBE's is displayed in Appendix A.2.2 as Eqs. (A.25) and (A.26), where we have used the definitions of Eqs. (3.24)-(3.26).

Also in this symmetric case, the OBE are less suited for an approximate analytical treatment with respect to the AV equations of the preceding section. In fact, if we consider the conditions $|\Omega_1/\Omega_2| \ll 1$ and $|\Omega_3/\Omega_4| \ll 1$ and, consistently with Eq. (3.47), we assume that

$$\sigma_{33} \approx 1, \tag{3.57a}$$

$$\sigma_{jj} \approx 0, \quad j = 1, 2, 4, 5, \tag{3.57b}$$

at the steady state, it is possible to see that by inserting Eqs. (3.27) into Eqs. (A.26) for the coherences, one gets a satisfactory expression for the probe linear susceptibility only. To be more specific, only the approximate linear susceptibility fits well with the numerical solution of the OBE. It is not easy to derive analytical expressions from Eqs. (A.25) and (A.26) for the nonlinear susceptibilities which would be as simple as those of Eqs. (3.52) and which would reproduce in the same way the exact numerical solution of the OBE within the EIT regime. Again, one could exactly solve analytically the OBE, but the resulting expressions are very cumbersome and not physically transparent as those of Eqs. (3.52). For this reason we will analytically derive from the OBE the probe linear susceptibility only, and we will then use the OBE only for the numerical determination of the atomic steady state. In addition, deriving this result will enable us to draw a formal analogy between the AV and OBE treatments (see Eqs. (3.60) below).

The probe and trigger susceptibilities are now defined as

$$\chi_P = \frac{N\mu_{32}}{V\varepsilon_0\mathcal{E}_1}\sigma_{32} = -\frac{N|\mu_{32}|^2}{V\hbar\varepsilon_0\Omega_1}\sigma_{32}, \tag{3.58a}$$

$$\chi_T = \frac{N\mu_{34}}{V\varepsilon_0\mathcal{E}_3}\sigma_{34} = -\frac{N|\mu_{34}|^2}{V\hbar\varepsilon_0\Omega_3}\sigma_{34}. \tag{3.58b}$$

Using Eqs. (3.57) and performing a series expansion at the lowest order in the probe and trigger

fields, we arrive at the following expressions for the probe and trigger linear susceptibilities

$$\chi_P^{(1)} = \frac{N|\mu_{32}|^2}{V\hbar\varepsilon_0} \frac{\delta_{12} - i\gamma_{13}/2}{[\delta_{12} - i\gamma_{13}/2]\,[\delta_1 - i\,(\Gamma_2 + \gamma_{12})/2] - |\Omega_2|^2}, \tag{3.59a}$$

$$\chi_T^{(1)} = \frac{N|\mu_{34}|^2}{V\hbar\varepsilon_0} \frac{\delta_{34} - i\gamma_{53}/2}{[\delta_{34} - i\gamma_{53}/2]\,[\delta_3 - i\,(\Gamma_4 + \gamma_{54})/2] - |\Omega_4|^2}. \tag{3.59b}$$

The probe linear susceptibility of Eq. (3.59a) coincides with that of the asymmetric $M$ scheme of Eq. (3.29), as it must be, since the linear properties of the probe in the two $M$ schemes are identical. Moreover, as noted before, due to the symmetry of the scheme, this probe linear susceptibility coincides with that of the trigger of Eq. (3.59b) when the corresponding parameters coincide, i.e., $\mu_{32} = \mu_{34}$, $\delta_1 = \delta_3$, $\delta_2 = \delta_4$, $\Omega_2 = \Omega_4$, $\Gamma_2 = \Gamma_4$, $\gamma_{54} = \gamma_{12}$ and $\gamma_{53} = \gamma_{13}$. By comparing Eqs. (3.59) with Eqs. (3.51), one can also see that the AV and OBE predictions for the linear susceptibilities again coincide provided that the phenomenological decay rates $\Gamma_i^{AV}$ are appropriately interpreted, i.e.,

$$\Gamma_2^{AV} \leftrightarrow \Gamma_2 + \gamma_{12}, \tag{3.60a}$$

$$\Gamma_1^{AV} \leftrightarrow \gamma_{13}, \tag{3.60b}$$

$$\Gamma_4^{AV} \leftrightarrow \Gamma_4 + \gamma_{54}, \tag{3.60c}$$

$$\Gamma_5^{AV} \leftrightarrow \gamma_{53}. \tag{3.60d}$$

This shows again that the intuitive interpretation of the phenomenological decay rates $\Gamma_i^{AV}$ as spontaneous emission total decay rates for the excited states, and as dephasing rates in the case of ground state sublevels, is essentially correct.

We then consider the numerical solution of the OBE and we compare it with the analytical treatment based on the AV approach. The numerical calculations are again performed in the limits discussed above, i.e., $|\Omega_1|, |\Omega_2| \ll |\Omega_3|, |\Omega_4|$ and we stay near the Raman resonance for both the probe and the trigger. In Figs. 3.10-3.12 we compare the analytical solutions of Eqs. (3.51) and Eqs. (3.52) with the numerical solution of the complete set of Bloch equations given in the Appendix B. Fig. 3.10 shows the linear susceptibilities and refers to a perfectly symmetric situation between probe and trigger, i.e., $\Gamma_2^{AV} = \Gamma_2 = \Gamma_4^{AV} = \Gamma_4 = \Gamma = 2\pi \times 6$ MHz, $\Omega_1 = \Omega_3 = 0.08\Gamma$, $\Omega_2 = \Omega_4 = \Gamma$, $\delta_2 = \delta_4 = 0$, $\forall$ i,j $\gamma_{ij} = \Gamma_1^{AV} = \Gamma_5^{AV} = 10^{-4}\Gamma$. As a consequence, the probe and trigger linear susceptibilities as a function of the respective detunings $\delta_1$ and $\delta_3$ are two indistinguishable curves. In such a case, group velocity matching is automatically guaranteed whenever $\mu_{32} = \mu_{34}$. Fig. 3.10 shows that Eqs. (3.51) work very well, except when the detunings correspond to the maximum probe (or trigger) absorption. In such a case, the detunings match the Rabi frequencies of the two pumps, and the probe (or trigger) field is in resonance with a single atomic transition. The atoms are significantly pumped to the excited levels and the population assumption of Eq. (3.47) is no more fulfilled.

Fig. 3.11 shows the cross-Kerr susceptibilities again in a perfectly symmetric situation between probe and trigger so that their plots as a function of the respective detunings $\delta_1$ and $\delta_3$ exactly coincide. However, in order to reduce as much as possible the influence due to the simultaneous presence of the self-Kerr susceptibility, we have considered a probe Rabi frequency $\Omega_1$ much smaller than that of the trigger in the $\chi_P^{(3,ck)}$ plot and *viceversa* a trigger Rabi frequency $\Omega_3$ much smaller than that of the probe in the $\chi_T^{(3,ck)}$ plot. To be more precise, Fig. 3.11 refers to $\Gamma_2^{AV} = \Gamma_2 = \Gamma_4^{AV} = \Gamma_4 = \Gamma = 2\pi \times 6$ MHz, $\Omega_2 = \Omega_4 = \Gamma$, $\delta_2 = \delta_4 = 0$, $\forall$ i,j $\gamma_{ij} = \Gamma_1^{AV} = \Gamma_5^{AV} = 10^{-4}\Gamma$, and $\Omega_1 = 0.002\Gamma$, $\Omega_3 = 0.08\Gamma$ in the case of the $\chi_P^{(3,ck)}$ plot, and

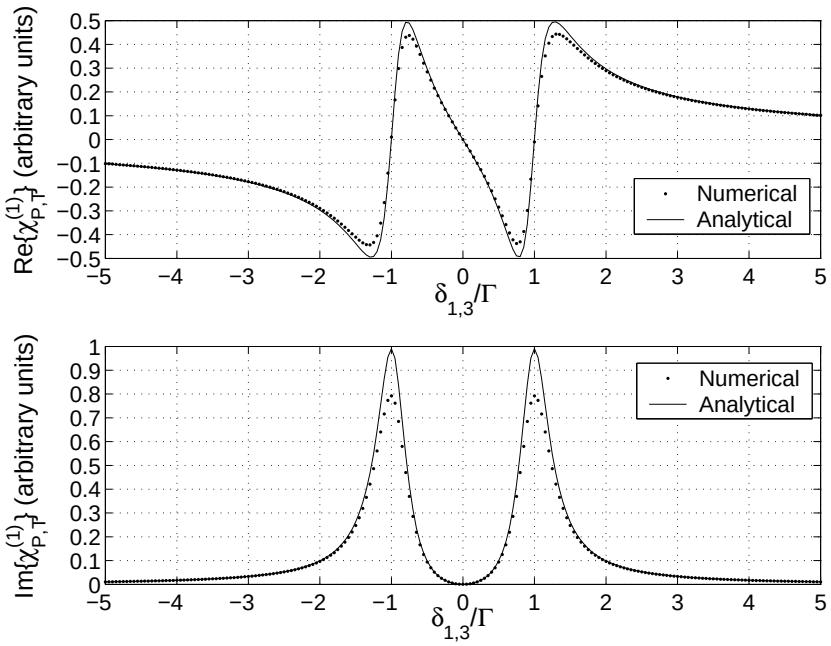


Figure 3.10: Comparison of the numerical solution (dotted line) of the OBE with the analytical prediction of Eqs. (3.51) (full line) for the real part (above) and imaginary part (below) of both probe and trigger linear susceptibilities versus their respective normalized probe detunings $\delta_1/\Gamma$ and $\delta_3/\Gamma$. Probe and trigger susceptibilities exactly overlap because we consider the perfectly symmetric situation $\Gamma_2^{AV} = \Gamma_2 = \Gamma_4^{AV} = \Gamma_4 = \Gamma = 2\pi \times 6$ MHz, $\Omega_1 = \Omega_3 = 0.08\Gamma$, $\Omega_2 = \Omega_4 = \Gamma$, $\delta_2 = \delta_4 = 0$, $\forall$ i,j $\gamma_{ij} = \Gamma_1^{AV} = \Gamma_5^{AV} = 10^{-4}\Gamma$, $\mu_{32} = \mu_{34}$, which guarantees perfect group velocity matching.

to $\Omega_3 = 0.002\Gamma$, $\Omega_1 = 0.08\Gamma$ in the case of the $\chi_T^{(3,ck)}$ plot. We can see from Fig. 3.11 that the AV approach gives a satisfactory description also for the cross-Kerr susceptibility, except when probe or trigger absorption is maximum, as it happens for the linear case.

Finally Fig. 3.12 shows the self-Kerr susceptibilities again in a perfectly symmetric situation between probe and trigger. As a consequence their plots versus the respective detunings $\delta_1$ and $\delta_3$ exactly coincide. Here, in order to reduce the influence due to the simultaneous presence of the cross-Kerr susceptibility, we have considered a trigger Rabi frequency $\Omega_3$ much smaller than that of the probe in the $\chi_P^{(3,sk)}$ plot and *viceversa* a probe Rabi frequency $\Omega_1$ much smaller than that of the trigger in the $\chi_T^{(3,sk)}$ plot. The parameters are the same as in Fig. 3.11, except that here we have chosen $\Omega_2 = \Omega_4 = 2\Gamma$, $\Omega_1 = 0.4\Gamma$, $\Omega_3 = 0.004\Gamma$ in the case of the $\chi_P^{(3,sk)}$ plot, and $\Omega_3 = 0.4\Gamma$, $\Omega_1 = 0.004\Gamma$ in the case of the $\chi_T^{(3,sk)}$ plot. The agreement between the AV prediction and the numerical solution of the OBE is satisfactory.

## 3.4 Group velocity matching

As we have seen in section 3.2.3, the condition of group velocity matching is of fundamental importance for achieving a large cross-phase modulation between probe and trigger fields. It is

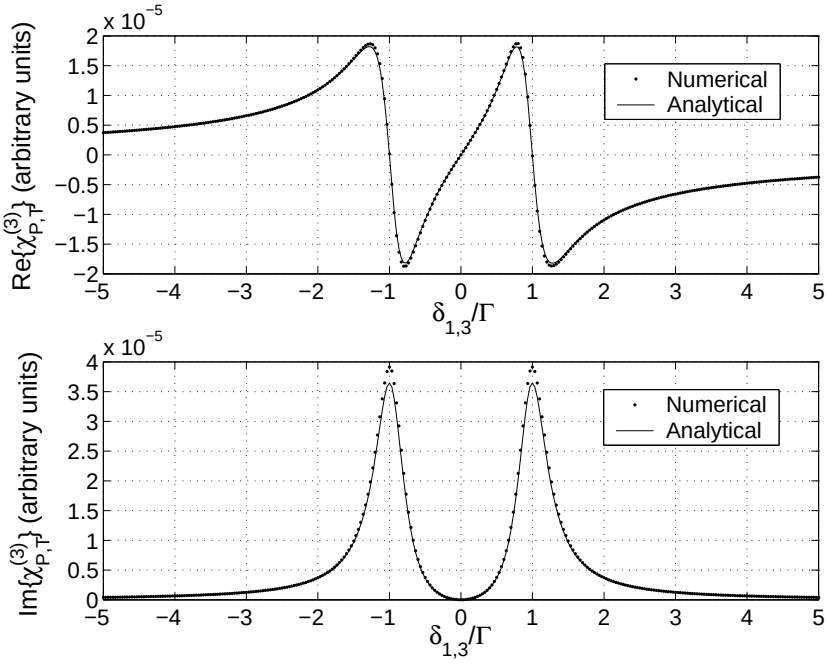


Figure 3.11: Comparison of the numerical solution (dotted line) of the OBE with the analytical prediction of Eqs. (3.52c,d) (full line) for the real part (above) and imaginary part (below) of both probe and trigger cross-Kerr susceptibilities versus their respective normalized probe detunings $\delta_1/\Gamma$ and $\delta_3/\Gamma$. Probe and trigger susceptibilities exactly overlap because we consider a perfectly symmetric situation: $\Gamma_2^{AV} = \Gamma_2 = \Gamma_4^{AV} = \Gamma_4 = \Gamma = 2\pi \times 6$ MHz, $\Omega_2 = \Omega_4 = \Gamma$, $\delta_2 = \delta_4 = 0$, $\forall$ i,j $\gamma_{ij} = \Gamma_1^{AV} = \Gamma_5^{AV} = 10^{-4}\Gamma$; moreover we have chosen $\Omega_1 = 0.002\Gamma$, $\Omega_3 = 0.08\Gamma$ in the case of the $\chi_P^{(3,ck)}$ plot, and *viceversa* $\Omega_3 = 0.002\Gamma$, $\Omega_1 = 0.08\Gamma$ in the case of the $\chi_T^{(3,ck)}$ plot, in order to reduce as much as possible the influence of the self-Kerr susceptibilities.

evident from the inherent symmetry of the present scheme that the condition of equal probe and trigger group velocities is automatically achieved when the corresponding parameters are equal i.e., $\mu_{32} = \mu_{34}$, $\delta_1 = \delta_3$, $\delta_2 = \delta_4$, $\Omega_2 = \Omega_4$, $\Gamma_2 = \Gamma_4$, $\gamma_{54} = \gamma_{12}$ and $\gamma_{53} = \gamma_{13}$, $\omega_1 \simeq \omega_3$. This is the main advantage of the symmetric $M$ scheme over the asymmetric one. The contribution of the nonlinear susceptibilities to $v_g$ is negligible with respect to that of the linear one, which is nonzero for both probe and trigger in this case (see Eqs. (3.50)). Therefore, approximating $\chi$ with the linear contribution $\chi^{(1)}$ and inserting Eqs. (3.51) into the definition (1.43), one gets the following expressions for the two group indices

$$n_g^P = \frac{N|\mu_{32}|^2}{2V\hbar\varepsilon_0}\mathrm{Re}\left\{\frac{d_1}{d_1 d_2 - |\Omega_2|^2} + \frac{\omega_1\left(d_1^2 + |\Omega_2|^2\right)}{\left(d_1 d_2 - |\Omega_2|^2\right)^2}\right\}, \tag{3.61a}$$

$$n_g^T = \frac{N|\mu_{34}|^2}{2V\hbar\varepsilon_0}\mathrm{Re}\left\{\frac{d_5}{d_5 d_4 - |\Omega_4|^2} + \frac{\omega_3\left(d_5^2 + |\Omega_4|^2\right)}{\left(d_5 d_4 - |\Omega_4|^2\right)^2}\right\}, \tag{3.61b}$$

where we have used the definitions of Eqs. (3.46) for $d_j$, $j = 1, 2, 4, 5$. The symmetry between probe and trigger discussed above is evident also in these expressions. Eqs. (1.42) and (3.61)

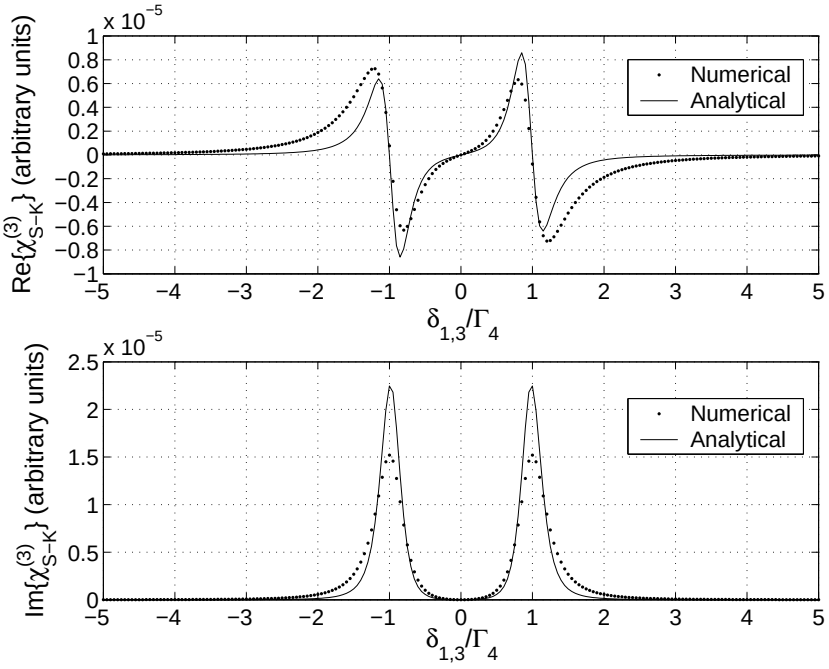


Figure 3.12: Comparison of the numerical solution (dotted line) of the OBE with the analytical prediction of Eqs. (3.52a,b) (full line) for the real part (above) and imaginary part (below) of both probe and trigger self-Kerr susceptibilities versus their respective normalized probe detunings $\delta_1/\Gamma$ and $\delta_3/\Gamma$. Probe and trigger susceptibilities exactly overlap because we consider a perfectly symmetric situation: $\Gamma_2^{AV} = \Gamma_2 = \Gamma_4^{AV} = \Gamma_4 = \Gamma = 2\pi \times 6$ MHz, $\Omega_2 = \Omega_4 = 2\Gamma$, $\delta_2 = \delta_4 = 0$, $\forall$ i,j $\gamma_{ij} = \Gamma_1^{AV} = \Gamma_5^{AV} = 10^{-4}\Gamma$; moreover we have chosen $\Omega_1 = 0.4\Gamma$, $\Omega_3 = 0.004\Gamma$ in the case of the $\chi_P^{(3,sk)}$ plot, and *viceversa* $\Omega_3 = 0.4\Gamma$, $\Omega_1 = 0.004\Gamma$ in the case of the $\chi_T^{(3,sk)}$ plot, in order to reduce as much as possible the influence of the cross-Kerr susceptibilities.

are now compared with the corresponding ones obtained from the integration of the full set of Bloch equations of Appendix A.2.2. The comparison is shown in Fig. 3.13, which refers to the completely symmetric situation between probe and trigger defined above and therefore shows exact group velocity matching for all values of the detunings $\delta_1 = \delta_3$. Fig. 3.13 shows an excellent agreement between analytical and numerical results. The only points in which the two curves do not coincide exactly are when the detunings match the Rabi frequencies of the two pumping field. In fact in this conditions the fields are in resonance with a single atomic transition and the atoms are pumped to the excited levels. The other points that determine the disagreement are in the vicinity of the peaks. In fact in these regions the derivatives are small, because of the change in slope of the real part of the susceptibilities. Hence, the group index of Eqs. (3.61) is small, and the group velocity jumps near $c$.

In some cases, the perfectly symmetric conditions guaranteeing group velocity matching, i.e., $\mu_{32} = \mu_{34}$, $\delta_1 = \delta_3$, $\delta_2 = \delta_4$, $\Omega_2 = \Omega_4$, $\Gamma_2 = \Gamma_4$, $\gamma_{54} = \gamma_{12}$ and $\gamma_{53} = \gamma_{13}$, are difficult to realize in practice. In fact, sometimes it may be convenient to use transitions with different Clebsch-Gordan coefficients, yielding therefore a significant discrepancy between $\mu_{32}$ and $\mu_{34}$. The other symmetry conditions above are less problematic because detunings and Rabi frequencies can

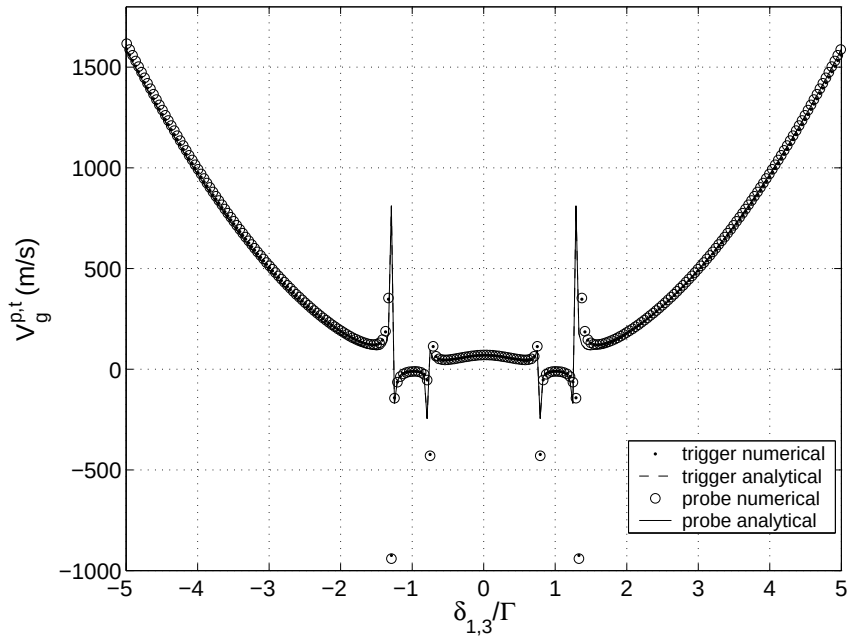


Figure 3.13: Group velocity of the probe and trigger pulses versus the normalized detunings $\delta_1/\Gamma = \delta_3/\Gamma$. Lines denote the analytical predictions of Eqs. (1.42) and (3.61) (the full line refers to the probe and the dashed line to the trigger). Circles and dots refer to the numerical solution of the OBE for the probe and trigger group velocity, respectively. Parameters correspond to the perfectly symmetric situation considered in Fig. 3.10, that is, $\Gamma_2^{AV} = \Gamma_2 = \Gamma_4^{AV} = \Gamma_4 = \Gamma = 2\pi \times 6$ MHz, $\Omega_1 = \Omega_3 = 0.08\Gamma$, $\Omega_2 = \Omega_4 = \Gamma$, $\delta_2 = \delta_4 = 0$, $\forall$ i,j $\gamma_{ij} = \Gamma_1^{AV} = \Gamma_5^{AV} = 10^{-4}\Gamma$, and we have chosen $\mu_{32} = \mu_{34} = 10^{-29}$ C ·m, and $N/V = 3.0 \times 10^{13}$ cm$^{-3}$. Due to symmetry, one has perfect group velocity matching within a large interval of values for the detunings.

always be made equal by the experimenter, and moreover decay and dephasing rates, even though not perfectly equal, are often comparable to each other. Just to give an example, one could implement the symmetric $M$ scheme of Fig. 3.9 by using the $D_1$ and $D_2$ line of the $^{87}$Rb spectrum.The Zeeman sublevels $|5P_{1/2}F = 1, m = 0\rangle$ and $|5P_{3/2}F = 1, m = 0\rangle$ could be chosen as levels $|2\rangle$ and $|4\rangle$, respectively, while the Zeeman sublevels $|5S_{1/2}F = 1, m = -1\rangle$, $|5S_{1/2}F = 2, m = 1\rangle$ and $|5P_{1/2}F = 1, m = 1\rangle$ could chosen as levels $|1\rangle$, $|3\rangle$ and $|5\rangle$, respectively (see also Ref. [59] for a similar choice). For these levels the atomic transitions related to the probe and trigger have dipole moment matrix elements $\mu_{32}$, $\mu_{34}$ differing by a factor $\sqrt{10}$, violating therefore the symmetry condition.

It is evident however that this slight asymmetry can be compensated (so that group velocity matching can be still achieved in a restricted but still useful range of detunings) by properly adjusting the Rabi frequencies of the tuner field $\Omega_4$ and of the coupling field $\Omega_2$, which will be no more equal. In fact, by imposing group velocity matching at the center of the transparency window, i.e., for $\delta_{12} = \delta_{34} = 0$, we derive the condition

$$\Omega_2 = \alpha\Omega_4, \tag{3.62}$$

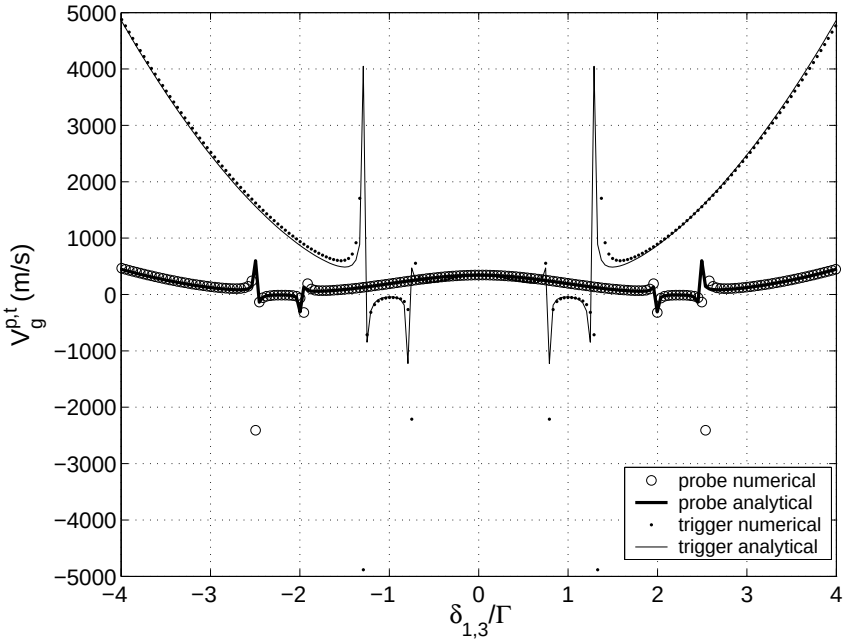


Figure 3.14: Group velocity of the probe and trigger pulses versus the normalized detunings $\delta_1/\Gamma = \delta_3/\Gamma$. Full lines denote the analytical predictions of Eqs. (1.42) and (3.61) (the thick line refers to the probe and the thin line to the trigger). Circles and dots refer to the numerical solution of the OBE for the probe and trigger group velocity, respectively. Parameters correspond to the five–level scheme derived from the $D_1$ and $D_2$ lines of the $^{87}$Rb spectrum described in the text, $\Gamma_2^{AV} = \Gamma_2 \simeq 36$ MHz, $\Gamma_4^{AV} = \Gamma_4 \simeq 38$ MHz, $\mu_{32} = 1.27 \times 10^{-29}$ C·m, $\mu_{34} = 5.7 \times 10^{-30}$ C·m, $\Omega_4 = \Gamma$, $\Omega_2 = 2.22\Gamma$, $\Omega_1 = \Omega_3 = 0.08\Gamma$, $\delta_2 = \delta_4 = 0$, $\forall$ i,j $\gamma_{ij} = \Gamma_1^{AV} = \Gamma_5^{AV} = 10^{-4}\Gamma$, $N/V = 3.0 \times 10^{13}$ cm$^{-3}$. The asymmetry between the two dipole moment matrix elements has been compensated by adjusting the value of $\Omega_2$. In this way group velocity matching is achieved within the entire EIT window.

where the *correction factor* $\alpha$ is given by

$$\alpha = \sqrt{\frac{|\mu_{32}|^2}{|\mu_{34}|^2}\frac{\omega_1}{\omega_3}}. \tag{3.63}$$

As shown in Fig. 3.14, if the adjustment condition of Eqs. (3.62) and (3.63) is taken into account, one still gets equal probe and trigger group velocities in the case of the $^{87}$Rb five–level scheme specified above, at least within the entire EIT window.

### 3.4.1 Role of the dephasings on absorption and group velocity matching.

The studied M-scheme show good performances for the nonlinear interactions and for the group velocity reduction even in presence of realistically dephasing process. Here we want to illustrate how destructive are the dephasing process, in particular for the group velocities matching. Group velocity matching is a crucial condition for the realization of a strong XPM. In previous

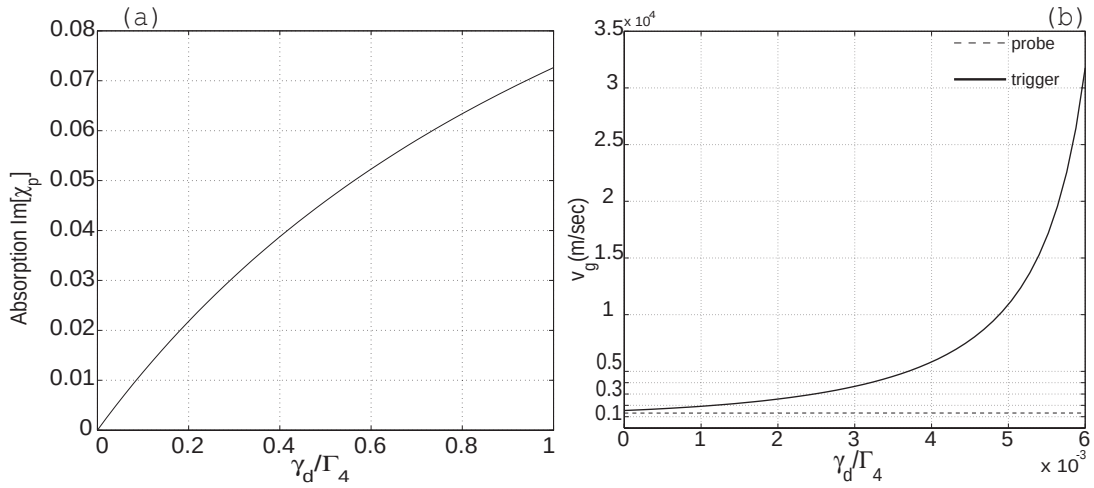


Figure 3.15: Numerical estimation of the effects of the ground states dephasings on the probe group velocity and on the linear absorption for the probe field. Parameters are $\Omega_1 \simeq 0.08\Gamma_4$, $\Omega_2 \simeq 2\Gamma_4$, $\Omega_3 \simeq 0.04\Gamma_4$ ,$\Omega_4 \simeq \Gamma_4$ and $\delta_1 = \delta_2 = 0$ , and $\delta_4 \simeq \delta_3 \simeq 20\Gamma_4$, with $\Gamma_4 \sim 38$Mhz, all the dephasings of the ground state are assumed to be equal.

section we have taken dephasing process three order of magnitude smaller then the spontaneous decay rate. Here we want to illustrate the effect of dephasing process on the matching of the two group velocity for the two M-schemes studied in the previous sections, and the effect on the imaginary part of linear susceptibility, i.e., on the absorption process. We have solved numerically the master equation of both the M-schemes and we have plotted the group velocity and the absorption in function of dephasing process $\gamma_d$. An improvement of the absorption in the middle of the transparency window of an EIT profile take place, and the steep variation of the real part of the linear susceptibility is reduced inducing on the pulse a larger group velocity. This situation is depicted in Fig.3.15(a).

From Fig.3.15(b) we can see how the probe is more sensitive to the introduction of dephasing. The result is that as we increase the dephasing, the absorption of the probe pulse grows, and becomes several orders of magnitude larger, while the dispersion is less sensitive. The largest effect of the increase of the dephasing on the trigger pulse is on its group velocity, which rapidly increases (see Fig.3.15) and group velocity matching could be compromised.
The symmetry of the M-scheme, implies a better tolerance of group velocity matching against dephasing (Fig.3.16). Fig.3.16 shows that increasing the dephasing, the absorption increases and analytical prediction starts to fails. In fact absorption of the fields means that the system start to have a non negligible probability of being in the excited level $|2\rangle$ and $|4\rangle$.

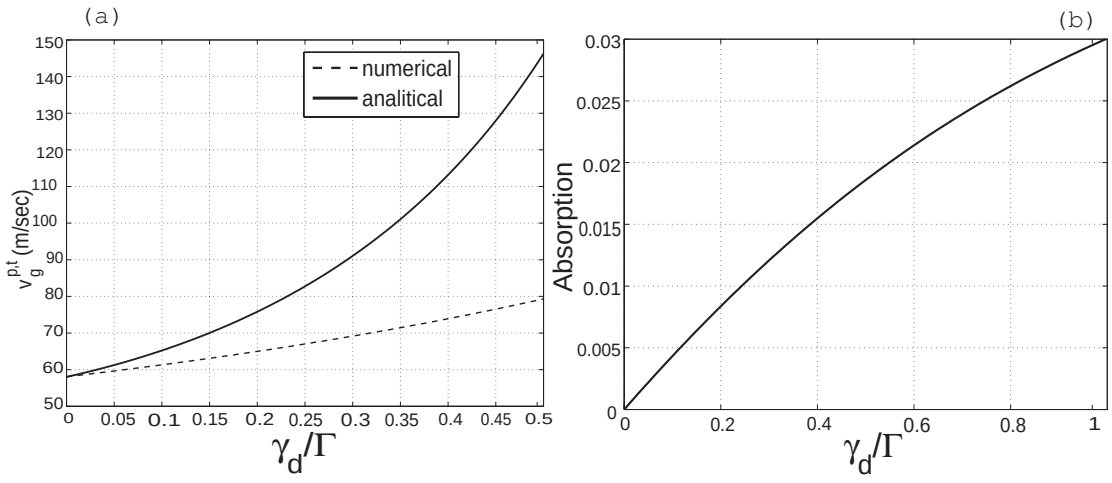


Figure 3.16: Probe and trigger group velocity, Fig.3.16a, and the absorption at the center of the transparency window Fig.3.16b, for the SMS scheme. The numeric calculation of the group velocity (continuous line in Fig.3.16a) is compared with the analytical expression for the group velocity provided by eq(3.61). It is evident how the group velocity matching starts to disagree when absorption mechanisms become important and the population assumption $b_{33} \simeq 1$ is no more well fulfilled. Parmeters are the same of Fig.(3.13).

# Chapter 4

# Cross-phase modulation at the single-photon level: Full quantum calculation

*Adopting a non degenerate perturbation theory, we analyze the performance, for QPG implementation based on the symmetric M-scheme described semiclassically in the previous chapter. The adoption of the perturbative treatment permits us to develop a full quantum treatment of the system dynamics.*
*The performance, i.e. the conditional phase shift $\phi$ and fidelity $\mathcal{F}$, of this two-qubit quantum phase gate for travelling single-photon qubits is thoroughly examined in the steady-state and transient regimes. In the steady-state regime, we find a general trade-off between the size of the conditional phase shift and the fidelity of the gate operation. However, this trade-off can be bypassed in the transient regime, where a satisfactory gate operation is found to be possible, significantly reducing the gate operation time.*

## 4.1 Introduction

In this chapter we perform a full quantum description of the interaction of two quantum probe and trigger fields with $\mathcal{N}_a$ in the five-level symmetric M-scheme, studied in the previous chapter from the semiclassical point of view. The two quantum fields undergo cross-phase modulation induced by EIT. The performance of this two-qubit quantum phase gate for travelling single-photon qubits is thoroughly examined in the steady-state and transient regimes, by means of a full quantum treatment of the system dynamics. In the steady-state regime, we find a general trade-off between the size of the conditional phase shift and the fidelity of the gate operation. However, this trade-off can be bypassed in the transient regime, where a satisfactory gate operation is found to be possible, significantly reducing the gate operation time.

The scope of this chapter is to assess the performance of a two-qubit quantum phase gate (QPG) for travelling single photon qubits [59, 66, 71, 77, 91–93], based on the cross-Kerr nonlinearity which is generated in a five-level atomic medium.

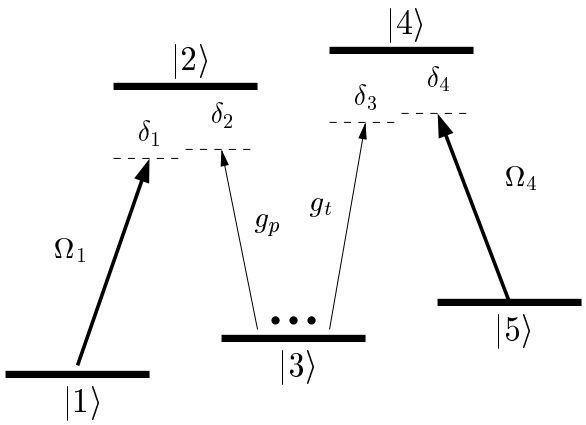


Figure 4.1: Energy levels of the "M"-scheme. $\Omega_j$ are the Rabi frequencies of classical fields, while $g_{p,t}$ denote couplings of the quantized probe and trigger fields to their respective transitions. $\delta_j$ are the detuning of the fields from resonance.

Most of the literature focused only on the evaluation of the CPS and on the best conditions for achieving $\phi = \pi$ [59, 66, 71, 77, 91–93], while the gate fidelity, which is the main quantity for estimating the efficiency of a gate, has been evaluated in the full quantum limit in Ref. [83] for the first time. Here we provide the details of the calculation of the fidelity and the CPS of Ref. [83], which showed the presence of a general *trade–off* between a large CPS and a gate fidelity close to one, hindering the QPG operation, in the stationary state. However, we shall see that this trade-off can be partially bypassed in the transient regime, which has never been considered before in EIT situations, still allowing a satisfactory gate performance.

The qubits are given by polarized single-photon wave packets with different frequencies, and the phase shifts $\phi_{ij}$ are generated when these two pulses cross an atomic ensemble in a five-level "M" configuration (see Fig. 4.1). The population is assumed to be initially in the ground state $|3\rangle$. From this ground state, it could be excited by either the single-photon *probe* field, with central frequency $\omega_p$ and coupling to transition $|3\rangle \leftrightarrow |2\rangle$, or by the single-photon *trigger* field, with central frequency $\omega_t$ and coupling to transition $|3\rangle \leftrightarrow |4\rangle$. We assume that the five levels are Zeeman sub-levels of an alkali atom, and that both pulses have a sufficiently narrow bandwidth. In this way, the Zeeman splittings can be chosen so that the atomic medium is coupled only to a given circular polarization of either the probe or trigger field, while it is transparent for the orthogonally polarized mode, which crosses the gas undisturbed [59]. As a consequence, the logical basis for each qubit practically coincides with the two lowest Fock states of the mode with the "right" polarization, $|0_j\rangle$ and $|1_j\rangle$ ($j = p, t$), while the "wrong" polarization modes will be neglected from now on.

A classical pump field, with frequency $\omega_1$ and Rabi frequency $\Omega_1$, couples to the transition $|1\rangle \leftrightarrow |2\rangle$, while a second classical pump field, with frequency $\omega_4$ and Rabi frequency $\Omega_4$, couples to the transition $|4\rangle \leftrightarrow |5\rangle$ (see Fig. 4.1). We consider a cylindrical, quasi-1D, atomic medium with the two classical pump beams propagating along its axis, collinear with the two quantum fields in order to avoid Doppler broadening. When the probe field is on two-photon resonance with the pump field with Rabi frequency $\Omega_1$, and the trigger field is on two-photon resonance with the pump field with Rabi frequency $\Omega_4$, the system exhibits EIT for probe and trigger

simultaneously. As in the semiclassical SMS scheme this simultaneous EIT condition is achieved when

$$\delta_1 = \delta_2, \qquad \delta_3 = \delta_4, \tag{4.1}$$

where the detunings $\delta_j$ are defined by

$$E_2 - E_1 = \hbar\omega_1 + \hbar\delta_1, \tag{4.2a}$$
$$E_2 - E_3 = \hbar\omega_p + \hbar\delta_2, \tag{4.2b}$$
$$E_4 - E_3 = \hbar\omega_t + \hbar\delta_3, \tag{4.2c}$$
$$E_4 - E_5 = \hbar\omega_4 + \hbar\delta_4. \tag{4.2d}$$

A nonzero CPS occurs whenever a nonlinear cross-phase modulation (XPM) between probe and trigger is present. For small frequency mismatch $\epsilon_{12} = \delta_1 - \delta_2$ and $\epsilon_{34} = \delta_3 - \delta_4$ (both chosen to be within the EIT window), absorption remains negligible and the cross-Kerr interaction between probe and trigger photons may be strong. The consequent CPS may become large, of the order of $\pi$, if the probe and trigger pulse interact for a sufficiently long time. If the two single photon pulses enter simultaneously the atomic medium, their interaction time $t_{int}$ is optimized when the group velocities of the two pulses are equal, so that $t_{int} = L/v_g$, where $v_g$ is the common group velocity of the pulses and $L$ is the length of the gas cell. The inherent *symmetry* of the scheme guarantees perfect group velocity matching for probe and trigger whenever $\delta_1 = \delta_4$, $\delta_2 = \delta_3$ and $g_p/\Omega_1 = g_t/\Omega_4$, where $g_j = \mu_j\sqrt{\omega_j/2\hbar\epsilon_0 V_j}$ $(j = p, t)$ is the coupling constant between the quantum mode with frequency $\omega_j$ and mode volume $V_j$, and the corresponding transition with electric dipole moment $\mu_j$.

The chapter is organized as follows. In Sec. 4.2 we describe the model used in the remainder of the chapter. Sec. 4.3 shows the results of a perturbative calculation for the CPS. These are used as a motivation to pass to a density matrix based calculations in Sec. 4.4, describing a QPG operation in a steady-state. Then, the transient regime in explored in Sec. 4.5, while in Sec. 4.7 a scheme for the experimental verification of the QPG operation is discussed in detail.

## 4.2 Model

In this Section, we present the model we have adopted for a full quantum description of the interaction of the two single-photon wave-packets with the atomic medium possessing the level structure outlined in Fig. 4.1. To this end, we make the following two assumptions which, even though not simple to realize experimentally, are more technical than physical in nature:

1. We assume perfect spatial mode matching between the input single-photon pulses entering the gas cell and the optical modes naturally excited by the driven atomic medium, and which are determined by the geometrical configuration of the gas cell and of the pump beams [85]. This allows us to describe the probe and trigger fields with the right polarization in terms of *single* travelling optical modes, with annihilation operators $\hat{a}_{p,t}$.

2. We assume that the pulses are tailored in such a way that they simultaneously enter gas cell and completely overlap with it during the interaction (see Fig. 4.2). This means that their length (compressed inside a medium due to group velocity reduction) is of the order

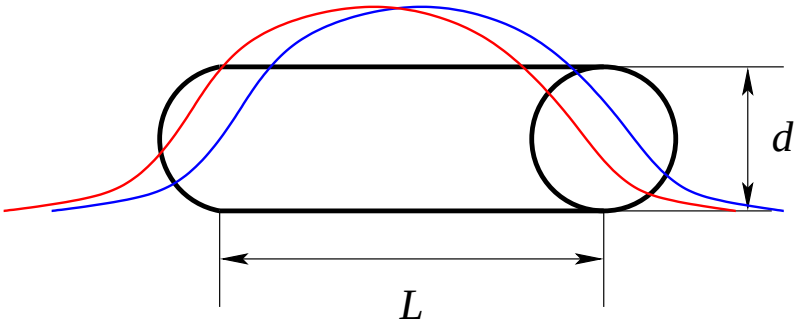


Figure 4.2: A schematic plot of the assumed single-photon pulse propagation through the gas cell of length $L$ and diameter $d$ (color online). The pulse length is assumed to coincide with the cell length $L$, and the pulse waist $w$ is assumed to be of order of cell diameter $d$.

of the cell length $L$ and their beam waist is of the order of the cell radius. In this way, the two pulses interact with *all* $N_a$ atoms in the cell at once, and moreover, one can ignore spatial aspects of pulse propagation.

With these assumptions, and neglecting dipole-dipole interactions, the interaction picture Hamiltonian may be written as

$$\begin{aligned} H &= \hbar\epsilon_{12}\hat{S}_{11} + \hbar\delta_2\hat{S}_{22} + \hbar\delta_3\hat{S}_{44} + \hbar\epsilon_{34}\hat{S}_{55} \\ &+\hbar\Omega_1\sqrt{N_a}\left(\hat{S}_{21} + \hat{S}_{12}\right) + \hbar g_p\sqrt{N_a}\left(\hat{a}_p\hat{S}_{23} + \hat{S}_{32}\hat{a}_p^\dagger\right) \\ &+\hbar g_t\sqrt{N_a}\left(\hat{a}_t\hat{S}_{43} + \hat{S}_{34}\hat{a}_t^\dagger\right) + \hbar\Omega_4\sqrt{N_a}\left(\hat{S}_{45} + \hat{S}_{54}\right), \end{aligned} \tag{4.3}$$

where we have defined the collective atomic operators

$$\hat{S}_{kl} = \frac{1}{\sqrt{N_a}}\sum_{i=1}^{N_a}\sigma_{kl}^i, \quad k \neq l = 1, \ldots, 5, \tag{4.4}$$

$$\hat{S}_{kk} = \sum_{i}^{N_a}\sigma_{kk}^i, \tag{4.5}$$

with $\sigma_{kl}^i \equiv |k\rangle_i\langle l|$ being the operator switching between states $k$ and $l$ of the $i$th atom. The initial state of the system corresponds to a probe and a trigger single-photon pulse with generic polarization, simultaneously entering the medium in which all the atoms are initially in state $|3\rangle$. Since we consider only the polarization mode interacting with the medium, both for the probe and the trigger, the initial state can be written as

$$\begin{aligned} |\psi_{in}\rangle = \bigotimes_{i=1}^{N_a}|3\rangle_i \otimes (&c_{00}|0_p\rangle \otimes |0_t\rangle + c_{01}|0_p\rangle \otimes |1_t\rangle \\ &+c_{10}|1_p\rangle \otimes |0_t\rangle + c_{11}|1_p\rangle \otimes |1_t\rangle). \end{aligned} \tag{4.6}$$

Due to the above assumptions, the passage of the two pulses through the atomic medium of length $L$ corresponds to the time evolution of this state, for a time $t_{int} = L/v_g$, according to

the master equation [6]

$$\begin{aligned}\dot{\sigma} &= -\frac{i}{\hbar}[H,\,\sigma] + \sum_k \frac{\gamma_{kk}}{2}\sum_{j=1}^{N_a}\left(2\sigma_{kk}^j\sigma\sigma_{kk}^j - \sigma_{kk}^j\sigma - \sigma\sigma_{kk}^j\right), \\ &+ \sum_{kl}\frac{\gamma_{kl}}{2}\sum_{j=1}^{N_a}\left(2\sigma_{kl}^j\sigma\sigma_{kl}^{j\dagger} - \sigma_{kl}^{j\dagger}\sigma_{kl}^j\sigma - \sigma\sigma_{kl}^{j\dagger}\sigma_{kl}^j\right), \end{aligned} \tag{4.7}$$

including not only the coherent interaction described by the Hamiltonian of Eq. (4.3), but also the spontaneous emission from the excited states $l = 2, 4$ to the ground states $k = 1, 3, 5$ ($\gamma_{kl}$ denotes the corresponding decay rate) and the dephasing of levels $|k\rangle$, $k = 1, 2, 4, 5$, with dephasing rate $\gamma_{kk}$. Typically the dephasing rates are much smaller than the decay rates, $\gamma_{kl} \gg \gamma_{kk}$, $\forall\, k, l$.

Since the initial state of Eq. (4.6) contains at most two excitations, the coherent time evolution driven by Eq. (4.3) is simple and restricted to a finite-dimensional Hilbert space involving few symmetric collective atomic states. In fact, each component of the initial state of Eq. (4.6) evolves independently in a different subspace. The component with no photon is an eigenstate of $H$ and does not evolve. The $\bigotimes_{i=1}^{N_a}|3\rangle_i|0_p\rangle \otimes |1_t\rangle$ component evolves in a three-dimensional Hilbert space which it spans together with the two states $|e_4^{(0,0)}\rangle$ and $|e_5^{(0,0)}\rangle$. Here, we have defined the symmetric collective states

$$|e_r^{(n_p,n_t)}\rangle = \frac{1}{\sqrt{N_a}}\sum_{i=1}^{N_a}|3_1, 3_2, \ldots, r_i, \ldots, 3_{N_a}\rangle \otimes |n_p\rangle \otimes |n_t\rangle, \tag{4.8}$$

where $r = 1, 2, 4, 5$. In a similar fashion, the component with only one probe photon evolves in a three-dimensional Hilbert space spanned by the three states $\bigotimes_{i=1}^{N_a}|3\rangle_i|1_p\rangle \otimes |0_t\rangle$, $|e_1^{(0,0)}\rangle$ and $|e_2^{(0,0)}\rangle$. The component with one probe and one trigger photon evolves in the five dimensional subspace spanned by the four collective states $|e_1^{(0,1)}\rangle$, $|e_2^{(0,1)}\rangle$, $|e_4^{(1,0)}\rangle$, and $|e_5^{(1,0)}\rangle$ and the state $\bigotimes_{i=1}^{N_a}|3\rangle_i|1_p\rangle \otimes |1_t\rangle$.

### 4.2.1 Decoherence Effects

Decoherence effects, and more specifically spontaneous emission from each atom complicates this dynamics. However, we are in the weak excitation limit where, for $l \neq 3$, $\langle\sigma_{ll}^j\rangle \simeq N_a^{-1} \ll 1$, as shown by the fact that the Hamiltonian dynamics involve only the symmetric atomic states of the form of Eq. (4.8). This limit allows a drastic simplification of the effective time evolution. Following Duan *et al.* [86], we can introduce Fourier transforms of the individual atomic operators $s_{kl}^\mu = \sum_{j=0}^{N_a-1}\sigma_{kl}^j e^{ij\mu/N_a}/\sqrt{N_a}$, where $s_{kl}^0 = \hat{S}_{kl}$ are the collective operators defined in Eq. (4.4). The sum over the atoms in Eq. (4.7) then transforms to the sum over the collective atomic modes with index $\mu$. In the weak excitation limit, the operators $s_{kl}^\mu$ approximately commute with each other. This means that they represent independent collective atomic modes, and one can trace over the $\mu \neq 0$ modes, so that the spontaneous emission term in the master equation becomes

$$\sum_{kl}\frac{\gamma_{kl}}{2}\left(2\hat{S}_{kl}\sigma\hat{S}_{kl}^\dagger - \hat{S}_{kl}^\dagger\hat{S}_{kl}\sigma - \sigma\hat{S}_{kl}^\dagger\hat{S}_{kl}\right), \tag{4.9}$$

where the sum is now over the six "collective" spontaneous decay channels only, each characterized by the *single-atom* decay rate $\gamma_{kl}$. A similar argument applies to the dephasing term in the

master equation (4.7). In fact, if we restrict to the subspace of the symmetric collective states of Eq. (4.8) involving only single atomic excitations, we can approximate in the dephasing terms of the master equation,

$$\sum_k \gamma_{kk} \sum_{j=1}^{N_a} \sigma_{kk}^j \sigma \sigma_{kk}^j \simeq \sum_k \gamma_{kk} \hat{S}_{kk} \sigma \hat{S}_{kk}, \tag{4.10}$$

where $\hat{S}_{kk}$ is given by Eq. (4.5). Using Eqs. (4.9) and (4.10), the master equation of Eq. (4.7) in the weak excitation limit becomes

$$\begin{aligned} \dot{\sigma} &= -\frac{i}{\hbar}[H, \sigma] + \sum_k \frac{\gamma_{kk}}{2}\left(2\hat{S}_{kk}\sigma\hat{S}_{kk} - \hat{S}_{kk}\sigma - \sigma\hat{S}_{kk}\right) \\ &\quad + \sum_{kl} \frac{\gamma_{kl}}{2}\left(2\hat{S}_{kl}\sigma\hat{S}_{kl}^\dagger - \hat{S}_{kl}^\dagger\hat{S}_{kl}\sigma - \sigma\hat{S}_{kl}^\dagger\hat{S}_{kl}\right), \end{aligned} \tag{4.11}$$

that is, it involves only the operators of the collective atomic mode with index $\mu = 0$. This actually means that the single photon probe and trigger pulses excite only a restricted number of collective atomic states, so that the atomic medium behaves as an effective *single* 5-level atom, with a *collectively enhanced* coupling with the optical modes $g_j\sqrt{N_a}$, but with single-atom decay rates $\gamma_{kl}$, dephasing rates $\gamma_{kk}$, Rabi frequencies $\Omega_i$, and detunings $\delta_i$.

Spontaneous emission causes the four independent Hilbert subspaces corresponding to the four initial state components to become coupled. Moreover, the "cross" decay channels $|4\rangle \to |1\rangle$ and $|2\rangle \to |5\rangle$ couple the above-mentioned collective states with six new states, $|e_1^{(1,0)}\rangle$, $|e_2^{(1,0)}\rangle$, $|e_3^{(2,0)}\rangle$ (populated if $\gamma_{41} \neq 0$), and $|e_5^{(0,1)}\rangle$, $|e_4^{(0,1)}\rangle$, $|e_3^{(0,2)}\rangle$ (populated if $\gamma_{25} \neq 0$). Therefore Eq. (4.11) actually describes dynamics in a Hilbert space of dimension 18, which we have numerically solved in order to establish the performance of the QPG. Notice that, due to the combined action of the cross-decay channels and of the Hamiltonian (4.3), the states $|e_1^{(1,0)}\rangle$, $|e_2^{(1,0)}\rangle$, $|e_5^{(0,1)}\rangle$ and $|e_4^{(0,1)}\rangle$ are coupled also to *doubly excited* atomic collective states without photons which are neglected by our treatment. However, as we shall see below in the chapter, a good QPG performance is possible only when spontaneous emission events are rare. Under this condition, the probability to populate these doubly excited atomic collective states during the atom-field interaction is completely negligible, and therefore our model based on the effective single five-level atom description provided by Eq. (4.11) is essentially correct.

### 4.2.2 Definition of the *Fidelity*

The main objective of this work is the determination of the performance of the full optical quantum phase gate. The quantity to be evaluated is the *fidelity*, that in general is a measure of how much an output state overlap the state of an ideal device. Evaluate the Fidelity is of crucial importance to realize if an all optical quantum phase gate can be used in realistic technological devices.

Here to characterize the QPG operation, we calculate both the CPS $\phi$ of Eq. (1.64) and the fidelity of the gate. The accumulated CPS $\phi$ as a function of the interaction time $t_{int}$ is obtained by using the fact that the phase shifts $\phi_{ij}$ of Eq. (1.64) are given by combinations of the phases of the off-diagonal matrix elements (in the Fock basis) of the reduced density matrix of the probe and trigger modes, $\sigma_f(t) = \mathrm{Tr}_{atoms}\{\sigma(t)\}$.

The gate fidelity is given by [24]

$$\mathcal{F}(t) = \sqrt{\langle \psi_{id}(t) | \sigma_f(t) | \psi_{id}(t) \rangle}, \tag{4.12}$$

where

$$|\psi_{id}(t)\rangle = c_{00}\exp\{i\phi_{00}(t_{int})\}|0_p,0_t\rangle + c_{01}\exp\{i\phi_{01}(t)\}|0_p,1_t\rangle + c_{10}\exp\{i\phi_{10}(t)\}|1_p,0_t\rangle + \\ + c_{11}\exp\{i\phi_{11}(t)\}|1_p,1_t\rangle \tag{4.13}$$

is the ideally evolved state from the initial condition (4.6), with phases $\phi_{ij}(t)$ evaluated from $\sigma_f(t)$ as discussed above. The overbar denotes the average over all initial states (i.e., over the $c_{ij}$, see Poyatos *et al.* [87]). The above fidelity characterizes the performance of the QPG as a deterministic gate. However, one could also consider the QPG as a *probabilistic* gate, whose operation is considered only when the number of output photons is equal to the number of input photons. This analysis will be performed by means of the quantum trajectories analysis (A.3). The performance of this probabilistic QPG could be experimentally studied by performing a conditional detection of the phase shifts, and it is characterized by the *conditional* fidelity $\mathcal{F}^c(t)$, which will be discussed in Sec. 4.4.

## 4.3 Perturbative Regime

Now that we have clarified how we will evaluate the two quantities that characterize the QPG we analyze the system in the perturbative regime. The conditional fidelity is always larger than the unconditional one, but they become equal (and both approach 1) for an ideal QPG in which the number of photons is conserved and all the atoms remain in state $|3\rangle$. This ideal condition is verified in the limit of large detunings $\delta_j \gg \gamma_{kj}$ so that spontaneous emission is significantly suppressed and can be neglected, and very small couplings $g_j\sqrt{N_a} \ll \Omega_j$. In this limit, each component of the initial state of Eq. (4.6) practically coincides with the dark state of the four independent Hamiltonian dynamics discussed in Sec. 4.2. The system with the initial state containing zero probe and trigger photons does not evolve, i.e. stays in the initial state $\bigotimes_{i=1}^{N_a}|3\rangle_i|0_p\rangle\otimes|0_t\rangle$ all the time. The subsystem containing one probe and zero trigger photons as the initial state evolves according to a reduced three-dimensional Hamiltonian, which in the basis formed by the states $\bigotimes_{i=1}^{N_a}|3\rangle_i|1_p\rangle\otimes|0_t\rangle$, $|e_2^{(0,0)}\rangle$ and $|e_1^{(0,0)}\rangle$, is given by

$$H_p = \begin{pmatrix} 0 & g_p\sqrt{N_a} & 0 \\ g_p\sqrt{N_a} & \delta_1 & \Omega_1 \\ 0 & \Omega_1 & \epsilon_1 \end{pmatrix}. \tag{4.14a}$$

Similarly, the subsystem containing one trigger and zero probe photons as the initial state evolves according to a reduced three-dimensional Hamiltonian, which in the basis formed by the states $\bigotimes_{i=1}^{N_a}|3\rangle_i|0_p\rangle\otimes|1_t\rangle$, $|e_4^{(0,0)}\rangle$ and $|e_5^{(0,0)}\rangle$, is given by

$$H_t = \begin{pmatrix} 0 & g_t\sqrt{N_a} & 0 \\ g_t\sqrt{N_a} & \delta_3 & \Omega_4 \\ 0 & \Omega_4 & \epsilon_2 \end{pmatrix}. \tag{4.14b}$$

Finally, the subsystem containing initially one photon each in probe and trigger modes evolves according to a reduced five-dimensional Hamiltonian, which in the basis formed by the states

$|e_1^{(0,1)}\rangle$, $|e_2^{(0,1)}\rangle$, $\bigotimes_{i=1}^{N_a}|3\rangle_i|1_p\rangle\otimes|1_t\rangle$, $|e_4^{(1,0)}\rangle$, and $|e_5^{(1,0)}\rangle$, is given by

$$H_{pt}=\begin{pmatrix}\delta_1 & \Omega_1 & g_p\sqrt{N_a} & 0 & 0\\ \Omega_1 & \epsilon_1 & 0 & 0 & 0\\ g_p\sqrt{N_a} & 0 & 0 & g_t\sqrt{N_a} & 0\\ 0 & 0 & 0 & \delta_3 & \Omega_4\\ 0 & 0 & g_t\sqrt{N_a} & \Omega_4 & \epsilon_2\end{pmatrix}. \tag{4.14c}$$

The phase accumulation experienced by the various components of the quantum state of the fields will be proportional to the eigenvalues of these matrices. The four phase shifts $\phi_{ij}$ can be evaluated as a fourth-order perturbation expansion of the eigenvalue corresponding to the dark state in each subspace, multiplied by the interaction time $t_{int}$. The CPS is then calculated as

$$\phi=(\lambda_{H_{pt}}-\lambda_{H_p}-\lambda_{H_t})t_{int}, \tag{4.15}$$

where the $\lambda$'s denote the eigenvalues of the corresponding reduced Hamiltonian, with $\lambda_{pt}\leftrightarrow\phi_{11}$, $\lambda_p\leftrightarrow\phi_{10}$, $\lambda_t\leftrightarrow\phi_{01}$ and $\phi_{00}=0$, in agreement the with general definition of Eq. (1.64)

$$\phi=\phi_{11}+\phi_{00}-\phi_{10}-\phi_{01}.$$

Then the conditional phase shift have to be evaluated calculating the eigenvalues of the previous hamiltonian. This has been done adopting a fourth order perturbation theory, where the perturbation parameters are the small single photon coupling $g_p$ and $g_t$ (see Appendix B). The order of perturbation, the fourth, is needed to take into account the effects that depends on the square of the probe and trigger coupling $g_p$ and $g_t$ to which the cross Kerr interaction is proportional.
Following the procedure described in the Appendix B, the zeros order eigenvalues are

$$\lambda_\pm^t = \frac{\delta_3-\epsilon_2}{2}\pm\sqrt{\Big(\frac{\delta_3-\epsilon_2}{2}\Big)^2+\Omega_4^2}, \tag{4.16}$$

$$\lambda_\pm^p = \frac{\delta_1-\epsilon_1}{2}\pm\sqrt{\Big(\frac{\delta_1-\epsilon_1}{2}\Big)^2+\Omega_2^2}. \tag{4.17}$$

At second order we get (see Appendix B)

$$\delta\lambda^{(2)}_{trigger}=-g_t^2\Omega_4^2\Big[\frac{1}{\lambda_+^t(\Omega_4^2+d_{+,t}^2)}+\frac{1}{\lambda_-^t(\Omega_4^2+d_{-,t}^2)}\Big], \tag{4.18}$$

where with $d_{\pm,t}=\lambda_\pm^t-\delta_3$. The correction of the eigenvalues at the fourth order is

$$\delta\lambda^{(4)}_{trigger}=g_t^4\Omega_4^4\Big[\frac{1}{\lambda_+^t(\Omega_2^2+d_{+,t}^2)}+\frac{1}{\lambda_-^t(\Omega_4^2+d_{-,t}^2)}\Big]\times\Big[\frac{1}{(\lambda_+^t)^2(\Omega_2^2+d_{+,t}^2)}+\frac{1}{(\lambda_-^t)^2(\Omega_4^2+d_{-,t}^2)}\Big]. \tag{4.19}$$

In the case of the probe field, it is sufficient replace $\lambda_\pm^t\to\lambda_\pm^p$, $g_t\to g_p$, and $\Omega_4\to\Omega_2$.
The phases $\phi_{10}$ and $\phi_{01}$ of the QPG are defined by

$$\phi_{01} = (\lambda_\pm^t+\delta\lambda^{(2)}_{trigger}+\delta\lambda^{(4)}_{trigger})t_{int}, \tag{4.20}$$

$$\phi_{10} = (\lambda_\pm^p+\delta\lambda^{(2)}_{probe}+\delta\lambda^{(4)}_{probe})t_{int}. \tag{4.21}$$

We have illustrated the solution for the trigger field, the same results holds for the probe up to a suitable redefinition of $d_{\pm,p} = \lambda^p_{\pm} - \delta_1$. Now we calculate the eigenvalues of the $H_{pt}$ matrix, that will include a cross Kerr interaction term. We proceed as before for the Hamiltonian that describes the single photon evolution. The unperturbed eigenvalues for matrix $H_{pt}$ are the same of the two separate cases $H_p$ and $H_t$, the second and third order perturbative terms are

$$\begin{aligned}\delta\lambda^{(2)}_{pt} &= -g_t^2\Omega_4^2\Big[\frac{1}{\lambda^t_+(\Omega_4^2+d^2_{+,t})}+\frac{1}{\lambda^t_-(\Omega_4^2+d^2_{-,t})}\Big] \\ &\quad -g_p^2\Omega_2^2\Big[\frac{1}{\lambda^p_+(\Omega_2^2+d^2_{+,p})}+\frac{1}{\lambda^p_-(\Omega_2^2+d^2_{-,p})}\Big].\end{aligned} \tag{4.22}$$

Adopting the $\Lambda_{t,p}$ and $\Theta_{t,p}$ variables defined by eq(B.17) to simplify the expressions, we obtain an expression that gives the fourth order term of the eigenvalue of the $H_{pt}$ matrix that describe, in practice, the conditional interaction

$$\phi_{11} = \delta\lambda^{(4)}_{pt} = \Big[g_t^2\Omega_4^2\Lambda_t + g_p^2\Omega_2^2\Lambda_p\Big]\Big[g_t^2\Omega_4^2\Theta_t + g_p^2\Omega_2^2\Theta_t\Big]t_{int}. \tag{4.23}$$

This term is the key term, responsible for the cross-phase modulation. In fact expanding the product we obtain four terms. The two proportional to $g_p^4\Omega_2^4$ and $g_t^4\Omega_4^4$ cancel with the $\lambda^{(4)}_{H_t}$ and $\lambda^{(4)}_{H_p}$, and the residual terms give the conditional phase shift. In fact putting all these results together and applying eq.(1.64) we have

$$\phi = (\lambda^{(4)}_{pt} - \delta\lambda^{(4)}_{probe} - \delta\lambda^{(4)}_{trigger})t_{int} = g_p^2 g_t^2\Omega_2^2\Omega_4^2 t_{int}\Big\{\Lambda_t\Theta_p + \Lambda_p\Theta_t\Big\}. \tag{4.24}$$

After some algebra we arrive at the expression for the CPS

$$\phi = \frac{g_p^2 g_t^2 N_a^2 t_{int}}{(\epsilon_{34}\delta_3 - \Omega_4^2)(\epsilon_{12}\delta_1 - \Omega_1^2)} \times \left[\frac{\epsilon_{34}(\epsilon_{12}^2+\Omega_1^2)}{(\epsilon_{12}\delta_1 - \Omega_1^2)} + \frac{\epsilon_{12}(\epsilon_{34}^2+\Omega_4^2)}{(\epsilon_{34}\delta_3 - \Omega_4^2)}\right]. \tag{4.25}$$

This prediction is verified by the numerical solution of Eq. (4.11) in the limit of large detunings and small couplings.

However the resulting CPS is too small, even for very long interaction times (i.e., long gas cells): for example, for $g_{p,t}\sqrt{N_a} = 0.5$ MHz, $\epsilon_{12,34} = 1.9$ MHz, $\Omega_{1,4} = 65$ MHz and $\delta_{1,3} = 1.9$ GHz, we obtain a tiny CPS of only $3\times10^{-4}$ radians when $t_{int} = 10^{-4}$ s, which corresponds to $L \simeq 30$ Km. This is not surprising because this limit corresponds to a dispersive regime far from EIT. In this regime, transparency is achieved by means of a strong coupling field, producing a well-separated Autler-Townes doublet [6]. At the same time, the size of nonlinearity is small due to the extremely weak coupling of the quantized fields to their respective transitions. The results are, therefore, not different from those expected from XPM in a standard nonlinear optical fiber. Therefore, one has to explore the non-perturbative regime of larger couplings in order to exploit the low-noise, large-nonlinearity properties of EIT and achieve a satisfactory QPG operation.

## 4.4 Steady-State QPG Operation

A large amount of work exploring EIT-based nonlinear optical phenomena considers the steady-state of a generic EIT-based system as being the natural state in which to predict and test

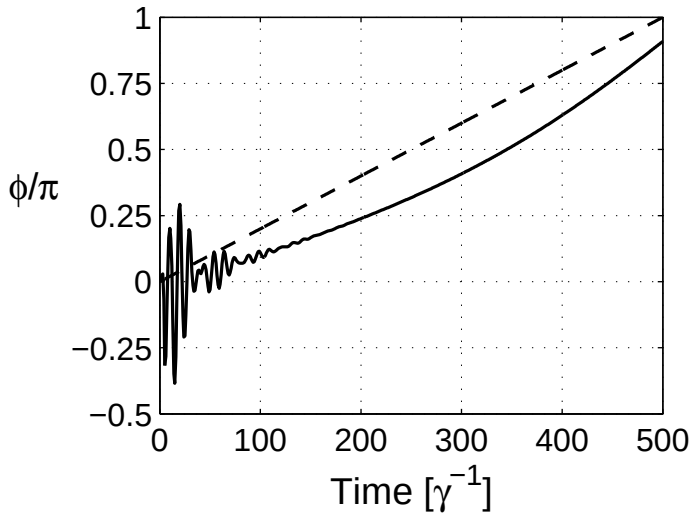


Figure 4.3: Conditional phase shift as a function of the interaction time for $N_a = 10^8$, $\delta_1 = \delta_3 = 7.5\gamma$, $\epsilon_{12} = \epsilon_{34} = 0.05\gamma$,$g_p = g_t = 0.0011\gamma$, $\Omega_1 = \Omega_4 = 1.875\gamma$ and $\gamma_{kk} = \gamma_{ph} = 10^{-3}\gamma$, $\forall\, k$. We have taken equal decay rates, $\gamma_{21} = \gamma_{23} = \gamma_{25} = \gamma_{41} = \gamma_{43} = \gamma_{45} = \gamma/3$, with $\gamma = 2\pi \times 6$ MHz. Solid line represents the phase shift, as calculated from the full master equation, while the dashed line gives the perturbative prediction of Eq. (4.25).

different phenomena [13,18,59,76]. We shall see in this Section that it is not possible to achieve a satisfactory QPG performance in such a steady-state regime.

In this Section, we analyze the performance of the QPG at the steady state. To this end, we consider two different parameter regimes:
*(i)* the regime of long interaction times, a natural extension of the perturbation analysis of Sec. 4.3,
*(ii)* the regime of short interaction times, corresponding to a non-perturbative regime with strong atom-field coupling.

### 4.4.1 Long Interaction Time

Naturally extending the perturbative analysis, we solve the master equation (4.11), and show the results in Figs. 4.3 and 4.4. Fig. 4.3 shows the result for the conditional phase shift. Solid line has been calculated from the solution of Eq. (4.11), as explained in Sec. 4.2. The dashed line is the 'benchmark' solution, obtained from the eigenvalues of the associated Hamiltonian, by using Eq. (4.15). The eigenvalues of the Hamiltonians of Eqs. (4.14) have been calculated numerically for the set of parameters of Fig. 4.3.

It is evident that the 'benchmark' solutions offers a reasonably good estimate for the size of the CPS. The exact dynamics driven by the master equation (4.11) presents an additional oscillatory behavior both on a short time scale (transient processes), and on a long-time scale. The longer time scale comes from the fact that to induce the cross-Kerr nonlinearity, one has to detune the fields away from the dark resonance. This detuning is very small and is seen in

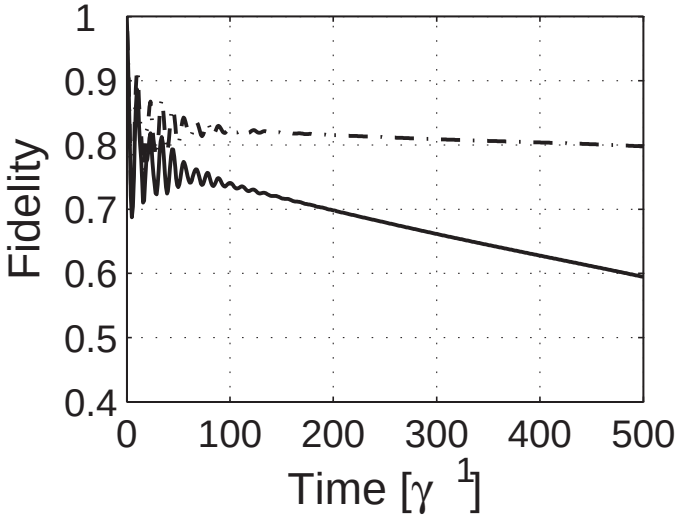


Figure 4.4: Gate fidelity of Eq. (4.12) versus the interaction time, for the same set of parameters as in Fig. 4.3. The solid line is the unconditional gate fidelity $\mathcal{F}(t)$, while the dot-dashed line is the conditional one, $\mathcal{F}^c(t)$.

the oscillations on a long time-scale. As both probe and trigger fields are detuned by the same amount, only one frequency of long-time oscillations is observed.

In Fig. 4.4, fidelities (averaged over all possible two-qubit initial states) are shown in two cases. Both are calculated by using Eq. (4.12), but they differ in the way $\sigma_f(t)$ is defined. The solid line in Fig. 4.4 refers to the *unconditional* fidelity $\mathcal{F}(t)$, which is calculated from Eq. (4.12) by taking $\sigma_f(t) = \mathrm{Tr}_{at}\{\sigma(t)\}$, where $\sigma(t)$ is the solution of the master equation (4.11). The unconditional fidelity quantifies the performance of the QPG as a *deterministic* gate for single-photon qubits.

The dot-dashed line in Fig. 4.4 refers to the *conditional* fidelity $\mathcal{F}^c(t)$, which is evaluated according to Eq. (4.12), but with $\sigma_f(t)$ replaced by $\sigma_f^c(t) = \mathrm{Tr}_{at}\{|\psi_{nj}(t)\rangle\langle\psi_{nj}(t)|\}/\langle\psi_{nj}(t)|\psi_{nj}(t)\rangle$, where $|\psi_{nj}(t)\rangle$ is the (non-normalized) evolved atom-field state conditioned to the detection of no quantum jumps [112], i.e., of no photon loss by spontaneous emission. This fidelity can be measured by post-selecting those measurement results that conserve photon number, i.e., discarding those data sets where at least a photon from the initial two-qubit state has been lost to the environment. The conditional fidelity quantifies the performance of the QPG as a *probabilistic* two-qubit gate.

In Figs. 4.3 and 4.4, we have found at best a CPS of $\sim \pi$ in correspondence with fidelities $\mathcal{F}(t_{int})$ and $\mathcal{F}^c(t_{int})$ equal to 60% and 80%, respectively. This is due to the general presence of a *trade-off between the size of the CPS and of the gate fidelity*, as well as to the atomic

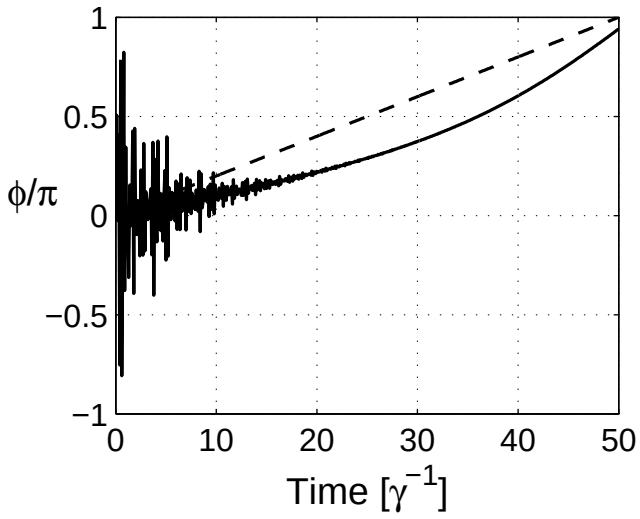


Figure 4.5: Conditional phase shift as a function of the interaction time for $N_a = 10^8$, $\delta_1 = \delta_3 = 9.5\gamma$, $\epsilon_{12} = \epsilon_{34} = 0.2\gamma$, $g_p = g_t = 0.018\gamma$ and $\Omega_1 = \Omega_4 = 19\gamma$ and $\gamma_{kk} = \gamma_{ph} = 10^{-3}\gamma$, $\forall\ k$. We have taken equal decay rates, $\gamma_{21} = \gamma_{23} = \gamma_{25} = \gamma_{41} = \gamma_{43} = \gamma_{45} = \gamma/3$, with $\gamma = 2\pi \times 6$ MHz. Solid line represents the phase shift, as calculated from a density matrix, while the dashed line gives the eigenvalue solution.

dephasing [1]. This is an important result of our chapter, which actually holds true in *any* EIT-based nonlinear optics systems. In fact, both the conditional and the unconditional gate fidelity approach 1 in the limit of very small $g_j$, but this limit yields a CPS which becomes appreciable only for unrealistically long gas cells. Therefore a larger CPS requires a larger ratio $g_j\sqrt{N_a}/\Omega_j$. This condition however increases the population of the collective atomic states $|e_1^{(n_p,n_t)}\rangle$ and $|e_5^{(n_p,n_t)}\rangle$ at the expense of the initial atomic state $|3\rangle$, thus unavoidably decreasing the gate fidelity. Similar conclusions hold for other options, such as increased detunings $\delta_j$, or adjusting two-photon detunings $\epsilon_{ij}$. Therefore, just the pure coherent unitary evolution of the system, governed by the Hamiltonian of Eq. (4.3) causes this inherent trade-off.

### 4.4.2 Short Interaction Time

To further illustrate our findings, we calculate the CPS and the gate fidelities in the range of parameters where the total interaction time is an order of magnitude smaller than in Sec. 4.4.1. The CPS and the gate fidelities are calculated as described in Sec. 4.4.1, and the results are shown in Figs. 4.5 and 4.6. To obtain a CPS of the order of $\pi$ in a shorter interaction time ($t_{int} \sim 50/\gamma$), we have assumed a larger ratio $g_j\sqrt{N_a}/\Omega_j$. The trade-off between the amount of accumulated nonlinear phase shift and the gate fidelity is now even more pronounced: we find at best a CPS of $\sim \pi$ in correspondence with fidelities $\mathcal{F}(t_{int})$ and $\mathcal{F}^c(t_{int})$ equal to 65% and 73%, respectively. As expected, having a stronger atom-field coupling enhances the processes

[1] Without the dephasing, steady-state fidelities reach the values of 77% and 83% for unconditional and conditional cases, respectively

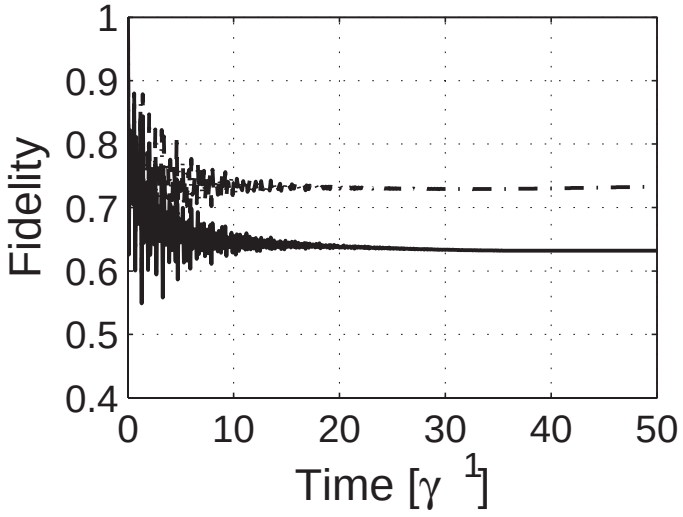


Figure 4.6: Fidelity, averaged over the initial states of a two-qubit system, for the same set of parameters as in Fig. 4.5. Solid line is the unconditional gate fidelity, while dot-dashed line is the conditional one.

lowering the fidelity. The system ends up with a large CPS faster, but this is achieved with a final state in which the probability of loosing the probe and trigger photons by spontaneous emission or within the atomic medium is no more negligible. We notice that in this short interaction time case dephasing does not have an appreciable effect, that is, the results without dephasing are indistinguishable from those with dephasing shown in Figs. 4.5 and 4.6, due to fact that dephasing rates in a dilute gas are typically much smaller than decay rates. The only possible way to circumvent this trade-off is to explore the transient regime, which will be discussed in the following Section.

## 4.5 QPG Operation in Transient Regime

In Sec. 4.4, we have found that the QPG operation of EIT-based nonlinear system in a steady-state is plagued by the trade-off between the phase shift size and the gate fidelity. In an attempt to find favorable conditions for the QPG operation, we consider the transient regime, when $\gamma t_{int} \lesssim 1$. As discussed above, in order to accumulate a significant CPS in such a short time one has to consider the strong coupling regime with a large ratio $g_j\sqrt{N_a}/\Omega_j$. Therefore, the trade-off between fidelity and a large nonlinear interaction is present also in the transient regime. However, when $g_j\sqrt{N_a}/\Omega_j$ is large, the transient dynamics is characterized by Rabi-like oscillations of the atomic populations and of the photon number, determining, as a consequence, coherent oscillations of the gate fidelity. In such a case one cannot exclude the existence of special values of the interaction time $t_{int}$ corresponding to a maximum of the gate fidelity close to one, and at the same time, to a value of the CPS close to $\pi$.

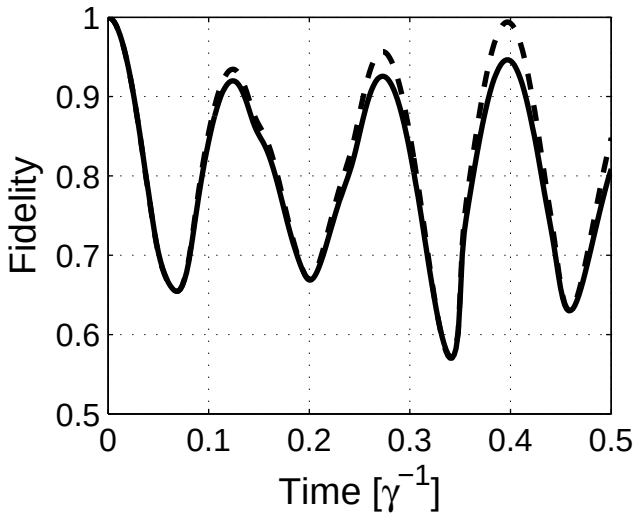


Figure 4.7: Fidelity of the QPG operation for $N_a = 10^8$, $\delta_1 = \delta_3 = 15\gamma$, $\epsilon_{12} = \epsilon_{34} = 0.01\gamma$, $g_p = g_t = 0.0022\gamma$, $\Omega_1 = \Omega_4 = 4\gamma$ and $\gamma_{kk} = \gamma_{ph} = 10^{-3}\gamma$, $\forall\ k$. We have taken equal decay rates, $\gamma_{21} = \gamma_{23} = \gamma_{25} = \gamma_{41} = \gamma_{43} = \gamma_{45} = \gamma/3$, with $\gamma = 2\pi \times 6$ MHz. The unconditional fidelity (solid) and conditional fidelity (dashed) are shown. See text for details.

We show that this fact is actually possible in Figs. 4.7 and 4.8, where we see that a CPS of $\sim \pi$ radians is obtained in the transient regime for $t_{int} \approx 0.4/\gamma \sim 10$ ns. At the same interaction time, the unconditional gate fidelity (Fig. 4.7, full line) is about 94%, while the conditional gate fidelity reaches the value of 99% (Fig. 4.7, dashed line). The conditional gate fidelity is obtained in correspondence with a success probability of the gate equal to 0.94, calculated from the norm of the Monte-Carlo wave function [112]. The probe and trigger group velocities are calculated to be $v_g \simeq 3 \times 10^6$ ms$^{-1}$, yielding a gas cell length $L = v_g t_{int} \simeq 3.1$ cm. The value of $g_j$ yields an interaction volume $V \simeq 2 \cdot 10^{-3}$ cm$^3$, corresponding to a gas cell diameter of about 330 $\mu$m and to an atomic density $N_a/V \simeq 5 \cdot 10^{10}$ cm$^{-3}$.

It is interesting to note that the quantity that we calculate, the conditional phase shift $\phi$, effectively depends upon the mutual interaction that takes place between the probe and trigger photons when the M type interaction take place. This can be argued from Fig4.9a. This figure shows that for the interaction time for which we have the $\pi$ conditional phase shift and the maximum in fidelity, corresponds to a maximum of probability of finding the atoms in the level $|3\rangle$. More important, when the probability of having the fields in the Fock states $|0,1\rangle$, $|1,0\rangle$, and $|1,1\rangle$ are in phase at their maximum, we get simultaneously the maximum fidelity $\mathcal{F}$ and the maximum CPS.

The maximum value of the CPS is obtained when the nonlinear cross Kerr interaction takes place; and this happens when the probability of being in states $|0,1\rangle$, $|1,0\rangle$, and $|1,1\rangle$ is simultaneously maximum. Moreover the fact that the oscillating collective atomic state returns to the level $|3\rangle$ (see Fig.4.9b), ensures the high fidelity of the transient process.

A comment about the calculation of the common group velocity of the two wave-packets, $v_g$, is in order. As mentioned earlier, EIT is stationary phenomenon, and in fact, the conventional

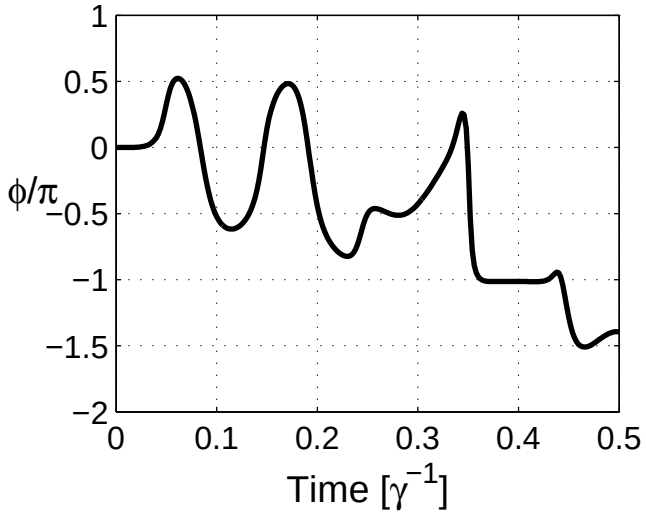


Figure 4.8: Conditional phase shift $\phi$ versus the interaction time, for the parameters of Fig. 4.7. See text for details.

$v_g$ is a steady-state quantity which it is obtained from the susceptibility $\chi$ according to eq.(4.26)

$$v_g = c\left[1 + \frac{1}{2}\mathrm{Re}[\chi] + \frac{\omega_0}{2}\left(\frac{\partial \mathrm{Re}[\chi]}{\partial \omega}\right)_{\omega_0}\right]^{-1} \tag{4.26}$$

($\omega_0$ is the central frequency of wave-packet), where the susceptibility of the $j$-th field, $\chi_j$ ($j = p, t$), is evaluated from the associated steady-state atomic coherence $\sigma_j^{ss}$ as

$$\chi_j = \frac{N|\mu_j|^2}{V\hbar\varepsilon_0\Omega_j}\sigma_j^{ss}. \tag{4.27}$$

Instead, the above results are obtained in the transient regime where $\gamma t_{int} < 1$, and for this reason we have estimated the group velocity in a different way. We have evaluated the relevant time-dependent atomic coherence $\sigma_j(t)$ and the corresponding "instantaneous susceptibility" $\chi_j(t)$ from the reduced atomic density matrix $\sigma_{red}(t) = \mathrm{Tr}_{fields}\{\sigma(t)\}$, with $\sigma(t)$ being the solution of Eq. (4.11). The corresponding "instantaneous"group velocity $v_g(t)$ has been then averaged over the time interval between 0 and $t_{int}$, providing in this way our estimate of the "transient" non-stationary group velocity of the single-photon wave-packets. For the parameters of Figs. 4.7 and 4.8, this non-stationary $v_g$ is approximately equal to $c/100$ and it is about one order of magnitude smaller than the conventional $v_g$ obtained from the steady-state susceptibility. This appreciable slowing down of the group velocity is a signature of a sort of "non-stationary" EIT process.

In order to verify that this non-stationary dynamics are really reminiscent of EIT, in the next subsection we compare these results with a numerical study of the three-level ladder atomic scheme (see Fig. 4.10), yielding XPM without EIT. Here we anticipate that we have found a smaller gate fidelity ($\sim 78\%$) for a corresponding set of parameters, providing therefore further

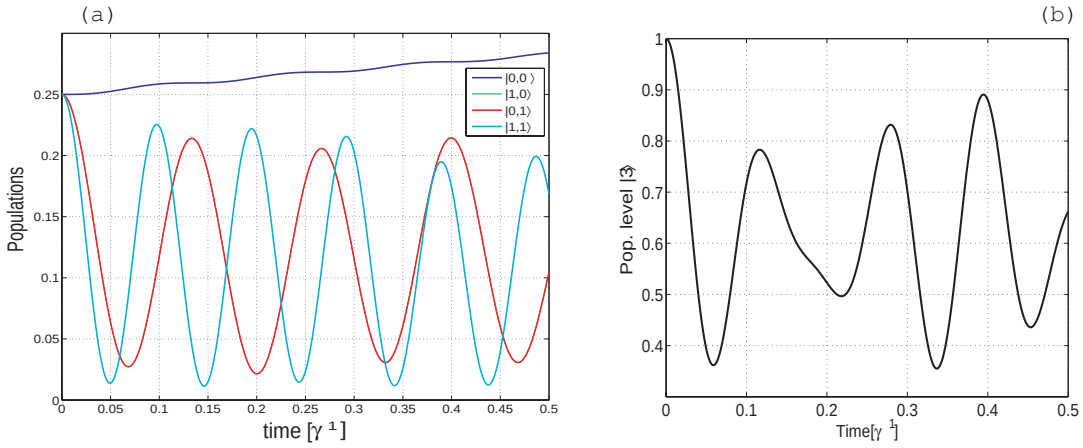


Figure 4.9: Figure (a) shows the Rabi oscillations of the probability of finding the system in level $|0,0\rangle$, $|1,0\rangle$, $|0,1\rangle$, $|1,1\rangle$, respectively, when the atom is on atomic level $|3\rangle$. Fgure (b) shows the probability of finding the atoms in the atomic level $|3\rangle$.

support to the presence of a moderate, non-stationary EIT process in the transient dynamics of our five-level $M$ scheme.

### 4.5.1 The Conventional Three-Level Scheme

The atomic ladder scheme (see Fig. 4.10) is well-known to exhibit XPM of the two fields involved [13]. In order to achieve a reasonable size of cross-phase shift, the detuning of the intermediate state $\delta_p$ needs to be large. This minimizes spontaneous emission ($\sim \gamma_2/\delta_p^2$), but also the size of XPM $\sim 1/\delta_p^2$.

In order to evaluate the XPM in a manner comparable to what we have done for the M-scheme, we make similar assumptions and arrive at a description analogous to the one described in Sec. 4.2. The Hamiltonian is now given by

$$\begin{aligned} H_3 &= \hbar\delta_p\hat{S}_{22} + \hbar(\delta_p - \delta_t)\hat{S}_{33} + \hbar g_p\sqrt{N_a}\left(\hat{a}_p\hat{S}_{21} + \hat{S}_{12}\hat{a}_p^\dagger\right) \\ &\quad + \hbar g_t\sqrt{N_a}\left(\hat{a}_t\hat{S}_{23} + \hat{S}_{32}\hat{a}_t^\dagger\right). \end{aligned} \tag{4.28}$$

Following the same reasoning as in Sec. 4.2, we arrive at the effective master equation (we neglect here atomic dephasing)

$$\begin{aligned} \dot{\sigma} &= \mathcal{L}_3\sigma = -\frac{i}{\hbar}\left[H_3,\,\sigma\right] + \frac{\gamma_{21}}{2}\left(2\hat{S}_{12}\sigma\hat{S}_{21} - \hat{S}_{21}\hat{S}_{12}\sigma - \sigma\hat{S}_{21}\hat{S}_{12}\right) \\ &\quad + \frac{\gamma_{32}}{2}\left(2\hat{S}_{23}\sigma\hat{S}_{32} - \hat{S}_{23}\hat{S}_{32}\sigma - \sigma\hat{S}_{23}\hat{S}_{32}\right), \end{aligned} \tag{4.29}$$

where $\gamma_{12}$ and $\gamma_{23}$ denote the spontaneous emission rates from levels $|2\rangle$and$|3\rangle$ to levels $|1\rangle$and$|2\rangle$ respectively, and the operators $\hat{S}_{ij}$ denote collective atomic operators, in the spirit of Eq. (4.4).

The results of the calculation of unconditional quantities are shown in Fig. 4.11, for a parameter regime comparable to that discussed above for the five-level $M$ scheme. The atoms are assumed to be in the collective state $\bigotimes_{i=1}^{N_a}|2\rangle_i$ initially, as this is found to give better results.

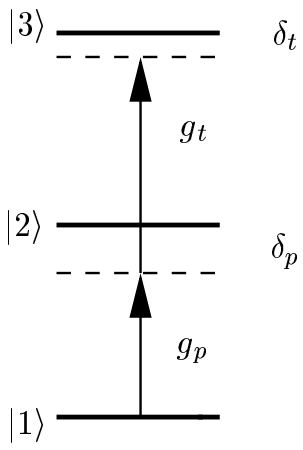


Figure 4.10: Energy levels of the ladder scheme. $g_{p,t}$ denote couplings of the quantized probe and trigger fields to their respective transitions. $\delta_{p,t}$ are detunings of the probe and trigger fields from resonance.

The reason is a more efficient photon-photon interaction since the initial state is symmetric with respect to probe and trigger photons. At the interaction time $t_{int} \approx 0.12/\gamma$, the CPS reaches the value $\sim \pi$ and at the same time the unconditional fidelity is found to be $\sim 78\%$. It is possible to see that the conditional fidelity, even though higher, always remains significantly lower than that obtained in the $M$-scheme.

Therefore, we conclude that the optimal results for the QPG operation can be found in the "transient EIT-regime". The general trade-off between the nonlinear phase shift and the fidelity is still present, but it is compensated by the transient oscillations in the populations of atomic levels. In fact, the numerical results show that, in the parameter regime under consideration, the population of the excited states $|e_2^{(n_p,n_t)}\rangle$ and $|e_4^{(n_p,n_t)}\rangle$ is always negligible, and one has coherent oscillations of the population between the states $|e_1^{(n_p,n_t)}\rangle$, $\bigotimes_i |3\rangle_i \otimes |n_p, n_t\rangle$ and $|e_5^{(n_p,n_t)}\rangle$. At the interaction time $t_{int}$ corresponding to the maxima of the gate fidelity in Fig. 4.7, atoms are largely found in state $\bigotimes_i |3\rangle_i \otimes |n_p, n_t\rangle$, and the relative populations *and* phase relations between the states of the two photonic qubits are consistent with the "ideal" state of Eq. (4.13).

## 4.6 QPG operation with longer pulses

In a recent experiment [98], performed in Paris by the group of Grangier, a single photon emitter has been realized. This single photon source adopts a coherent adiabatic passage procedure on a single multilevel Rubidium atom. The atomic transition involved in the experiments are the same we have used to propose the experimental implementation of the all-optical quantum phase gate. This experiment produces a single photon pulse of a duration determined by the lifetime of the excited level and it is therefore ..... and approximately equal to 25 nsec.
In this section we recalculate numerically the conditional dynamics, and the expected group velocity adopting the properties and the parameters of the pulses generated in the recent experiment [98]. The pulses' duration for the Grangier experiment is more or less the double of that one we adopted in the section of the transient regime. Assuming that the probe and trigger fields are single photon pulses of duration of 25 nanoseconds, compared to the previous set up

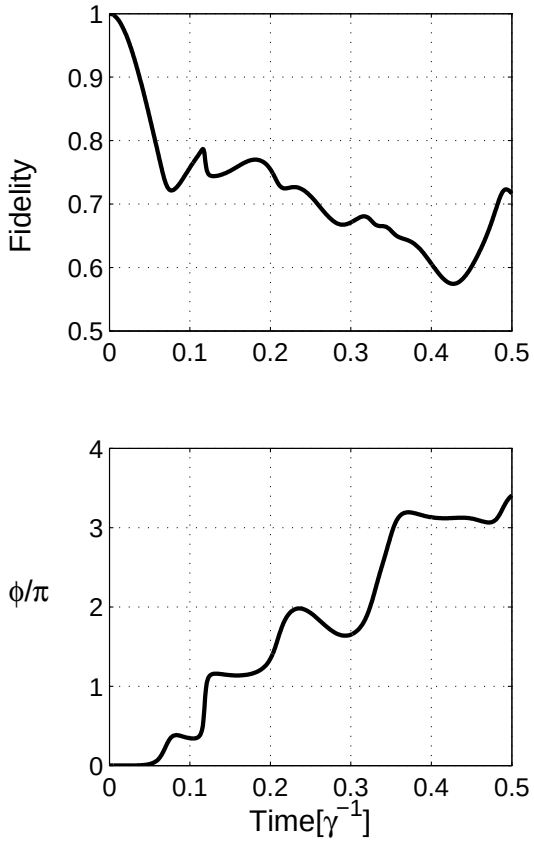


Figure 4.11: Average fidelity (top figure) and conditional phase shift (bottom figure) as a function of time for the three-level ladder scheme of Fig. 4.10 and for $N_a = 10^8$, $\delta_p = 10\gamma$, $\delta_t = 0$ and $g_p = g_t = 0.0022\gamma$. The spontaneous emission rate is $\gamma_{21} = \gamma_{32} = \gamma = 2\pi \times 6$ MHz.

we have to adapt the dimensions of the atomic cloud and consequently all the other parameters, like coupling $g_{p,t}$ and the density. Results for the new parameters are represented in Fig.(4.12).

The results of the numeric simulations are obtained, as in the preious sections, for all possible initial states, and show that for a conditional phase shift of $\pi$, corresponds a fidelity of around 90%. The difference between the deterministic fidelity (continous-blue line) and that from the post-selection scheme (dashed line) is smaller than in the transient regime transient regime of the previous Section. This is because the larger interaction time of 25 ns determines a larger probability for jumps to take place. The fidelity in the transient regime is maximum when the probabilities of find the atomic-field system in the states $|3,1,1\rangle, |3,1,0\rangle, |3,0,1\rangle$ are at their maximum and in phase. Here, the adoption of pulses longer than in the previous case determines an exponential reduction of this probability resulting in a reduction of the best achievable fidelity. Also the non stationary group velocity has been evaluated as in the previous Section: the results gives a smaller group velocity of $1.5 \times 10^6$m/sec. Also in this new parameter regime the behaviour of the group velocity is consistent with the presence of a weak EIT regime.

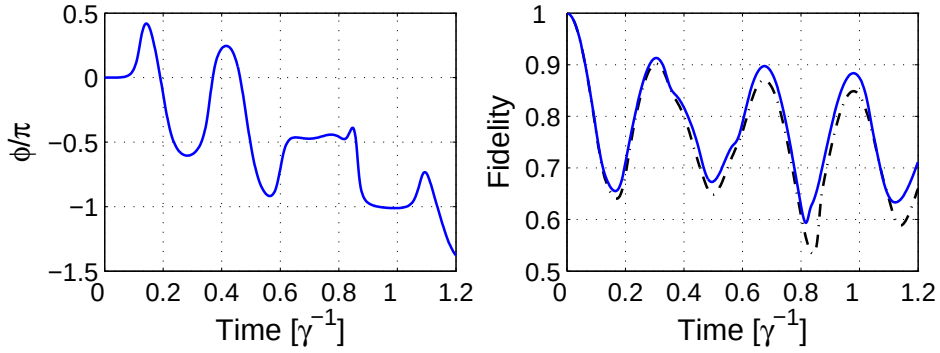


Figure 4.12: Conditional phase shift (*left*) and the fidelity (*right*) of a QPG operation for $N_a = 10^8$, $\delta_2 = \delta_3 = 6\gamma$, $\epsilon_{12} = \epsilon_{34} = 0.05\gamma$, $g_p = g_t = 0.0009\gamma$ and $\Omega_1 = \Omega_4 = \gamma$. For $^{87}$Rb, $\gamma = 2\pi \times 6$ MHz, giving the interaction time (i.e. pulse length) of $\simeq 25$ ns for $|\phi| \simeq \pi$. Dot-dashed line denotes the deterministic fidelity, while solid line denotes the conditional fidelity.

## 4.7 Proposal for an experimental verification of a QPG

*Occupation number logical basis* – In this section we describe a Michelson-like interferometer (see Fig 4.13) for two-photons product state $|1_{\rm R}\rangle|1_{\rm B}\rangle$ with the 'right' $\sigma^-$ circular polarization, where R (red) refers to the *probe* field and B (blue) to the *trigger*. We show that the interferometer is able to reveal and measure the QPG phase shift. The probe and trigger fields with a bandwidth of $40 \div 100$ MHz (corresponding to $25 \div 10$ ns 1/e half width pulse duration) are separated in frequency by $\sim$7 THz and are resonant with the $^{87}$Rb hyperfine transitions $D_1F = 2 \rightarrow F' = 1$ at 794.7 nm (377.228 THz), and $D_2F = 2 \rightarrow F' = 1$ at 780.2 nm (384.225 THz), respectively.

The interferometer is realized by a 50/50 beam splitter (BS) and using a Fabry-Perot cavities ($\rm FP_{1,2}$) instead of mirrors. The FPs reflect back the probe field, which is then superimposed on the BS and detected by an APD ($\rm D_R$), and transmit the trigger field detected by an APD in each arm ($\rm D_{B1}$ e $\rm D_{B2}$). This implies that only the trigger frequency is resonant with the FPs' cavity, which has a cavity length of 2 mm corresponding to a FSR is 74.85 GHz, while the probe frequency falls in the middle of the previous $93^{\rm th}$ and $94^{\rm th}$ FSRs. According to the photon bandwidth a Finesse of $10^3$ determines a reflectivity for the probe field of 99.9% (see the spectra in the *Right Inset* of Fig. 4.13).

As the bandwidth of the two photons are well distinct in frequency and the FPs filter out the trigger field, the apparatus determine an interferometer only for the probe field. The coincidence probabilities $P(\rm R, B1)$, between $\rm D_R$ and $\rm D_{B1}$, and $P(\rm R, B2)$, between $\rm D_R$ and $\rm D_{B2}$, post-select the events in which the trigger photon was either in the arm 1 or arm 2, with any informations on the probe, which interferes. In this case the coincidence probabilities are equal and given by

$$P(\rm R, B1) = P(\rm R, B2) = [1 + \cos \Phi]/8 \tag{4.30}$$

where $\Phi$ represents the phase difference due to the different optical paths of the two arms the probe experiences. In arm 2 a delay line (DL) is added to compensate the difference in the optical path and to scan for the interference pattern. In the *Left Inset* of Fig. 4.13 is shown a Sagnac-like version of the interferometer, which allows for an auto-compensation of the optical path delay as the two arms coincide.

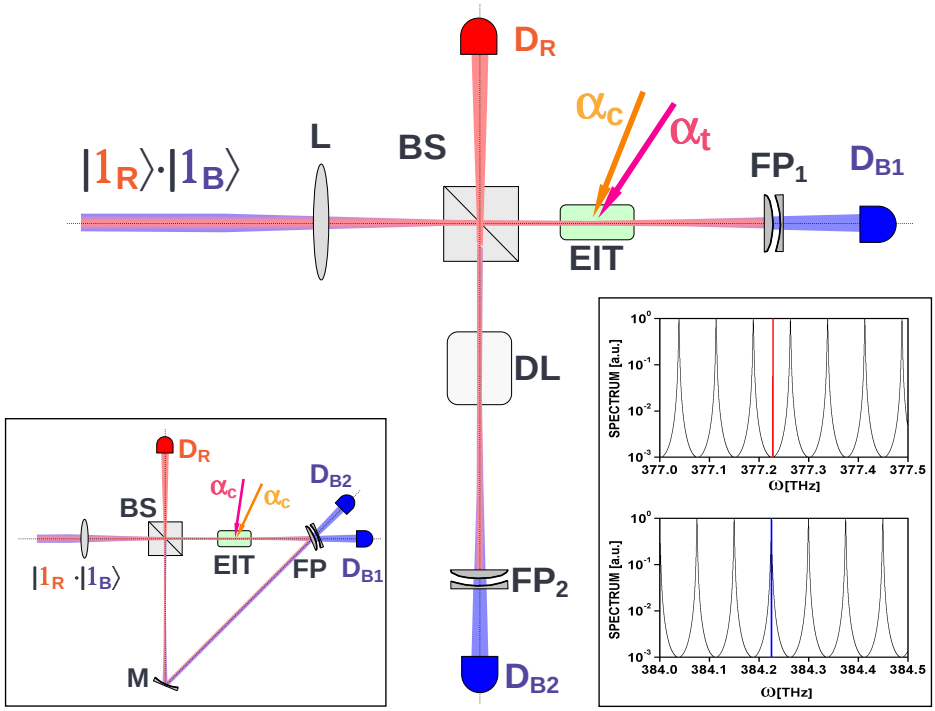


Figure 4.13: Scheme of the proposed experiment for a measurement of the non-linear phase shift in a QPG. A Michelson-like interferometer with a two-photons input state $|1_{\mathrm{R}}\rangle|1_{\mathrm{B}}\rangle$, *probe* and *trigger*, respectively, allows to measure the non-linear phase induced by the EIT on the logical basis of the qubits, which coincide with the two lowest Fock states. Two intense classical fields $\alpha_t$ and $\alpha_c$, *tuner* and *coupling* respectively, are necessary to the 5-levels EIT process. L is a lens for the mode matching in the EIT. BS a 50/50 beam splitter. DL a delay line. $\mathrm{FP}_{1,2}$ Fabry-Perot cavities. $\mathrm{D}_{R,B1,B2}$ are avalanche-photodiodes APDs. *Left Inset* – Scheme using a Sagnac interferometer for avoiding the optical path difference. M is a mirror. *Right Inset* – Frequency spectrum for a 2 mm FP cavity length and Finesse equal to $10^3$. In the plots are also reported the spectra of the probe and trigger photon.

When an EIT system is considered in one arm, let's say the arm 1, a non-linear contribution to the phase is added by the QPG, whether the trigger photon is present in the arm 1 or not. The EIT requires two intense classical fields resonant to the $D_2F = 1 \rightarrow F' = 1$ (384.232 THz) and $D_1F = 1 \rightarrow F' = 1$ (377.235 THz), $\sigma^-$ circularly polarized *tuner* field ($\alpha_t$), and $\sigma^+$ circularly polarized *coupling* field ($\alpha_c$), respectively. The coincidence probabilities $P(\mathrm{R}, \mathrm{B1})$, between $\mathrm{D_R}$ and $\mathrm{D_{B1}}$, and $P(\mathrm{R}, \mathrm{B2})$, between $\mathrm{D_R}$ and $\mathrm{D_{B2}}$, post-select the events in which the trigger photon is in the arm 2 and hence a non-linear phase is not added to the interference amplitude. Instead a non-linear contribution to the phase is expected when detections on $\mathrm{D_R}$ are post selected by the detection on $\mathrm{D_{B2}}$. Fig. 4.14 represents the diagram of the four amplitude probabilities after the action of the BS and the FPs on the two-photons state. The non-linear phase $\phi_{11}$ is added only to the first diagram.
According to the true-table and the amplitudes of Fig. 4.14, the coincidence probabilities can

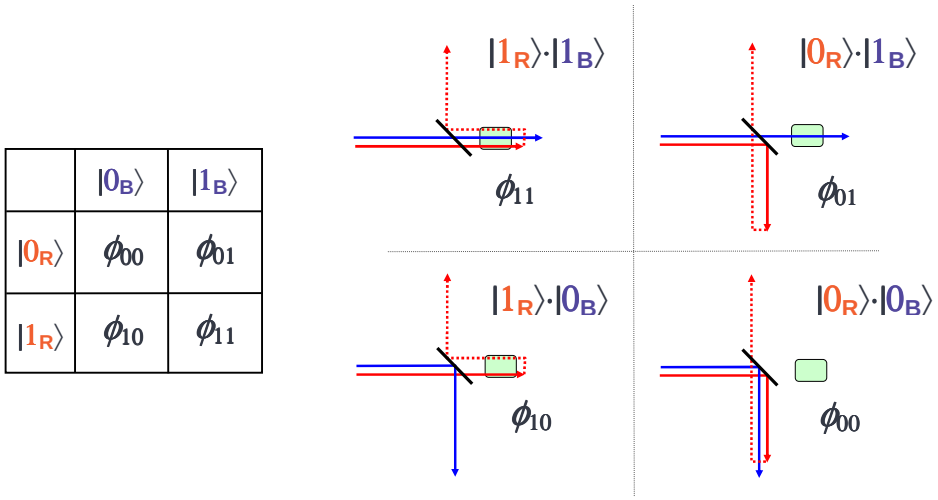


Figure 4.14: True-table of the QPG for a logical basis of the qubits determined by the two lowest Fock states. On the right the diagrams corresponding to the probability amplitudes after the action of the BS and the FPs on the two-photons input state.

be evaluated to be

$$P(\mathrm{R},\mathrm{B1}) = [1+\cos(\widetilde{\Phi}+\phi)]/8 \quad (4.31)$$
$$P(\mathrm{R},\mathrm{B2}) = [1+\cos\widetilde{\Phi}]/8 \quad (4.32)$$

with $\tilde{\Phi}=\Phi+(\phi_{10}-2\phi_{00}+\phi_{+0})$, $\phi_{+0}$ the phase due to the probe photon reflected in arm 1 with 'wrong' $\sigma^+$ circular polarization. The phases $\phi_{10}$ and $\phi_{00}$ were introduced in Eqs. (4.15,1.64) as the QPG phase $\phi=\phi_{11}-\phi_{01}-\phi_{10}+\phi_{00}$. The phase difference between the two interference patters determined by the two coincidence probabilities determines univocally the value of $\phi$. In the case of an ideal QPG for which $\phi=\pi$ the two coincidence probabilities are in opposition of phase.

*Polarization logical basis* – The previous proposal indirectly tests the QPG based on the EIT detecting the non-linear phase shift by a Michelson interferometer and coincidence measurements. A direct measurement of the true table or a test on a general qubit state requires a control and measurement of a superposition of vacuum and one photon state. While the generation of a superposition of vacuum and single photon state has been already achieved [98], the measurement of such a superposition requires a difficult homodyne measurement [99,100]. However a logical basis for the qubits can be chosen as the circular polarization basis of the probe and trigger photons. A test of the QPG will then require the detection of both the photons solving the problem of the detection of Fock states superposition.

The experimental setup is the same as in Fig. 4.13, but the qubits are now encoded in the polarization of the input two-photon state. According to the true-table and the amplitudes in Fig. 4.7 it is possible to derive the coincidence probabilities $P(\mathrm{R_i},\mathrm{B1_j})$ and $P(\mathrm{R_i},\mathrm{B2_j})$, with $i,j=\{+,-\}$, as

$$P(\mathrm{R_i},\mathrm{B1_j}) = [1+\cos(\overline{\Phi}+\overline{\phi}_{ij})]/8 \quad (4.33)$$
$$P(\mathrm{R_i},\mathrm{B2_j}) = [1+\cos\overline{\Phi}]/8 \quad (4.34)$$

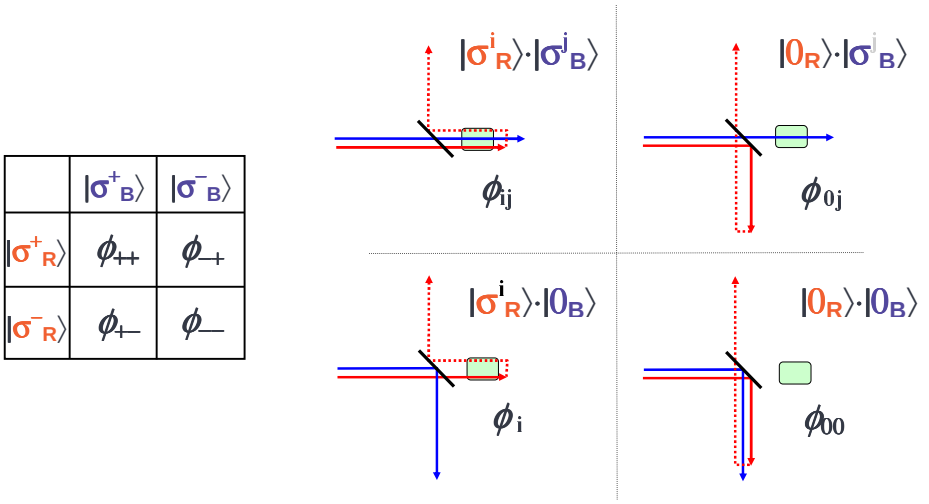


Figure 4.15: True-table of the QPG for a logical basis of the qubits determined by orthogonal circular polarization basis. On the right the diagrams corresponding to the probability amplitudes after the action of the BS and the FPs on the two-photons input state.

with $\overline{\Phi} = \Phi + (\phi_{i0} - 2\phi_{00} + \phi_{(i\oplus 1)0})$, where $i \oplus 1$ is the sum mod 2. The phase $\overline{\phi}$ is now given as $\overline{\phi}_{ij} = \phi_{ij} - \phi_{i0} - \phi_{0j} + \phi_{00}$, where $\phi_{i0}$ is the phase due to the EIT for the probe photon with polarization $i$ and no trigger photon present, and same meaning for the other phases. It is notable that for $i = j = `-' \equiv 1$ it is obtained the previous expression of the QPG phase for the logical Fock states basis. Four possible choices of the probe and trigger polarizations determine the phases

$$\begin{aligned}
\overline{\phi}_{--} &= \phi_{--} - \phi_{-0} - \phi_{0-} + \phi_{00} \\
\overline{\phi}_{-+} &= \phi_{-+} - \phi_{-0} - \phi_{0+} + \phi_{00} \\
\overline{\phi}_{+-} &= \phi_{+-} - \phi_{+0} - \phi_{0-} + \phi_{00} \\
\overline{\phi}_{++} &= \phi_{++} - \phi_{+0} - \phi_{0+} + \phi_{00}\,,
\end{aligned} \tag{4.35}$$

which satisfies the relation $\overline{\phi}_{--} - \overline{\phi}_{+-} - \overline{\phi}_{-+} + \overline{\phi}_{++} = \phi_{--} - \phi_{+-} - \phi_{-+} + \phi_{++} = \phi$. In the case of an ideal EIT for which $\phi_{+0} = \phi_{0+} = \phi_{++} = \phi_{00}$, $\phi_{-+} = \phi_{-0} = \phi_R$ and $\phi_{+-} = \phi_{0-} = \phi_B$, where $\phi_{A,B}$ are the phases acquired by the single photons, we have $\overline{\phi}_{--} = \phi$, and $\overline{\phi}_{-+} = \overline{\phi}_{+-} = \overline{\phi}_{++} = 0$. In a way the phases between the two coincidence interference patterns allows a measurement of the QPG phases in the diagonal basis, i.e. in the single qubit states for which the only QPG phase non zero is the conditional phase shift $\phi$.

*General polarization qubit input states* – The polarization logical basis allows for a direct observation of coherence and production of entanglement as necessary conditions for a QPG. Let assume to encode the information on the polarization state of a two photons, and then send them into the EIT system for QPG, as shown in Fig. 4.7. The outpout photons, as shown in Fig. 4.7, are split by a dichroic mirror (an angled FP cavity with the same parameters as before) and then collected in two APDs ($D_R$ and $D_B$) for coincidence counting. In front of each detector a tomographic system constituted by a QWP, HWP and a PBS, is placed for the complete reconstruction of the polarization state of the output state gaining information on the coherence properties of the gate. It has also been shown [97] that an input state for the QPG

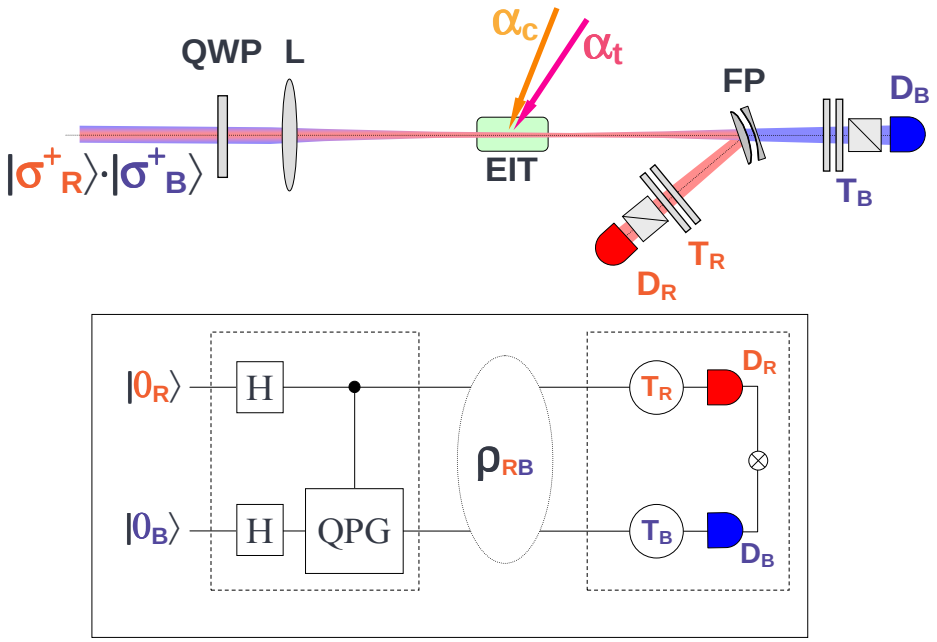


Figure 4.16: Scheme of the proposed experiment for a complete characterization of the QPG. Two photons in the $\sigma^+$ polarization state (logical state $|0_R\rangle \otimes |0_B\rangle$) are transformed by a QWP, corrisponding to two Hadamar single-qubit gates, and then to the EIT (QPG). A Fabry-Perot cavitiy with the same parameter as before transmits the trigger photon and reflect the probe to two tomographic measurement systems ($T_{R,B}$) and detected by APDs.

given by $[(|\sigma_R^+\rangle + |\sigma_R^-\rangle) \otimes (|\sigma_B^+\rangle + |\sigma_B^-\rangle)\rangle)]/2$ can quantify the entanglement of the output state, for which the CHSH inequality is $2\sqrt{1+\sin^2\phi}$ where 2 is the upper classical limit.

# Chapter 5

# A Quantum Error Correction scheme by Atoms and Cavities

*The correction of the errors has been of fundamental importance for the development of contemporary computing devices and also in the advances in communications. In this chapter we focus our attention to the possible realization of a Quantum Error Correction Code (QECC). The goal of this chapter is to show how it is possible to implement a QECC by adopting the interaction of circular Rydberg atoms with the quantized mode of a cavity field.*
*We illustrate the basic ideas of error correction and we show the main difference between classical and quantum error correction. A QECC protocol based on atoms-cavity QED interaction is described. Then we give and describe the results of the simulation of an experimental realization of the protocol under realistic experimental conditions.*

## 5.1 Basic Principles of Quantum Error Correction

Let us assume that we have two distant stations, *Alice* and *Bob*, that share a message. In general the communication channel over which the information is sent is a noisy one, i.e. it is affected by unknown errors of various type [24, 101, 103, 104]. The origin of these errors is the coupling of the system with the environment Fig.(5.1), and the degradation of the information encoded in the quantum state is named *decoherence*. The ability to reveal the errors that have affected the sent message, and finding a way to correct them constitute the central task of Quantum Error Correction (QEC).

Any classical or quantum error correction scheme is based on the main steps:

- *Encoding:* Generating several copies of the original message we want to send.
- *Decoding:* The application of a measurement procedure for the encoded states permits to reveal if errors have occurred.
- *Correction:* With the information obtained from the previous step we can decide which kind of operation has to be applied (if needed).

The objects that are transferred from a station (*Alice*) to another (*Bob*) is a set of qubits

$$|\psi_s\rangle = \alpha|0\rangle + \beta|1\rangle, \tag{5.1}$$

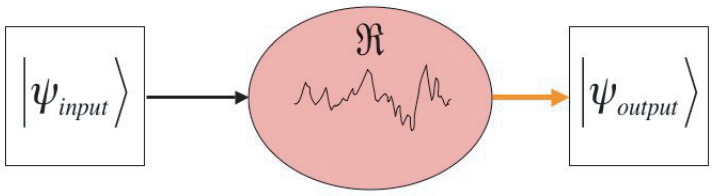


Figure 5.1: Sketch of a transmission's channel affected by noise due to the interaction with the environment

where $|\alpha|^2 + |\beta|^2 = 1$. When we send a qubit through the noisy channel, it interacts with the environment and its state evolves to a different state. The environment can be described in terms of a collection of operators $\{\Gamma_{\mathcal{R}}^{(i)}\}$, that act on the quantum states of the system, and a collection of states $|\psi\rangle_{\mathcal{R}}$. For each qubit sent from Alice to Bob we can apply the following interaction scheme. At $t = 0$, we assume that the system and the environment are factorized

$$|\psi\rangle_{in} = |\psi\rangle_s \otimes |\psi\rangle_{\mathcal{R}}. \tag{5.2}$$

After the transmission of the state, due to the influence of the environment's operators $\Gamma_{\mathcal{R}}^{(i)}$ we have

$$|\psi\rangle_{out} = \sum_i |\psi\rangle_{\mathcal{R}} \Gamma_{\mathcal{R}}^{(i)} |\psi\rangle_s, \tag{5.3}$$

The reduced state at Bob's site is

$$\rho_{Bob} = Tr_{\mathcal{R}}(|\psi\rangle_{out}\langle\psi|), \tag{5.4}$$

which is, in general, a mixed state because Bob does not have access to the environment variables and he has to trace over all possible degrees of freedom of the environment. Moreover the state will differ from the pure one sent by Alice.
In the transmission of quantum systems the errors that can affect the qubits are more numerous than those in the classical counterpart. Together with *bit-flip errors* that cause a flip in the quantum state of the system, also *phase-flip errors* can occur. These cause the flip of the relative phase between the two components of a qubit.

To fight against decoherence, the key resource, in quantum as well as in classical error correction, is *redundancy*. It is the simplest approach to correct errors, and it consists in the

encoding of the information in a redundant way so that it is possible to identify the errors and recover them. During the encoding procedure the first step is to prepare many copies of the information to send. Moreover while making copies of a classical bit is easy, with qubits things are different. In the *quantum domain* we have some additional considerations that have to be taken into account. For qubits the following limitations hold

- *The no cloning theorem* states that it is not possible to make copies of a quantum state.
- *Measurements typically destroy quantum information.*

The resource that can be used in QEC to complete the encoding step is *entanglement*. By enlarging the Hilbert space we can build a non separable state of two or more systems, starting from the original one (5.1). The additional quantum systems "helping" the principal qubit are named *ancillas*. The quantum state describing the composite system of the principal system $S$ and the ancillas $a_1, a_2$ will be part of a Hilbert space given by the tensor product of the Hilbert space of the each system $H_{S,a1,a2} = H_S \otimes H_{a1} \otimes H_{a2}$.

Let consider our qubits in the state (5.1). It is possible to define the encoded basis

$$|0_L\rangle = |0\rangle \otimes |0\rangle \otimes |0\rangle \tag{5.5}$$
$$|1_L\rangle = |1\rangle \otimes |1\rangle \otimes |1\rangle, \tag{5.6}$$

and the initial state (5.1) of the qubit that we are sending can be mapped, by applying a suitable unitary evolution $\mathcal{U}$, into the state

$$\alpha|0\rangle + \beta|1\rangle \rightarrow \alpha|0_L\rangle + \beta|1_L\rangle, \tag{5.7}$$

which means the implementation of the logical state $|\psi_L\rangle$ (*encoding*).

The QEC protocol continues by the next three steps:

- To avoid the perturbation of the encoded qubit during the measurement of the ancillas states, we have to decouple ancillas from the states of the encoded qubit before we measure them. For that Bob applies an unitary operation to the qubits on the logical basis sent by Alice in such a way the ancillas are decoupled from the principal qubit (*decoding*).
- We have to detect the two ancillas. From their state we can know which error occurred, so that we can correct it.
- We can perform the *recovery* procedure, applying a unitary operation $\mathcal{U}^\dagger$ on the qubit that, in practice, invert the effect of the environment.

Now if errors occur with probability $p$, we can calculate the probabilities that a bit-flip error occurs on one of the three qubits that composes the encoded state of eq.(5.7) see Tab.5.1 The final state, after the correction protocol, can be written as

$$\rho_{final} = [(1-p)^3 + 3p(1-p)^2]|\psi\rangle_L\langle\psi|_L + \ldots, \tag{5.8}$$

and depends on the total probability that error can occur in one of this three qubits. The additional terms, non showed here, depend upon the probability that a two-qubit flip occurs,

Table 5.1: Probability of errors through a channel that affected by bit flip errors.

| Input state | Output state | Probability |
|---|---|---|
| $\|\psi_L\rangle = \alpha\|0_L\rangle + \beta\|1_L\rangle$ | $\alpha\|000\rangle + \beta\|111\rangle$ | $(1-p)^3$ |
| $\|\psi_L\rangle$ | $\alpha\|001\rangle + \beta\|110\rangle$<br>$\alpha\|010\rangle + \beta\|101\rangle$<br>$\alpha\|100\rangle + \beta\|011\rangle$ | $p(1-p)^2$ |
| $\|\psi_L\rangle$ | $\alpha\|011\rangle + \beta\|100\rangle$<br>$\alpha\|101\rangle + \beta\|010\rangle$<br>$\alpha\|110\rangle + \beta\|001\rangle$ | $p^2(1-p)$ |
| $\|\psi_L\rangle$ | $\alpha\|111\rangle + \beta\|000\rangle$ | $p^3$ |

they give a positive contribution to $\rho_{final}$ but they are much smaller than the terms showed when $p < 1/2$. This is an important assumption for the validity of the bit-flip error correction schemes and in general is easily fulfilled.

The final goal of the QECC is to improve the fidelity $\mathcal{F}$ of the transfer of information. The evaluation of the overlap between the sent qubit $|\psi_L\rangle$ and the transmitted final state given by $\rho_{final}$ gives

$$\mathcal{F} = \sqrt{\langle\psi_L\,|\rho_{final}|\,\psi_L\rangle} \geqslant \sqrt{1-3p^2+2p^3}, \tag{5.9}$$

The important point is that QEC *cancels errors at first order in* $p$, so that when $p \to 0$, the *fidelity* in the presence of QEC, *converges* to *unity* much faster than in the case of no QEC

### 5.1.1 Quantum Error Correction with Cavity-QED

We now describe a protocol for the correction of the bit flip errors that occurs on an encoded qubit. The protocol is expected to work in the limit of $p < 1/2$ so that the probability that a two bit flip occurs is exponentially small, as seen in the previous section. The reason for which we focus on the use of a cavity-QED (C-QED) system to implement the error correction algorithm is due to the high degree of control nowadays available on C-QED devices. In particular as we cannot copy a qubit (5.1) we need the ability to entangle the encoded qubits with the two ancillas, and C-QED permits to implement the gates needed for this operation. Moreover the long decoherence time, available in C-QED based set up, permits to store quantum information in the cavity modes. This storage is useful because the information recorded in the cavity mode can be read-out by an appropriately prepared atom, and the detection of the atomic states permits to recover the quantum information with a good fidelity.

## 5.2 The Interaction Hamiltonian

Here we describe the model we adopted to take into account the interaction of the atoms with the quantized mode inside an cavity. We have already described the interaction of a two level system with an electromagnetic field, where the field was treated semi-classically. Here we introduce

the Jaynes-Cummings model [105], in which the field is treated quantum mechanically.
Let us consider a two level system as for example the one given in Fig.1.1. The atom are now placed inside a cavity $\mathcal{C}$. The atom will interact with the electromagnetic field associated with a single cavity mode quasi-resonant with the atom. In the passage from a semiclassical to a quantum description, the field is described [2,11,105] by the creation and destruction operators of the field $\hat{a}$ and $\hat{a}^\dagger$,

$$\hat{E}(t) = E_0(t)\mathcal{E}(\vec{r})\Big(\hat{a} + \hat{a}^\dagger\Big), \tag{5.10}$$

where $\mathcal{E}(\vec{r})$ is the mode function. The free evolution Hamiltonians are given by the Hamiltonian of the field $H_{field} = \hbar\omega_{\mathcal{C}}(\hat{a}^\dagger\hat{a} + 1/2)$, and that of the atom $H_{atom} = \hbar\omega_2|2\rangle\langle 2| + \hbar\omega_1|1\rangle\langle 1|$.
These terms, together with the interaction Hamiltonian $H_{int} = -\mu\hat{E}(t) = \imath g(r)\hbar(|2\rangle\langle 1|\hat{a} - \hat{a}^\dagger|1\rangle\langle 2|)$, in the RWA approximation give the total Hamiltonian

$$\begin{aligned} H &= H_{atom} + H_{cavity-field} + H_{int}, \\ &= \hbar\omega_2|2\rangle\langle 2| + \hbar\omega_1|1\rangle\langle 1|) + \hbar\omega_{\mathcal{C}}\hat{a}^\dagger\hat{a} + \imath g(r)\hbar(|2\rangle\langle 1|\hat{a} - \hat{a}^\dagger|1\rangle\langle 2|), \end{aligned} \tag{5.11}$$

where $g(\mathbf{r}) = \mathbf{g_0}\mathcal{E}(\mathbf{r}) = -\mathbf{E_0}\mathcal{E}(\mathbf{r})\mu/\hbar$ is the space dependent coupling of the atom with the cavity mode depending upon the atomic dipole $\mu$ and on the quantization volume. $\mathcal{E}(\mathbf{r})$ is the mode function, and $E_0 = \sqrt{\hbar\omega_C/2\epsilon_0 V}$ is the electric field of the vacuum where $V$ is the quantization volume defined as $\int d^3\mathbf{r}|\mathcal{E}(\mathbf{r})|^{\mathbf{2}}$,i.e. the volume occupied by the field's mode.
In what follows, we place the zero of energy between the two atomic levels, so that $H_{atom} = \hbar\omega_{21}(|2\rangle\langle 2| - |1\rangle\langle 1|)$, and applying the IP with respect to it, we can write the Hamiltonian as

$$H = \Delta\hat{a}^\dagger\hat{a} + \imath\frac{g(\mathbf{r})}{2}(\hat{a}^\dagger|1\rangle\langle 2| - |2\rangle\langle 1|\hat{a}), \tag{5.12}$$

$\Delta$ is the detuning between the frequency of the cavity mode and the atomic transition.
This Hamiltonian describes the unitary time evolution of the atom-field system when an atom is injected inside the cavity.

## 5.3 The QECC Protocols

For the realization of the protocol we need two cavities (see Fig.5.2) $\mathcal{C}_1$ and $\mathcal{C}_2$ placed one after the other. Four different atoms $A_1, A_2, A_3, A_4$, are injected through the cavities interacting sequentially with $\mathcal{C}_1$ and $\mathcal{C}_2$.
The atoms are three level atoms in the *cascade* configuration $|i\rangle, |g\rangle, |e\rangle$, where $|i\rangle$ is the ground state, $|g\rangle$ is the intermediate state, and $|e\rangle$ is the excited state. The quantum information that we want protect, is encoded in the first atom $A_1$, while the second ($A_2$) and the third atom ($A_3$) are the "ancillas" atoms, that have the role of revealing the syndrome. Finally the fourth atom $A_4$ is the *detector*. It is the atom on which the information, originally encoded in the the quantum state of $A_1$, has to be transferred and, if needed, corrected.

The zones indicated with $R_i$ are usually named Ramsey zone, where the atoms interact with a classical electromagnetic field.
In the *First step*, the first atom $A_1$ is prepared in level $|e\rangle$ before entering the first cavity $\mathcal{C}_1$.

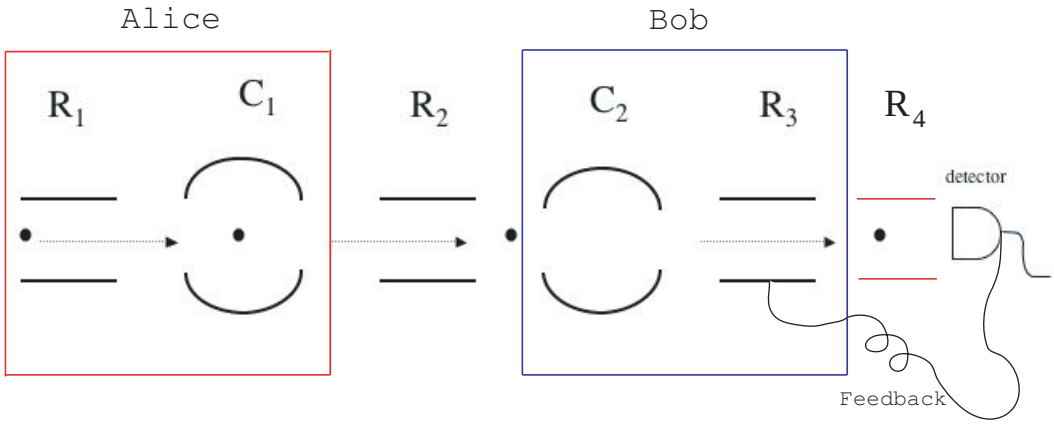


Figure 5.2: Scheme for atom cavity interaction based QECC.

This can be done by applying a $\pi$-pulse in the first Ramsey zone $R_1$, in resonance with the atomic transition $|g\rangle \rightarrow |e\rangle$. In fact in the Ramsey zone the Hamiltonian is

$$H_{Ramsey} = \hbar\Delta|e\rangle\langle e| + \frac{\hbar}{2}\Big(\Omega_{R1}|e\rangle\langle g| + \Omega_{R1}^{\star}|g\rangle\langle e|\Big). \tag{5.13}$$

The consequent atomic evolution at resonance, $\Delta = 0$, starting from $|g\rangle$, is (see eq.(1.15))

$$|\psi(t)\rangle = \cos\frac{\Omega_{R1}t}{2}|g\rangle - \imath e^{-\imath \arg(\Omega_{R1})}\sin\frac{\Omega_{R1}t}{2}|e\rangle. \tag{5.14}$$

Therefore, the $|e\rangle$ state is prepared by applying a $\pi$ pulse, i.e. if a the duration of the interaction $t_{int}$ and Rabi frequency $\Omega_R$ satisfy $\Omega_R t_{int}/2 = \pi$.
*Second step.* The first atom enters cavity $\mathcal{C}_1$. The cavity has to be initially prepared in the vacuum state and when $A_1$ crosses it the Hamiltonian (5.12) determines the evolution

$$|e, 0_{\mathcal{C}_1}\rangle \rightarrow \cos\frac{|\Omega_{C1}|t}{2}|e,0\rangle - \imath e^{-\imath \arg(\Omega_{C1})}\sin\frac{|\Omega_{C1}|t}{2}|g,1\rangle. \tag{5.15}$$

By controlling the atom-cavity interaction time we can prepare an effective initial qubit, involving both $A_1$ and $C_1$ in the generic superposition

$$|\psi\rangle_{enc} = \alpha(t)|e,0\rangle + \beta(t)|g,1\rangle, \tag{5.16}$$

with $|\alpha(t)|^2 + |\beta(t)|^2 = 1$.
At the *third step* we prepare the encoding of the principal qubit with the two ancillas to obtain a state of the (5.5) type. The two ancillas $A_2, A_3$, are chosen to be atoms emitted in state $|i\rangle$. When they pass through the first Ramsey zone $R_1$ they resonantly interact with the EM field and after a $\pi/2$-pulse they are prepared in the state

$$|+\rangle_{A_1,A_2} = \frac{1}{\sqrt{2}}\big(|i\rangle + |g\rangle\big). \tag{5.17}$$

Crossing $\mathcal{C}_1$ they experience a $2\pi$ interaction resonant with the $|g\rangle \rightarrow |e\rangle$ transition. The $2\pi$ interaction determines a controlled phase accumulation on the atomic state $|g\rangle_{A_2,A_3}$ resulting in

$$|1\rangle_{C_1}|g\rangle_{A_{2,3}} \rightarrow -|1\rangle_{C_1}|g\rangle_{A_{2,3}}.$$

When both the ancillas have crossed $\mathcal{C}_1$, the final atoms-cavity state will be

$$\alpha(t)|e,0\rangle + \beta(t)|g,1\rangle \rightarrow \alpha(t)|e_{A_1},+_{A_2},+_{A_3},0_{C_1}\rangle + \beta(t)|g_{A1},-_{A_2}-_{A_3},1_{C_1}\rangle, \tag{5.18}$$

where $|\pm\rangle_{A_j} = \frac{1}{\sqrt{2}}\big(|i\rangle_{A_j} \pm |g\rangle_{A_j}\big)$, with $j = 1,2,3$.
At the next step, *the fourth*, atoms are sent from Alice to Bob through the noisy channel, which in the experimental proposal is represented by the second Ramsey zone $R_2$.
Let us for the moment assume that no error has taken place during the passage through the noisy channel. In what follows we describe the evolution of the global system's state as all the other steps of the protocols are realized in the three possible situation, *no error*, error on *one of the ancilla* atom, *error on the encoded* qubit .

We are faced with three possible situations:

- **Case 1: No bit-flip error.**
  At *step five* the $A_1$ will interact with the cavity $\mathcal{C}_2$ by a $\pi$-pulse. The only part of the state (5.26) that evolves, is $|e_{A_1},0_{C_1}\rangle$. This interaction *disentangles* the first atom from the other system giving

  $$|\psi\rangle = \big[\alpha(t)|+_{A_2},+_{A_3},0_{C_1},1_{C_2}\rangle + \beta(t)|-_{A_2}-_{A_3},1_{C_1},0_{C_2}\rangle\big]|g\rangle_{A_1}. \tag{5.19}$$

  This transformation transfers the encoded qubit from the cavity-atom $\mathcal{C}_1 - A_1$ given by the relation (5.15) to the an encoded qubit that involves the two cavities $\mathcal{C}_1 - \mathcal{C}_2$. When the two ancillas pass through the second cavity they experience the same transformation than in $C_1$, applying the $2\pi$-pulse to atoms $A_{2,3}$, so that the two ancillas are decoupled from the encoded $\mathcal{C}_1 - \mathcal{C}_2$ state as it must be for a decoding process. The resulting state will be an entangled state of the two cavities only,

  $$|\psi\rangle = \big[\alpha(t)|0\rangle_{C_1}|1\rangle_{C_2} + \beta(t)|1\rangle_{C_1}|0\rangle_{C_2}\big]|-\rangle_{A_2}|-\rangle_{A_3}. \tag{5.20}$$

  We arrive at the final *sixth step* of this error correction protocol. Here the detection of the ancillas' states is performed, and if an error is revealed the correction procedure is applied. In this step the fourth atom $A_4$ starts to play its role. The $A_4$ has the function to reload the information now encoded in the $\mathcal{C}_1 - \mathcal{C}_2$ entangled state and record the information stored in the atomic state. The need for this fourth atom is in fact evident, the only information that can be easy to read by the detector is that recorded in the atomic state. Atoms $A_4$ is prepared in the $|g\rangle$ state, it passes, without any interaction, through the first cavity and the first two Ramsey zones. Assuming that no error takes place on this atom, it arrives in the state $|g\rangle$ at $\mathcal{C}_2$. To $A_4$ we apply a $\pi$-pulse resonant interaction as before, the only part of the global state that evolves is $|g\rangle_{A_4}|1\rangle_{C_2} \rightarrow -|e\rangle_{A_4}|0\rangle_{C_2}$. The evolution of the whole cavities-atoms system, after the passage of the last atom, is

  $$|\psi\rangle = \big[-\alpha(t)|0\rangle_{C_1}|e\rangle_{A_4} + \beta(t)|1\rangle_{C_1}|g\rangle_{A_4}\big]|-\rangle_{A_2}|-\rangle_{A_3}. \tag{5.21}$$

Now we detect the two ancilla states. If we obtain the ancillary state $|-\rangle_{A_2}|-\rangle_{A_3}$, we can argue that the qubit has not been affected by any bit-flip error. The state of eq.(5.21) and (5.17) are not identical. Although the amplitude probabilities are exactly the same, they differ by a difference of $\pi$ in the relative phase. This is a consequence of the sequence of pulses that permits the entanglement and disentanglement that constitute the protocol, but there is a simple way to correct this "problem". As it is a relative phase difference that affect the final state with respect to the encoded one, it is sufficient to apply a classical resonant $2\pi$-pulse in the $R_4$ zone to the final state. This will change the phase of the $A_4$ state only, permitting to obtain a perfect matching of the final and of the initially encoded state.

- **Case 2: bit-flip error on the ancillas.** The possible situation is that a single bit-flip error on *one* of the ancilla atoms takes place. We have assumed that two bit-flip errors are much less probable than single bit-flip errors. If such an error on one of the ancilla takes place, the final state (5.21) will have one of the decoupled ancillary state flipped $|-\rangle_{A_2}|-\rangle_{A_3} \rightarrow |+\rangle_{A_2}, |-\rangle_{A_3}, |-\rangle_{A_2}, |+\rangle_{A_3}$. By detecting such a state on the ancillas, we can distinguish that the error has not involved the qubit we are sending, and therefore no correction is needed. As before the only thing we have to do is to apply a classical pulse to correct the relative phase as in the previous case.

- **Case 3: bit-flip error on the encoded qubit.** If a bit-flip error occurs during the passage of $A_1$ in $R_2$, the effect will be the exchange between $|g\rangle_{A_1} \leftrightarrow |e\rangle_{A_1}$. The state after the first atom has interacted with $\mathcal{C}_2$ now becomes

$$|\psi\rangle = \alpha(t)|0\rangle_{C_1}|g\rangle_{A_1}|++\rangle_{A_{2,3}} + \beta(t)|1\rangle_{C_1}|e\rangle_{A_1}|--\rangle_{A_{2,3}}, \tag{5.22}$$

and after the passage of $A_4$ we have

$$|\psi\rangle = \left[\alpha(t)|0\rangle_{C_1}|g\rangle_{A_4} - \beta(t)|1\rangle_{C_1}|e\rangle_{A_4}\right]|++\rangle_{A_{2,3}}. \tag{5.23}$$

In this case we have to apply the error correction, that consists of a feedback $\pi$ pulse in $R_3$ that flip the $|e\rangle \leftrightarrow |g\rangle$ in $A_4$, followed by a $2\pi$-pulse that change the phase of the $|g_{A_4}, 1_{C_1}\rangle$ state. After the measurement of the two ancillas we obtain a final state

$$|\psi\rangle_{final} = \alpha(t)|0\rangle_{C_1}|g\rangle_{A_4} + \beta(t)|1\rangle_{C_1}|e\rangle_{A_4}, \tag{5.24}$$

that is exactly the initial atom-cavity state provided the we make the exchange $A_1 \leftrightarrow A_4$. The original encoded state is restored and quantum information has been safely transferred from Alice to Bob.

## 5.4 Experimental set-up, Cavity and Rydberg states

The proposed QECC scheme gives the result of eq.(5.24) provided that all the evolutions at each step, are unitary. In general this is not true due to the fact that cavities and atoms experience their own interaction with the environment. This makes time evolution only approximately

unitary. For what concerns the atoms spontaneous emission is present, and depends on the type of atoms that we use in the experiment. For the cavity we have to take into account photon leakage. The photons can remain inside a cavity only for a limited time, after which the photons are lost mainly by scattering, but also transmission and absorption of the mirrors play a role. For a realistic analysis of the performance of the QECC protocol we have to include these losses in the treatment. This analysis shows us how the atoms and the cavities involved have to be chosen so to reduce the effect of the environment. To this end the protocol has been tailored for the experimental set-up involving microwave cavities and Rydberg atoms studied at the ENS in Paris.

### 5.4.1 The Circular Rydberg States

Adopting atoms with the right properties, namely long decay time and right velocities, is of crucial importance in the realization of the protocol. The circular Rydberg states [108] are excellent candidates for the protocol's implementation. They are atoms possessing large principal quantum number $n$, i.e. of the order of 50, and maximum angular momentum $l = n - 1$. The large principal quantum number and the large $l$ permit to describe the orbital in a classical way, and the electron orbital is a circular. The three level cascade structure can be found around $n = 50$, more precisely we can choose $n = 51, 50, 49$ for $|e\rangle, |g\rangle, |i\rangle$ respectively. Circular Rydberg states in this configuration represents a well studied experimental set-up [107, 109–111] that has been adopted by the Haroche's group in a number of experiment during last years. Rydberg atoms posses interesting properties because the radiative lifetime of the three levels $|e\rangle, |g\rangle, |i\rangle$ is of the order of $T_{atoms} = 30ms$. This long radiative time permits to have negligible effect on the atomic coherence from the spontaneous decay rate. The dipole moment matrix elements are very large, of the order of 1250 a.u for the $|e\rangle \leftrightarrow |g\rangle$ transition.
The circular atoms can be prepared with a purity of $\geq 98\%$ [106] and the velocity of the atoms emitted by the atoms gun can be controlled with great precision (the precision is $\sim \pm 2$ m/sec). The position of each atoms inside the apparatus is known with a $\pm 1$-mm precision. The process of optical pumping devoted to the preparation of the circular states has an efficiency of 0.2 "right" atoms for pulse, with a Poissonian statistics.

### 5.4.2 The Cavity

The cavity that is adopted in [106, 107, 110, 111] is an open Fabry-Perot resonator made with two spherical superconducting niobium mirrors facing each other at a distance $d = 27.6$ mm, the diameter $D$ of the cavity is $D = 50$ mm, and the radius of the mirrors is $R = 40$ mm. The resonator is in resonance with the $e \leftrightarrow g$ transition, with a photon storage of $T_{cavity} = 1 \div 10$ms, this correspond to a very large quality factor of $Q = 3 \times 10^8$. To obtain an optimal atom-cavity mode interaction we need that the cavity is as much as possible in the vacuum state at the beginning of the various steps. To this end, the cavity is cooled down, to avoid the presence of thermal photons. Moreover, as after the cooling the mean number of photons is still $\sim 0.7$, every experiment includes at the beginning a flux of resonant atoms in $|g\rangle$ that passing through the cavity, have the role of absorbing the residual photons. Adopting this technique the cavity can be prepared to contain 0.1 photons after a cooling sequence.

Passing through the cavity, the atoms are coupled with the field by the $g$ factor which is a Gaussian function due to the profile of the cavity field, that depends on the interaction time, the time spent by the atom within the cavity, on the atoms' velocity $v$, and on the parameter

$\omega_0$ is the width of the Gaussian. $\omega_0$ depends on the specific parameters of the cavity, like the distance $d$ between the cavity's mirrors and the radius $R$ of the mirrors.
Therefore the resulting time dependent coupling is a Gaussian with the envelope given by the relation

$$g(t) = \frac{g_0}{2}\mathcal{E}(vt) = \frac{g_0}{2}\exp\Big(-\frac{(vt)^2}{\omega_0^2}\Big). \tag{5.25}$$

The control over the interaction time between the cavities and the atoms, can reach an high degree of accuracy in the cavities we are thinking to adopt [106]. This control is based on Stark-shift tuning [106, 107] of the atoms injected inside the cavities. This approach to the control of the interaction time is based on a rapid modification of the resonance condition under which the atom interacts with the cavity mode. In practice, applying a tension at the end of the two mirrors, we can rapidly modify the field inside the cavity. This induces a quadratic Stark-shift of the atomic levels that for the Rydberg atoms is particularly strong [107], permitting to modulate the interaction between the atoms and the cavity. In this way it is possible to build all possible superposition of atom-cavity state generated by the Rabi angle $\Omega t_{int} \in [0, 2\pi]$.

## 5.5 Numerical Simulation

The sequence of the operation needed by the protocol has been simulated adopting the parameters of the realistic devices adopted in a real experimental set-up as for example that of references [106, 107, 110, 111]. The quantum trajectories approach [112], is adopted to perform the numerical simulation of the protocol. Three different initial encoding configuration have been adopted, i.e. different values of the $\alpha$ and $\beta$ after the first atom has passed the first cavity. The main source of decoherence, apart from the noisy channel is the cavity decay rate $k$. For this reason the simulations have been performed to find out the role of such a decay process in the efficiency of the algorithm.

### 5.5.1 Simulation of the Noisy Channel

The Rydberg states are affected by a strong quadratic Stark shift. Let us now see how the quadratic Stak shift effect can be used to engineer a noisy channel.
In the second Ramsey zone $R_2$ the atoms interact for a controllable time with a classical electromagnetic field. Appling a $\pi/2$ pulse to the $A_1$ atom the state

$$|\psi\rangle = \alpha(t)|+_{A_1}, +_{A_2}, +_{A_3}, 0_{C_1}\rangle + \beta(t)|-_{A1}, -_{A_2} -_{A_3}, 1_{C_1}\rangle, \tag{5.26}$$

is produced. On the basis of the $|\pm\rangle$ states a phase-flip error is equivalent to a bit-flip error on the basis of the $|e\rangle_{A_1}$ and $|g_{A_1}\rangle$. The reason for which we have to rotate the $A_1$ state before applying the noise is due to the fact that from an experimental point of view the random effect of the environment on the atomic states of $A_1$, on which the qubit is encoded, can be modeled as a random Stark shift on the atomic energy levels of the $A_1$. This random fluctuation of the energy levels will reflect as a random spin-flip on the $|\pm\rangle$ basis's state. After the application of the random noise, we can return back re-applying an inverse $\pi/2$ interaction. In this way, if there have been no error, the $A_1$ state at the entrance of the second cavity $\mathcal{C}_2$, when the qubits

starts to be processed by Bob, it will be exactly the same than at the exit of $\mathcal{C}_1$.

The error induced by the noisy channel, in our experiment is then given by the application of a random electric field in the Ramsey zone $R_2$. What is random is the intensity of this electric field. This random electric field induces a shift of the energies of the three levels of interest, $i, g, e$, due to quadratic Stark effect. Therefore we have three energy shifts, $\Delta E_k$, $k = i, g, e$ on each state,

$$\psi_k \to \psi_k \exp\left\{-\imath \frac{T}{\hbar} \Delta E_k\right\} \quad k = i, g, e, \tag{5.27}$$

where $T$ is the duration of the random electric field pulse in $R_2$.
As a consequence, the density matrix elements of the whole system will acquire random phase shifts. Each off-diagonal matrix element with respect to atomic indices, i ,e , g, will acquire a random phase shift given by

$$\rho_{k,l} \to \rho_{k,l} \exp\left\{-i \frac{T}{\hbar} \left(\Delta E_k - \Delta E_l\right)\right\} \quad k, l = i, g, e \tag{5.28}$$

Referring to real Rydberg atoms we need the knowledge of the shifts $\Delta E_k$. This is provided by the following relation [107]

$$\Delta E^{(2)} = -\frac{1}{8}\Big[7n^2 - 6(|m|^2 + n_1)^2 + 6n_1(|m| - 1) + 6n(|m| + 1) - \frac{3}{2}|m| + 8\Big] n^4 |\mathcal{E}|^2, \tag{5.29}$$

where $n_1$ is the parabolic quantum number (zero for the circular Rydberg states), $n$ is the principal quantum number ($n = 49, 50, 51$ for $|i\rangle, |g\rangle, |e\rangle$ respectively), and $|m| = n - 1$ is the magnetic quantum number. For circular Rydberg states we have

$$\Delta E_n = -\frac{1}{8}\left[7n^2 + \frac{21}{2}n + \frac{7}{2}\right] n^4 |E|^2 \equiv \alpha_n |E|^2, \tag{5.30}$$

in appropriate atomic units, which however, we shall see, will be unimportant. In fact, thanks to this formula, the change of the off-diagonal matrix element due to the application of the "error", i.e., of the random electric field, can be written as

$$\rho_{k,l} \to \rho_{k,l} \exp\left\{-i \frac{T|E|^2}{\hbar} \left(\alpha_k - \alpha_l\right)\right\} = \rho_{k,l} \exp\left\{-i\phi \left(\alpha_k - \alpha_l\right)\right\}, \tag{5.31}$$

where $\phi$ *is a random phase proportional to the intensity of the Stark field* and which becomes the random variable with flat distribution. The knowledge of the atomic physics of circular Rydberg states is important only for the determination of the $n$-dependent factors in the phase shift, $\alpha_n$, which are needed in order to know the effect on each atomic level, $|i\rangle, |g\rangle, |e\rangle$.
The QT approach permits to manipulate the evolution of the wave function instead of a density matrix, as it happens in master equation simulation. This means, from the numerical point of view, manipulating smaller objects. In fact the evolution takes place in a Hilbert space of dimension $324 \times 324$ (dims $(H_{atoms}) = 81 = 3^4$, while the state of the two cavities with one photon has dimensions $(H_{cavi}) = 2^2$). With quantum trajectories we study the evolution of a vector of 324 elements and only at the end of the time evolution we determine the density matrix

by averaging over the trajectories. The result of a simulation of the QECC protocol over 1000 trajectories is showed in Fig.5.3. During each trajectory a flat-distributed random error between $[0, \phi_{max}]$ on the encoded qubit is induced, by applying a flat-distributed random electric field. At the end of each *evolution* the overlap of the initial and final state is evaluated and the fidelity 5.9 calculated in both cases, when we apply correction and when we do not complete the final correction step,i.e. we do not turn on the interaction on the $R_3$ Ramsey zone for the fourth atoms.
It is evident there is a great difference in the final fidelity if we do not apply the feedback correction procedure. Both the corrected and uncorrected fidelity are oscillating function of the error, that converges for large values of the error.
In the case of Fig.(5.3) the encoded qubit is obtained by applying a pulse of tailored duration on $\mathcal{C}_1$ so that the final encoded state is $\sqrt{0.6}|g\rangle_{A_1} + \sqrt{0.4}|e\rangle_{A_1}$. If we do not apply the correction the fidelity of the transmission is reduced down to $60 \div 65\%$ of the initial value. The fact that for a perfect channel, i.e. when the applied random error is zero ($\phi_{MAX} = 0$), the fidelity with and without the feedback, do not start from unity, depends on the fact that the evolution is not unitary. In fact, also for a perfect channel, the losses that come from the cavity decay rate (fixed at $k = 100Hz$ that correspond to a time of storage of 10 milliseconds, a realistic value for the current cavity technology), and the spontaneous emission rate $\gamma$, that is $k/30$, determine a non zero probability of errors. On the other hand, we have to consider that the high quality factor of the cavities and the adoption of the circular Rydberg states permits to maintain under control these latter loss terms. In fact if compared to the time scale of the efficient interaction inside the cavity, that is around $20\mu$sec (for a Gaussian mode of 6 mm of width), they affect only partially the time evolution of the system.
The mean fidelity represented in Fig.(5.3) shows how, for realistic parameters, the correction of the error is possible. Moreover we have to stress the fact that, in the simulation, a perfect efficiency of the detectors is assumed. The inclusion of imperfect detectors is another source of loss of fidelity.

The parameters adopted, as said, are realistic. On the other hand, in what follows, we want to show the performance of the protocol for different values of the initial encoding, i.e. different $\alpha$ and $\beta$, and for larger values of the decay rate of the cavities. In Fig.5.4 we have plotted the fidelity averaged over 1000 trajectories for different values of the cavity's decay rate with the same initial encoding of $\alpha \simeq \sqrt{0.6}$ and $\beta \simeq \sqrt{0.4}$. From left to right in clockwise, we see the fidelity for $k = 2\pi$ 0.1 KHz, $k = 2\pi$ 0.3 KHz, $k = 2\pi$ 0.4 KHz . Up to this value of the decay rate, it is possible to fight against the deterioration of the information induced by the noisy channel. Moreover large loss from the cavities and the effect of the noisy channel determine the failure of the QECC protocol. This means that, as expected, the QECC is able to correct for the phase errors added in $R_2$, but it is not able to correct the errors due to cavity damping.

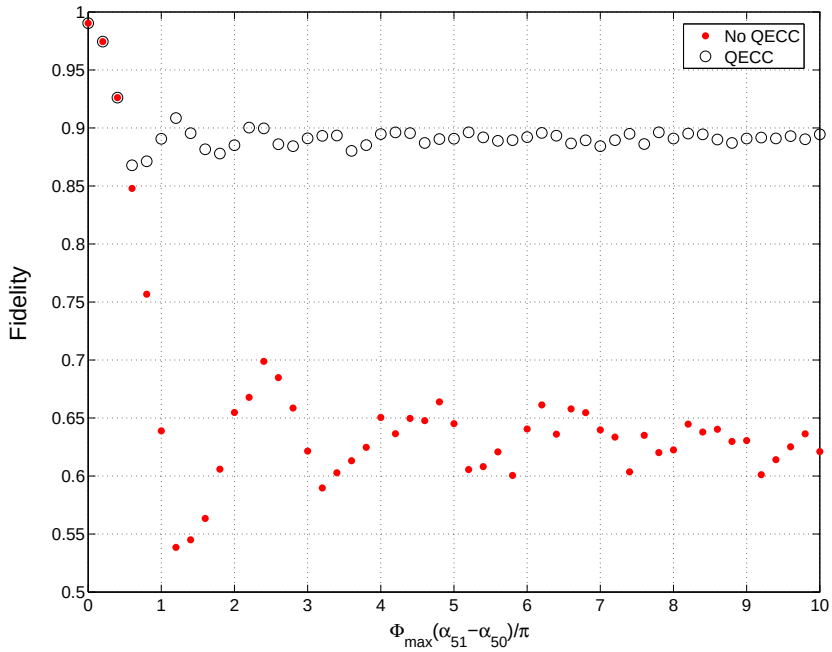


Figure 5.3: Fidelity of the QECC scheme based on the CQED. Parameters are those of the experiment performed in [106]. Cavity's decay rate is $k = 2\pi$ 0.1 KHz, that means a photon's storage time of 10 msec. The electric field inside the cavity is $\Omega = 2\pi$ 47 KHz, and the spontaneous decay time $T_\gamma$ is fixed at $T_\gamma = 30$ msec

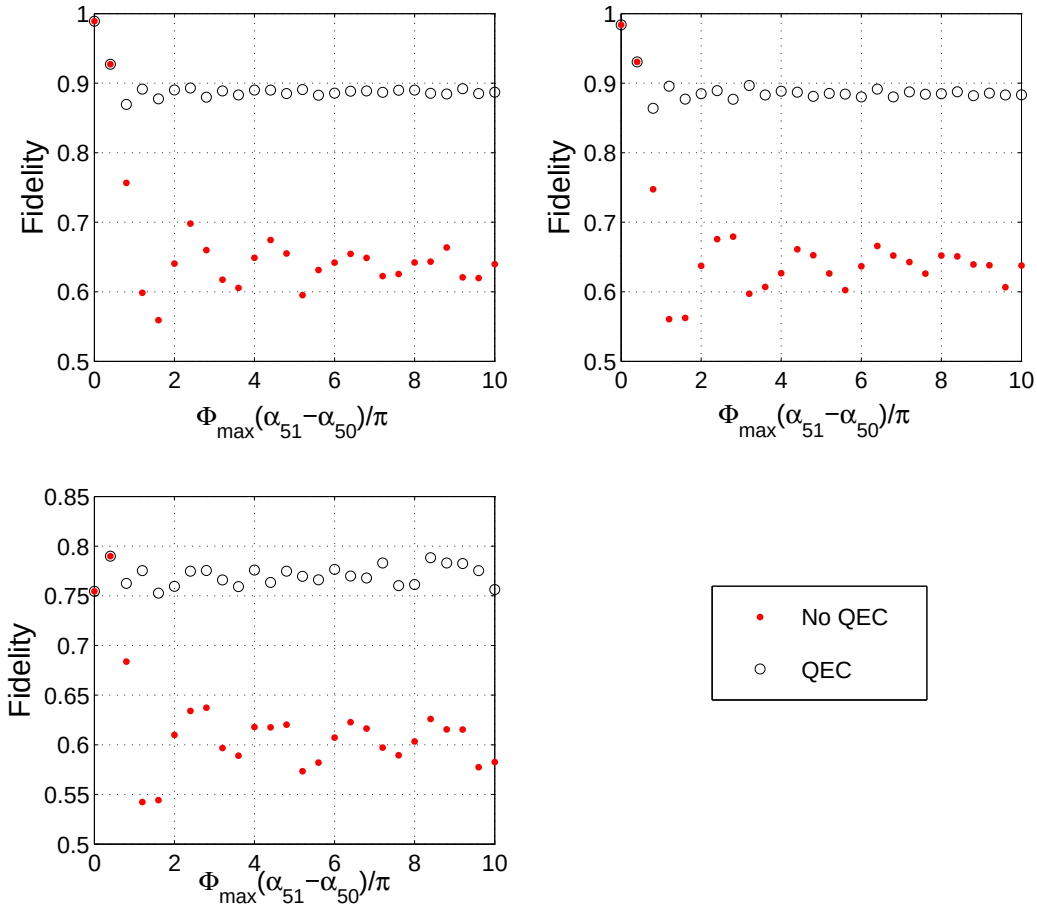


Figure 5.4: Fidelity of the QECC scheme based on the CQED. Parameters are the same of previous plot. The only change is the cavity's decay rate that is from left to right in clockwise direction, $k = 2\pi$ 0.2 KHz, $k = 2\pi$ 0.3 KHz, $k = 2\pi$ 0.4 KHz.

# Conclusions and perspectives

This thesis has been devoted primarily to the evaluation of the performance of a QPG based on the giant non-linear effect that the phenomenon of Electromagnetically Induced Transparency permits. In particular we have addressed our work to the determination if at the single photon level the performances for he production of conditional photon-photon dynamics is strong enough to permit the implementation of an all-optical quantum phase gate. To this end, the efficiency of the process has been evaluated rigorously, calculating numerically and analytically for the first time the fidelity and the conditional phase shift of the device, in presence of noises and losses. To this end a perturbation theory at order higher then the second has been developed.

To reach the final goal of the study of EIT in the full quantum regime, we have preliminarly analyzed other configuration schemes for the atoms-field interaction.
In the second chapter we have studied the nonlinear response of a four-level atomic sample in a *tripod configuration* for an incident probe and trigger field. The resulting large cross-Kerr modulation between probe and trigger enables one to implement a phase gate with a conditional phase shift of the order of $\pi$. This feature has been shown to be valid for both, semiclassical and quantum adiabatic case. The main advantage of this scheme lies in its experimental feasibility which has been assessed through a detailed study of the requirements needed to observe such a large shift in a realistic sample of magnetically trapped ultracold $^{87}$Rb atoms.

Then we have studied a five-level atomic system in two different but related $M$-configurations. We focused on the nonlinear properties of the system and specifically on the conditions for the optimization of the cross-phase modulation between two weak fields of interest, which we have named probe and trigger fields. Both systems have been studied from a semiclassical point of view, i.e., by describing all the fields in terms of their Rabi frequencies. We have seen that both linear and nonlinear properties are well described by an approach based on amplitude variables, which has been shown to reproduce well the numerical solution of the exact optical Bloch equations describing the system.

We have showed that both the asymmetric and the symmetric $M$ scheme are able to provide a giant cross-Kerr modulation, which may be useful for many applications. Both $M$ schemes can be seen as a "duplication" of the usual three-level $\Lambda$ scheme at the basis of EIT, one for the probe and one for the trigger fields. In the asymmetric scheme, only the probe drives a significantly populated transition and a large cross-Kerr effect is obtained when either the probe or the trigger is slightly detuned from the two-photon resonance condition. The corresponding nonlinear phase shift, yielding for example the conditional phase shift of Eq. (4.3) of a quantum phase gate for photonic qubits, can become very large, especially when the probe and trigger group velocities, slowed down by EIT, become equal. In the asymmetric scheme, this group velocity matching can be achieved by properly adjusting the detuning and the intensity of the control field of the trigger $\Lambda$ system. In the symmetric $M$ scheme, the atomic population is equally shared by the probe

and trigger transitions. Adjusting the corresponding parameters (Rabi frequencies, detunings) so that the two $\Lambda$ systems become identical, probe and trigger experience the same interaction with the atomic medium and group velocity matching is achieved automatically. In this case a significant nonlinear cross-phase modulation is achieved only if both $\Lambda$ schemes are slightly and equally detuned from two-photon resonance, so to remain still within the transparency window.

Then the full quantum analysis of EIT based system have been performed, individuating in the symmetric M-scheme a very good candidate for the implementation of the conditional dynamics between photons. The main result of our study is that the implementation of efficient EIT-based nonlinear two-qubit gates for travelling single-photons is possible, even though experimentally challenging. The main limitation is due to the existence of a trade-off between the size of the CPS and the fidelity of the gate, limiting the achievable gate fidelity in the stationary regime, but which can be partially bypassed in the transient regime. In the transient regime a pair of parameters set-up has been studied to fit with the single photon pulse recently realized at Orsay by the Grangier Group.
Another important conclusion of our work is that since the trade-off in the stationary regime is a general consequence of the coherent interaction between the atomic medium and the single-photon wave-packets, we expect that these considerations apply to all EIT-based crossed-Kerr schemes [59, 77], regardless the specific level scheme considered. Instead, this consideration does not apply to situations where the nonlinearity comes from independent processes (e.g. collisions of dipole-dipole interactions) [91–93], nor the similar solid-state based processes [94–96]. Moreover the experimental set up of the last section, shows how with present technology the implementation of conditional dynamics between flying qubit could be realized.

Finally in the last chapter we have turned our attention to the study of the controlled interaction in cavity QED set up. We have studied analytically and simulated numerically the performance of a Quantum Error Correction Scheme for the protection of the quantum information during the transmission through a noisy channel. The scheme is based upon the high degree of control of the coherent interaction between atoms and cavity. The results obtained has showed that the experimental realization of the quantum correction code protocol is within contemporary technological possibilities.

Perspectives for this work are numerous. With this work, we have demonstrated that, although difficult, the realization of a conditional dynamics between photon is possible. This would permit to apply this work to open problems of fundamental research interest like the generation of macroscopical quantum object [114], or could find application in the field of quantum communication, in particular in quantum cryptography. The work on the QECC has its main application in quantum information science. The main result of the work is that our analysis has showed promising results for the realistic experimental realization. The only loss mechanisms that has not been taken into account is the efficiency of the detectors. This could reduce the performance of the QECC, but the general validity and the experimental feasibility could be demonstrated experimentally.

# Appendix A

# Open quantum systems description

In the following pages we describe some technical tools that permit the analysis of an open quantum system $S$ interacting with the environment $R$. Here we review two formalisms usually adopted to describe the influence of the environment in the dynamic of quantum system, the Master Equation (ME) approach, and the Quantum Trajectories (QT) formalism.

## A.1 Master equation

Let us consider a quantum system $\mathcal{S}$. The most general form to describe its state, is assuming that it is in a mixed states, i.e. its state is composed by a statistical mixture of different quantum state, each occurring with a probability $p_i$

$$\hat{\rho}_S = \sum_i p_i |i\rangle\langle i|. \tag{A.1}$$

The system is open, and interacts with a reservoir $\mathcal{R}$ The dynamics of the whole system can be described by the time evolution of the density matrix, $\rho_{S+R}$, of the total system $\mathcal{S} + \mathcal{R}$. Its time evolution is determined by the Hamiltonian of the system and the environment, given by $H_\mathcal{S}$ and $H_\mathcal{R}$ respectively. The Hamiltonian that describes the whole system also includes their mutual interaction and is given by

$$H = H_\mathcal{S} + H_\mathcal{R} + H_{\mathcal{S}-\mathcal{R}}, \tag{A.2}$$

where $H_{\mathcal{S}-\mathcal{R}}$ describes the system-reservoir interaction.
The time evolution is given by the *Von Neumann* equation of motion

$$\dot{\rho}_{S+R} = -\frac{\imath}{\hbar}\Big[H, \rho_{S+R}\Big]. \tag{A.3}$$

If we assume that the interaction between the system and the environment is weak, if compared to the two other terms in eq.(A.2), it is useful to describe the dynamics of the system in the IP

representation with respect to the Hamiltonian $H_0 = H_S + H_R$. In this way we can take into account only the effects of the $H_{SR}(t)e^{\frac{\imath}{\hbar}H_0 t}H_{sr}e^{-\frac{\imath}{\hbar}H_0 t}$ on the dynamics of the system. The Von Neumann equation in the IP can be written as

$$\dot{\rho} = -\frac{\imath}{\hbar}\Big[H_{SR}(t), \rho\Big]. \tag{A.4}$$

This equation can be solved formally by integration giving

$$\rho(t) = \rho(0) - \frac{\imath}{\hbar}\int_0^t dt'[H_{SR}(t'), \rho(t')]. \tag{A.5}$$

The previous formal solution can be repeated iteratively, finding the time evolution of the density matrix, at all orders in the interaction Hamiltonian $H_{SR}$ and at all times. Inserting the eq.(A.5) into the eq.(A.4), we will obtain the general expression for the time evolved density matrix

$$\begin{aligned}\rho(t) &= \sum_{k=0}^{\infty}\frac{(-\imath)^k}{\hbar^k}\int_0^t dt_1\int_0^{t_1} dt_2\ldots \\ &\quad \int_0^{t_{k-1}} dt_k[H_{SR}(t_1),[H_{SR}(t_2),\ldots[H_{SR}(t_k),\rho(0)]]].\end{aligned} \tag{A.6}$$

In the previous formal solution we can retain only terms of lower orders in the eq.(A.6). The assumption, is in general well verified if the interaction Hamiltonian is smaler than all other terms in the Hamiltonian. It is known as the *Born approximation*. Let stops the perturbative development at the second order in eq.(A.6), we obtain

$$\dot{\rho} = -\frac{\imath}{\hbar}[H_{SR}(t), \rho(0)] - \frac{1}{\hbar^2}\int_0^t dt'[H_{SR}(t),[H_{SR}(t'),\rho(t')]]. \tag{A.7}$$

Assuming that no correlation exists between the system and the environment at $t = 0$ we can write the density matrix of the whole system $\rho$ in a factorized way,

$$\rho(0) = \rho_S(0)\rho_R(0). \tag{A.8}$$

Now we have to note that the eq.(A.7) is not what we are looking for, because it contains much more information than the required to describe the time evolution of the state of the system. Tracing over the degrees of freedom of the environment we can obtain the evolution of the density matrix of the quantum system only.
The first commutator on the rhs of eq.(A.7) can be eliminated by assuming that the operators of the environment have zero mean on the state of the reservoir itself. Moreover while it is reasonable to assume that, starting from the initial state given by eq.(A.7), the environment will be much more less affected by the weak interaction $H_{SR}$, the system-environment whole state can be written as follows

$$\rho(t) = \rho_S(t)\rho_R, \tag{A.9}$$

this equation describe how the time evolution of the $S - R$ system is largely due only to the $S$

evolution, leaving the environment , in practice, unchanged during time.
After tracing over the degrees of freedom of the environment, we obtain

$$\dot{\rho}_S(t) = -\frac{1}{\hbar^2}\int_0^t dt' Tr_R\Big\{[H_{SR}(t),[H_{SR}(t'),\rho(t')\otimes\rho_R]]\Big\}, \tag{A.10}$$

where we have assumed that the the reservoir's operators have zero mean in the state $\rho_R$. This permits to eliminate the first commutator in the eq.(A.7).
This equation is still hard solve, because it is not Markovian,i.e. it states how the future evolution of the system at time $t$, depends upon its past history at time $t'$. This difficulty can be avoided adopting an additional assumption on the physical nature of the interaction, i.e applying the *Markov approximation*. The Markov approximation consists in assuming that the future evolution of a system depends only on its present history. This holds if the $S-R$ system possess two much different time scales, i.e. if the time scale over which $R$ changes is faster then the time scale over which $S$ changes. This permits us to neglect the change of the system induced by the back-action of the reservoir.
If this condition is verified we can substitute the $\rho(t')$ with $\rho(t)$ in eq.(A.10). The equation that we obtain

$$\dot{\rho}_S(t) = -\frac{1}{\hbar^2}\int_0^t dt' Tr_R\Big\{[H_{SR}(t),[H_{SR}(t'),\rho(t)\otimes\rho_R]]\Big\}, \tag{A.11}$$

is the *Master equation in the Morn-Markov approximation.*

### A.1.1 Two level atom's Master Equation

Now we calculate the ME (A.11) for a more specific model of the system-environment interaction. Let us consider a two level atomic system left free to interact with the environment, formed by the vacuum electromagnetic field, with creation and annihilation operators defined by the operators $\Gamma_k^\dagger$ and $\Gamma_k$ respectively. The interaction with the electromagnetic field of the environment will determine the radiative decay of the density matrix elements. The system-environment interaction energy can be written as

$$H_{SR} = \hbar\sum_k g_k\Big[\Gamma_k^\dagger|_\rangle\langle 1|2e^{-i(\omega-\omega_k)} + |_\rangle\langle 2|1\Gamma_k e^{-i(\omega-\omega_k)}\Big], \tag{A.12}$$

The label $k$ describes the interaction of the atom with the $k-$mode of the environment, defined by the frequency $\omega_k$, detuned from the atomic transition by $\omega-\omega_k$. The coefficient $g_k$ gives the coupling of the mode $k$ with the atomic transition. Inserting this interaction energy in the eq.(A.11), we obtain eight terms given by the following relation

$$\begin{aligned}
\dot{\rho}_S = &-\int_0^t dt' \sum_{k,k'} g_k g_{k'} \\
&\Big\{\Big[\sigma_{12}\sigma_{12}\sigma(t') - 2\sigma_{12}\sigma(t')\sigma_{12} + \sigma_S(t')\sigma_{12}\sigma_{12}\Big]\times e^{-\imath(\omega-\omega_k)t - i(\omega-\omega_{k'})t'}\langle\Gamma_k^\dagger\Gamma_{k'}^\dagger\rangle \\
&+[\sigma_{12}\sigma_{21}\sigma(t') - \sigma_{21}\sigma(t')\sigma_{12}]\times e^{-\imath(\omega-\omega_k)t + i(\omega-\omega_{k'})t'}\langle\Gamma_k^\dagger\Gamma_{k'}\rangle \\
&+[\sigma_{21}\sigma_{12}\sigma(t') - \sigma_{12}\sigma(t')\sigma_{21}]\times e^{\imath(\omega-\omega_k)t - i(\omega-\omega_{k'})t'}\langle\Gamma_k\Gamma_{k'}^\dagger\rangle\Big\} + h.c.,
\end{aligned} \tag{A.13}$$

where $\sigma_{ij} = |i\rangle\langle j|$ for $i,j = 1,2$.

The correlation functions, represented in the previous relation by the expressions of the form $\langle \dots \rangle$, depend strictly on the nature of the reservoir. If we consider a reservoir at thermal equilibrium at temperature $T$, the mean photon number is given by the relation

$$\bar{n}_k = \frac{1}{\exp\left(\frac{\hbar\omega_k}{k_B T}\right) - 1}, \tag{A.14}$$

where $k_B$ is the Boltzmann constant, and the calculation of the correlation functions gives the following expression for the ME

$$\begin{aligned}\dot{\rho}_S = -\int_0^t dt' \sum_k g_k^2 \Big\{ &[\sigma_{12}\sigma_{21}\sigma(t') - \sigma_{21}\sigma(t')\sigma_{12}] \times \bar{n}_k e^{-\imath(\omega-\omega_k)(t-t^{prime}} \\ &+[\sigma_{21}\sigma_{12}\sigma(t') - \sigma_{12}\sigma(t')\sigma_{21}] \times e^{\imath(\omega-\omega_k)(t-t')}(\bar{n}_k + 1)\Big\} + h.c.,\end{aligned} \tag{A.15}$$

we have dropped out those terms with correlation functions equal to zero, $\langle \Gamma_k \Gamma_{k'} \rangle = \langle \Gamma_k^\dagger \Gamma_{k'}^\dagger \rangle = 0$, and where the relations $\langle \Gamma_k^\dagger \Gamma_{k'} \rangle = \bar{n}_k \delta_{k,k'}$ and $\langle \Gamma_k \Gamma_{k'}^\dagger \rangle = (1+\bar{n}_k)\delta_{k,k'}$, for the reservoir's photon numbers, hold.
If the mode of the reservoir's field are closely spaced in frequency, we can transform the summation over $k$ in an integral. Adopting the definition of the delta function

$$2\pi\delta(t-t') = \int_{-infty}^{\infty} d\omega_k e^{\imath(\omega-\omega_k)(t-t')}$$

, we arrive at the following expression for the decay process of an atomic two level system

$$\begin{aligned}\dot{\rho}_S(t) &= \bar{n}\frac{\gamma_{21}}{2}[2\sigma_{21}\sigma(t)\sigma_{12} - \sigma_{12}\sigma_{21}\sigma(t) - \sigma(t)\sigma_{12}\sigma_{21}] \\ &\quad +(1+\bar{n})\frac{\gamma_{21}}{2}[2\sigma_{12}\sigma(t)\sigma_{21} - \sigma_{21}\sigma_{12}\sigma(t) - \sigma(t)\sigma_{21}\sigma_{12}].\end{aligned} \tag{A.16}$$

Where $\bar{n}$ represents the mean number of photons at the resonance frequency $\omega$. If the system is also under the influence of an applied field, we have to add the effective Hamiltonian given by the eq.(1.9) in the calculation of the master equation. For an applied field detuned by an amount $\Delta$ from the atomic resonance, we obtain an additional part to previous relation that describes the deterministic dynamic

$$\begin{aligned}\dot{\rho} &= \imath\frac{1}{2}\Delta\big[\sigma_{22},\sigma\big] + \imath\frac{\Omega}{2}\big[\sigma_{21}+\sigma_{12},\sigma\big] + \\ &\quad +\frac{\gamma_{21}}{2}[2\sigma_{12}\sigma(t)\sigma_{21} - \sigma_{21}\sigma_{12}\sigma(t) - \sigma(t)\sigma_{21}\sigma_{12}],\end{aligned} \tag{A.17}$$

where we have assumed zero mean photon number, $n = 0$.

### Inclusion of dephasing process

To complete the description of the interaction of a quantum system with the environment, we have to include phase destroying processes. The interaction with the environment causes the atomic systems a loss of energy from the atom, and damping of the atomic polarization. This

latter damping results from a randomization of the phases of the atomic wavefunctions, causing the overlap between different states to decay in time. Moreover it is often necessary to take into account the additional dephasing interaction caused, for example, by elastic collisions in an atomic vapor.
These processes do not affect the atomic population, but destroy the quantum coherence varying, randomly, the relative phase in the wave function of the quantum system. To describe dephasing processes we can phenomenologically add, to the interaction Hamiltonian of eq.(A.12), two further reservoir interaction Hamiltonian

$$H_{SR_1} = \Gamma_1^{deph}\sigma_{22} \tag{A.18}$$
$$H_{SR_2} = \Gamma_2^{deph}\sigma_{11}. \tag{A.19}$$

The operators depend only on operators projectors on level $|2\rangle$ and $|1\rangle$, to take into account the fact that the dephasing do not affect population. The complete reservoir seen by the system is now composed by $R_{tot} = R \bigoplus R_1 \bigoplus R_2$. Within the Born - Markov approximation, we can evaluate the correlation functions, that for dephasing process are of the form $\langle \Gamma_1(t)\Gamma_1(t')\rangle = \delta(t-t')$.
If the time scale of the dephasing process is fast, we arrive at an additional term in eq.(A.17). In two level atoms,

$$\frac{\gamma_{deph}}{2}(\sigma_z\rho\sigma_z - \rho), \tag{A.20}$$

where $\sigma_z = |2\rangle\langle 2| - |1\rangle\langle 1|$.

The generalization to multilevel systems is straightforwardly obtained from the previous expression, including the deterministic part of the evolution and by considering a reservoir for each radiative decay channel. What we obtain is an expression of the form

$$\dot{\rho} = -\frac{i}{\hbar}[H_{eff},\sigma] + \sum_{i,j}^{level}\left\{\frac{\gamma_{ji}}{2}[2\sigma_{ij}\sigma\sigma_{ji} - \sigma_{ji}\sigma_{ij}\sigma - \sigma\sigma_{ji}\sigma_{ij}]\right\} + \sum_{l=1}^{level}\frac{\gamma_{deph}^{l}}{2}(\sigma_{ll}\sigma\sigma_{ll} - \sigma_{ll}\sigma - \sigma\sigma_{ll}), \tag{A.21}$$

where the index $l$ describes the numbers of level composing the atomic system. The Optical Bloch Equation (OBE), are straightforwardly obtained by evaluating the matrix elements of the time evolved density matrix

$$\rho_{ij} = \langle i|\rho|j\rangle. \tag{A.22}$$

## A.2 Optical Bloch Equations for Five level M-schemes

Adopting the the receipt given by eq.(A.22) we have obtained the following density matrix element for the five level atomic system. The capital $\Gamma$s describe the collective radiative decay rate from the two excited level $|2\rangle$ and $|4\rangle$, while the $\gamma_{ij} = \gamma_{ii} + \gamma_{jj}$ for $i,j = 1,2,3,4,5$ describes the dephasing process of levels $|i\rangle$ with $i = 1,2,3,4,5$.

### A.2.1 Optical Bloch Equations - Asymmetric Case

From Eqs. (3.5) and (3.23), and using the definitions of Eqs. (3.24)-(3.26), one gets the following set of equations for the atomic populations $\rho_{ii}$

$$\begin{aligned}
\dot{\rho}_{11} &= i\Omega_1\rho_{21} - i\Omega_1^\star\rho_{12} + \Gamma_{41}\rho_{44} + \Gamma_{21}\rho_{22}, && \text{(A.23a)}\\
\dot{\rho}_{22} &= -i\Omega_1\rho_{21} + i\Omega_1^\star\rho_{12} - i\Omega_2\rho_{23} + i\Omega_2^\star\rho_{32} - \Gamma_2\rho_{22}, && \text{(A.23b)}\\
\dot{\rho}_{33} &= i\Omega_3\rho_{43} - i\Omega_3^\star\rho_{34} + i\Omega_2\rho_{23} - i\Omega_2^\star\rho_{32} + \Gamma_{43}\rho_{44} + \Gamma_{23}\rho_{22}, && \text{(A.23c)}\\
\dot{\rho}_{44} &= i\Omega_3^\star\rho_{34} - i\Omega_3\rho_{43} - i\Omega_4\rho_{45} + i\Omega_4^\star\rho_{54} - \Gamma_4\rho_{44}, && \text{(A.23d)}\\
\dot{\rho}_{55} &= i\Omega_4\rho_{45} - i\Omega_4^\star\rho_{54} + \Gamma_{25}\rho_{22} + \Gamma_{45}\rho_{44}, && \text{(A.23e)}
\end{aligned}$$

and the following set of equations for the atomic coherences $\rho_{ij}$, $i \neq j$,

$$\begin{aligned}
\dot{\rho}_{12} &= -i\delta_1\rho_{12} + i\Omega_1(\rho_{22} - \rho_{11}) - i\Omega_2\rho_{13} - \frac{\Gamma_2 + \gamma_{12}}{2}\rho_{12}, && \text{(A.24a)}\\
\dot{\rho}_{13} &= -i\delta_{12}\rho_{13} + i\Omega_1\rho_{23} - i\Omega_3^\star\rho_{14} - i\Omega_2^\star\rho_{12} - \frac{\gamma_{13}}{2}\rho_{13}, && \text{(A.24b)}\\
\dot{\rho}_{14} &= -i\delta_{13}\rho_{14} + i\Omega_1\rho_{24} - i\Omega_3\rho_{13} - i\Omega_4\rho_{15} - \frac{\gamma_{14} + \Gamma_4}{2}\rho_{14}, && \text{(A.24c)}\\
\dot{\rho}_{15} &= -i\delta_{14}\rho_{15} + i\Omega_1\rho_{25} - i\Omega_4^\star\rho_{14} - \frac{\gamma_{15}}{2}\rho_{15}, && \text{(A.24d)}\\
\dot{\rho}_{23} &= i\delta_2\rho_{23} + i\Omega_1^\star\rho_{13} - i\Omega_3^\star\rho_{24} + i\Omega_2^\star(\rho_{33} - \rho_{22}) - \frac{\Gamma_2 + \gamma_{23}}{2}\rho_{23}, && \text{(A.24e)}\\
\dot{\rho}_{24} &= i\delta_{23}\rho_{24} - i\Omega_3\rho_{23} - i\Omega_4\rho_{25} + i\Omega_2^\star\rho_{34} + i\Omega_1^\star\rho_{14} - \frac{\Gamma_2 + \Gamma_4 + \gamma_{24}}{2}\rho_{24}, && \text{(A.24f)}\\
\dot{\rho}_{25} &= i\delta_{24}\rho_{25} + i\Omega_1^\star\rho_{15} + i\Omega_2^\star\rho_{35} - i\Omega_4^\star\rho_{24} - \frac{\Gamma_2 + \gamma_{25}}{2}\rho_{25}, && \text{(A.24g)}\\
\dot{\rho}_{34} &= -i\delta_3\rho_{34} + i\Omega_3(\rho_{44} - \rho_{33}) + i\Omega_2\rho_{24} - i\Omega_4\rho_{35} - \frac{\Gamma_4 + \gamma_{34}}{2}\rho_{23}, && \text{(A.24h)}\\
\dot{\rho}_{35} &= -i\delta_{34}\rho_{35} + i\Omega_3\rho_{45} + i\Omega_2\rho_{25} - i\Omega_4^\star\rho_{34} - \frac{\gamma_{35}}{2}\rho_{35}, && \text{(A.24i)}\\
\dot{\rho}_{45} &= i\delta_4\rho_{45} + i\Omega_3^\star\rho_{35} + i\Omega_4^\star(\rho_{55} - \rho_{44}) - \frac{\Gamma_4 + \gamma_{45}}{2}\rho_{45}, && \text{(A.24j)}
\end{aligned}$$

where we have also defined the composite detunings $\delta_{23} = \delta_2 - \delta_3$, $\delta_{24} = \delta_2 - \delta_3 + \delta_4$, and $\delta_{34} = \delta_3 - \delta_4$.

### A.2.2 Optical Bloch Equations - Symmetric Case

From Eqs. (3.44) and (3.23), and using the definitions of Eqs. (3.24)-(3.26), one gets the following set of equations for the atomic populations $\rho_{ii}$

$$\begin{aligned}
\dot{\rho}_{11} &= \imath\Omega_2\rho_{21} - \imath\Omega_2^\star\rho_{12} + \Gamma_{41}\rho_{44} + \Gamma_{21}\rho_{22}, && \text{(A.25a)}\\
\dot{\rho}_{22} &= \imath\Omega_2\rho_{12} - \imath\Omega_2^\star\rho_{21} - \imath\Omega_1\rho_{23} + \imath\Omega_1^\star\rho_{32} - \Gamma_2\rho_{22}, && \text{(A.25b)}\\
\dot{\rho}_{33} &= \imath\Omega_3\rho_{43} - \imath\Omega_3^\star\rho_{34} + \imath\Omega_1\rho_{23} - \imath\Omega_1^\star\rho_{32} + \Gamma_{43}\rho_{44} + \Gamma_{23}\rho_{2}, && \text{(A.25c)}\\
\dot{\rho}_{44} &= \imath\Omega_3^\star\rho_{34} - \imath\Omega_3\rho_{43} - \imath\Omega_4\rho_{45} + \imath\Omega_4^\star\rho_{54} - \Gamma_4\rho_{44}, && \text{(A.25d)}\\
\dot{\rho}_{55} &= \imath\Omega_4\rho_{45} - \imath\Omega_4^\star\rho_{54} + \Gamma_{45}\rho_{44} + \Gamma_{25}\rho_{22}, && \text{(A.25e)}
\end{aligned}$$

while the equations for the coherences are

$$\dot{\rho}_{12} = -\imath\delta_2\rho_{12} + \imath\Omega_2(\rho_{22} - \rho_{11}) - \imath\Omega_1\rho_{13} - \frac{\Gamma_2 + \gamma_{12}}{2}\rho_{12}, \tag{A.26a}$$

$$\dot{\rho}_{13} = \imath(\delta_1 - \delta_2)\rho_{13} + \imath\Omega_2\rho_{23} - \imath\Omega_3^\star\rho_{14} - \imath\Omega_1^\star\rho_{12} - \frac{\gamma_{13}}{2}\rho_{13}, \tag{A.26b}$$

$$\dot{\rho}_{14} = \imath(\delta_1 - \delta_2 - \delta_3)\rho_{14} + \imath\Omega_2^\star\rho_{24} - \imath\Omega_3\rho_{13} - \imath\Omega_4\rho_{15} - \frac{\Gamma_4 + \gamma_{14}}{2}\rho_{14}, \tag{A.26c}$$

$$\dot{\rho}_{15} = \imath(\delta_1 - \delta_2 - \delta_3 + \delta_4)\rho_{15} + \imath\Omega_2^\star\rho_{25} - \imath\Omega_4^\star\rho_{14} - \frac{\gamma_{15}}{2}\rho_{15}, \tag{A.26d}$$

$$\dot{\rho}_{23} = \imath\delta_1\rho_{23} + \imath\Omega_2^\star\rho_{13} - \imath\Omega_3^\star\rho_{24} + \imath\Omega_1^\star(\rho_{33} - \rho_{22}) - \frac{\Gamma_2 + \gamma_{23}}{2}\rho_{23}, \tag{A.26e}$$

$$\dot{\rho}_{24} = \imath(\delta_1 - \delta_3)\rho_{24} - \imath\Omega_3\rho_{23} - \imath\Omega_4\rho_{25} + \imath\Omega_2^\star\rho_{14} + \imath\Omega_1^\star\rho_{34} - \frac{\Gamma_2 + \Gamma_4 + \gamma_{24}}{2}\rho_{24}, \tag{A.26f}$$

$$\dot{\rho}_{25} = \imath(\delta_1 + \delta_4 - \delta_3)\rho_{25} + \imath\Omega_2\rho_{15} + \imath\Omega_1^\star\rho_{35} - \imath\Omega_4^\star\rho_{24} - \frac{\Gamma_2 + \gamma_{25}}{2}\rho_{25}, \tag{A.26g}$$

$$\dot{\rho}_{34} = -\imath\delta_3\rho_{34} + \imath\Omega_1\rho_{24} - \imath\Omega_4\rho_{35} + \imath\Omega_3(\rho_{44} - \rho_{33}) - \frac{\Gamma_4 + \gamma_{34}}{2}\rho_{34}, \tag{A.26h}$$

$$\dot{\rho}_{35} = -\imath(\delta_3 - \delta_4)\rho_{35} - \imath\Omega_3\rho_{45} + \imath\Omega_1\rho_{25} - \imath\Omega_4^\star\rho_{34} - \frac{\gamma_{35}}{2}\rho_{35}, \tag{A.26i}$$

$$\dot{\rho}_{45} = \imath\delta_4\rho_{45} + \imath\Omega_4^\star(\rho_{55} - \rho_{44}) + \imath\Omega_3^\star\rho_{35} - \frac{\Gamma_4 + \gamma_{45}}{2}\rho_{45}. \tag{A.26j}$$

From the solution of this set of equation we can obtain the population and coherence' s information on the five level atomic system.

## A.3 Quantum Trajectories Approach

Quantum Trajectories (QT) approach [112, 113] provides a tool to describe the dynamics of quantum systems alternative to the ME description. While the Master Equation provides an ensemble description of the evolution of quantum system, the QT approach is based upon the observation of a single sequence of events. This is possible, because we monitor the time evolution of the wave equation rather than observe the evolution of the density matrix.
The interaction of quantum systems with the environment and the consequent possibility that *quantum jumps* take place, poses the problem of how to describe any single realization of the system's evolution in the presence of quantum jumps. Quantum jumps occur randomly, and their effect is to collapse the wave function.
Within the QT approach, once we have obtained the time evolution of the wave function from an effective Stochastic the Schrödinger equation, we evaluate the expectation values by this single wave function. Repeating this process a large number of time, we thus evaluate the mean values over all possible stochastic evolutions.
The general expression of the time evolution of the density matrix can be written as

$$\dot{\rho} = \mathcal{L}\rho, \tag{A.27}$$

where $\mathcal{L}$is the a Louivillian super-operator. The formal solution of this equation gives

$$\rho(t) = e^{\mathcal{L}t}\rho(0). \tag{A.28}$$

Adding and subtracting the superoperator $\mathcal{O}$ to the exponential function, and expanding the exponential, we obtain

$$\begin{aligned}\rho(t) &= e^{(\mathcal{L}-\mathcal{O}+\mathcal{O})t}\rho(0) \\ &= \sum_{n_0}^{\infty}\int_0^t dt_n \int_0^{t_n} dt_{n-1}\ldots\int_0^{t_2} dt_1 e^{(\mathcal{L}-\mathcal{O})(t-t_n)}\mathcal{O}\times e^{(\mathcal{L}-\mathcal{O})(t_n-t_{n-1})}\mathcal{O}\ldots\mathcal{O}e^{(\mathcal{L}-\mathcal{O})t_1}\rho(0).\end{aligned} \tag{A.29}$$

The quantity under the integral is the evolved, unormalized density matrix,

$$\bar{\rho}_c(t) = e^{(\mathcal{L}-\mathcal{O})(t-t_n)}\mathcal{O}\times e^{(\mathcal{L}-\mathcal{O})(t_n-t_{n-1})}\mathcal{O}\ldots\mathcal{O}e^{(\mathcal{L}-\mathcal{O})t_1}\rho(0), \tag{A.30}$$

conditioned to the presence of $n$ quantum jumps events, described by the application of the operator $\mathcal{O}$ at times $t_1, t_{2,}, \ldots, t_n$.
The sum describes all possible physical preparations, determined by the number of jumps $n$, to go from the initial time $t = 0$ to the final time $t_n$. Each path can have an arbitrary number of emissions, i.e. the jumps go from zero to $\infty$. The conditioned state can be defined as $\bar{\rho}_c(t) = |\psi_c(t)\rangle \otimes \langle\psi_c(t)|$, where $|\psi_c(t)\rangle$ represent the time evolved wave equation between a jump determined collaps and an other. The normalized conditioned density matrix is then obtained by dividing by its trace

$$\rho_c(t) = \frac{\bar{\rho}_c(t)}{Tr[\bar{\rho}_c(t)]}. \tag{A.31}$$

From a numerical point of view, the advantage, with respect to the ensemble-based description, relies on the fact that the problem involves the time evolution of an object of dimension $N$ rather than $N \times N$.

Let us now give an example of how an atomic system can be treated. The general approach is based on considering a state vector $|\psi\rangle$ evolved in time by means of the Schrödinger equation

$$\imath\hbar\frac{d|\psi\rangle}{dt} = H_{eff}(t)|\psi\rangle, \tag{A.32}$$

where the general expression for the effective non-Hermitian Hamiltonian is

$$H_{eff}(t) = H_{int}(t) - \frac{i\hbar}{2}\sum_n C_n^{\dagger}(t)C_n(t), \tag{A.33}$$

where the set $\{C_n(t)\}$ represent the family of collapse operators describing the dissipation. The example above corresponds to a single kind of jump, with $C_1 = \mathcal{O}$.
Eq.(A.33) determines the continuous evolution of the state $|\psi\rangle$ punctuated by quantum jumps at time $\tau$ at which the wave function changes according to

$$|\psi(t)\rangle = \frac{C_n(t)|\psi(\tau)\rangle}{||C_n(t)|\psi(\tau)\rangle||}, \tag{A.34}$$

where $\tau < t$. Evaluating the evolution of the eq.(A.32) for a number of trajectories we can

evaluate the expectation values over the number of trajectories obtaining the average quantities that represent the expectation values of physical quantities.

The only difference from a quantum system to another is in the way we define the interaction Hamiltonian $H_{int}$ and how we define the quantum jumps operators. For example if we apply the above procedure to multilevel atomic systems, e.g. the five level symmetric M scheme system, we adopt the Hamiltonian given by eq.(4.3) as $H_{int}$ and each collapse operator, related to each decay channel, is defined as

$$C_{ij} = \sqrt{\gamma_{ij}}|i\rangle\langle j| \qquad \text{for } \; i,j = 1,2,3,4,5, \tag{A.35}$$

# Appendix B

# Fourth order Wigner-Brillouin Perturbation theory

In this section we give much details of the perturbative calculation of the quantum phase due to a cross Kerr interaction expressed by the results of eq.(4.3). The aim of this Appendix is to show how we can calculate the eigenvalues and eigenvectors of a multilevel system described in the chapter *IV* by means of the perturbation theory at fourth order. For simplicity we consider only the non-degenerate case.

## B.1 Formulas

Let us consider a quantum system under the influence of an Hamiltonian that can be separated in a large term plus a perturbative term, much smaller than the other, i.e.

$$H = H_0 + V. \tag{B.1}$$

The general formula describing the perturbation of the energy of the unperturbed eigenstate $|n\rangle$ of $H_0$ is given by

$$\begin{aligned} E_n &= E_n^0 + \langle n|V|n\rangle + \sum_{k\neq n} \frac{\langle n|V|k\rangle\langle k|V|n\rangle}{E_n - E_k^0} + \sum_{k,k'\neq n} \frac{\langle n|V|k\rangle\langle k|V|k'\rangle\langle k'|V|n\rangle}{(E_n - E_k^0)(E_n - E_{k'}^0)} \\ &\quad + \sum_{k,k',k''\neq n} \frac{\langle n|V|k\rangle\langle k|V|k'\rangle\langle k'|V|k''\rangle\langle k''|V|n\rangle}{(E_n - E_k^0)(E_n - E_{k'}^0)(E_n - E_{k''}^0)} + \dots . \end{aligned} \tag{B.2}$$

Now the form of the perturbation at the various orders depends on the perturbative treatment of the $E_n$ term. In fact, the expressions of the perturbation at all orders are obtained by developing $E_n$ in the denominators of the previous expression at the correct order. Taking into account that

$$|V_{nm}| \ll |E_n^{(0)} - E_m^{(0)}|, \tag{B.3}$$

i.e, assuming that the matrix elements of the perturbation $V$ are much smaller than the absolute

values of the difference between the unperturbed energies $E_k^{(0)}$.
To find the complete expression of the correction at the second order, we can take $E_n = E_n^{(0)}$ in the second order term in the eq.(B.2) obtaining

$$E_n^{(2)} = E_n^{(0)} + V_{nn} + \sum_{k\neq n} \frac{|V_{nk}|^2}{E_n^{(0)} - E_k^{(0)}}, \tag{B.4}$$

In the same way the third order correction can be obtained by developing at first order $E_n$ in the term of eq.(B.2) proportional to the $V^2$ of the perturbative part of the Hamiltonian, and at *zero*th order in $V^3$, we obtain

$$\begin{aligned} E_n^{(3)} &= E_n^{(0)} + V_{nn} + \sum_{k\neq n} \frac{|V_{nk}|^2}{E_n^{(0)} - E_k^{(0)}} - V_{nn} \sum_{k\neq n} \frac{|V_{kn}|^2}{(E_n^{(0)} - E_k^{(0)})^2} \\ &+ \sum_{k,k',\neq n} \frac{V_{nk}V_{kk'}V_{k'n}}{(E_n^{(0)} - E_k^{(0)})(E_n^{(0)} - E_{k'}^{(0)})}. \end{aligned} \tag{B.5}$$

Now we can apply the same procedure to include the fourth order correction. We have to develop at second order $E_n$ in the $V^2$ term, at first order in the $V^3$ term, and at the zero order in the $V^4$ term. We give the final result

$$\begin{aligned} E_n^{(4)} = &= E_n^{(0)} + V_{nn} + \sum_{k\neq n} \frac{|V_{nk}|^2}{E_n^{(0)} - E_k^{(0)}} - V_{nn} \sum_{k\neq n} \frac{|V_{kn}|^2}{(E_n^{(0)} - E_k^{(0)})^2} \\ &- \sum_{k\neq n} \frac{|V_{kn}|^2}{E_n^{(0)} - E_k^{(0)}} \sum_{k\neq n} \frac{|V_{kn}|^2}{(E_n^{(0)} - E_k^{(0)})^2} \\ &- V_{nn} \sum_{k,k'\neq n} \left[ \frac{V_{nk}V_{kk'}V_{k'n}}{(E_n^{(0)} - E_k^{(0)})(E_n^{(0)} - E_{k'}^{(0)})^2} + \frac{V_{nk}V_{kk'}V_{k'n}}{(E_n^{(0)} - E_k^{(0)})^2(E_n^{(0)} - E_{k'}^{(0)})} \right] \\ &+ \sum_{k,k',k''} \frac{V_{nk}V_{kk'}V_{k'k''}V_{k''n}}{(E_n^{(0)} - E_k^{(0)})(E_n^{(0)} - E_{k'}^{(0)})(E_n^{(0)} - E_{k''}^{(0)})}, \end{aligned} \tag{B.6}$$

where the summations labels refer to the eigenstates of the unperturbed part of the Hamiltonian.

## B.2 Application to the symmetric M-scheme

We apply the previous results to the specific case of an atom in the symmetric M-scheme configuration.
Let us consider a single five - level atom, interacting with an EM field, and described by the following Hamiltonian (see chapter IV)

$$\begin{aligned} H &= \hbar\epsilon_{12}|1\rangle\langle 1| + \hbar\delta_2|2\rangle\langle 2| + \hbar\delta_3|4\rangle\langle 4| + \hbar\epsilon_{34}|5\rangle\langle 5| + \hbar\Omega_1\left(|2\rangle\langle 1| + |1\rangle\langle 2|\right) + \\ &+\hbar g_p\left(\hat{a}_p|2\rangle\langle 3| + |3\rangle\langle 2|\hat{a}_p^\dagger\right) + \hbar g_t\left(\hat{a}_t|4\rangle\langle 3| + |3\rangle\langle 4|\hat{a}_t^\dagger\right) + \hbar\Omega_4\left(|4\rangle\langle 5| + |5\rangle\langle 4|\right), \end{aligned}$$

We assume that the terms proportional to $g_{p,t}$, in the equation above, are much smaller than all the others, so that they represent the perturbation V in the Hamiltonian in the form of eq.(B.1). If the trigger field possesses only one photon, while the probe field is in the vacuum state, the

Hilbert space within which the dynamics takes place can be represented by the following basis $B_t = \{e_1 = |3\rangle \otimes |0\rangle_p \otimes |1\rangle_t, e_2 = |4\rangle \otimes |0\rangle_p \otimes |0\rangle_t, e_3 = |5\rangle \otimes |0\rangle_p \otimes |0\rangle_t\}$, we obtain (see chapter IV)

$$H_t = \begin{pmatrix} 0 & 0 & 0 \\ 0 & \delta_3 & \Omega_4 \\ 0 & \Omega_4 & \epsilon_2 \end{pmatrix} + \begin{pmatrix} 0 & g_t & 0 \\ g_t & 0 & 0 \\ 0 & 0 & 0 \end{pmatrix}, \tag{B.7}$$

Similarly for the one probe photon, we have

$$H_p = \begin{pmatrix} 0 & 0 & 0 \\ 0 & \delta_1 & \Omega_2 \\ 0 & \Omega_2 & \epsilon_1 \end{pmatrix} + \begin{pmatrix} 0 & g_p & 0 \\ g_p & 0 & 0 \\ 0 & 0 & 0 \end{pmatrix}, \tag{B.8}$$

in the basis $B_p = \{e_1 = |3\rangle \otimes |1\rangle_p \otimes |0\rangle_t, e_2 = |2\rangle \otimes |0\rangle_p \otimes |0\rangle_t, e_3 = |1\rangle \otimes |0\rangle_p \otimes |0\rangle_t\}$.
If the probe and the trigger possess one photon each, we have the Hilbert space spanned by the five states $e_1 = |2\rangle \otimes |0\rangle_p \otimes |1\rangle_t, e_2 = |1\rangle \otimes |0\rangle_p \otimes |1\rangle_t, e_3 = |2\rangle \otimes |1\rangle_p \otimes |1\rangle_t, e_4 = |4\rangle \otimes |1\rangle_p \otimes |0\rangle_t, e_5 = |5\rangle \otimes |1\rangle_p \otimes |0\rangle_t$. Writing the Hamiltonian in the perturbative representation of eq.(B.1), we have

$$H_{pt} = \begin{pmatrix} \delta_1 & \Omega_2 & 0 & 0 & 0 \\ \Omega_2 & \epsilon_1 & 0 & 0 & 0 \\ 0 & 0 & 0 & 0 & 0 \\ 0 & 0 & 0 & \delta_3 & \Omega_4 \\ 0 & 0 & 0 & \Omega_4 & \epsilon_2 \end{pmatrix} + \begin{pmatrix} 0 & 0 & g_p & 0 & 0 \\ 0 & 0 & 0 & 0 & 0 \\ g_p & 0 & 0 & g_t & 0 \\ 0 & 0 & g_t & 0 & 0 \\ 0 & 0 & 0 & 0 & 0 \end{pmatrix}. \tag{B.9}$$

We can immediately note how the odd terms in the perturbative expansion give zero contribution, as they depend on the diagonal matrix elements $V_{nn}$ or $V_{kk'}$ of the perturbation Hamiltonian that are identically zero. For eq.(B.7) and eq.(B.8), the Hamiltonians are the same, and it is sufficient to study only one of the two cases and then modify the obtained results by switching $g_t \to g_p$, $\Omega_4 \to \Omega_2$, $\delta_3 \to \delta_1$ and $\epsilon_2 \to \epsilon_1$.
Calculating the eigenvalues of eq.(B.9), together with the eigenvalues of the unperturbed eigenstate $e_1$, that is zero (as it has to be for a dark state), we obtain

$$\lambda_\pm^t = \frac{\delta_3 - \epsilon_2}{2} \pm \sqrt{\left(\frac{\delta_3 - \epsilon_2}{2}\right)^2 + \Omega_4^2}, \tag{B.10}$$

corresponding to the eigenvectors

$$v_{t,\pm} = \frac{\Omega_4 e_2 + (\lambda_\pm^t - \delta_3)e_3}{\sqrt{\Omega_4^2 + (\lambda_\pm^t - \delta_3)^2}}. \tag{B.11}$$

In this basis $B = \{v_{t,+}, v_{t,-}\}$, the term $V_\pm^t$ that determines the perturbation to the state $e_1$ can be calculated

$$V_\pm^t = \langle e_1 | V | v_{t,\pm} \rangle = \frac{\Omega_4 g_t}{\sqrt{\Omega_4^2 + (\lambda_\pm^t - \delta_3)^2}}, \tag{B.12}$$

with this result we can calculate the second and fourth order correction to the unperturbed state

in the case of one photon on the trigger field, or one photon on the probe field (switching the label of the fields and of the detunings). We obtain

$$\delta\lambda^{(2)}_{trigger} = -\frac{|V^t_+|^2}{\lambda^t_+} - \frac{|V^t_-|^2}{\lambda^t_-}. \tag{B.13}$$

Applying eq.(B.10) and eq.(B.12) we have the eq.(4.18) given in Chapter IV and at the fourth order by adopting the following relation

$$\delta\lambda^{(4)}_{trigger} = -\sum_{k=+,-}\frac{|V^t_k|^2}{\lambda^t_k}\sum_{k=+,-}\frac{|V^t_k|^2}{\lambda^t_k}, \tag{B.14}$$

we obtain the eq.(4.19).
In the same way we can proceed for the $5\times 5$ dynamics. The unperturbed eigenvectors are the same of the previous lines, being the $5\times 5$ unperturbed Hamiltonian a block matrix. We have $v_{+1}, v_{-1}$ for the block belonging to the probe field, $e_3$ is the unperturbed state, and $v_{+2}, v_{-2}$ for the block related to the trigger field. The perturbative development give the cross interaction between the two $\Lambda$ dynamics, and then produces the cross Kerr photon-photon interaction. As for the trigger case eq.(B.12), the perturbation term on level $e_1$ proportional to the probe field is

$$V^p_\pm = \frac{\Omega_2 g_p}{\sqrt{\Omega_2^2 + (\lambda^p_\pm - \delta_1)^2}}. \tag{B.15}$$

In the evaluation of the second order perturbative term, we can note that the structure of the matrix $H_{pt}$ will give the same terms of each separated $\Lambda$ eqns.(4.18)

$$\delta\lambda^{(2)}_{pt} = \delta\lambda^{(2)}_p + \delta\lambda^{(2)}_t, \tag{B.16}$$

while the fourth order terms give contributions from the cross interaction. Defining

$$\Lambda_t = \frac{1}{\lambda^t_+(\Omega_4^2 + d^2_{+,t})} + \frac{1}{\lambda^t_-(\Omega_4^2 + d^2_{-,t})} \tag{B.17}$$

$$\Theta_t = \frac{1}{(\lambda^t_+)^2(\Omega_4^2 + d^2_{+,t})} + \frac{1}{(\lambda^t_-)^2(\Omega_4^2 + d^2_{-,t})} \tag{B.18}$$

$$\Lambda_p = \frac{1}{\lambda^p_+(\Omega_2^2 + d^2_{+,p})} + \frac{1}{\lambda^p_-(\Omega_2^2 + d^2_{-,p})} \tag{B.19}$$

$$\Theta_p = \frac{1}{(\lambda^p_+)^2(\Omega_2^2 + d^2_{+,p})} + \frac{1}{(\lambda^p_-)^2(\Omega_2^2 + d^2_{-,p})}, \tag{B.20}$$

we obtain the fourth order perturbation from terms of the form

$$\delta\lambda^{(4)}_{pt} = \Big[g_t^2\Omega_4^2\Lambda_t + g_p^2\Omega_2^2\Lambda_p\Big]\Big[g_t^2\Omega_4^2\Theta_t + g_p^2\Omega_2^2\Theta_t\Big]t_{int}. \tag{B.21}$$

In this equation we have four terms, the two terms proportional to $g_t^4\Omega_4^4$ and $g_p^2\Omega_2^4$ are equal to the fourth order term $\delta\lambda^{(4)}_{probe}$ and $\delta\lambda^{(4)}_{trigger}$; however there are two more terms that are produced by the cross products that give the cross interaction.

# Appendix C

# Multimode Coherent States

In section 2.6 we have described the Tripod system in the quantum limits when probe and trigger fields are represented by two weak coherent fields. Here we give the basic definition and properties of *coherent states* and *multimode coherent state*.
The coherent state formalism provides a powerful approach to find solution to many problems in quantum optics. They have an indefinite number of photons, which allows them to have a more precisely defined phase than a number state for which the uncertainty principle states that the phase is completely random. They describe the closest field to the classical one. This states can be seen as *generated* by the unitary displacement operator $\hat{D}$ defined as follows

$$D(\alpha) = e^{(\alpha\hat{a}^\dagger - \alpha^\star \hat{a})}, \tag{C.1}$$

where $\alpha$ is an arbitrary complex number, and $\hat{a}$ and $\hat{a}^\dagger$ are destruction and creation operators of the field. The coherent states are eigenstates of the destruction operator $\hat{a}$, they can be expressed in terms of the Fock states and they are not orthogonal. For different $\alpha$, moreover it can be proved that the set of all coherent states is *overcomplete*. Let us prove some of these assertions.
By the Baker-Hausdorff formula for operators $A$ and $B$, one has

$$e^{A+B} = e^A e^B e^{-[A,B]/2}, \tag{C.2}$$

when

$$[A,[A,B]] = [B,[A,B]] = 0. \tag{C.3}$$

The operator $\hat{D}$ can be written as

$$D(\alpha) = e^{|\alpha|^2/2} e^{\alpha a^\dagger} e^{-\alpha^\star a}, \tag{C.4}$$

and it has the following properties

$$D^\dagger(\alpha)\hat{a}D(\alpha) = \hat{a}^\dagger + \alpha, \tag{C.5}$$

The coherent state id obtained by applying $\hat{D}$ to the vacuum state

$$|\alpha\rangle = D(\alpha)|0\rangle. \tag{C.6}$$

Adopting the relations (C.5, and C.6) we see that the coherent states are eigenstates of the annihilation operator $\hat{a}$,

$$D^\dagger(\alpha)a|\alpha\rangle = D^\dagger(\alpha)aD(\alpha)|0\rangle = (\hat{a}+\alpha)|0\rangle, \tag{C.7}$$

applying the $D$ operator on the left of both side of the previous equation we have

$$a|\alpha\rangle = \alpha|\alpha\rangle. \tag{C.8}$$

The expression of the coherent states on the Fock basis is

$$|\alpha\rangle = e^{|\alpha|^2/2}\sum_{n=0}^{\infty}\frac{\alpha^n}{\sqrt{n!}}|n\rangle. \tag{C.9}$$

Coherent states of more than one field modes are simply formed as products of single-mode coherent states. For two modes $P, T$ with annihilation operators $a_P$ and $a_T$, the two-mode coherent state $|\alpha_P, \alpha_T\rangle$ is generated by the action of two displacement operators $\hat{D}_P(\alpha_P)$ and $\hat{D}_T(\alpha_T)$ on the two-mode vacuum state $|0_P, 0_T\rangle$ so that

$$\begin{aligned} |\alpha_P, \alpha_T\rangle &= \hat{D}_P(\alpha_P)\hat{D}_T(\alpha_T)|0_P, 0_T\rangle & \text{(C.10)}\\ &= e^{(\alpha_P a_P^\dagger - \alpha_P^\star a_P)}e^{(\alpha_T a_T^\dagger - \alpha_T^\star a_T)}|0_P, 0_T\rangle. & \text{(C.11)}\end{aligned}$$

The properties of this state follow from those described above of the single-mode state. In particular, $|\alpha_P, \alpha_T\rangle$ is a right eigenstate of both $\hat{a}_P$ and $\hat{a}_T$ with eigenvalues $\alpha_P$ and $\alpha_T$, respectively, and therefore expectation values of normal ordered products of $\hat{a}_P, \hat{a}_P^\dagger$, and $\hat{a}_T, \hat{a}_T^\dagger$ can be found simply by replacing these operators by $\alpha_P, \alpha_P^\star$ and $\alpha_T, \alpha_T^\star$. For example to evaluate the normal ordered operators' $\hat{a}_P^{\dagger k}\hat{a}_T^{\dagger l}\hat{a}_T^l\hat{a}_P^m$ expectation value, we have

$$\langle\alpha_P, \alpha_T|\hat{a}_P^{\dagger k}\hat{a}_T^{\dagger l}\hat{a}_T^l\hat{a}_P^m|\alpha_P, \alpha_T\rangle = \alpha_P^{\star k}\alpha_T^{\star l}\alpha_P^m\alpha_T^n. \tag{C.12}$$

## C.1 Nonlinear phase in Tripod system by weak multimode coherent field

Here we give the detail of the calculation of the non linear phase accumulation for a weak coherent field, interacting in the *Tripod* configuration, expressed by eq.(2.33). When the equations (2.29)

are dominated by the nonlinear terms, after the interaction of a multimode field $|\alpha_P(t), \alpha_T(t)\rangle$ where the coherent state amplitudes $\alpha_{P,T}$ are defined

$$\alpha_{P,T}(t) = \sqrt{\frac{2\pi c}{l}} \sum_k \alpha^k_{P,T} e^{\imath kct}. \tag{C.13}$$

The evolved operators after the passage throgh an interaction region of length $l$ will be

$$\hat{E}_{P,T}(z,t) = \hat{E}_{P,T}(t') e^{\imath\eta \hat{E}^\dagger_{T,P}(t')\hat{E}_{T,P}(t')l}, \tag{C.14}$$

where $t' = t - z/v_g$, with $v_g$ the pulse's group velocity. Evaluating the mean field operator over the evolved coherent states, we have

$$\begin{aligned} \langle \hat{E}_{T,P}(z,t)\rangle &= \langle \beta_P, \beta_T | \hat{E}_{P,T}(t') e^{\imath\eta \hat{E}^\dagger_{T,P}(t')\hat{E}_{T,P}(t')} | \alpha_P, \alpha_T\rangle, \\ &= \langle \alpha_P, \alpha_T | \hat{O} | \alpha_P, \alpha_T\rangle, \end{aligned} \tag{C.15}$$

where we have defined $\hat{O} = e^{-\imath\eta \hat{E}^\dagger_{T,P}(t')\hat{E}_{T,P}(t')} \hat{E}_{P,T}(t') e^{\imath\eta \hat{E}^\dagger_{T,P}(t')\hat{E}_{T,P}(t')}$. Rewriting the operator $\hat{O}$ by the Baker-Hausdorff formula we have

$$\hat{O} = -\imath\eta l \Delta\omega \hat{E}_{P,T} - \frac{(\eta l \Delta\omega)^2}{2!}\hat{E}_{P,T} - \imath\frac{(\eta l\Delta\omega)^3}{3!}\hat{E}_{P,T} + \ldots \tag{C.16}$$

where we have defined the commutators of the field operators as

$$\begin{aligned} -\Delta\omega \hat{E}_{P,T} &= \left[\hat{E}^\dagger_{T,P}(t')\hat{E}_{T,P}(t'), \hat{E}_{T,P}(t')\right] \\ \Delta\omega^2 \hat{E}_{P,T} &= \left[\hat{E}^\dagger_{T,P}(t')\hat{E}_{T,P}(t'), \left[\hat{E}^\dagger_{T,P}(t')\hat{E}_{T,P}(t'), \hat{E}_{T,P}(t')\right]\right], \\ -\Delta\omega^3 \hat{E}_{P,T} &= \left[\hat{E}^\dagger_{T,P}(t')\hat{E}_{T,P}(t'), \left[\hat{E}^\dagger_{T,P}(t')\hat{E}_{T,P}(t'), \left[\hat{E}^\dagger_{T,P}(t')\hat{E}_{T,P}(t'), \hat{E}_{T,P}(t')\right]\right]\right]. \end{aligned}$$

Applying the previous sequence of the operators in the evaluation of the expectation value of the applied field, grouping the odd terms and even terms, and defining $\Phi = c\eta\Delta\omega$, we have

$$\langle \hat{E}_{P,T}(z,t)\rangle = \alpha_{P,T}(t') e^{[-2sin^2(\Phi/2) + \imath sin(\Phi)]\frac{|\alpha_{T,P}(t')|^2}{\Delta\omega}}, \tag{C.17}$$

that gives the eq.(2.33).

# Bibliography


[1] S. E. Harris, Phys. Today **50**, 36 (1997);

[2] M. O. Scully and M. S. Zubairy, *Quantum Optics* (Cambridge University Press,Cambridge, UK, 1997).

[3] H.R. Gray et al., Optocs Lett. **3**, 218-220 (1978).

[4] E. Arimondo, in *Progress in Optics*XXXV, ed. by E. Wolf, (Elsevier, Amsterdam, 1996).

[5] Arimondo and G. Alzetta et al. 1976 *Nuovo Cimento B*, **36**, 5.

[6] M. Fleischhauer, A. Imamoğlu and J. Marangos,RMP **77**, 633 (2005).

[7] J.D. Jackson, Classical Electrodynamics, 2nd ed., John Wiley & Sons, New York (1975).

[8] Quantum Mechanics: Non-Relativistic Theory, Vol.3, Lifshitz-Landau, Elsevier-Science, 1981.

[9] P.A.M. Dirac, The Principles of Quantum Mechanics, Oxford University Press, London, 1958.

[10] C.W.Gardiner and P. Zoller, *Quantum Noise*, (Springer 2nd Edition, 2000).

[11] Walls and Milburn,*Quantum Optics*, Springer Berlin,(1994).

[12] M.D. Lukin, RMP, 2004

[13] H. Schmidt and A. Imamoğlu, Opt. Lett. **21**, 1936 (1996).

[14] H. Schmidt and A. Imamoğlu, Opt. Lett. **23**, 1007 (1998).

[15] R. W. Boyd, *Nonlinear Optics*, (Academic, San Diego, Calif., 1992).

[16] A. Sinatra, J. F. Roch, K. Vigneron, Ph. Grelu, J.-Ph. Poizat, K. Wang, and P. Grangier, Phys. Rev. A 57, 2980 (1998),

[17] J.-F. Roch, K. Vigneron, Ph. Grelu, A. Sinatra, J.-Ph. Poizat, and Ph. Grangier, Phys. Rev. Lett. 78, 634-637 (1997).

[18] Wang, Goorskey, and Xiao, Phys. Rev. Lett, **87**, 073601 (2001).

[19] M.Fleischhauer and M.O. Scully Phys. Rev. Lett. **72**, 989 (1994).

[20] S.E. Harris et al., Phys. Rev. Lett. 57, **62**(9) 1033 ,(1989),

[21] S.E.Harris et al., **64**, 1107-1110 (1990).

[22] H. Kang, G. Hernadez, and Y. Zhu, Phys. Rev. A **70**, 061804(R), (2004).

[23] H. Kang, G. Hernandez, and Y. Zhu, Phys. Rev. Lett. **93**, 073601(2004).

[24] M. A. Nielsen and I. L. Chuang, *Quantum Computation and Quantum Information*, (Cambridge University Press, Cambridge 2000.)

[25] M. D. Lukin and A. Imamoğlu, (London) **413**, 273 (2001) and references therein.

[26] C. W. Chou et al., Nature **438**, 828-832 (8 December 2005).

[27] M.D. Eisaman et al., Nature **438**, 837-841 (08 Dec 2005).

[28] M. Bajcsy et al., Nature **426**, 638-641 (11 Dec 2003).

[29] A. Kuzmich et al., Nature **423**, 731-734 (12 Jun 2003).

[30] B.Julsgaard et al., Nature **432**, 482-486 (25 Nov 2004).

[31] S. E. Harris and L. V. Hau, Phys. Rev. Lett. **82**, 4611 (1999).

[32] L. V. Hau, S. E. Harris, Z. Dutton and C. H. Berhoozi, Nature (London) **397**, 594 (1999);

[33] M. M. Kash, V. A. Sautenkov, A. S. Zibrov, L. Hollberg, G. R. Welch, M. D. Lukin, Y. Rostovtsev, E. S. Fry and M. O. Scully, Phys. Rev. Lett. **82**, 5229 (1999).

[34] D. F. Phillips, A. Fleischhauer, A. Mair, R. L. Walsworth and M. D. Lukin, Phys. Rev. Lett. **86**,783 (2001).

[35] Eugene Polzik,Nature **428**, 129-130 (11 Mar 2004).

[36] B. Darqui, Science 15 July 2005 **309**: 454-456.

[37] H. Kang and Y. Zhu, Phys. Rev. lett. **91**, 093601 (2003);

[38] H. Kang, G. Hernandez and Y. Zhu, Phys. Rev.Lett. **93**, 073601 (2004);

[39] H. Kang, G. Hernandez and Y. Zhu, Phys. Rev. A **70**, 061804 (2004);

[40] H. Kang, G. Hernandez and Y. Zhu, Phys. Rev. A **70**, 011801 (2004).

[41] R.P.Feynman, Int.J. Theor. Phys. 21, 467, 1982.

[42] D.Deutsch, *Proc. R. Soc. Lond. A*, 400:97, 1985.

[43] D. P. Di Vincenzo, *Science*, 270, 1995 and in the arXive e-print quant-ph/9503016.

[44] P.W.Shor, arXiv:quant-ph/9508027, (1996).

[45] J. Preskill, arXiv quant-ph/9712048, (1997).

[46] A.Ekert, Phys. Rev. Lett., **67**(6), 661-663, (1991).

[47] Gisin, Ribordy,Tittel, and Zbinden, Rev. Mod. Phys., **74**, 145, (2002).

[48] Grosshans, Assche,Wenger, Brouri, Cerf, and Grangier, Nature, **421**, 238 (2003).

[49] Bouwmeester,Pan, Mattle, Eibl, Weinfurter, and Zeilinger, Nature,**390**, 575 (1997).

[50] Boschi, Branca,DeMartini, Hardy, and Popescu, Phys. Rev. Lett., **80**, 1121 (1998).

[51] Furusawa, Srensen, Braunstein, Fuchs, Kimble, and Polzik , Science, **282**, 706 (1998).

[52] Bowen, Treps,Schnabel, and Lam , Phys. Rev. Lett., **89**, 253601 (2002).

[53] Zhang, Goh, Chou, Lodahl, and Kimble, Phys. Rev. A, **67**, 033802 (2003).

[54] Knill, Laflamme, and Milburn, Nature, **409**, 46 (2001).

[55] O'Brien, Pryde,White, Ralph, and Branning, Nature, **426**, 264 (2003).

[56] Sanaka, Jennewein,Pan, Resch, and Zeilinger, Phys. Rev. Lett., **92**, 017902 (2004).

[57] Boller, Imamoğlu, and Harris, Phys. Rev. Lett.**66**, 2593 (1991).

[58] Resch, Lundeen, and Steinberg, Phys. Rev. Lett., **89**, 037904 (2002).

[59] C. Ottaviani, D. Vitali, M. Artoni, F. Cataliotti and P. Tombesi, Phys. Rev. Lett. **90**, 197902 (2003).

[60] Unanyan, Fleischhauer, Shore, and Bergmann, Opt. Comm., **155**,144 (1998).

[61] Paspalakis and Knight, J. Opt. B: Quantum Semiclass. Opt., **4**, S372 (2002).

[62] Paspalakis, Kylstra, and Knight, Phys. Rev. A, **65**, 053808 (2002).

[63] Paspalakis and Knight, J. Mod. Opt., **49**, 87 (2002).

[64] Malakyan, e-print, quant-ph/0112058.

[65] Petrosyan and Malakyan, e-print, quant-ph/0402070.

[66] Petrosyan and Kurizki, Phys. Rev. A, **65**, 033833 (2002).

[67] A. Rauschenbeutel, G. Nogues, S. Osnaghi, P. Bertet, M. Brune, J. M. Raimond, and S. Haroche, Phys. Rev. Lett. **83**, 5166-5169 (1999).

[68] M. Fleischhauer and M. D. Lukin, Physical Review. A, **65**, 022314 (2002).

[69] S. Rebić, A.S.Parkins and S.M.Tan, Phys. Rev. A., **65**,043806 (2002).

[70] S. Rebić, A.S.Parkins and S.M.Tan, Phys. Rev. A., **65**,063804 (2002).

[71] S. Rebić, D. Vitali, C. Ottaviani, P. Tombesi, M. Artoni, F. Cataliotti and R. Corbalàn, Phys. Rev. A **70**, 032317 (2004).

[72] S. Rebić, D. Vitali, C. Ottaviani, P. Tombesi, M. Artoni, F. Cataliotti and R. Corbalàn, Optics and Spectroscopy, Vol.99. No.2,pp.264-269, (2005).

[73] D. Petrosyan and G. Kurizki, Phys. Rev. A **65**,033833 (2002).

[74] M. S. Zubairy, A. B. Matsko, and M. O. Scully, Phys. Rev.A **65**, 043804 (2002);

[75] A. D. Greentree, D. Richards, J. A. Vaccaro, A. V. Durrant, S. R. de Echaniz, D. M. Segal, and J. P. Marangos, Phys. Rev. A **67**, 023818 (2003).

[76] A. B. Matsko, I. Novikova, G. R. Welch, and M. S. Zubairy, Opt. Lett. **28**, 96 (2003).

[77] M. D. Lukin and A. Imamoğlu, Phys. Rev. Lett. **84**, 1419 (2000).

[78] D. Vitali, M. Fortunato, and P. Tombesi, Phys. Rev. Lett. **85**, 445 (2000).

[79] S. Lloyd, Phys. Rev. Lett. 75, 346-349 (1995).

[80] A.Barenco, D.Deutsch, A.Ekert, R.Jozsa, Phys. Rev. Lett. **74**, 4083-4086 (1995)

[81] M.J. Werner and A. Imamoglu, Phys. Rev. A. **61**, 011801(R) (1999).

[82] Q. A. Turchette, C. J. Hood, W. Lange, H. Mabuchi and H. J. Kimble, Phys. Rev. Lett. 75, 4710 (1995).

[83] C. Ottaviani, S. Rebić, D. Vitali and P. Tombesi, Physical Rev. A, 010301(R), (2006).

[84] C. Ottaviani, S. Rebić, D. Vitali and P. Tombesi, physics/0510200, (2005).

[85] L. -M. Duan, J. I. Cirac, and P. Zoller, Phys. Rev. A **66**, 023818 (2002).

[86] L. M. Duan, M. D. Lukin, J. I. Cirac and P. Zoller, Nature (London) **414**, 413 (2001); J. I. Cirac, L. Duan and P. Zoller, in *Experimental Quantum Computation and Information*, ed. by F. De Martini and C. Monroe, (IOS Press, Amsterdam 2002.), also available as e-print quant-ph/0405030

[87] J. F. Poyatos, J. I. Cirac and P. Zoller, Phys. Rev. Lett., **78**, 390 (1997).

[88] E. Knill, R. Laflamme and G. J. Milburn, Nature **409**, 46 (2001).

[89] D. A. Braje, V. Balic, G. Y. Yin, and S. E. Harris, Phys. Rev. A **68**, 041801 (2003);

[90] D. A. Braje, V. Balic, S. Goda,G. Y. Yin, and S. E. Harris, Phys. Rev. Lett. **93**, 183601 (2004).

[91] M. Mašalas and M. Fleischhauer, Phys.Rev. A, **69**, 061801(R) (2004);

[92] I. Friedler, G. Kurizki and D. Petrosyan, Phys. Rev. A, **71**, 023803 (2005);

[93] A. Andrè *et al.*, Phys.Rev. Lett. **94**, 063902 (2005).

[94] J.J.Longdell *et al.*, Phys.Rev. Lett. **93**, 100503-1 (2004).

[95] E.Fraval *et al.*, Phys.Rev. Lett. **92**, 077601-1 (2004).

[96] J.J. Longdell *et al.*, Phys.Rev. A **69**, 032307 (2004).

[97] A. Turchette, C.J. Hood, W. Lange, H. Mabuchi, H. J. Kimble, Phys. Rev. Lett., **75**, 4710 (1995),

[98] B. Darquié, M. P. A. Jones, J. Dingjan, J. Beugnon, S. Bergamini, Y. Sortais, G. Messin, A. Browaeys, P. Grangier, Science, **309**, 454 (2005),

[99] A. Zavatta, S. Viciani, M. Bellini, Science, **306**, 660 (2004),

[100] S. A. Babichev, B. Brezger, A. I. Lvovsky, Phys. Rev. Lett.",**92**, 047903(2004),

[101] John Preskill *Lectures on Quantum Information*, Physics 219 Course Information.

[102] S.Pirandola, PhD Thesis, University of Camerino, Italy, (2005).

[103] I. Chuang's lectures on QECC for the QL&QI School 2004, Cargese, France.

[104] A.Ekert, C.Machiavello, Phys. Rev. Lett. **77**, 2585-2588 (1996)

[105] E.T. Jaynes and F.W. Cummings, Proc. IEEE, **51**, 89 (1963).

[106] J.M.Raimond, M. Brune, S. Haroche, Rev. Mod. Phys, **73**, July 2001

[107] A. Rauschenbautel, PhD. Thesis, Ecole Normale Superieur, Paris (2001).

[108] Hulet R.G. and D. Kleppner, Phys.Rev.Lett., **51**, 1430 (1983).

[109] S.Haroche and J.M Raimond, Physics Today, **49**(8), 51 (1996).

[110] A.Rauschenbeutel et al., Phys.Rev.Lett, **83**, 5166 (1999).

[111] A.Rauschenbeutel et al., Science **288**, 2024 (2000).

[112] H.Carmicahel, An Open System Approach to Quantum Optics, Lecture Notes in Physycs, **m18**, Springer-Verlag, 1993.

[113] M.Plenio and P. Knight, Rev. Mod. Phys. **70**, 101-144 (1998).

[114] E.Scrödinger, Naturwissenschaften **23**, 807 (1935).